DESIGN AND FABRICATION OF CONVENTIONAL AND UNCONVENTIONAL SUPERCONDUCTORS

(NASA-CR-170753) DESIGN AND FABRICATION OF CONVENTIONAL AND UNCONVENTIONAL SUPERCONDUCTORS Final Report, 17 Mar. 1980 - 15 Apr. 1983 (Battelle Columbus Labs., Ohio.) 234 p HC A11/MF A01 CSCL 09C G3/33

N83-24765

Unclas
03684

E. W. Collings
Battelle Memorial Institute
Columbus Laboratories
Columbus, Ohio 43201

Final Report covering the period March 17, 1980 to April 15, 1983 prepared under Contract Number NAS8-33722 to the George C. Marshall Space Flight Center, Marshall Space Flight Center, Alabama 35812.

April 15, 1983

ABSTRACT

The design and fabrication of conventional and unconventionally processed Ti-Nb-base and A15-compound-base, respectively, composite superconductors is discussed in a nine-section review. The first two sections introduce the general properties of alloy and compound superconductors, and the design and processing requirements for the production of long lengths of stable low-loss conductor. Section 3 deals with all aspects of flux-jump stability, and the general requirements of cryogenic stabilization. Section 4 discusses conductor design from an a.c.-loss standpoint; some basic formulae describing hysteretic and eddy-current losses are presented, and the influences on a.c. loss of filament diameter, strand (conductor) diameter, twist pitch, and matrix resistivity are discussed. Section 5 describes the basic techniques used in the fabrication of conventional multifilamentary conductors. This description is generic and applicable to the pre-heat-treatment phases of both alloy and compound conductor fabrication. Section 6 considers conventional Ti-Nb-base composite conductors. Commencing with a brief description of meta-equilibrium and equilibrium Ti-Nb phases, the metallurgical prerequisites for high current-carrying capacity are discussed. With this as a foundation, the section goes on to consider the thermomechanical process optimization of alloy superconductors and the directions that have recently been taken toward the development of high-performance Ti-Nb-base alloy superconductors. Titanium-alloy superconductors are nowadays made by the extrusion of fabricated composite billets and the wire-drawing of the product. Nevertheless it is both interesting and instructive to consider some unconventional fabrication routes that have been suggested from time to time during the development of Ti-Nb-alloy technology. In treating "unconventional" Ti-alloy composite-conductor fabrication, Section 7 refers to a method for continuously coating a superconducting wire or tape with a stabilizing layer of some simple or noble metal, and two methods reminiscent of unconventional approaches that have recently been developed for the production of A15 composites, *viz.* *"in-situ"* composite conductor processing using directional solidification, and a powder-metallurgical technique. Section 8 deals briefly with the conventional processing of A15 conductors, which in this context implies the use of bronze-process chemistry in association with fabricated-billet metalworking. Emphasis is placed on the various ways in which Sn can be introduced to the Nb, process-control of flux-pinning strength, and the effect of multicomponent alloying on the superconducting properties. A.c. loss is only briefly mentioned in Section 8. The influence of strain on the current-carrying capacity is not considered in it at all, since stress effects in both conventionally and unconventionally processed conductors are treated jointly in the final section. As a reflection of the strong interest that has been taken in recent years in

"unconventionally processed" A15 superconductors, the final section of this review, Section 9, places emphasis on conductors produced by techniques other than bronze-processing or by powder-metallurgical or "*in-situ*" variants of that process. Both "hot" and "cold" powder processing techniques for the production, primarily, of Nb_3Sn conductors are considered. Other powder approaches discussed are the "infiltration" method and the so-called "ECN" process which involves the further heat treatment of pre-reacted powdered compounds. Experimental samples of Nb_3Al conductors have been prepared by conventional macroscopic metalworking techniques followed by direct solid-state reaction between the elements; also by variants of this approach which, through the use of laminated microcomposites, reduces the diffusion length and lowers the reaction temperature. Under the heading "solid-state precipitation processes" are considered techniques for preparing V_3Ga and Nb_3Al conductors by a method which involves the administering of an ordering heat treatment to a previously metalworked β-quenched supersaturated solid-solution alloy. The discussion of unconventional processing concludes with a description of the *in-situ* technique which, as the name suggests, uses as its starting point an interconnected array of Nb (or V, as the case may be) precipitates suspended in a Cu matrix as formed by the chill casting of the appropriate liquid alloy. Section 9 then goes on to deal with flux-pinning and critical-current optimization in both powder-metallurgically and *in-situ* processed conductors achieved through the addition of metallic elements either internally or externally, and through the control of fiber size and reaction-layer grain size. The stress effect in conventionally processed conductors is not the subject of a separate subsection, the topic having already been adequately dealt with in several recent reviews and reports. Of particular interest and relevance, however, are *comparisons* of the extents to which the critical current densities of conventionally and unconventionally processed conductors respond to stress (strain), and this is where the emphasis has been placed. Section 9 concludes with a discussion of a.c. loss. A general introduction to the subject of hysteretic and eddy-current losses in conventional composite conductors is provided. Then, although the remaining subsections deal primarily with a.c. loss in untwisted and twisted *in-situ* composites, a comparison with the behaviour of conventionally processed material is implied throughout.

The review is illustrated with 44 line drawings, 29 photographs, and lists 245 references.

TABLE OF CONTENTS

SECTION 1

INTRODUCTION

SECTION 2

THE DESIGN AND FABRICATION OF COMPOSITE CONDUCTORS

SECTION 3

STABILITY CONSIDERATIONS IN CONDUCTOR DESIGN

SECTION 4

A.C. LOSS CONSIDERATIONS IN CONDUCTOR DESIGN

SECTION 5

FABRICATION OF COMPOSITE CONDUCTORS -- GENERAL CONSIDERATIONS

SECTION 6

CONVENTIONAL TITANIUM-ALLOY SUPERCONDUCTORS

SECTION 7

SECTION 8

CONVENTIONAL A15 SUPERCONDUCTORS

SECTION 9

UNCONVENTIONAL A15 SUPERCONDUCTORS

SECTION 9 -- continued

SECTION 1

INTRODUCTION

1.1 Alloy and Compound Superconductors

Although superconductors based on A15 intermetallic compounds such as Nb_3Sn, V_3Ga, and so on possess tempting high-field superconducting properties, manufacturing and handling difficulties have tended to restrict their use to fairly straightforward, usually small-scale, solenoidal-magnet applications. On the other hand conductors using the binary-alloy Ti-Nb, or multicomponent alloys based on it, because of their relative ease of manufacture and excellent mechanical properties are being pressed into service in numerous small- and large-scale devices.

The use of Ti-Nb as a superconductor for magnet applications was first proposed by MATTHIAS in a U.S. patent applied for in 1961 [1]. Since then superconducting Ti-alloy development has paralleled that of type-II superconductivity itself, the alloys having been frequently employed in experimental case studies during the development of the subject. At the same time, superconductivity has provided a useful context for discussions of the microstructural properties of Ti alloys. In the beginning attempts were made to exploit the flux-pinning potentialities of ω-phase precipitation in suitably heat-treated, low-concentration Ti-Nb alloys ($\sim$22 at .% Nb); but after recognizing the poor workability of such alloys, attention turned towards the deformation subband structure, suitably decorated with α-phase precipitates, as a flux-pinning agent. At the present time Ti-Nb-base superconductors are favored over the A15 materials for use in magnets for energy storage, energy conversion (i.e., generators and motors) and in high-energy particle detectors and beam-handling magnets. The goal of the recent and on-going rather intense series of investigations into the electrical and mechanical properties of A15 superconductors is to counteract this tendency, and through finding ways to exploit their advantages, and at the same time to overcome their disadvantages, to cause them to replace Ti-Nb alloys in the next generation of superconducting devices.

The A15 intermetallic compound Nb_3Sn was the first superconductor to be prepared in wire form; the fabrication method described by KUNZLER in 1961 [2], and which bears his name, consists of packing mixtures of Nb and Sn powders into a Nb tube, drawing the composite down to wire and reacting them at elevated temperatures to promote formation of the desired A15 Nb_3Sn compound. The Kunzler method, which was also used in the fabrication of test coils by the "wind-and-react" technique, might be regarded as the forerunner of some of the powder-metallurgy conductor-fabrication processes currently under consideration. It was followed by the development of several tape-processing techniques involving the deposition of Nb_3Sn onto an inert substrate and the reaction of Nb (or V) ribbons with molten Sn (or Ga) either with or without the presence of Cu as a catalyst. The introduction of Cu led to the Cu-V_3Ga and subsequently the Cu-Nb_3Sn "bronze processes" in which filaments of V (or Nb) imbedded in Cu-Ga (or Sn) bronze matrices were suitably heat treated in order to convert them to, or at least encrust them with, the A15 compound. Although some forty-seven binary A15 compounds are known to be superconducting, only six have transition temperatures above 15 K and of these only three, *viz* Nb_3Sn, V_3Ga, and V_3Si, are amenable to bronze-process fabrication. Other members of the group must be prepared by what are herein referred to as "unconventional" methods, for example: CVD or sputtering (Nb_3Ge), or direct reaction between the elements (Nb_3Al). Unconventional processing techniques have also been adapted to the bronze-process fabrication of Cu-Nb_3Sn and Cu-V_3Ga composites in order to confer on them special mechanical and electrical properties. We are referring of course to: (a) the various powder-metallurgical approaches to the preparation of A15 conductors; (b) the so-called "*in-situ*" method pioneered by TSUEI [3], which uses as starting point for Cu-Nb_3Sn fabrication, for example, a fine dispersion of Nb particles precipitated during the solidification of a molten mixture of Nb and Cu.

1.2 The Critical Superconducting Parameters

1.2.1 The Critical Surface

The three cardinal superconducting parameters of hard type-II superconductors are the critical temperature, T_c, the upper critical field, H_{c2}, and the critical current density, J_c. In that T_c depends only on the electronic properties of the material, H_{c2} depends on T_c and to some extent on metallurgically influenced variables, and J_c at intermediate fields depends almost entirely on the metallurgical state of the specimen, they have been referred to as the *primary*, *secondary*, and *tertiary* properties, respectively [4]. A critical surface is imagined to exist within the positive octant of T-H-J-space such that: (a) it cuts the axes at T_c, H_{c2}, and J_c; (b) points within the surface correspond to superconducting states--those without to normal states of the specimen.

1.2.2 The Upper Critical Field

The secondary nature of the upper critical field is demonstrated by the following zero-K expression:

$$H_{c20} = 3.06 \times 10^4 \rho_n \gamma T_c \qquad \text{(Oe)} \qquad (1\text{-}1)$$

where ρ_n is the normal-state residual resistivity in Ω cm and γ is the electronic specific heat coefficient in erg cm^{-3} K^{-2}. The latter, as with T_c, are electronic properties, while ρ_n may be adjusted in magnitude by altering the densities and strengths of electron-scattering defects such as dislocation cores and strain fields, and point defects of various kinds.

1.2.3 The Critical Current Density

It was discovered very early in the history of hard (hence current-carrying) type-II *alloy* superconductors that the critical current density responded strongly to (a) cold work, and (b) cold work followed by moderate-temperature aging. Cold deformation is the natural accompaniment of the

wire-drawing process, the type of deformation structure which results being referred to as "fibrous", "cellular", or "subband". The cell walls have been found to be very suitable for the pinning of flux, hence the stabilization of transport-current flow. The moderate-temperature heat treatment (~380°C), since it is able to activate atomic motion in general, is equally responsible for clarifying the subband structure and in inducing precipitates to grow within the dislocation tangles which constitute the cell walls. Hence in optimizing high-field current transport in alloy superconductors recent interest has focussed on determining the relative merits, from a flux-pinning standpoint, of the deformation-cell structure and the α-phase precipitation which may, in the composition range of interest to the manufacturers of practical superconducting-alloy wire (47~54 wt. % Nb), be associated with it.

The situation is quite different in A15 conductor processing in which, of course, the actual superconductor does not appear until the reaction heat treatment is administered as the final production step. Thus, grain boundaries must be relied on as the principal seat of flux-pinning; and, as was the case with the alloy conductors, great care must be taken to ensure that the grain structure is as fine as possible.

1.3 Conductor Design and Fabrication Considerations -- Plan of the Review

Before embarking upon any superconductor fabrication program, it is necessary to select a superconducting alloy or compound capable of supporting a suitably high critical current density in the intended combination of self-field and applied magnetic field at not too low an operating temperature. As indicated above, the choice is usually between a binary alloy such as Ti-50Nb, or a ternary or quaternary alloy based on it, and an A15 compound such as Nb_3Sn or V_3Ga. Satisfactory values of superconducting transition temperature, T_c, and upper critical field, H_{c2}, both being intrinsic materials properties, are then assured. Critical current density, J_c, in moderately strong applied fields is a more elusive quantity depending as it does on the bulk pinning strength -- a metallurgical variable. In the

alloys, flux-pinning is the responsibility of heat-treatment-optimized cold-work-induced deformation-cell (subband) boundaries and the precipitation that can be induced to form within them. In the A15 compounds, flux-pinning takes place primarily in the boundaries of the grain structure which has to be specially refined, again by paying careful attention to the processing details. Process optimization in both alloy and compound conductors is considered in the following sections.

But excellent superconducting properties alone are of little value if the device wound from the selected conductor switches permanently to the normal state upon being exposed to some electrical or thermal disturbance. The conductor must be both intrinsically stable against internal disturbances -- i.e., flux-jump stable -- and stable against externally applied heat pulses -- i.e., cryostable. In one of the following sections it will be pointed out that flux-jump stability can be achieved in superconducting filaments of sufficiently small diameter. It will also be shown that cryostability of varying degree -- i.e., from *full* to *limited* cryostability depending on the length of normal zone which will spontaneously return to the superconducting state after removal of the disturbance -- can be achieved by associating the superconductor with varying amounts of He-cooled high-purity Cu.

A superconductor will transport a direct current without dissipating energy; not so an alternating current. Associated with the time-varying magnetic field of the alternating current are hysteresis losses in the superconductor itself and eddy-current losses in the normally conducting matrix which stabilizes it. In the section on a.c. loss it will be shown that the hysteretic component can be reduced by reducing the superconducting filament diameter -- but this time to a small fraction of the value sufficient to achieve flux-jump stability alone -- while eddy-current loss can be suppressed by increasing the transverse electrical resistivity of the matrix, to some extent in conflict with the requirements of cryostability.

Stability and a.c. loss, both of which are of central importance in conductor design, are dealt with in Sections 3 and 4, respectively. These are followed, in Section 5, by a description of the basic techniques used in the fabrication of conventional multifilamentary conductors. This description is generic and applicable to the pre-heat-treatment phases of both alloy and compound conductor fabrication. Section 6 considers conventional Ti-Nb-base composite conductors. Commencing with a brief description of meta-equilibrium and equilibrium Ti-Nb phases, the metallurgical prerequisites for high current-carrying capacity are discussed. With this as a foundation, the section goes on to consider the thermomechanical process optimization of alloy superconductors and the directions that recent advances are taking toward the development of high-performance Ti-Nb-base alloy superconductors. Titanium-alloy superconductors are nowadays made by the extrusion of fabricated composite billets and the wire-drawing of the product. Nevertheless it is both interesting and instructive to consider some unconventional fabrication routes that have been suggested from time to time during the development of Ti-Nb-alloy technology. In treating "unconventional" Ti-alloy composite-conductor fabrication, Section 7 refers to: a method for continuously coating a superconducting wire or tape with a stabilizing layer of some simple or noble metal; also two methods reminiscent of unconventional approaches that have recently been developed for the production of A15 composites, *viz.* "*in-situ*" composite conductor processing using directional solidification, and a powder-metallurgical technique. Section 8 deals briefly with the conventional processing of A15 conductors, which in this context implies the use of bronze-process chemistry in association with fabricated-billet metalworking. Emphasis is placed on the various ways in which Sn can be introduced to the Nb, process-control of flux-pinning strength, and the effect of multicomponent alloying on the superconducting properties. A.c. loss is only briefly mentioned in Section 8. The influence of strain on the current-carrying capacity is not considered in it at all, since stress effects in both conventionally and unconventionally processed conductors are to be treated jointly in the final section.

In recent years considerable attention has been devoted to the study of "unconventional" A15 superconductors -- conductors produced by techniques other than bronze-processing or by powder-metallurgical or "*in-situ*" variants of that process. Accordingly, in this review strong emphasis is placed on the preparation and properties of unconventionally processed A15 conductors. Both "hot" and "cold" powder processing techniques for the production primarily, of Nb_3Sn conductors are considered. Other powder approaches discussed are the "infiltration" method and the so-called "ECN" process which involves the further heat treatment of pre-reacted powdered compounds. Experimental samples of Nb_3Al conductors have been prepared by conventional macroscopic metalworking techniques followed by direct solid-state reaction between the elements; also by variants of this approach which, through the use of laminated microcomposites, reduces the diffusion length and lowers the reaction temperature. Under the heading "solid-state precipitation processes" are considered techniques for preparing V_3Ga and Nb_3Al conductors by a method which involves the administering of an ordering heat treatment to a previously metalworked β-quenched supersaturated solid-solution alloy. The discussion of unconventional processing concludes with a description of the *in-situ* technique which, as the name suggests, uses as its starting point an interconnected array of Nb (or V, as the case may be) precipitates suspended in a Cu matrix as formed by the chill casting of the appropriate liquid alloy. Section 9 then goes on to deal with flux-pinning and critical-current optimization in both powder-metallurgically and *in-situ* processed conductors achieved through the addition of metallic elements either internally or externally, and through the control of fiber size and reaction-layer grain size. The stress effect in conventionally processed conductors is not the subject of a separate subsection, the topic having already been adequately dealt with in several recent reviews and reports. Of particular interest and relevance, however, are *comparisons* of the extents to which the critical current densities of conventionally and unconventionally processed conductors respond to stress (strain), and this is where the emphasis has been placed. Section 9 concludes with a discussion of a.c. loss. A general introduction to the subject of hysteretic and eddy-current losses in conventional composite

conductors is provided. Then, although the remaining subsections deal primarily with a.c. loss in untwisted and twisted *in-situ* composites, a comparison with the behaviour of conventionally processed material is implied throughout.

Information for this review has been drawn from the copious body of material which has appeared in the recent journal literature as well as in the proceedings of the biennial Applied Superconductivity and International Cryogenic Materials Conferences. Information has also been obtained from the books "Metallurgy of Superconducting Materials" (Academic Press, 1979) edited by T.S. Luhman and D. Dew-Hughes [5] and "Filamentary A15 Superconductors" (Plenum Press, 1980) edited by M. Suenaga and A.F. Clark [6]. For further discussions of the topics referred to herein the following books are recommended: *SUPERCONDUCTOR MATERIALS SCIENCE -- METALLURGY, FABRICATION, AND APPLICATIONS* (The proceedings of the 1980 NATO Advanced Study Institute) edited by S. Foner and B. B. Schwartz, Plenum Press (1980); *A SOURCEBOOK OF TITANIUM ALLOY SUPERCONDUCTIVITY*, by E. W. Collings, Plenum Press (1983); *APPLIED SUPERCONDUCTIVITY, METALLURGY AND PHYSICS OF TITANIUM ALLOYS*, by E. W. Collings, Plenum Press Cryogenic Monograph Series -- *to be published* .

SECTION 2

THE DESIGN AND FABRICATION OF COMPOSITE CONDUCTORS

2.1 The Current-Carrying Component -- Flux-Pinning

The principal applications of superconductors are generally the production of strong magnetic fields by the passage, through coils wound from them, of heavy electric currents. But under such conditions each "current-element" experiences a Lorentz force as a result of the field acting on it produced by the same current flowing through the rest of the coil (its "external field"). This would sweep the current dissipatively across the wire were it not "pinned" in place by metallurgical defects. Actually it is not the current that is pinned but the "external field" penetrating the conductor; nevertheless, if the flux penetrating the conductor is immobilized, so also is the path of the current flowing through it. The design of the superconductive current-carrying element of the composite conductor focusses largely on the development within it of suitable flux-pinning microstructures.

2.2 Stability

If the Lorentz force, i.e., the product of the current density, J, and the applied field, H, becomes excessive, the flux penetrating the conductor can become dislodged catastrophically from its pinning sites. The mechanical analog of such a "flux jump", as it is called, is brittle fracture under the influence of excessive tensile stress. There are numerous ways of dealing with this phenomenon, i.e., of "stabilizing" the conductor. Two principal philosophies apply: the first is to produce an *intrinsically stable* superconducting wire by giving it a sufficiently small diameter, and then using a number of such filaments in parallel in order to carry the requisite current; the second is to associate the superconducting filament with sufficient Cu to enable the current to be safely shunted about the length of superconductor (SC) that has just experienced a flux jump while it cools

back down to its operating temperature. Most large-scale conductors are *cryostabilized* in this way with Cu/SC ratios varying from about 7:1 (the U.S. MFTF conductor [8]) through 10:1 (the Japanese 8-T LCT conductor [9]) to 20:1 (the Japanese 5-T LCT conductor [9]). The purity and state of strain of the Cu, i.e., the degree of residual cold work, needed to provide adequate stabilization in strong magnetic fields is such that its zero-field residual-resistance ratio ($RRR \equiv R_{300K}/R_{4K}$) is equal to or greater than about 150; in strong magnetic fields (>5T) the residual resistances of all coppers with purities greater than this coalesce onto a single curve [10].

Although Cu, and in particular the OFHC-purity of it, has been referred to as the stabilizing material, high-purity Al is also a serious contender. As discussed by numerous authors (e.g., [11] and further references contained therein) Al as a stabilizer has the following advantages: (i) 99.999% Al with RRR $\sim$ 1000 possesses a higher 4.2-K electrical conductivity than OFHC Cu; (ii) Al (RRR = 1000) possesses a higher thermal conductivity than either OFHC Cu (RRR $\sim$ 150) or specially purified Cu (RRR $\sim$ 1000); (iii) Al possesses a lower 4.2-K specific heat than Cu (purity is not specified since specific heat is much less sensitive to the presence of impurities than the electrical and thermal transport properties); (iv) Al, even when reinforced with stainless steel, possesses a lower 300-0 K enthalpy ("heat capacity during cool-down" [11]) than Cu; (v) since Al is more radiation transparent than Cu, it is required as the stabilizing matrix in superconducting magnets associated with high-energy particle detection and analysis; (vi) the density of Al is less than one-third that of Cu. This property, which has also contributed to characteristics (iii), (iv) and (v) listed above, is an advantage in its own right, especially in mobile applications when weight reduction is important; (vii) high-purity Al is self-annealing at room temperature; this may be advantageous if winding strain is to be removed or radiation damage repaired; (viii) the surface of the Al can be conveniently anodized for the purpose of depositing a thin, strong layer of insulation if required; (ix) finally, the cost per unit volume of high-purity Al is less than that of OFHC Cu.

The disadvantages of Al are mostly mechanical in nature and impinge on both fabricability and serviceability; they have to do with its low yield strength which (a) renders it incompatible with Ti-Nb during conductor fabrication, and (b) requires it to be reinforced, usually with stainless steel, for most applications. But in addition although, as pointed out by DESPORTES *et al.* [12] the radiation length of high-purity Al is six times longer than that of Cu (cf. item (v) above). It should be remembered, especially when tokamak applications are being considered, that if high-flux neutron damage is incurred, Al will increase in resistivity to a larger extent than Cu.

Having decided to use small-diameter superconducting filaments in the interests of flux-jump stability and to imbed them in a conductive matrix in order to achieve dynamic flux-jump stability and cryostability, one is faced with the fact that an array of *parallel* filaments so imbedded is mutually intercoupled *via* circulating currents and prone to flux-jump instability just as if it had not been subdivided in the first place [13]. This difficulty can be partially alleviated by twisting (which is available to monolithic composites) and by transposition (which can be applied to braids woven from twisted composite strands). Twisting will eliminate flux jumping in a time-varying *external* magnetic field [14] and at the same time will significantly reduce a.c. losses [15]. Transposition does both of these and in addition, is the only way to eliminate *self-field* instabilities [16], [17], [18].

2.3 A.C. Loss

The power dissipated in a composite conductor passing an alternating current and exposed to an alternating magnetic field is the sum of two quantities: (a) a hysteretic loss arising from the irreversible magnetization of the cores and which is proportional to filament diameter; (2) a loss due to normal eddy-currents crossing the matrix, which is unrelated to filament diameter but depends on the transverse matrix resistivity, $\rho_{\perp}$.

2.3.1 Hysteretic Loss

The rate of hysteretic heating, $\dot{Q}_h$, is directly proportional to the filament diameter, w, the volume of the superconducting component in the composite, and to the frequency, f. It seems, therefore, that the a.c. losses associated with cores that have been electrically decoupled by twisting could, for a given superconductor volume (hence conductor current-carrying capacity), be indefinitely reduced by making the filaments smaller and smaller. But mechanical metalworking difficulties, also electrical and mechanical filament-surface effects, eventually intervene to impose practical limitations on the pursuit of ultrafine filaments. As a result there appears to be no inducement to lower the filament diameters of low-a.c.-loss superconductors below the 5 μm achieved some time ago by POPLEY *et al.* [19] in the fabrication of a complex Cu/Cu-Ni/Ti-Nb composite.

2.3.2 Eddy Current Loss

The rate of eddy-current heating is independent of the filament diameter, dependent in a complicated way on the frequency and inversely proportional to the transverse resistivity of the matrix, $\rho_\perp$. At "low" and "intermediate" frequencies the eddy-current power loss per unit frequency, $\dot{Q}_e/f$, follows a relaxation-dispersion type of law and thereby subdivides itself into two regimes separated by a characteristic frequency, f_{c1}, which depends on $\rho_\perp$ and the twist pitch. In the low-frequency regime usually encountered in practice, the eddy-current loss is proportional to f^2. The high matrix resistivity needed to suppress $\dot{Q}_e$ is achieved by introducing some high-resistivity components into the composite matrix, usually in the form of cylindrical eddy-current barriers, while at the same time preserving sufficient pure Cu to maintain the cryostability.

2.4 The Design of Stranded Conductors -- Stability and A.C. Loss

The product of a single extrusion instead of being rebundled for use in a two-or-more stage monolithic composite may be drawn down to wire for use as the basic strand of a cabled or braided conductor. There are several advantages to this approach: (a) a single wire product, the "basic strand", can form the basis of conductor of unlimited current-carrying capacity; (b) in its final form as a flat cable, the conductor is fully transposed in the direction normal to the flat face, or as a flat or lattice braid it is fully three-dimensionally transposed; (c) the construction of the stranded conductor is modular -- by combining the standard basic strand with Cu wire and other materials, conductors can be fabricated so as to conform to almost any required performance level or stability criterion; (d) by adjusting the porosity, the access to liquid He can be controlled. A flexible conductor can be produced; or it can be associated with reinforcement during the cabling or (tubular) braiding processes.

With regard to the stabilization of stranded conductors, no single criterion has been adhered to. A conductor may be flux-jump stabilized, using the principles of dynamic stabilization, then operated at almost any desired performance level (α-value or mean conductor current density, cf. Section 4) depending on whether cryostabilization or quench protection is to be relied on to deal with contingencies not otherwise included in the design. Successful practical conductors can be cited which exemplify both ends of the stabilization-philosophy spectrum. On one hand there is the Fermilab cable which has both a low Cu/SC ratio and restricted access to liquid He, while on the other there are cables of the type recommended by WANG *et al.* [20] which in addition to having low a.c. losses and dynamic stability are also fully cryostabilized by the presence of abundant amounts of additional Cu wire. But whatever the final conductor design there is a strong similarity among many of the basic strands.

2.5 Fabrication Techniques

2.5.1 Conventional Processing Steps for Alloy and Compound Conductors

The goal of superconductor fabrication is generally to produce a very long length of wire in the form of a metal-matrix composite consisting of a large number (up to say ∿ 1000) of fine filaments (of diameter say between 5 and 50 μm) imbedded in a high-conductivity matrix usually of OFHC Cu (but occasionally of Al). The conventional way of doing this is to assemble the required number of Cu-clad superconductor rods, plus Cu filler pieces, into a Cu can fitted with nose-cone and tail plug and suitably evacuated in readiness for extrusion. The "conventionally"- or hydrostatically-extruded product is cold drawn to rod on a drawbench and further cold drawn to wire using in succession a bullblock and a multidie machine. The output of this process is a multifilamentary strand which, after insulation, can either be used in that form for the winding of small solenoidal magnets, or can be assembled with many others of its kind into a cable in order to enable the transportation of heavy supercurrents in large-scale applications. A typical superconducting strand and two views of a flat cable wound from it are depicted in Figure 2-1.

2.5.2 Thermomechanical Processing of Alloy and Compound Conductors

If a Ti-Nb alloy conductor is being produced, a carefully designed sequence of interleaved heat treatments (at ∿ 380°C) and wire drawing steps is inserted just prior to a final cold reduction by wire-drawing of about 200:1 followed by twisting and a stress-relief of the Cu at about 300°C. If on the other hand the product is an A15 conductor, although some intermediate heat treatments may be introduced during fabrication in order to counteract work-hardening, the actual reaction heat treatment at temperatures in the vicinity of 800°C (cf. Chapters 8 and 9) takes place after all the metalworking steps have been completed.

2.5.3 Unconventional Processing Methods

As indicated in the Introduction, most "unconventional" A15 superconductor processing involves practically the same general production steps as those just outlined. The principal difference between conventional and unconventional superconductor fabrication has to do with extrusion-billet assembly. Thus, in powder or *in-situ* processing, instead of the billet's being fabricated from clad rods and filler pieces it consists, respectively, of either a mixture of elemental powders (say, Cu and Nb) or a precipitate-bearing chill casting poured from a molten mixture of the starting elements.

SECTION 3

STABILITY CONSIDERATIONS IN CONDUCTOR DESIGN

3.1 Introduction -- Stability of a Composite Superconductor

Stability in the present context is a measure of the ability of a conductor or device to return spontaneously to the superconducting state after the passage of a disturbance which had either triggered, or driven, an excursion into the normal state (i.e., a "quench"). The term stabilization is loosely used to describe (a) methods of improving the stability of the conductor itself but more frequently, since the problems of intrinsic conductor stability have by now been solved, (b) system design procedures which may be adopted for the suppression or limitation of the effects of conductor instability brought about either through the deliberate use of a minimally stabilized conductor or through some mechanical or thermal perturbation external to the conductor. Conductor instability is diagrammed in Figure 3-1(a). Whatever the source of the disturbance the focus of the instability is the conductor itself, processes associated with which are indicated by the circular portion of the diagram. As indicated in Figure 3-1(b) any feedback cycle which results in a continuous enhancement of ΔT, the initial temperature change experienced by some portion of the superconductor, represents an instability; conversely stability is represented by an inward-turning spiral. Stabilization has to do with the various ways in which this spiraling can be controlled.

It is usual to address first of all the intrinsic flux-jump stability of the isolated conductor, either (a) the bare superconducting wire, or (b) a superconducting wire in close association with a highly conductive normal metal. Stability considered under this heading would, for example, describe the performance of the conductor during short-sample testing. But the conductor is eventually to be used in one or other of numerous possible large-scale superconducting devices, all of which except

one (the transmission line) utilize the high-intensity magnetic fields generated by superconducting solenoids. In designing such devices it is sometimes necessary to discard some of the principles of intrinsic conductor stability especially if high average current densities are required and substitute for them some means of *coping* with the instabilities that will inevitably follow [21]. Furthermore an unstable response may be triggered by sources which have nothing to do with the electrical properties of the conductor itself, but which again must be dealt with in terms of conductor as well as device design; this generally entails either the suppression or the control of magnetically, thermally or mechanically instigated heat pulses.

A conductor which is immune to flux-jumping is "intrinsically stable" or "flux-jump stable" [22].† By now the methods for achieving flux-jump stability are well known and have been fully discussed in the classical paper by WILSON *et al.* [13]. They include the techniques of "adiabatic", "dynamic", and "enthalpy" stabilization. Most other stabilization techniques may be included under the general heading "cryogenic stabilization". Thus, if (a) in the isolated conductor the conditions for intrinsic stability have for one reason or another been relaxed, or (b) a pulse of internal heat is generated through some mechanical stress effect taking place within the superconductor, or (c) an otherwise stabl conductor when wound into a magnet experiences a device-generated magnetic, thermal, or mechanical disturbance, then superconductivity is restored following the resultant

---

† The term "intrinsic stability" is no longer in favor [23], and does not appear among the list of terms defined by the NBS group [22] who favor "flux-jump stability". WIFP has suggested [23] that the term should be reserved for the condition $dJ_c/dT>0$. It could be argued that the term does serve a useful purpose in distinguishing the stability of a conductor from that of the device wound from it.

quench through the intervention in one way or another of the cooling properties of liquified or gaseous He. Some writers contend that flux-jump and cryogenic stabilization bear a "prevention" and "cure" relationship one to the other.

The applicability of the term "cryostabilization" is obviously very broad. For further definitions of the terminologies of stability, and other properties of practical superconductors, the article by READ, EKIN, POWELL and CLARK [22] of the National Bureau of Standards (NBS), Boulder, U.S.A., is recommended.

3.2 Flux-Jump Stabilization

The aim of this class of stabilization is to prevent incipient flux motion from developing into a flux-jump, i.e., to suppress the initiation of a cycle of disturbances that will drive the conductor normal. Flux-jump stability depends heavily on materials properties such as: (i) the critical current density and the several metallurgical and other factors, including temperature, which influence it; (ii) K_{sc}, the thermal conductivity of the superconducting alloy; (iii) ρ_{Cu}, the electrical resistivity of the Cu matrix; (iv) C, the specific heats of the superconducting alloy and other materials with which it is closely in contact. It also depends on geometrical factors such as: (i) w, the filament diameter; (ii) N, the number of filaments in the strand; (iii) L_p, the filament twist pitch, and their degree of transposition if any.

3.3 Cryogenic Stabilization

The purpose of cryogenic stabilization is to restore superconductivity once a major thermal disturbance has taken place. In cryostabilization, as it is also called, the quenched supercurrent is temporarily provided with a shunt path in the form of a normal-metal cladding or substrate which in turn

is supplied with sufficient cooling to enable heat to be removed from it more rapidly than it is produced by Joule heating. The term "cryostable" is most usefully applied to the state of the conductor in conjunction with the device wound from it. Crystabilization may be either "full" or "limited". According to READ *et al.* [22] an individual conductor may be fully cryostabilized by associating it with sufficient, adequately cooled, normal metal to enable it to recover after the passage of a large and extensive disturbance which has driven the entire length normal. Limited cryostability refers to the ability of the conductor to recover after a *local* quench. It is this aspect of cryostability that is particularly relevant to machine design since *global-scale* winding disturbances are not expected. This continuum of cryostability levels can be generated by varying the Cu/SC ratio. On one hand there is the Stekly-stabilized[†] conductor which, although operating at a current-density in the superconductor equal to the critical value, J_c, will recover from a so-called "global" disturbance in which the entire length of the conductor has become normal. At the other extreme are the high-performance conductors, possessing minimal amounts of Cu, which recover only from local disturbances of carefully engineered magnitude.

3.4 Factors Controlling the Stability of a Conductor

The flux-jump stability of a conductor is established by subdividing the superconductor into a bundle of fine transposed, or at least twisted, filaments (adiabatic stabilization). Should an internal disturbance still quench the conductor a return to the superconducting state (i.e., stability) can be assured by associating it intimately with a large volume-fraction of liquid-He-cooled Cu or Al (dynamic stabilization).

[†] Full (zero-dimensional) cryostability as defined as $\dot{G} = \dot{Q}$ or $\alpha_{st} i^2 = 1$. Stekly cryostability is the extreme case of this when $\alpha_{st} = 1$. The symbols are defined below.

The means used to achieve dynamic flux-jump stability are also compatible with those needed to confer cryostability to the conductor or the device wound from it, usually against external disturbances. Different degrees of stability are achieved by variation of the Cu/SC ratio (i.e., the "design stabilization") or the average current density (i.e., by adjustment of the "operational stability").

The starting point for a discussion of steady-state cryostability is usually Figure 3-2 in association with an expression for the power balance such as:

$$\dot{G}_d + \dot{G} = \alpha_1 \nabla^2 T + \alpha_2 \partial T/\partial t + \alpha_3 \Delta T \qquad (3\text{-}1)$$

whose five components after adjustment to a common dimensionality, usually W cm^{-2} of conductor surface, represent the following heat fluxes:

$\dot{G}_d$, W cm^{-2}, the global or local initiation *disturbance*;

$\dot{G} \rightarrow (A/P)_{tot} \rho_{as} J^2_{av}$, W cm^{-2}, the specific power *generated* in the matrix as a result of current sharing or transfer;

$\dot{G}_d$, W cm^{-2}, the global or local initiating *disturbance*;

$\dot{G} \rightarrow (A/P)_{tot} \rho_{av} J^2_{av}$, W cm^{-2}, the specific power *generated* in the matrix as a result of current sharing or transfer;

$\alpha_1 \nabla^2 T \rightarrow \left(\frac{AK}{P}\right)_{Cu} \partial^2 T/\partial X^2$, W cm^{-2}, the dimensionally adjusted heat *conducted* away to cold parts of the device;

$\alpha_2 \partial T/\partial t \rightarrow \left(\frac{A}{P}\right)_{tot} C(T) \partial T/\partial t$, W cm^{-2}, the rate of *heat storage* within the conductor or its immediate surroundings;

$\alpha_3 \Delta T \rightarrow h(T-T_b)$, W cm^{-2}, the *cooling rate* to the cryogen per unit area of conductor surface.

Each steady-state stability criterion can be described in terms of some, but usually not all, of these terms.

Of considerable interest to the magnet designer is the "performance" of the conductor or device [24, 25]. To achieve high performance it is usually necessary to sacrifice some of the stabilizing substrate. The average critical current density increases as the Cu/SC ratio decreases; very soon the conductor is no longer fully cryostable and must be operated under different criteria, more and more reliance being placed on a knowledge of the expected disturbance power and energy. Under current sharing or transfer the ohmic heating in the conductor or the stabilizer (i.e., the "heat generation", $\dot{G}$) is $\rho_{av}J_{av}^2$ W cm^{-3}, where ρ_{av} is the average resistivity of the conductor and J_{av} is the current density averaged over its cross section. As the superconductor volume fraction increases (and current transfer rather than sharing soon becomes the only alternative to the fully superconducting mode) heat generation follows suit; and expressed in terms of heat dissipation per unit cooled surface area of the conductor (W cm^{-2}) makes a convenient measure of conductor performance. The performance level of a fully cryostabilized conductor is usually about 0·2 W cm^{-2}.

If a global instability develops in a conductor of cooled perimeter P_{Cu} in a conductor carrying current I_c, the critical value in the ambient design field, such that current is transferred completely to the stabilizer, the heat generated is:

$$\dot{G} = I_c^2(\rho/PA)_{Cu} \quad \text{(full transfer)} \tag{3-2}$$

where the subscript, Cu, applies to all the quantities within the brackets. Since cooling to the cryogen bath (temperature T_b) is given by:

$$\dot{Q} = h(T_c - T_b) \tag{3-3}$$

where "h" is the unit-area heat-transfer coefficient and T_c is the conductor critical temperature in the operating field, an equilibrium non-runaway state is achieved when:

$$1 = \frac{\dot{G}}{\dot{Q}} = \frac{\rho_{Cu}I_c^2}{hP_{Cu}A_{Cu}(T_c - T_b)} \equiv \alpha_{st} \tag{3-4}$$

Here α_{st} is the Stekly cryostability parameter. If a calculation shows that $\alpha_{st} < 1$, the conductor will be able to recover upon removal of the disturbance which resulted in its entire length going normal. An enormous Cu/SC ratio is called for; for example, at least 20:1 for a 10,000-A conductor. If less Cu is employed, α_{st} immediately increases; but an "$\alpha = 1$" condition can be restored by operating the conductor at some current $I < I_c$ (i.e., at $i \equiv I/I_c < 1$) and this is usually done. Thus, a general condition for full cryostability is:

$$\alpha \equiv i^2\alpha_{st} \lesssim 1 \qquad (3\text{-}5)$$

The foregoing discussions have indicated that the design of a conductor that is to be flux-jump and cryogenically stable while operating under given conditions of temperature, current, and field, results in the specification of such quantities as: filament diameter, w; number of filaments, N; twist pitch, L_p; strand diameter, D; Cu/SC ratio, R_s. A series of equations governing the choice of these quantities is presented below.

3.5 Filament Diameter

3.5.1 Adiabatically Stable Filament Diameter

Calculations based on a double-sided slab have indicated that an isolated filament is adiabatically stable against flux-jumping (i.e., will self-recover) provided its diameter w satisfies:

$$w^2 < 10^9 f_i (C/J_c^2)\Delta T_o \qquad (3\text{-}6)^{\dagger}$$

---

† This equation, which assumes flux-jumping in a two-sided slab yields a critical thickness four times larger than the equivalent expression in Reference [13]; but this discrepancy may be removed by the introduction into the latter

where "f_i" is a model-dependent numerical factor lying between about 0.6 and 0.9, "C" is the volume specific heat of the superconductor and "ΔT_o" $\equiv J_c/(-dJ_c/dT)$. The equation contains a wealth of information about intrinsic stability. Stability is obviously aided by factors which: (a) tend to suppress the temperature rise accompanying a given heat input and (b) diminish the decrease in J_c which accompanies that temperature increase. Item (a) refers to "enthalpy" stabilization; item (b) indicates that flux-jump instability is a more serious problem in a conductor operating to full capacity at low winding field strengths than when it is operating in a device designed for high-field applications when the J_c is much lower. In an attempt to attain the highest possible values of J_c in an alloy superconductor some designs call for operation at temperatures below 4.2 K. This involves an additional investment in cryogenics the return for which would be the sought-after higher J_c. Implicit in this approach, however, is that the superconductor possesses a suitably large value of $-dJ_c/dT$. But Equation (3-6) indicates that the conductor which provides the largest increase in J_c upon cooling from 4.2 K to 2 K, say, has the highest tendency towards flux-jump instability.

However, Equation (3-6) has only limited utility. Since in practice the filament is imbedded in a normal high-conductivity matrix, although the equation makes a useful starting point for general discussions of flux-jump stability, as a predictor of filament diameter it must be replaced by the following relationships based upon dynamic and (what appeared to be) cryogenic stability considerations.

3.5.2 Dynamically Stable Filament Diameter

The filament size limitation based on dynamic stability considerations is given by:

---

equation of a factor of 4 to take into account Hancox' limited-flux-jump stability margin (see also [13]). Equation (3-6) is identical to the filament-size criterion for intrinsic stability as defined by SMITH *et al.* [26].

$$w^2 \gtrsim 8\left(\frac{K_{SC}}{\rho_{Cu}}\right)\left(\frac{1-\lambda}{\lambda}\right)\Delta T_o/J_c^2 \qquad (3\text{-}7)$$

i.e.,
$$w^2 \gtrsim 8\left(\frac{K_{SC}}{\rho_{Cu}}\right)(1-\lambda)\Delta T_o/J_{av}J_c \qquad (3\text{-}8)$$

where K_{SC} is the thermal conductivity of the superconductor and in which $\rho_{Cu}/(1-\lambda)$ is taken as the effective resistivity (or transverse resistivity) of the matrix, λ being the filling factor, A_{sc}/A_{tot}.

The condition for dynamic stability is a little stricter than the adiabatic condition, but the principle does provide a ready means of escape for the internally generated heat, and must of course be applied when the filaments are imbedded in Cu. The ratio of the maximum filament diameters provided under the two conditions referred to (with $f_i = 0.8$) is given by:

$$\frac{w_{max}^{dynamic}}{w_{max}^{adiabatic}} \cong \left[\frac{D_{TH}^{SC}}{D_{EM}^{Cu}}\left(\frac{1-\lambda}{\lambda}\right)\right]^{\frac{1}{2}} \qquad (3\text{-}9)$$

where the D's are the thermal (TH) and electromagnetic (EM) diffusivities, respectively. Equation (3-9) clearly indicates the parameters which would need to be adjusted in order to raise $w^{dynamic}$ up to the adiabatic value.

3.5.3 Cryostable Filament Diameter

Within the context of a steady-state analysis of the conditions for full cryostability STEKLY [27, 28, 29] has also derived an expression for the maximum stable filament diameter, *viz:*

$$w^2 \lesssim 8\left(\frac{K_{SC}}{\rho_{Cu}}\right)(T_c - T_b)/J_{Cu}J_c \qquad (3\text{-}10)$$

where T_c and T_b have already been defined, J_c is the critical current density corresponding to I_c and J_{Cu} represents the current density in the matrix after the entire conductor has gone normal. Close examination of the

analysis, however, reveals that the underlying physics in fact involves the *dynamics* of the superconductive/normal transition, and the ability of the superconducting core (each filament) to dissipate its heat to a surrounding Cu matrix at some uniform temperature just above the bath temperature. For this reason it is satisfying to note that the substitution of ΔT_o for $T_c - T_b$ [which is the same as requiring that $-dT/dJ_c = (T_c - T_b)/J_c$] and $\lambda J_c/(1 - \lambda)$ for J_{Cu} (based on the assumption that $\rho_{Cu} << \rho_{SC}$) transforms Equation (3-10) into Equation (3-7).

3.6 Twist Pitch

3.6.1 Filament Decoupling

In order for a group of filaments to be able to maintain their stability in the presence of a time-varying external field, $\dot{H}_a$, they must be twisted to a pitch, L_p, tighter than some calculable characteristic value. Based on a model consisting of a pair of parallel superconductive plates of thickness w and separation D_s imbedded in a conducting matrix of transverse resistivity $\rho_\perp$, WILSON *et al.* [13] have predicted that their individuality can be preserved provided that the quarter-wavelength, ℓ_p, of the twist which must be imparted is small compared to some ℓ_c, given by:

$$\ell_c^2 = 2 \times 10^8 \, (\rho_\perp \lambda^{\frac{1}{2}} w) \left(\frac{J_c}{\dot{H}_a}\right) \frac{D_s}{D_s + w} \qquad (3\text{-}11)$$

Next, since the eddy currents which "couple" the filaments (and which also produce the a.c. losses to be considered in the next section) also give rise to a diamagnetic moment, magnetization measurements provide a ready means of gauging both flux-jump instability (*via* interfilamentary coupling) and a.c. loss.

Based on an analysis of a multifilamentary composite, WILSON *et al.* [13] went on to develop the following expression for the magnetization as a function of a filament-coupling parameter, $v \equiv (\ell_p/\ell_c)^2$:

$$\frac{M}{M_o} = 1 + \frac{4\eta_c}{\lambda^{\frac{1}{2}}}\left(1 - 0.5\,\frac{w}{D}\right)v - \frac{4\eta_c}{\lambda}\left(\frac{w}{D}\right)v^2 \qquad (3\text{-}12a)$$

(where η_c (= $2/3 \sim 1$) is an efficiency factor which takes into account the variation of coupling along the length of the conductor) a simplified version of which (for $\eta_c = 2/3$) is:

$$\frac{M}{M_o} \cong 1 + \frac{8}{3\lambda^{\frac{1}{2}}}\left(\frac{\ell_p}{\ell_c}\right)^2 - \cdots \qquad (3\text{-}12b)$$

$$\equiv 1 + \alpha_m \qquad (3\text{-}13)$$

Figure 3-3 based on Equation (3-12a) with $\eta_c = 0.8$, $\lambda \equiv Nw^2/D^2 = 0.5$, and N = 200 filaments shows the relative magnetization rising to a saturation value given by $M/M_o \cong D/w$. CARR [30][32] has identified α_m as the ratio of the eddy-current to hysteretic losses, $\dot{Q}_e/\dot{Q}_h$ (cf. Section 4); accordingly, Figure 3-3 can be interpreted as showing the eddy-current loss component building up, as the "coupling" between the filaments increases, to a maximum at point P. Returning to Equation (3-12b) and inserting $\lambda = 0.33$, a typical value, it can be seen that the decoupling will be better than 70% effective (i.e., $\alpha_m \lesssim 0.3$) provided ℓ_p/ℓ_p is reduced below about 0.25 (i.e., if $L_p \lesssim \ell_c$).

Twist involves an additional fabrication step which although unable to be avoided in most cases should not be made unnecessarily difficult, or hazardous from the standpoint of filament integrity, by the imposition of an excessively short twist pitch. For several reasons L_p is never reduced below about 5 to 10 wire diameters. With the aid of Equation (3-11), Equation (3-12b) can be rewritten (in c.g.s. - practical units):

$$\frac{M}{M_o} \cong 1 + \frac{4}{3 \times 10^8} \left(\frac{1}{w\lambda J_c}\right) \frac{\ell_p^2 \dot{H}_a}{\rho_\perp} \qquad (3\text{-}14)$$

If $\dot{H}_a$ in this equation is so large that a value of $4\ell_p$ shorter than $5 \sim 10D$ would be called for, since w, λ, and $\rho_\perp$ are more-or-less fixed by filamentary and dynamic stability requirements, α_m can only be kept within bounds by "artificially" increasing $\rho_\perp$ through the introduction of eddy-current barriers. However, in such cases the applied field would be changing so rapidly that a.c. loss may be just as serious a problem as flux-jump stability. The subject of matrix resistivity will, therefore, be reintroduced in Section 4.

3.6.2 Twist-Pitch Selection for Low $\dot{H}_a$

For magnets intended for steady-state operation (i.e., superconducting "permanent-magnets" such as those needed for bubble chambers, particle-beam bending, MHD generators, magnetic mirrors, NMR spectrometers, and so on) the filament twist pitch is dictated only by the proposed magnetic charging rate [33] and the desire to achieve $L_p \tilde{<} \ell_c$ and may, therefore, be relatively long.

3.6.3 Twist Pitch Selection for High $\dot{H}_a$

As indicated by Equation (3-11) a large applied-field ramp rate, $\dot{H}_a$, can drastically reduce ℓ_c, thereby placing a severe restriction on the twist pitch $L_p \tilde{<} \ell_c$. By equating the second terms of Equations (3-13) and (3-14) and substituting, where appropriate, the usual definition $\lambda \equiv Nw^2/D^2$ the relative twist pitch can be expressed in the form:

$$\left(\frac{L_p}{D}\right)^2 = \frac{12 \times 10^8}{\dot{H}_a} \left(\frac{\alpha_m \lambda^2}{Nw}\right) \rho_\perp J_c \qquad (3\text{-}15a)$$

$$= \frac{3 \times 10^8}{\dot{H}_a} (\pi \alpha_m w \lambda^2) \rho_\perp \frac{J_c^2}{I_c} \qquad (3\text{-}15b)$$

where I_c is the critical current in the conductor. As indicated above, the

goal of this stage of conductor design is to maintain L_p/D greater than $5 \sim 10$ in the face of large $\dot{H}_a$ and fixed values of $\rho_\perp$, α_m, and λ as dictated by coupling and cryostability requirements, respectively. The importance of large $\rho_\perp$ is apparent; a large J_c is advantageous from all standpoints; a small w is generally beneficial, but N needs to be as large as possible to achieve a reasonable current-carrying capacity for the strand.

3.7 Strand Diameter and Number of Filaments

3.7.1 Strand Diameter Under Twist-Pitch Limitation

As mentioned above, a large value of $\dot{H}_a$ demands a short twist pitch, Equation (3-11); but for mechanical and other reasons [34][35], L_p is lower bounded by the requirement that $L_p/D \nless 5$. These factors combine to place an upper limit on the diameter of the multifilamentary conductor to be flux-jump stabilized against external-field variation. With reference to Equation (3-15), the statement $(L_p/D)_{min} = 5$ is equivalent to:

$$N_{max} = \frac{12 \times 10^8}{25w} (\lambda^2 \rho_\perp J_c)\left(\frac{\alpha_m}{\dot{H}_a}\right) \qquad (3\text{-}16)$$

For example, suppose a pulse-magnet for $\dot{H}_a$ = kOe s^{-1} is to be wound with a maximally twisted conductor conforming to w = 9 μm, Cu/SC = 1.8:1 (λ = 0.357), Jc(4.2 K, 5T) = 2.18×10^5 A cm^{-2} and $\rho_\perp$ (4.2 K, 5T)= 4.6×10^{-8} Ω cm, and that α_m is to be 0.25; then Equation (3-16) yields N_{max} = 1700 filaments. The maximum possible flux-jump-stabilized strand current under the conditions stipulated is therefore 236 A. Thus, in order to construct a high-amperage pulse-magnet conductor, a multiplicity of such strands would be required. For example, to carry 5000 A with some margin of safety it would be necessary to cable (or braid) together more than 21 of them.

3.7.2 Strand Diameter Under Adiabatic Self-Field Limitation

Just as in the case of external-field stability, in which the adiabatic approach had eventually to be replaced by a dynamic model (cf. Sections 3.5.1 and 3.5.2) a discussion of self-field instability couched in adiabatic terms makes a useful introduction to the physics of the problem.

According to a model due to WILSON *et al.* [13], a flux-jump will occur as soon as the self-field difference, H_s, across the half-width, D/2, of the entire composite is equal to H_{fj}, the usual minimum flux-jump field. In other words:

$$D_{max} = 2H_{fj} \Big/ \left[\left(\frac{4\pi}{10}\right) \lambda J_c\right] \tag{3-17}$$

$$\cong 2H_{fj} \Big/ \lambda J_c \tag{3-18}$$

The substitution of H_{fj} = 2.4 kOe (a typical value) and other data from the previous sub-section leads to the prediction that, under adiabatic conditions, self-field instability could be expected in conductors with diameters larger than $D_{max} \cong 6.2 \times 10^{-2}$ cm. With a filament diameter of 9 μm the other specifications would be N = 1680 and I_c = 233 A.

According to the more recent model of DUCHATEAU and TURCK [35] the maximum composite outside diameter for adiabatic self-field stability is:

$$D_{max} \cong \frac{2}{(4\pi/10)} \left(\frac{1}{J_c}\right) \sqrt{10^9 C_{av} \Delta T_o} \tag{3-19}$$

which leads to comparable results.

If the stabilizing influence of a 50-kOe external field is then to be taken into consideration, it is possible to double the number of filaments while still maintaining adiabatic self-field stability. Furthermore, if operation at current levels lower than I_c is satisfactory, even larger strand diameters are permissible. But for d.c. applications, it would be desirable not to have to be constrained, through adiabatic self-field

limitations to such small wire sizes. At first pointed out by WILSON *et al.* [13], subsequently to be confirmed by the calculations of DUCHATEAU and TURCK [17], significant relief can be expected under dynamic conditions.

3.7.3 Strand Diameter Under Dynamic Self-Field Limitation

According to the DUCHATEAU and TURCK [16, 17] approach to dynamic self-field stability, a conductor can be assigned a dimensionless parameter β given by:

$$\beta = (\pi/10^9)(\lambda J_c)^2 D^2 / C_{av}\, \Delta T_o \qquad (3\text{-}20)$$

such that it is dynamically self-field stable at some degraded current $i = I/I_c$ provided β is less than some critical value β_c; or stable at $i = 1$ (no degradation) provided its β is less than a special value β_s given (for cylindrical conductors) by:

$$\beta_s \equiv \beta_c(i = 1)$$

$$= 2.7(1 + 1{\cdot}1\sqrt{h^+ d} + 0.72\, h^+ d) \text{ (valid for } h^+ < 0.1) \qquad (3\text{-}21)$$

Here $d = D_{TH}^{av}/D_{EM}^{av}$, the ratio of the thermal and magnetic diffusivities (a function of λ) and h^+ is a reduced coefficient of heat transfer to the cryogen bath a not atypical value for which is 0.25*. Obviously, since under adiabatic conditions $h^+ = 0$, it is possible to make the comparison

---

* $h^+ = h' R_o / K_{av}$ where h' is the dynamic heat-transfer coefficient $\cong h$, the steady-state value; $R_o = D/2$; K_{av} is the average thermal conductivity of the composite $= (1 - \lambda^{\frac{1}{2}})K_{Cu}$. Then inserting the values $h' = 5$ W cm^{-2}, $D = 2.5$ mm, $\lambda = 0.357$, $K_{Cu} = 6$ W cm^{-1}K^{-1}, $h^+ = 0.259$.

$$\beta_s^{\text{dynamic}} / \beta_s^{\text{adiabatic}} = (1 + 1.1\sqrt{h^+ d} + 0.72\, h^+ d) \qquad (3\text{-}22)$$

following which, since according to Equation (3-20) $D^2 \propto \beta$, it is apparent that upon the removal of the adiabatic constraint the maximum self-field-stable wire diameter (for i = 1) is able to be increased in the ratio:

$$\frac{D_{max}^{\text{dynamic}}}{D_{max}^{\text{adiabatic}}} = \left[\frac{\beta^{\text{dynamic}}}{\beta^{\text{adiabatic}}}\right]^{\frac{1}{2}} = (1 + 1.1\sqrt{h^+ d} + 0.72\, h^+ d)^{\frac{1}{2}} \qquad (3\text{-}23)^*$$

For example, with $h^+ = 0.25$ and $d = 150$ (appropriate for a λ-value of 0.36), it is clearly possible for the diameter of a previously adiabatically stable wire to be increased by a factor of 6. Of course to render the modified conductor flux-jump stable under the terms of Equation (3-16) the transverse matrix resistivity would have to be increased and in such a way as to preserve the d of Equation (3-23). The new resistivity could be achieved by the insertion of Cu-Ni barriers.

3.7.4 Strand Diameter Under Full Critical-Current (i.e., Steckly) Crystability

It should be stated at the outset that there is no electrical limitation on the size of strand that can be stabilized under the full cryostability criterion. The design variable in this case is the Cu/SC ratio, R_S.

When designing conductors for pulse- and a.c.-magnet applications, it is important to adhere to the design requirements outlined above -- and also to those to be considered in the next section which have to do with a.c. loss. However, if in the design of a d.c. conductor it has been

---

* A similarity between this expression and Equation (3-9) for the *filament-diameter* enhancement is obvious.

decided to relax one or more of the flux-jump stability requirements having to do with filament diameter, twist pitch, and so on, safe operation can still be achieved by applying the principles of steady-state cryostability.

The point of departure for all cryostable conductor designs is Stekly-type full cryogenic stability in which a conductor, operating at a current density $J = J_c$, is provided with sufficient Cu that should its entire length go normal and transfer its current to the matrix, the steady-state heat generation in it is less than about 0.2 W cm^{-2} and as such can be dissipated into the cryogen bath, with only modest temperature drop at the interface, until the initiating disturbance has passed and the conductor has relaxed back into the superconducting state. There are numerous mechanical and electrical causes of magnet quench; current surge is not generally regarded as one of them. They all tend to be local in extent, consequently, it is difficult to envision the need for stabilization against global disturbances, yet such designs are contemplated when the stabilities of large systems are at stake. Other less conservative, and consequently more restrictive, cryostability criteria are arrived at in turn by peeling off more and more of the Cu stabilizer.

Returning to full Stekly-cryostability we recall that the heat generated per unit area of conductor surface, $\dot{G}$, after the current has transferred to the stabilizer is given by the identity:

$$\dot{G} = I_c^2(\rho/PA)_{Cu} \text{ (full transfer)} \qquad (3\text{-}24)$$

Under steady-state $\alpha_{st} = 1$ conditions this is equal to $\dot{Q}$ the cooling capacity of the exposed conductor surface. Next by applying the definitions $I_c \equiv J_c A_{SC}$ and $R_s \equiv A_{Cu}/A_{SC}$ to Equation (3-24) it is possible to arrive at the following two conditions sufficient for the description of a fully cryostable conductor of current-carrying capacity $I = I_c$:

(a) for the Cu/SC ratio, R_s:

$$R_s^2(R_s + 1) = \frac{\rho_{Cu}^2 J_c^3}{4\pi\dot{Q}^2} I_c \quad ; \qquad (3\text{-}25)$$

(b) hence for the resulting strand diameter:

$$D = \frac{4\dot{Q}}{\rho_{Cu} J_c^2} R_s(R_s + 1) \qquad (3\text{-}26)$$

For example suppose J_c (4.2 K, 7.5 T) = 7.7×10^4 A cm^{-2}, ρ_{Cu} (4.2 K, 7.5 T) = 4.6×10^{-8} Ω cm as for the MFTF conductor [8, 33], and furthermore suppose $\dot{G} = \dot{Q} = 0.2$ W cm^{-2} and that a critical current of 5.8 kA is to be carried. Then from the above relationships, $R_s = 22$ and D = 14.8 mm. Since application of the principle of full critical-current cryostability results in such large Cu/SC ratios, hence conductor diameters, it is not used in its unmodified form in the design of high-amperage conductors.

As pointed out in Section 3.4, by operating the conductor at some current $I < I_c$ (i.e., $i < 1$), full cryostability (i.e., full, but not Stekly-type) is assured provided that:

$$i \lesssim 1/\sqrt{\alpha_{st}} \qquad (3\text{-}5)$$

which is a generalization of the Equation (3-4) result. Obviously α_{St} can now be larger than 1, and the Cu/SC ratio reduced.

The next step in performance increase is achieved by permitting only half of the conductor to go normal, and requiring it to relax by a combination of radial surface-cooling as before plus longitudinal *conduction* to the colder still-superconducting half. This is the Maddock-James-Norris [36] so-called "cold-end" principle which permits stable operation under the condition:

$$i_{CE} \lesssim (1/\sqrt{\alpha_{St}}) \left[\frac{-1 + \sqrt{1 + 8\alpha_{St}}}{2\sqrt{\alpha_{St}}} \right] . \qquad (3\text{-}27)$$

The essence of Equation (3-5) was of course the possibility that $\alpha_{St} > 1$; under this condition Equation (3-27) permits $i_{CE} > i$.

3.8 Summary -- General Requirements for Stable Conductor Design

3.8.1 Flux-Jump Stability

The adiabatic relationship, Equation (3-6), controls the flux-jump stability of the windings of a potted magnet. Under such conditions a large conductor heat capacity is beneficial ("enthalpy stabilization"). But in most practical situations the windings are exposed to liquid He to which the heat of the jump is supposed to be delivered as quickly as possible. Under dynamic stabilization the stable filament diameter, according to Equation (3-7) is proportional to $\sqrt{K_{SC}/\rho_{Cu}}$. Although K_{SC} is fixed it is clearly beneficial to reduce the resistivity of the matrix (in the design field of the magnet) as far as possible. Increasing the purity of the Cu, even in the presence of a magnetic field, always lowers its resistance [37]; and Al in a magnetic field can have a considerably lower resistance than Cu [37] itself. With regard to dynamic self-field stability, Equation (3-21) shows that the self-field-stable strand diameter (proportional to $\beta^{\frac{1}{2}}$ -- Equation (3-20)) increases with the product $h^{+}d$ which, according to Section 3.7.3, being by definition equal to $(h'R_o/K_{av})(D^{av}_{TH}/D^{av}_{EM})$ is in turn proportional to $(h'R_o/K_{av})K_{av}(1 - \lambda)/(C_{av}\rho_{Cu})$. Beneficial to conductor dynamic self-field stability is efficient dynamic heat transfer (coefficient, h') to the cryogen bath; on the other hand a large conductor heat capacity, which increases the thermal time-constant of the flux-jump, is detrimental in this case. An interesting exception to this is when the heat capacity is that of the He itself, which suggests that in some cases an open winding (referring now to a stranded conductor) may be preferable to one that is filled with solder.

3.8.2 Cryostability

Attention is drawn to the essence of full cryostability theory as embodied in Equations (3-4) and (3-5) and, therefore, expressible in the forms:

$$I^2 \lesssim \sigma_{Cu} A_{Cu} P h (T_c - T_b) \quad . \qquad (3\text{-}28)$$

Equation (3-28) demonstrates explicitly the need for a large volume of high-conductivity Cu and emphasizes the further benefits that can be derived from: (a) a large He-exposed surface area (P per unit length); (b) a large heat transfer coefficient, h, for cooling across that surface -- which we have just been reminded is also beneficial to the dynamic self-field stability.

In order to acquire higher performance than that available under full cryostability more and more reliance may be placed on longitudinal conduction to yield in succession cold-end stability and finally MPZ stability as defined in Figure (3-4).

SECTION 4

A.C. LOSS CONSIDERATIONS IN CONDUCTOR DESIGN

4.1 Introduction -- Components of A.C. Loss in a Composite Superconductor

4.1.1 Flux-Jump Stability and Hysteresis Loss

Experiments such as those depicted in Figure 4-1 serve to illustrate the close relationship that exists between the flux-jump stability of a multifilamentary conductor and its hysteretic lossiness in an applied a.c. field. Both are gauged by the amount of net flux which is able to be enclosed by any pair of filaments. As pointed out in Section 3.6 the flux-jump stability of a given composite is maximized if the filaments are decoupled by twisting; likewise the a.c. loss is minimized, becoming simply the sum of the hysteretic losses of the individual filaments.

But in most applications as well as being exposed to an external field, the conductor is subjected to the local "self-field" of the current passing through it. Losses associated with this are not able to be reduced by twisting since the self-field system rotates with the twist. However, as pointed out by WILSON [39], it is conceivable that in the presence of a strong external field the electric center lines of the individual filaments will be shifted in such a way as to assist the external field in partially cancelling the internal one linking the filaments, thereby tending to reduce the self-field effect [39]. Self-field loss may also be minimized by filament transposition which then becomes an important element in conductor design.

4.1.2 Cryostability and Eddy-Current Loss

In addition to hysteretic loss, the conductor is subject to Joulean heating associated with the normal-state eddy-currents which cross the matrix between the filaments. Thus, cryostability and low a.c. loss are conflicting requirements which call for a careful blending of design philosophies when stable low-loss conductors are required for the generation of pulsed or alternating fields. Section 3.4 has shown that a conductor designed primarily for a steady-state application will tend to use massive amounts of high-conductivity Cu in intimate contact with the superconducting component on one hand and the He bath on the other. But for a.c. applications it will soon become obvious that monolithic conductors must generally be abandoned in favor of some form of stranded conductor -- either a cable or a braid.

4.1.3 Hysteretic and Eddy-Current Losses -- General Description

To a first approximation the frequency dependence of a.c. loss may be divided into two regimes separated by a characteristic frequency f_{cl} related to the conditions for the interfilamentary coupling referred to above, and consequently the twist pitch. (a) With $f \ll f_{cl}$ all of the filaments are fully decoupled, the hysteretic power loss $\dot{Q}_h$ is minimal, is proportional to f, and may be treated separately from the matrix eddy-current loss, $\dot{Q}_e$, which has an f^2 frequency dependence. At "low" frequencies and modest alternating-field amplitudes H_m, the total a.c. loss is approximately:

$$\dot{Q} = \dot{Q}_h + \dot{Q}_e \qquad (4\text{-}1a)$$

$$= aH_m f + bH_m^2 f^2 \qquad (4\text{-}1b)$$

where a and b are constants.

Theoretical results are usually expressed in terms of power-loss per unit volume. Experimental results are also often reduced to that format, although results expressed in terms of loss per unit length of conductor [40] or per experimental coil [41] are also to be found. It is also common practice to refer to $\dot{Q}/f$, the power-loss per unit frequency. This leads to a convenient format for the representation of low-frequency experimental data in that a plot of $\dot{Q}_t/f$ *versus* f, being linear with intercept, a, enables the low-frequency hysteretic and eddy-current components to be easily separated [42]. Since $\dot{Q}\ f^{-1} \equiv Q\ \text{cycle}^{-1}$ the *unit-frequency power loss* is identical to the *energy loss per cycle*, the latter being a format which has often been used in hysteretic-loss calculations, particularly within the framework of critical-state models.

4.2 Frequency and Amplitude Dependences of A.C. Loss

The per-cycle eddy-current loss does not of course continue to increase in frequency at the rate prescribed by Equation (4-1). In fact it turns out that $\dot{Q}_e/f$ passes through a maximum at $f \sim f_{c1}$ [41]. The functional form of $\dot{Q}_e/f$, according to the early theory of MORGAN [43] (cf. also [40, 41] for further discussion), was of the relaxation-dispersion type, *viz.*:

$$\dot{Q}_e/f \propto \frac{\omega}{1 + \omega^2\tau^2} \qquad (4\text{-}2)$$

where $\omega \equiv 2\pi f$, and τ is a characteristic relaxation time. Equation (4-2) confirms the f^2 dependence of $\dot{Q}_e$ at low frequencies and predicts that at higher frequencies $\dot{Q}_e$ will tend to be proportional to f^0. At $f > f_{c1}$ the outer filaments of a composite become coupled by the eddy currents. The hysteretic and eddy-current losses then become physically interrelated, although mathematically it is still possible to assign to the total loss, hysteretic and eddy-current components [32, 44, 45].

Although to satisfy the needs of simple theory and many practical applications two frequency regimes are adequate to describe the dependence of a.c. loss on the frequency and amplitude of the applied field [40, 41, 43], the full theory subdivides the upper-frequency region into two more at a critical frequency f_{c2} according to the manner in which the high-frequency current is distributed within the composite, which in turn depends on the relative magnitudes of the skin depth and the radius of the conductor. The anisotropic-continuum model of CARR [30, 31] (see also CARR, WALKER, and MURPHY [32, 44, 45, 46] describes a.c. loss within the framework of three frequency regimes: (a) *low frequencies*, $f \ll f_{c1}$, where the losses are associated with independent fully-field-penetrated filaments and the normal-state matrix between them with its transversely crossing eddy-currents; (b) *intermediate frequencies*, $f_{c1} < f < f_{c2}$, where the above effects are confined to the "core" of the conductor which is then surrounded by a cylindrical shell, set up by the axis-parallel return paths of the eddy-currents, and which simulates the current-saturated shell that shields the interior of a partially penetrated ($H_a < H^*$) solid superconductor; (c) *very high frequencies*, $f \gg f_{c2}$, where the effects described under (a) above take place within the skin depth, while the current-saturation effect mentioned directly above is confined to the outermost portion of the skin. The frequency- and amplitude-dependences of both $\dot{Q}_h$ and $\dot{Q}_e$ have been calculated and measured by CARR *et al.* for all these regimes. For $f \ll f_{c1}$, $\dot{Q}_e$ turned out to be proportional to f^2 as before; but for $f > f_{c1}$ an f^0 dependence was observed, while at very high frequencies, $f \gg f_{c2}$, skin-effect theory dictates an $f^{\frac{1}{2}}$ frequency dependence.

A.c. losses are experienced by open-circuited conductors when exposed to alternating transverse or longitudinal applied magnetic fields; in addition, just as current-carrying conductors experience *self-field* instability, they may also suffer self-field-induced hysteretic loss, $\dot{Q}_{hs}$. In general it is necessary to deal with a.c. loss in *current-carrying* conductors under *various combinations* of field and current conditions. The most important causes of a.c. loss are usually the external-field hysteretic loss, $\dot{Q}_h$, in the individual filaments and the eddy-current loss, $\dot{Q}_e$, due to the circulating matrix currents. If the self-field of the

transport current is small compared to the field at the wire due to the other parts of the magnet, the self-field hysteretic loss, $\dot{Q}_{hs}$, is small compared to the external-field-induced hysteretic loss, $\dot{Q}_h$; their ratio, $\dot{Q}_{hs}/\dot{Q}_h$, is represented by α_s.

Although well founded in the work of WILSON *et al.* [13] of the Rutherford Laboratory, our present understanding of a.c. losses is due primarily to the work of CARR [30] and colleagues [32] (see also [44, 45, 47]) of the Westinghouse Research Laboratories to whom the development of the useful "anisotropic-continuum" model is due. In their summary of the essential results, MURPHY, WALKER, and CARR [32] have introduced for discussion nine equations (based on [30]) needed to completely describe the mixture of eddy-current and hysteretic losses which are encountered when the amplitude of the applied a.c. field is varied over several decades, and its frequency is varied over the three ranges referred to above. As a consequence of an interplay between numerous applied-field and conductor parameters, the principal among which are f, H_m, and L_p, the a.c.-loss regimes are distinguished by the extent to which flux is excluded from the intereior of the conductor.

4.3 Hysteretic and Eddy-Current Losses -- Some Basic Formulae

For reasons soon to be explained, of the nine equations referred to above the most generally useful are the three that describe the low-frequency hysteretic and eddy-current losses. These, together with some relationships between them, are presented below in c.g.s.-practical* units:

(a) the low-frequency hysteretic loss, $\dot{Q}_h$:

$$\frac{\dot{Q}_h}{V} \cong \left(\frac{8}{3\pi \times 10^8}\right) w\lambda J_c H_m f \qquad (4\text{-}3)$$

---

* In this case: amperes, oersteds, cm, watts.

(b) the low-frequency eddy-current (coupling) loss, $\dot{Q}_e$:

$$\frac{\dot{Q}_e}{V} \cong \left(\frac{1}{2 \times 10^{16}}\right)\left(\frac{L_p^2}{\rho_\perp}\right) H_m^2 f^2 \qquad (4\text{-}4)$$

(c) the ratio of the eddy-current to hysteretic loss, α_m (cf. Equation (3-13)) which from the above two equations, using $H_a = H_m \sin\omega t.$, is:

$$\alpha_m \cong \left(\frac{3}{2 \times 10^{8}}\right) \frac{1}{w\lambda J_c} \left(\frac{\ell_p^2}{\rho_\perp}\right) \dot{H}_a \qquad (4\text{-}5)$$

(d) the self-field hysteretic loss, $\dot{Q}_{hs}$:

$$\frac{\dot{Q}_{hs}}{V} = \eta_{sf}(5/10^{10})\pi f(\lambda J_c D)^2 \qquad (4\text{-}6)$$

where η_{sf} is an efficiency factor which combines a factor intended to take into account the crowding of current into the outer layers of the composite [39] with a function of i, the reduced current. A reasonable value for η_{st} is about 0.05.

(e) the ratio of self-field to external-field hysteretic losses, α_s:

$$\alpha_s \cong (0.185/H_m)\eta_{sf}\lambda J_c(D^2/w) \qquad (4\text{-}7)$$

(f) the critical frequency, f_{c1}, which upper bounds the "low-frequency" a.c.-loss regime:

$$f_{c1} = 10^9 \rho_\perp / L_p^2 \qquad (4\text{-}8)$$

The frequency f_{c1} is defined as that which maximizes the eddy-current loss (cf. Equation (4-2)), hence α_m. Obviously the conductor should be designed such that its operating frequency or sweep rate is remote from f_{c1}; and since frequencies *up to* the maximum operating frequency, $f_{op,\,max}$, should be allowed for, in order to avoid an intermediate resonance, the design frequency should be well below f_{c1}. This leads to two related conclusions: (a) conductor designs which include a magnetization-enhancement coefficient, α_m, of $0.1 \sim 0.5$ [39] already imply an $f_{op} << f_{c1}$; (b) the low-frequency hysteretic and eddy-current loss equations listed above are the ones which are generally of greatest interest to the designer of conductor for pulsed magnets.

4.4 Design Requirements for Low A.C. Losses

The design requirements for low a.c. losses, with due regard to the conditions just mentioned, are embodied in items (a) through (f) of Section 4.3 and particularly Equation (4-3) for $\dot{Q}_h$, Equation (4-6) for $\dot{Q}_{hs}$, and Equation (4-8) for f_{c1}. The basic philosophy consists in making $\dot{Q}_h$, which is proportional to $w\lambda J_c$ (a product of the *design-parameters*†), and $\dot{Q}_{hs} \propto (D\lambda J_c)^2$ as small as possible, and $f_{c1} \propto \rho_\perp / L_p^2$ (which consists of the design-parameters of $\dot{Q}_e$) as large as possible. These goals are achieved by attending to filament diameter, w, conductor diameter, D, twist pitch, L_p, and matrix transverse resistivity, $\rho_\perp$.

---

† H_m and f would then be regarded as *operational parameters*.

4.5 Filament Diameter, w

According to Equation (4-3) the filament diameter should be made as small as possible. In practice the filament diameter of the basic superconducting strands of even very large (e.g., 80 kA), non-steady-state-magnet cables tend to lie within the range 6-8 μm [48]. The only electrical argument against reducing the filament diameter even more than this has to do with the surface supercurrent. Since it has been shown that a surface sheath is responsible for a hysteretic loss equivalent to a 2-μm diameter filament [13], there is no incentive from a hysteretic-loss standpoint for the fabrication of ultrafine filaments. Small filaments are, moreover, difficult to produce without breakage -- for the detection of which no nondestructive test is available. On the other hand, small filaments are compatible with the attainment of high J_c's in alloy superconductors or during bronze-process heat treatment are able to be fully converted into the A15 compound; furthermore, according to Equations (3-6), (3-7), and (3-8) they are conducive to flux-jump stability.

4.6 Conductor (Strand) Diameter, D

4.6.1 Eddy-Current Loss

The eddy-current-controlled maximum number of filaments, N_{max}, which is proportional to $\rho_\perp$, is given by Equation (3-16). Maximum filament diameter then follows an application of $D_{max}^2 = N_{max} w^2/\lambda$.

4.6.2 Self-Field Loss

Equation (4-6) demonstrates that since the self-field hysteretic loss is proportional to D^2 the strand diameter should also be made as small as possible. Since this is in direct conflict with current-carrying capacity, which is also proportional to D^2, a compromise must be sought.

The approach usually taken is to ask that the $\dot{Q}_{hs}$ be some acceptable fraction of $\dot{Q}_h$ [13, 39]; $\alpha_s = 0.5$ has been suggested, although some large cabled conductors have been produced in which α_s is as small as 0.07 [49]. In designing for a selected α_s, Equation (4-7) may be used to provide a maximum conductor (strand) diameter or, for given λ, a maximum number of filaments using that equation rearranged in the following way:

$$N_{max} = (H_m \alpha_s)/(0.2\ \eta_{sf} J_c w) \quad . \tag{4-9}$$

The corresponding maximum strand diameter would be given by:

$$D^2_{max} = \frac{H_m w \alpha_s}{0.2\ \eta_{sf} \lambda J_c} \tag{4-10}$$

As a general example, suppose the field amplitude to be 45 kOe, the average critical current density to be 2.2×10^5 A cm^2 and w = 8 μm. Then assuming $\alpha_s = 0.1$ and $\eta_{sf} = 0.05$, it follows that $N_{max} \cong 2560$; and with $\lambda = 0.25$, the maximum strand diameter would be 0.81 mm and the critical-current-carrying capacity 280 A. If a 5-kA conductor operating at i = 0.75, and conforming to these hysteretic-loss guidelines, were needed it would be necessary to place 24 of these strands in parallel. In order to prevent an effective increase in D following this procedure the strands would need to be transposed in some way. Since transposition includes twist, additional eddy-current loss (coupling) would automatically be suppressed by this procedure.

4.7 Twist Pitch

According to Equations (4-4) and (4-8) the twist pitch, L_p, should be as short as possible. This requirement is compatible with flux-jump stability. The lower limit to L_p is dictated by: (a) the risk of filament fracture during fabrication; (b) the amount of additional filament elongation, with its attendant diameter reduction, which can be tolerated.

For ease of manufacture L_p should be as long as possible -- but how long? As with the self-field situation, the approach taken is to require $\dot{Q}_e$ to be some acceptable fraction of $\dot{Q}_h$. One such comparison led to the idea of a critical twist quarter-wavelength, ℓ_c, in the form, for example, of Equation (3-11). Equations (3-12b) and (3-13) then show that, provided ℓ_p ($\equiv L_p/4$) is less than 0.2 ℓ_c, then α_m ($\equiv \dot{Q}_e/\dot{Q}_h$) is less than $8/(3\lambda^{\frac{1}{2}})(0.2)^2$, (i.e., less than 0.21 if $\lambda = 0.25$). With reference to Figure 3-3 this then places the relative eddy-current loss well below the maximum in the α_m *versus* coupling parameter curve and securely in the "low-frequency" a.c.-loss regime. According to the above prescription, eddy-current loss is "acceptable" provided the twist pitch L_p is less than ℓ_c, the critical or characteristic length given by Equation (3-11). But if the field ramp-rate has already forced ℓ_c to be small, since L_p may not be less than 5 D the simultaneous requirement that $L_p < \ell_c$ may be difficult to meet. For example, if with the above conductor $\dot{H}_a = 10$ kOe s^{-1}, it follows that $\ell_c = 2.85$ mm, hence that $L_p (= \ell_c$, say) $= 3.5\ D_{max}$.

An equation to assist in the design of the basic strand, (relative twist pitch $L_p/D_{max} \geq n$) which connects the field amplitude, H_m, and ramp-rate, $\dot{H}_a$, with the relative self-field and eddy-current losses α_s and α_m, respectively, can be developed with the aid of Equation (4-10) for D_{max}, Equations (3-12) and (3013) for a relationship between (ℓ_p/ℓ_c) and α_m, and Equations (3-11) for ℓ_c itself. The result is:

$$\dot{H}_a H_m \leq 1.2 \times 10^7\ \rho_\perp \lambda^2 J_c^2 (1/n^2)(\alpha_m/\alpha_s) \qquad (4\text{-}11)$$

which after inserting typical values such as: $\rho_\perp = 4.6 \times 10^8$ Ωcm, $\lambda = 0.25$, and $J_c = 2.2 \times 10^5$ A cm^{-2}, reduces to:

$$\dot{H}_a H_m \leq 1.67 \times 10^9 (1/n^2)(\alpha_m/\alpha_s) \qquad (4\text{-}12)$$

In these equations note that (α_m/α_s) is the same as $(\dot{Q}_e/\dot{Q}_{hs})$.

As an example, consider the basic strand of a conductor intended for the cable of a tokamak ohmic heating coil for which $H_m = 4.5$ T and $\dot{H}_a \cong 10$ T s^{-1} [48]. This, if, as suggested in Section 4.6, an $\alpha_s = 0.1$

has been selected (leading to a 2560-fil., 212 A (i = 0.75), strand) and that a twist L_p = 8 D has been chosen, then Equation (4-12) yields α_m = 1.7, a factor of 10 larger than the value usually selected when free choice is available. The result shows that under such extreme operating conditions, if the basic strand has the resistivity of high-purity Cu, eddy-current losses within it equal to 1.7 times hysteretic must be anticipated. Under the circumstances, the only means of lowering the eddy-current loss would be to increase the matrix transverse resistivity.

4.8 Matrix Resistivity

4.8.1 Factors which Influence the Choice of Matrix Resistivity

According to Equations (4-4) or (4-8) it is beneficial from the standpoint of eddy-current loss to make $\rho_\perp$ as large as possible. But since there are some compromises to be made, it is important to be able to estimate just how much additional resistivity is adequate. This can be achieved with the aid of Equation (4-11).

Although high matrix transverse resistivity is necessary for eddy-current loss reduction, it may be disadvantageous from the standpoints of: (a) electrical stability; (b) cost and fabricability. In particular:

(i) According to Equation (3-7) an increase in $\rho_\perp$ is detrimental to dynamic flux-jump stability, and calls for a reduction in the maximum stable filament diameter. It turns out, fortunately, that the presence of Cu-10Ni (as an eddy-current barrier for the purpose of increasing $\rho_\perp$) leaves the average volume specific heat of the matrix practically unchanged. With regard to the cryostability, an increase in the matrix resistivity in the longitudinal direction results in an increase in $\dot{G}$ the heat generation which must be compensated for by: (a) an increase in the Cu/SC ration, R_s, (Equation (3-25)); or (b) a reduction in conductor diameter, D, at fixed R_s (Equation (3-26)). But through the use of a web of suitability located resistive eddy-current barriers (as in Figure 4-2) rather than a

general increase in the matrix resistivity, $\rho_\perp$ can be increased without seriously affecting the longitudinal component. This is particularly true for a cable made up of tin-alloy-plated† strands or filled cable.

(ii) With the introduction of eddy-current barriers, additional fabrication costs associated with the preparation of a more complicated billet must be taken into consideration. The material commonly used for the barriers is Cu-Ni (10 at. or wt.%) [50, 51] although some basic substrands conforming to the prescription SC/Cu/Cu-30Ni/Cu-10Ni, in which the Cu-30Ni is in the form of a barrier web, have been prepared [51]. The extra pressures normally needed to extrude cupronickel-containing billets may necessitate the use of smaller-diameter billets (hence lead to a shorter length of wire product) or may be reduced by the design of specially shaped extrusion dies.

4.8.2 Estimation of the Required Matrix Resistivities

Because of these disadvantages and difficulties no more cupronickel should be introduced then is necessary to achieve the desired twist pitch for a particular set of operating conditions. Equation (4-11), after the insertion of $\lambda = 0.25$, $J_c = 2.2 \times 10^5$ A cm^{-2}, hence in the form

$$\rho_\perp \geqslant \frac{n^2(\dot{H}_a H_m)}{3.63 \times 10^{16}(\alpha_m/\alpha_s)} \ (\Omega \text{ cm}) \qquad (4\text{-}13)$$

provides a useful guide to the selection of matrix resistivity. For example, suppose as before it is required to design a basic strand for the cabled conductor of a tokamak ohmic heating coil for which $\dot{H}_a = 10$ kOe s^{-1}, $H_m = 45$ kOe; that the L_p/D-ratio, n, is to be 10 and that $\alpha_m = \alpha_s$ (=say, 0.1 in order to satisfy a D_{max} requirement (Equation (4-10)). It then follows that $\rho_\perp \geqslant 1.24 \times 10^{-6}$ Ωcm, which is a factor of twenty-seven larger than the above-accepted resistivity of Cu (4.6×10^{-8} Ωcm at 4.2 K, 7.5 T) and factors of ten and thirty less than the residual resistivities of Cu-10Ni,

---

† An alloy commonly used is Sn-(4-5wt.%)Ag, known as "stabrite".

and Cu-30Ni, respectively. It is apparent that by deploying suitable mixtures of Cu and Cu-10Ni [50, 52] or Cu-30Ni [53] elements the desired resistivity can be achieved.

4.8.3 Location of the Eddy-Current Barriers -- Monoliths, Cables, and Braids

In order to isolate the filaments against coupling current -- the type of eddy-current that crosses the matrix transversely and completes its circuit by flowing through the filaments -- resistive barriers should surround the individual filaments. But in the interests of stability it is desirable for the barrier to be separated from its filament by a layer of Cu [54, p. 26]. Mixed-matrix conductors for pulsed magnets can be of either the monolithic or stranded (cable or braid) types. A solder-filled cable is a kind of "fabricated monolith". Examples can be cited in which the basic strand of the cable is itself a three-component composite similar in detail to the "first-stage-bundle" of the doubly-extruded monolith.

SECTION 5

FABRICATION OF COMPOSITE CONDUCTORS -- GENERAL CONSIDERATIONS

In superconductor fabrication, as in any other wire-production process, a massive billet of metal is converted into a long, continuous length of wire. Consequently a universal process could be described with the aid of a suitable flow diagram to trace the fabrication steps from billet assemply through extrusion and wire drawing to the final heat treatment and finishing stages. The processing of multifilamentary Ti-Nb-base, A15 compound, and *in-situ* composites can all be treated as variants of this universal process which for simplicity will first be discussed, with the aid of Figure 5-1, primarily in terms of the Ti-Nb-composite option.

The initial steps in conventional Ti-Nb-composite conductor fabrication are always the same independent of whether the finished product is to be a monolithic conductor, a cable, or a braid. Frequently, but not invariably (e.g., the conductor for the Mirror Fusion Test Facility (MFTF) [33]), the monolith is a double extrusion in which the product of the first extrusion is rebundled in preparation for a second. Otherwise the singly-extruded product passes down through the sequence of process steps delineated in the figure, to be used either as a single-strand wire or in one or other of the various possible multiply-stranded forms. It must be mentioned, however, that triply-extruded monoliths are not unknown [6, p. 47], and that doubly-extruded basic strands are in existence [6, p. 69].

The coextrusion process presently in use for the conventional fabrication of both alloy and A15 compound superconductors stems from a method invented in 1957 by LEVI (and described by him in U.S. patents granted in 1962 and 1966 [55, 56])intended for the preparation of highly elongated, fine ferromagnetic fibers with large coercive forces. Levi described the the bundling and drawing of 5% Sn-bronze-clad Fe wires, four stages of which resulted in a bundle of 0.1 μm^{ϕ} fibers. In a demonstration of the

applicability of the same method to Nb in Cu, CLINE *et al.* (1966)[57] described the fabrication by four stages of wire drawing of wire containing some 10^7 Nb filaments about 100 Å in diameter. GARWIN *et al.* [58] have suggested that by extending such operations to five or even more rebundlings enormous numbers of filaments with diameters as small as a few angstroms can be produced. Two effects were predicted: (a) in general the formation of a synthetic alloy with certain properties which are superior to those of the individual metals, and in particular; (b) a new superconductor whose properties are governed by the proximity effect. A scaled-up version of these composite wire drawing-methods, with extrusion as the first stage of reduction, is the one commonly in use today.

5.1 Billet Design -- Eddy-Current and Diffusion Barriers

With d.c. applications in mind a simple, two-component (superconductor plus stabilizer) composite is adequate; billet design is quite straightforward and governed primarily by metalworking rather than electrical considerations. On the other hand, for a.c. or pulsed-field applications the extensive network of eddy-current barriers which are needed for the control of transverse matrix resistivity calls for somewhat more complicated billet design and fabrication procedures. Probably the most complex double-extruded mixed-matrix monolithic Ti-Nb-base composite ever produced is the I.M.I. conductor described first by POPLEY *et al.* [19] and referred to subsequently by others [5, p. 57][59]. Today the tendency is to *fabricate* the high-current a.c. conductor starting with a singly-extruded-and-drawn basic mixed-matrix strand of the type illustrated in Figure 5-2.

The barrier material most commonly used to suppress transverse eddy-currents in Ti-Nb-base mixed matrix composites is Cu-10Ni. Cu-30Ni, with its three-times-higher residual resistivity has been used in the past, but has since been abandoned on account of its poor workability. It is generally agreed that, in the interests of *stability*, the Cu-Ni should not be placed in direct contact with the Ti-Nb [39][54, p. 26] although this

would be the most effective from an eddy (coupling)-current-loss standpoint. In the billet-stack, therefore, the Ti-Nb rod is first surrounded by a hexagonal-sided Cu jacket which in turn is, or has been, clad in Cu-Ni by some ancillary metalworking process. The results of so doing are illustrated in Figure 5-3. The average transverse resistivity of a matrix containing discrete eddy-current barriers can be adjusted by regularly intermingling jacketed and unjacketed Cu/SC elements.

With bronze-processed A15 conductors the problem is usually not to increase the transverse matrix resistivity but to reduce it. Solute-diffusion barriers, usually of Ta, replace the Cu-Ni eddy-current ones and permit the establishment within the matrix of strategically located regions of pure Cu. Obviously, in this case the higher resistivity component *is* in direct contact with the superconductor.

5.2 Billet Assembly

5.2.1 Ti-Nb Technology

Common commercial practice consists of inserting the cylindrical Ti-Nb alloy rods into hollow hexagonal-O.D. Cu tubes, assembling them into a close-packed bundle and, along with some extra filler pieces, slipping them into a cylindrical Cu shell -- the billet "can". In a research study conducted at MCA, and reported by COLLING *et al.* [61] Ti-Nb rods of diameters of 0.093", 0.126", 0.180", 0.278", and 0.368" installed in hexagonal-O.D. Cu tubes were the starting elements. In a production process for the Fermilab conductor, as reported by de WINTER *et al.* [62, p. 168], Ti-Nb rods of diameter 0.126" were inserted into prefabricated tubes of PDOF Cu with a 0.132"-round I.D. and a 0.177"-hexagonal O.D. In preliminary studies for the Fermilab program 0.084"-diameter Ti-Nb alloy rod (wire) was inserted into 10-ft. lengths of round Cu tube, 0.170" O.D., and 0.115" O.D. The Cu tube was "sunk" onto the Ti-Nb rod, and at the same time given a 0.120" flat-to-flat hexagonal cross-section by drawing through a hexagonal die mounted in a draw bench [63].

As an alternative to the *element-fabrication* approach just described, the deep-hole boring method of billet assembly has been considered. According to HILLMANN *et al.* [54, p. 23], who have explored the alternatives in detail, while the method has the following *advantages:*

(a) the Cu/Ti-Nb element fabrication step in avoided;
(b) filler-pieces do not need to be prepared;
(c) the network of Cu-Cu interfaces is no longer present, and the billet has a greater mechanical stability;
(d) a very high packing density is achieved.

The following *disadvantages* exist:

(a) accurate deep-hole boring in a metal as soft as OFHC Cu is difficult; rather large wall thicknesses must be left, which is satisfactory only if a high Cu/SC ratio is acceptable;
(b) the bore-hole depth-to-diameter ratio is necessarily restricted.

5.2.2 Conventional A15 Compound Technology

If the external-diffusion process is selected, the above prescription is followed but with Nb (or V) replacing the Ti-Nb component, while if the internal-bronze route is to be followed the Cu is replaced by a Cu-Sn (or Ga) bronze.

5.2.3 Unconventional A15 Compound Technology

Unconventional A15 conductors are the subject of Section 9. Among the various approaches outlined therein the most important are: the *in-situ* process, the "hot" and "cold" powder-metallurgical processes, and the "modified jellyroll" process. *In-situ* composites can be continuously cast in rod-like form [64] and as such need only be reduced to wire by swaging and/or rod and wire drawing. Alternatively, large cast ingots

may be canned in Cu and hot extruded [65] as the first step in wire fabrication. If the powder-metallurgy route is taken, the appropriate mixture of starting powders are compacted into cans prior to hot or cold extrusion as defined in Section 9. Only with the modified jellyroll process does anything approaching conventional billet assembly take place. As described by SHEN and McDONALD [66] and illustrated in Figure 5-4, a sheet of expanded Nb foil is rolled up along with other sheets of metals such as Cu, Ta, bronze, etc., about a mandrel of some suitable metal, sealed into a Cu container, and processed like conventional wire.

5.2.4 Eddy-Current and Diffusion Barriers

In Ti-Nb technology eddy-current barriers are needed only if it is necessary to guard against the effects of rapidly changing magnetic fields. The various ways in which Cu-10Ni can be incorporated into the basic strand are illustrated in Figure 5-5. One such barrier system has already been depicted in Figure 5-3. An interesting alternative method of installing eddy-current barriers was developed during the Fermilab wire production investigation [63, 67]. Pure Ni was electroplated to a thickness of $8 \sim 20$ μm onto the surface to be guarded -- either the Ti-Nb rods' hexagonal Cu jackets or the interior surface of the Cu extrusion can. During billet preheat (typically 30 min/650° C) some of the Ni diffused, as intended, into the underlying Cu to form a thin ($\sim$ 5 μm) Cu-Ni alloy interface layer.

In bronze technology, diffusion barriers are always needed in order to preserve regions of pure Cu for stabilization even in d.c. applications. They are usually introduced (in one of several ways, cf. Section 8) during the assembly of the second-stage billet.

5.2.5 Cleanliness During Assembly

Superconductor production is not a conventional metalworking process in that the billet elements, although large to begin with, are eventually reduced to some tens of μm in diameter. All necessary steps must, therefore, be taken to ensure that no foreign particles are trapped

in the billet during assembly. Typically the Ti-Nb rods, Cu tubes, and filler elements, are cleaned by acid dip, rinsed twice with water, twice with acetone, and blown dry in N_2 gas [62, p. 168]. Other solvents besides acetone may be used [67]. Cleaned materials are plastic bagged and stored under N_2 prior to assembly [33][62, p. 168]. Components and billets are assembled in a clean room using standard clean-room procedures [61][62, p. 168].

5.3 Billet Extrusion

(a) Types of Press. The three common types of extrusion press are illustrated schematically in Figure 5-6. In conventional extrusion the billet, which is machined to fit the bore of the container or its liner, and may be lubricated, is pushed through the die by the direct action of the stem. In this technique there are large frictional forces between the billet and the liner which both enhance the required stem force and add shearing components to the deformation force experienced by the outer elements of the billet. The pressure-displacement curve will generally exhibit a spike prior to the transition from sticking to sliding friction the height of which, although it may be reduced by lubrication (e.g., with graphite or MoS_2), generally amounts to ¼ to ½ of the applied force. Typical die-angles and billet-nose angles† are 2α = 90-100° [54, p. 31] [67, p. 33].

In indirect extrusion, Figure 5-6(b), the body of the billet remains motionless with respect to the container while the nose end is extruded through a die attached to the moving stem. With such an arrangement the absence of billet-container friction leads, in principle, to more uniform

† This so-called "included angle", 2α, is twice the semivertical angle (here α) of the cone.

deformation. In practice, however, in extrusion-tests of composite billets there turned out to be no significant difference between the results of applying the two processes [54, p. 28]. In indirect extrusion the extrusion ratio is lower-limited to about 7 by the compressive and buckling strengths of the hollow stem. This is no disadvantage in the present application since extrusion ratios of between $\sim$ 9 [68] and $\sim$ 12 [63] are commonly employed.

The principle of hydrostatic extrusion is illustrated in Figure 5-6(c). Since the hydraulic fluid -- a high-temperature liquid lubricant such as castor oil -- completely surrounds the billet not only is friction against the container eliminated, but the body of the billet is uniformly pressurized. The elimination of wall friction and billet "upset" (i.e., barrel-shape distortion) contribute to the uniformity of the reduction process. In hydrostatic extrusion it is not unusual to use specially contoured dies ("streamlined" dies of various kinds [69, p. 27] to still further improve the uniformity of the product. If conical dies are used the die angle is usually $2\alpha = 45°$; while the nose of the billet is tapered slightly more sharply than the die angle to enable it to seal the die entrance against fluid leakage during preparation for extrusion.

(b) Stem Force and Extrusion Pressure. The force needed to achieve an extrusion ration $R_e = A_o/A_e$, where A_o and A_e are, respectively, the billet and extruded rod cross-sectional areas are given by:

$$F_e(t) = K_w(t)A_o \ell n R_e + b \qquad (5\text{-}1)$$

where b is a constant, negligible in hot extrusion, and K_w is the deformation resistance of the billet -- a property of the billet composition and a function of temperature (hence time,t) during the extrusion. The extrusion pressure, $P_e = K_w \ell n R_e$ according to Equation (5-1), can be controlled by adjusting the extrusion ration, R_e, which according to HILLMANN [54, p. 30], should not be smaller than 7 if full densification of the billet in the extrusion press is required.

K_w is naturally related to the flow-stress, σ_f, of the billet material; typically $K_w \sim 4\sigma_f$ in lubricated conventional extrusion and $\sim 3\sigma_f$ in hydrostatic extrusion. σ_f for a composite billet is calculable from the short-time hot flow stresses of the constituents with the aid of the mixture rule [54, p. 31].

(c) Stem Speed. In conventional extrusion the stem speed must be chosen so that the energy produced by friction and deformation can be transferred to the liner [54, p. 34]; accordingly, HILLMANN *et al.* have, for Cu/Ti-Nb billets, recommended a stem speed within the range of 3-6 mm s^{-1}. In confirmation of this CURTIS and McDONALD [67] report that stem speeds of 2.1 and 4.2 mm s^{-1} were used in extruding an 8-inch diameter composite billet (at 600° C, R_e = 12.6) during manufacturing technology studies in support of the Fermilab Cu/Ti-Nb-conductor development program, and COLLING *et al.* [61] reported the use of stem speeds of less than 6.5 mm s^{-1} in the extrusion of 8-inch and 10-inch diameter billets of Cu/Ti-Nb to 2.5-inch diameter rod (R_e = 10¼ and 16) in support of a Los Alamos Scientific Laboratory wire production program.

On the other hand using hydrostatic extrusion FIORENTINO *et al.* [51, p. 32] were able to extrude 2.3-inch diameter Cu/Ti-Nb research billets (at 500° C, R_e = 53 to 167) at stem speeds of 34 mm s^{-1}.

(d) Billet Temperature. The extrusion temperature is an important parameter from the standpoints of both process technology and metallurgy. Since the flow stresses of metals generally decrease rapidly with increasing temperature press capacity would not be a limitation to the extrusion of large billets if the billet temperature could be freely chosen. However, such is not the case. If the billet temperature is too high, excessive interdiffusion and reaction between the elements will take place. In the case of Cu/Ti-Nb this can result in the formation of undeformable $Cu(Ti, Nb)_2$ nodules at the Cu/SC interface. Similarly with bronze/Nb billets premature formation of the brittle A15 compound may take place. Some Cu/Ti-Nb billet preheat temperatures and conditions which have been reported in the literature are: (1) (3/4)h/530-550° C plus (1/4)h/600-610° C [54, p. 33]; (2) 50 min/660° C or 40-46 min/600° C [67, p. 33]; (3) 650° C

(experimental) [70]; (4) 510-590° C [61]. For bronze/Nb billets preheat temperatures of 650 ± 10° C [62, p. 31] and 700-750° C [7, p. 345] have been reported.

5.4 Rod and Wire Drawing

The metalworking operations considered in this section have been depicted in Part (a) of Figure 5-1. Monolithic conductors or strands are produced by consecutive applications of: extrusion in a conventional or hydrostatic press, rod drawing, and wire drawing.

5.4.1 Rod Drawing

The extruded rod is drawn linearly through a single die installed on a draw bench during which a reduction of about 15% takes place. The dies are replaced and the process repeated until the rods attain the desired diameter or length. In the manufacture of the MFTF monolith [33] the extruded stock was drawn down from a rod of diameter about 90-100 mm to one of 20 mm with a length of about 50 m [33] using a 70-tonne, 122-m draw bench. In other facilities and for other applications rod drawing from 57 mm to 8.5 mm might be appropriate [63].

5.4.2 Wire Drawing and Finishing Stages

The drawn rod is transferred to a single-die bullblock, or a series of them, for reduction typically from 20 $mm^{\emptyset}$ [33], 8.5 $mm^{\emptyset}$ [63], or whatever the output of the draw bench is, down to a size, say $\sim$ 5 $mm^{\emptyset}$, suitable for coiling prior to transfer to the equipment used in the final phases of the process. The wire is next taken to a "multidie machine" and pulled through a series of dies of successively diminishing bores; a typical machine will be fitted with twenty of them, enabling a wire to be drawn down from, say,

5 $mm^{\emptyset}$ to 0.5 $mm^{\emptyset}$ at a mean reduction rate of 11% per die. The strand is next given a predetermined amount of twist after which, if the final product is to be rectangular in cross section the twisted wire goes on to pass through a double pair of orthogonally mounted rolls, commonly referred to as a "Turk's head."

5.4.3 Summary of Thermomechanical Processing

The point at which the product is transferred from one processing step to the next depends largely on the capacities of the available machines. For example entry into the 122-m draw bench used for processing the MFTF conductor took place at rod diameters of 90-100 mm; transfer to the usual bull block took place at 20 ∿ 25 $mm^{\emptyset}$ [33][62, p. 168], while multidie machines reduced the wire product from about 5 $mm^{\emptyset}$ down to a typical strand size of 0.55 $mm^{\emptyset}$. Similarly in the Fermilab conductor development program as described by CURTIS and McDONALD [67], conventional extrusion reduced a 20 $cm^{\emptyset}$ billet to a 13 $cm^{\emptyset}$ rod; rod drawing then reduced the diameter to 8.5 mm whereupon wire drawing, interspersed with heat treatment administered according to Table 5-1, took over to yield a strand either 0.62 mm or 0.95 mm in diameter.

The above processing sequences for composite alloy conductors can be rewritten to describe A15-conductor processing simply by changing the heat-treatment schedules and relocating them within the fabrication scheme. In particular if the internal-bronze process is selected it is necessary to administer heat treatments of ∿ 30 min/(490-500)° C at frequent intervals during the wire drawing to relieve the work hardening. As the wire drawing continues the interval between consecutive annealings can be raised from 30 ∿ 40% (area ratio) to upwards of 90% as the strand approaches its final diameter [62, p. 32]. After final reduction and twisting a reaction heat treatment at about 750° C (cf. Section 8, Figure 8-4) is administered. The strand is then passed on to Part (b) of Figure 5-1.

TABLE 5-1. WIRE DRAWING AND HEAT TREATMENT SCHEDULE FOR THE PROCESSING OF A MULTIFILAMENTARY Cu/Ti-Nb COMPOSITE CONDUCTOR. The schedule selected (one of four) was that which yielded the highest 50-kOe, 4.2-K, critical current density, *viz.* 1.70×10^5 A cm^{-2} -- after CURTIS and McDONALD [67, pp. 6, 7].

Superconductor Alloy:	Ti-b3.5Nb ("Nb46.5Ti")
Number of Filaments:	2860
Cu/SC Ratio:	$\sim$ 2:1

(1) Draw 0.335 in.$^{\phi}$ - 0.250 in.$^{\phi}$; 18 ± 2% R.A. per pass

(2) H.T. (65 ± 5) h/(400 ± 20)° C at 0.250 in.$^{\phi}$ (98.765%)

(3) Draw 0.250 in.$^{\phi}$ - 0.064 in.$^{\phi}$; 18 ± 2% R.A. per pass

(4) H.T. (0.5 ± 0.25) h/(300 ± 20)° C

(5) Draw 0.064 in.$^{\phi}$ - 0.040 in.$^{\phi}$; 18 ± 2% R.A. per pass

(6) H.T. (0.5 ± 0.25) h/(300 ± 20)° C

(7) Twist, 2.4 turns per inch

(8) Draw to 0.0375 in.$^{\phi}$

(9) H.T. (5 ± 1) h/(280 ± 20)° C at 0.0375 in.$^{\phi}$ (99.972%)

5.5 Stranded Conductors

5.5.1 Properties

High-amperage conductors can be processed in monolithic form by multiple iteration of the extrusion and rod-drawing processes. They can also be formed by the cabling or braiding together of numerous so-called "basic strands" -- the operation indicated in Part (b) of Figure 5-1. There are several advantages to this route: (1) First of all, regarding the basic strand as a module, there are the attributes of design flexibility and versatility usually associated with modular approaches; (ii) the strands can be mutually insulated in order to reduce eddy-current loss without recourse to a complex network of built-in eddy-current barriers; (iii) an opportunity exists, by braiding, to impose full transposition which increases self-field stability and at the same time (*via* its twist rather than transposition properties) increases external-field stability and reduces a.c. loss.

Then just as a high-amperage monolith can be prepared by multiple extrusion, a high-amperage cable can be built up from a single basic strand by several stages of cabling. Three examples of this are given in Figure 5-7. A Ti-Nb-alloy conductor prepared in this way will tend to have a higher current-carrying capacity than a monolith containing the same volume of superconductor, since the latter is not able to be given the optimal amount of cold work. On the other hand the monolith will tend to have a higher degree of mechanical stability than the cable. However, as will be indicated below, there are several ways of overcoming this drawback.

5.5.2 Fabrication of Cables

The essential elements of the stranding process which produces what is known in the ferrous-products industry as "rope" and in the electrical industry as "cable", can be understood with the help of Figure 5-8. Shown in Part (a) of the figure is a twelve-bobbin planetary strander. As

depicted it is arranged for no back-twist†, the spool axes retaining their original direction in space as the cage rotates. The wire tension, which in controlled by a brake, is supplied by a drawing unit (not shown in the figure) which may be either a capstan, or a "caterpillar" if straight-through pulling is preferred. Represented in Figure 5-8(b) is a detail of the cabling point, numerous proprietary variants of which have been developed. In the figure a flat core-less cable is being formed about a chisel-shaped mandrel, and directly after forming being compressed by a pair of rolls. A Turk's head arrangement may be used here to size the cable in width as well as in thickness. It is also possible, according to HILLMAN [54, p. 148] to dispense with the mandrel and the associated round nipple and to form the cable about a flat stainless-steel strip fed continuously through the hollow main shaft of the cabling machine.

Unless special precautions are taken the flattened coreless cable exiting from the machine will possess a residual twist. A trace of this was noticeable in Figure 2-1(b) (the edge-view). This may be corrected by over-twisting the cable between two sets of rolls, or by adjusting the backrotation of the spools, if provision for this has been made in the cabling machine.

5.5.3 Transposition in Flattened Twisted Monoliths and Cables

The need for twist and transposition has been discussed in Sections 3.6, 4.6, and 4.7. Monolithic conductors can only be twisted. Since in transposition, each strand occupies (as a function of distance along the conductor) every position in the bundle, full transposition in two dimensions can only be achieved by braiding. But with the aid of the diagram such as Figure 5-9, it is easily seen that the projection on a plane surface of a twisted cylindrical arrangement of strands is one-dimensionally transposed. The principle of flattening is frequently applied to a twisted monolith in order to achieve a semblance of transposition; while the

---

† In Europe the situation depicted in the figure is referred to as 100% or 360° backrotation [54, p. 120].

flat cable (i.e., the so-called Rutherford cable) as produced by the process just described is fully transposed within its plane. The flattened cable is called a Roebel transposition [72].

5.5.4 "Monolithic" Cables

A cable is able to combine dynamic stability with low a.c. loss. Another one of its advantages is mechanical flexibility; but if the relative strand movement to which flexibility is due takes place inopportunely, such as during the charging of the magnet, the resulting frictional heating can lead to a quench. To prevent strand movement it is often, but not always, customary (the Fermilab cable is a notable exception) to impregnate the cable with solder in which case Sn-5Ag is the usual choice. In a production process the cable is run in and out of the liquid-solder bath over rollers; a clean mirror surface at the entry and exit points is maintained, and care is taken to select the optimum traverse speed and keep it constant in order to ensure complete impregnation and a uniform layer of solder.

"Compacted cable" technology, a recent development by Airco, offers another approach to combining the heavy cold reductions and modest Cu/SC ratios available in strand fabrication with the strength and rigidity of a monolithic conductor. As pointed out by the Airco group [73], this fabrication technique was devised during the development of a 500-A (12 T) Nb_3Sn conductor for the High Field Test Facility at the Lawrence Livermore Laboratory. A cabled array of 18 (i.e., 6 triplets) strands each of diameter 2.3 mm and containing 15,895 (i.e., 187 x 85) filaments was continuously encased by TIG welding in high-purity Cu, as in Figure 5-10(a), and subsequently compacted to full density while being reduced to rectangular wire using standard procedures, Figure 5-10(b). The final heat treatment of 94h/750° C served not only to form the A15 compound but also was responsible for partially sinter-bonding the interfaces between the strands.

Although sinter-bonding is not available to Ti-Nb-alloy conductors the above technique was successfully adapted to the fabrication of both Cu-stabilized and mixed-matrix (Cu/Cu-10Ni) Ti-Nb-base composites [74].

For example, the 3-kA, 8-T, prototype poloidal field coil conductor depicted in Figure 5-11 was produced by continuously sheathing nineteen 517-filament Cu/Cu-10Ni/Ti-Nb strands in a tube mill prior to compaction, drawing through conventional wire dies and shaping to 5x2.8 mm^2 with Turck's head rolls and a final sizing die.

It is also possible to combine the strength, rigidity, and cryostability of a high-Cu/SC-ratio monolith with the high self-field stability and low a.c. loss characteristics of a flat cable. In order to do so the cable may be formed onto a rectangular Cu core, or a cable either with or without a core can be soldered into a suitably shaped recess in a thick bar of Cu or Al. Two good examples of the latter arrangement are the Japanese Large Coil Task (LCT) conductors which are heavily Cu-stabilized Rutherford cables and the conductor designed by MORPURGO *et al.* [75, 76] for a particle-detection magnet intended for CERN'S colliding-beam experiment, which consists of a stainless-steel-reinforced, "eleven-around-one" type of cable imbedded in high-purity Al, Figure 5-12.

Two further examples are given in Figures 5-13 and 5-14. The first of these shows a 15-strand Cu/Ti-Nb flat cable soldered into a slot formed into an OFHC-Cu bar, grooved in order to increase its cooled perimeter and to facilitate access to liquid He, and provided with a chemically oxidized surface to improve the heat-transfer coefficient of that surface; the second shows a 23-strand Cu/Ti-Nb flat cable imbedded in an Al matrix. Both of these conductors were designed with tokamak toroidal field coil applications in mind.

SECTION 6

CONVENTIONAL TITANIUM-ALLOY SUPERCONDUCTORS

6.1 Equilibrium and Nonequilibrium Phases

Precipitation in Ti-Nb alloys can be understood with reference to the metastable-equilibrium and equilibrium phase diagrams of Figure 6-1. These diagrams are based on information derived from the standard metallurgical literature, but have been modified by the observations of NEAL *et al.* [77] and WEST and LARBALESTIER [78][79][80] to the effect that α-phase precipitation is only a factor in flux pinning in alloys with Nb concentrations less than about 40 at.%.

6.2 Flux Pinning in Titanium-Niobium Alloys

6.2.1 Precipitate-Free Subbands

The seminal study of this topic was conducted by NEAL *et al.* [77], referred to above, using β-Ti-Nb. The composition of the alloy selected (an analyzed 42 at.% or 58 wt.%) placed it so close to the practical boundary of the α+β-phase field at, say, 400° C that its precipitate-free status needed to be confirmed by TEM. This was carried out, and although some traces of α-phase were detected its abundance was claimed to be inadequate to provide any significant degree of flux pinning. Samples were subjected to area reductions by cold work of between 33% and 99.999% (1.4×10^5:1) and final heat treatments, mostly for 1 h, at temperatures of 300 to 600° C, after which critical currents were measured at 4.2 K, using a 100 μV criterion, in fields of up to 60 kOe and converted to J_c's using measured wire cross-sectional areas. The electrical results were

correlated with fiber diameters (i.e., subband diameters, or cell sizes) determined by the intercept method from transverse-section electron micrographs. From the original article, and from other quantitative descriptions of the effects of cold drawing and heat treatment on the subband structure and the subband-related J_c the following conclusions can be drawn: (i) J_c appeared to be extremely sensitive to the initially administered cold work which in NEAL's experiments produced its greatest effect during the first stage of area reduction (*viz.* 10^2:10); further cold work in the range of 10^2:1 to 10^5:1 resulting in only moderate increases in J_c. This strong influence of deformation cell size on J_c is of course responsible for the anisotropy noted in early experiments with cold-rolled strip; (ii) in 1-h aging experiments, J_c increased rapidly as the temperature was raised above $\sim$ 300° C. This is interpreted as being due to a migration of dislocations from the interiors of cells to their walls, with little increase in cell diameter, a process which takes place all the more actively above about 400° C but which must compete with the deleterious effect of cell growth which begins to accelerate in the temperature range 400 - 500° C; (iii) after 5 x 10^4:1 area reduction by cold work the optimal 1-h aging temperature is 385 $\sim$ 425° C; (iv) during aging at 385° C, although the cell diameter appeared to be quite stable within any reasonable estimate of experimental uncertainty, J_c increased 5% to a maximum after 5 h; (v) cell growth data and the results of NEAL *et al.* [77] pointed to $\sim$ 400° C as an optimal heat treatment temperature. The fact that aging at this temperature can also yield ω-phase and α-phase precipitation in the appropriate concentration ranges has been a source of confusion in literature; (vi) according to NEAL *et al.* [77] and BAKER [81] before them, the bulk pinning force ($\propto J_c.H$) is proportional to the reciprocal of the cell diameter, d. As shown in Figure 6-2, $J_c.H(50kOe)$ *versus* d^{-1} for heat-treated Ti-58Nb wires is linear with slope 6.06 x 10^7 Å A cm^{-2}. The curve depicted represents a norm for optimized unprecipitated Ti-Nb superconductor, against which the effects of additional intrinsic α-phase precipitation, characteristic of less Nb-rich alloys, can be compared.

The effect of heat treatment on dislocation-cell structure within this context has been discussed in detail by CHARLESWORTH and MADSEN [82] with reference to FRIEDEL's classical work on dislocations and the contemporary

studies of BAKER [81] referred to above. All workers agree that critical current density is favored by a fine dislocation cell structure, and that an optimal heat treatment is one that clarifies the interiors of the cells while stopping short of cell growth. The case study of NEAL *et al.* [77], augmented by the results of more recent studies of flux pinning by α-phase precipitates to be considered below, and "interstitial"-element effects and intermetallic-compound precipitation discussed elsewhere, all point to the predominant influence of subband structure. Their investigation of precipitate-free alloys indicated that an optimal sub-cell structure must always be achieved as a basis for further improvements in flux pinning strength, whether it be by cell-wall precipitation, or more fundamentally *via* an alloying-effect increase in the upper critical field.

6.2.2 Subbands and Precipitates

From the very beginning when it was first recognized that flux penetrated a type-II superconductor in the form of an Abrikosov lattice, it was realized that in order to stabilize transport current, flux drift had to be prevented in some way. The metallurgical options available were *intrinsic* defects such as dislocations and grain boundaries, or *extrinsic* defects such as precipitates of one kind or another. Optimization then consisted of reducing the scale of these defects to that of the flux lattice to be pinned. Deformation and precipitation, as independent events, were treated early in the development of hard superconductors; but it has traditionally been difficult to separate improvements in J_c resulting from subband refinement from extra improvements which may result from precipitation. To accomplish this successfully an approach different from the usual method of intercomparing the J_c or $J_c.H$ *versus* composition curves of cold-worked-only and cold-worked-plus-heat-treated alloys is called for.

A brilliant solution to the problem was offered by LARBALESTIER [83] whose approach was to compare the optimized critical current densities of the precipitate-free alloys of NEAL *et al.* [77] (Ti-58Nb) with those of a

series of conventional α-precipitated alloys having compositions of from 31.6 to 37.2 at .% Nb using cell diameter as the common variable. Figure 6-3, which displays the results, shows that precipitation does little to increase flux pinning in large-subband material, but that provided the wire is already structurally optimized (*heat-treated* cell size $\lesssim$ 550 Å), precipitation may contribute an additional $\sim 0.5 \times 10^5$ A cm^{-2} to the critical current density. These results add strength to an accumulating body of opinion [84,85] that although a fine heat-treated subband structure is a necessary prerequisite for strong bulk flux pinning, full optimization demands the presence of a suitable dispersion of suitably dimensioned precipitates [86].

6.3 Process Optimization of Titanium-Niobium Superconductors

It has been shown how the critical current density of a heavily deformed Nb-rich Ti-Nb alloy may be optimized by the application of a moderate-temperature (385° C) heat treatment, and that further improvements can be obtained when the composition is such that precipitation, also as a result of moderate-temperature heat treatment (at 390° C -- WILLBRAND *et al.* [84] or 380° C -- HILLMANN *et al.* [86]) takes place in the cell walls. Optimization is the process of further increasing J_c, through fine adjustment of deformation structure and precipitate size and distribution. This is achieved: (a) by administering heat treatments in several stages interrupted by cold work during the wire drawing process (so-called intermediate heat treatment); (b) by administering a rather precise degree of final cold deformation.

6.3.1 Intermediate Heat Treatment

The literature is replete with examples of the steady increase in critical current density which accompanies the addition of more and more stages of intermediate heat treatment followed by, for the purpose of intercomparison, a fixed final cold reduction. A classical example is the early

work of PFEIFFER and HILLMAN [86], cited by several subsequent authors (e.g., [83]), which makes reference to the beneficial effects of properly administered final cold deformation.

6.3.2 Final Cold Deformation

It has been found empirically that it is better to terminate the alternating cold-work/anneal cycle of the intermediate-heat-treatment sequence with the cold-work option. Some of the first systematic studies of the effect of final cold deformation on the critical current densities of intermediate-heat-treated alloys were those of PFEIFFER and HILLMAN [86], mentioned above, on Ti-50Nb (34 at.%). Since even the *detection* of α-phase precipitates in heavily deformed wire is difficult, it has been possible in the past only to speculate on the basis of indirect evidence, on the manner in which precipitation is *affected* (i.e., refined or redistributed) by the final cold work. But more recent mechanical-property evidence [87] bolstered by direct TEM studies [80] suggest that the initially formed large α-phase particles are reduced in size, altered in shape, and distributed more uniformly during the post-anneal deformation. According to HILLMANN and coworkers [88], heat treatment of the fibrous structure yields a very anisotropic distribution of precipitate particles -- more abundant in the drawing direction than perpendicular to it. During final cold deformation, it is supposed that the density of α-particles increases in the transverse direction at the expense of that in the drawing direction, leading eventually to an isotropic distribution. This process should continue with further cold deformation leading once again to an anisotropic distribution. It follows that J_c should pass through a maximum at some optimal value of final cold work, and indeed this has been observed exterimentally. Further evidence in support of this hypothesis has been acquired by members of the same research group in studies of the J_c anisotropy of wires that had been removed from various stages of the final cold deformation sequence and flattened by rolling.

Optimization of the final cold-deformation process has been examined using two slightly differing experimental formats: (a) fixed overall reduction and fixed final wire diameter with variable reduction within the intermediate-heat-treatment segment [84]; (b) fixed reduction within the heat-treatment

segment and variable final wire diameter [88]. The results indicated that in Ti-50Nb at 50 kOe, for example, optimal final cold reduction as indicated by a maximum in J_c *versus* percent reduction in area lay somewhere within the range defined by (a) 91 ∿ 94% [84]; to (b) 94% [88]; optimization for higher fields called for higher levels of cold work, e.g., up to about 96% for 80 kOe. The significance of *total* reduction is considered below. The existence of a *maximum* in J_c implies the possibility of "overoptimization" through excessive final cold work. These effects which have to do with the redistribution of precipitate particles have been examined in the experiments on flattened wires mentioned above.

6.4 Recent Advances in Process Optimization

6.4.1 Total Area Reduction and Final Cold Deformation

Considered above were the effects of (multiple) intermediate heat treatment and variation of the level of final cold deformation on the critical current density of Ti-50Nb the alloy favored by European groups. In conductor optimization, composition is of course another important variable. Accordingly it is instructive to introduce into a continuation of the discussion of cold-work effects a pair of alloys, Ti-45Nb and Ti-53.5Nb, whose compositions bracket that of the alloy just treated. In the recent work of STEKLY *et al.* [89] commercial-size multifilamentary Cu/Ti-Nb composite billets (Ti-45Nb: 3 and 8 in.$^{\phi}$, 156, and 1272 cores, respectively; Ti-53.5Nb: 8 and 10 in.$^{\phi}$, 132 and 2046 cores, respectively) were reduced to wire of diameters ranging from ∿ 0.1 to 0.025 cm$^{\phi}$ during which various single-stage and multiple-stage (Ti-45Nb) intermediate heat treatments were administered. An optimal single-stage heat treatment was discovered for each composition (Ti-45Nb: 75h/350° C; Ti-53.5Nb: 75h/375° C) and in a two-part investigation an attempt was made to separate the influence on J_c of the *total* area reduction as distinct from the post-heat-treatment final cold work.

The mechanical processing, in conjunction with the single-stage "optimal" heat treatments specified above, took place according to the schema of Figure 6-4 after which J_c *versus* area-reduction data were required.

As indicated in Figures 6-4(a) and (b) the influence of final cold reduction, cw_2, on the critical current densities of Ti-45Nb and Ti-53.5Nb were intercompared. In either case the wires had been subjected to practically constant reduction, cw_1, prior to the heat treatment (*viz.* 9.7×10^3 and 5.1×10^3:1, respectively). According to (b) and (c) of the same figure a study was also made of the influence on J_c of variation of final cold reduction at fixed cw_1, ascompared to variation of final cold reduction at fixed overall reduction, cw, (implying a compensatory variation in cw_1). The results, presented in detail in the original article, and in summary form in the above figures themselves are as follows: (i) with the Ti-45Nb composite the critical current density decreased monotonically with final cold work suggesting that, for the magnetic field range under consideration, this alloy was already overoptimized at about 75% final cold deformation, (ii) with Ti-53.5Nb, J_c(1.9K, 13T) and J_c(4.2K, 10T) were found to be close to each other and to increase monotonically with increasing final cold work. Such a result is not inconsistent with the implicit high-field cold work response of Ti-50Nb referred to above in which the J_c-maximum shifted in the direction of smaller wire diamater as the applied field increased. In the present case it was noted that J_c increased insignificantly with final reductions greater than about 98%, which from a practical standpoint must be regarded as optimal, (iii) the purpose of the comparison represented by Figures 6-5(b) and (c) was to determine whether total reduction or final reduction had the greatest influence on critical current density. Unfortunately, the design of the experiment prevented that question from being definitively answered. To STEKLY *et al.* [89] the results depicted in the figure suggested that total area reduction, from pre-extrusion to final wire size, was the determining factor. On the other hand it could be argued that whereas in (b) a variation in final cold reduction ratio of 26:1 increased the critical current density by 58%, in (c) a variation of final cold reduction ratio of 3.8:1 increased J_c by 7% (in spite of the fact that in this case cw_1 was undergoing a large decrease). This remarkable proportionality of increase in J_c to increase

in final cold reduction ratio serves to emphasize the latter's importance as a determiner of current-carrying capacity in the magnetic field range under investigation.

6.4.2 Thermomechanical Process Optimization

Studies in the *heat-treatment* variables were undertaken by STEKLY *et al.* [89] on wire prepared from billets somewhat smaller than those referred to in Figure 5. With Ti-53.5Nb, heat treated for times of 40 to 150 h at temperatures between 350 and 400° C, it was found that J_c (1.9K and 4.2K, 12T) passed through a maximum in the vicinity of 50-75h/375° C. As a result of this investigation a single heat treatment of 75h/375° C was selected for the deformation studies just outlined. Similarly after subjecting Ti-45Nb to heat treatments definable by (50-150)h/(325-375)° C an optimal single heat treatment, based on J_c (1.1K, 12T), of 75h/350° C was chosen. Some attempts at investigating the effects of intermediate heat treatment were also made. It was noted that the J_c(1.9K, 12T) of singly-heat-treated Ti-45Nb could be raised 8% with one additional heat treatment or 25% with two more.

In a common J_c *versus* H plot, Figure 6-5, the curves for the two alloys referred to here lie below that for an intermediate (multiply) heat treated Ti-50Nb. It is not known whether this superiority will survive further attempts at optimizing the thermomechanical processing of Ti-53.5Nb. All evidence points to the technical desirability of multiple, rather than single-stage, cold work; thus, it is suspected that further improvements to the current-carrying capacity of Ti-53.5Nb are possible. Multiple heat treatment is more expensive to carry out than a single-stage process, but if successful the reward would be a conductor that is more workable than Ti-50Nb and one that may have a greater high-field critical current density.

6.4.3 Critical Field Limitation

(a) General Considerations. Having been carried as far as possible by empiricism in the form of thermomechanical process optimization, J_c is subject to further increase only if closer attention is paid to some of the fundamental aspects of flux pinning as reviewed in numerous standard works on the subject. Arising from Abrikosov theory, a factor $(1-H/H_{c2})$ appears in the expression for the bulk pinning force $F_p = J_c.H$. This has nothing to do with the strength of the elementary pinning force, of which F_p is the sum, but with the *existence* of the flux lattice itself. In this sense then there is an *existence cutoff* for flux pinning such that, as LARBALESTIER [83] has reminded us, at high fields J_c tends to become dominated by H_{c2}. The control that H_{c2} exerts over the high-field J_c is exemplified by the numerous figures that appear in the literature showing families of J_c *versus* H curves for given alloys under varying conditions of cold-work-plus-heat-treatment coalescing at very high fields before descending linearly and in unison upon a value of H_{c2} which depends primarily on the composition of the alloy and the temperature. The importance of H_{c2} as a controller of high-field J_c is adequately embodied in Figure 6-5: a small shift in H_{c2} to higher fields, carrying with it $J_c(H)$ with its high-field slope of typically close to -3.2 kA cm^{-2} kOe^{-1} (data for Ti-53.5Nb [83]) would reflect a significant improvement upon J_c in the high-field region. Thus, the optimization of existing superconductors having been dealt with, any further increases in J_c can only be won by increasing the upper critical field. There are two ways in which this can be done: (a) by reducing the temperature, and (b) through alloying.

(b) Temperature. According to the HELFAND and WERTHAMER nonparamagnetic theory of upper critical field temperature dependence [90], the zero-K H_{c2} may be expressed in the form:

$$H_{c20} = 0.68\ T_c(-dH_{c2}/dT)_{T_c} \quad . \qquad (6\text{-}1)$$

Inverting this, and replacing H_{c20} with its value from Equation (6-1) yields:

$$-dH_{c2}/dT = 4.50 \times 10^4 \rho_n \gamma \quad (\text{Oe K}^{-1}) \quad . \tag{6-2}$$

Substituting some numerical values, such as $\rho_n = 78 \times 10^{-6}\ \Omega\,\text{cm}$ and $\gamma = 1.04 \times 10^4$ erg $\text{cm}^{-3}\ \text{K}^{-2}$, yields:

$$-dH_{c2}/dT = 36.5\ \text{kOe K}^{-1} \tag{6-3}$$

in satisfactory agreement with the 26.4 kOe K^{-1} obtained experimentally by HAWKSWORTH and LARBALESTIER [91] with a Ti-52Nb monofilament.

Combining these data with the J_c field dependence quoted above yields for the H_{c2}-controlled high-field J_c temperature dependence the values:

$$\begin{aligned} dH_c/dT &= (dJ_c/dH)(dH/dT) \\ &= 84.5 \sim 116.8\ \text{kA cm}^{-2}\ \text{K}^{-1} \quad , \end{aligned} \tag{6-4}$$

in semiquantitative, but nevertheless useful, agreement with the 46.5 kA cm^{-2} K^{-1} obtained by comparing the 4.2-K and 2.05-K 8-T J_c's of Ti-53.5Nb as reported by HAWKSWORTH and LARBALESTIER [92] and depicted in Figure 6-5. The improvement in J_c acquired by reducing the temperature of operation of a Ti-Nb conductor from 4.2 to 2 K is adequately illustrated in that figure.

(c) Alloy Design. Having established the importance of the H_{c2}-control of critical current density, attention can also be directed towards alloying as a means of increasing H_{c2}, hence the high-field J_c. From the paramagnetic theories of the mixed state of type-II superconductors it can be concluded that an increase in the paramagnetic susceptibility of that state by increased conduction-electron scattering through the introduction of heavy-ion substitutional alloying should reduce the paramagnetic limitation on, hence increase, the upper critical field. With this in mind, the following substitutions have been made into the binary Ti-Nb base:

Hf for Ti ---- HAWKSWORTH and LARBALESTIER [91], WADA [93];
Ta for Nb ---- SUENAGA and RALLS [94], HAWKSWORTH and LARBALESTIER [91];
Zr for Ti and Ta for Nb ---- HORIUCHI *et al.* [95].

These deliberate attempts to increase H_{c2} through heavier-element substitutions for the basic components of Ti-Nb alloys have resulted in the development of some promising ternary (Ti-Nb-Ta) and quaternary (Ti-Zr-Nb-Ta) alloy superconductors.

SECTION 7

EARLY AND UNCONVENTIONAL TITANIUM-ALLOY SUPERCONDUCTORS

In an early demonstration of tandem-extrusion technology CLINE *et al.* [57] have demonstrated the feasibility of fabricating by four successive stages of extrusion a wire containing filaments as small as 100 Å in dimaeter. Although such filament sizes are presently being achieved using the *in-situ* technique, in the conventional fabrication of large monolithic conductors usually no more than two stages of processing are now employed. In fact for many applications, high-current conductors are assembled in a modular fashion by cabling or bundling from a single-stage multifilamentary strand. When this is done, it is usual to insulate the strands from each other, or at least to increase the transverse resistivity, by plating them with a metallic coating, a technique invented by GEBALLE in 1960 and patented in the U.S. by him in 1963 [96]. Whereas at the time electroplated layers of simple or noble metals were considered, current practice is to coat with a molten alloy such as Sn-5Ag ("stabrite"). A liquid-metal-coating technique was also suggested by DOI and KUDO in a U.S. patent application filed in 1968 (granted, 1973) [97]. In this method, which might be regarded as an extension of one of the techniques of continuous casting, a superconducting wire or tape was drawn vertically through a bath of molten metal (noble and simple metals, particularly Al were suggested) exiting out of the bottom to be gathered, after solidification of the layer, on a take-up spool. This process was intended to provide the superconducting wire with a well-bonded coating of metal for the purpose of *stabilization* rather than "insulation".

An early suggested method of conductor fabrication, fairly similar to those in use today was recommended by FAIRBANKS *et al.* [98] in a 1967 U.S. patent application (granted, 1970). In it extrusion was the first step, the billet being assembled by the deep-hole-boring method; but after extrusion, further reduction was to take place by rolling, in order to produce a conductor suitable for magnet designs requiring ribbon-like conductors.

BOGNER *et al.*, in a German patent applied for in 1966 (granted, 1971) [99], also considered applying a stabilizing strip to a group of superconducting wires, but could see certain disadvantages in a simple roll-bonding approach, *viz:* (a) difficulties in securing a good contact between the superconductor and the matrix; and (b) the possible disadvantage that during the rolling the softer matrix material would elongate more than the superconductor. To avoid these drawbacks BOGNER *et al.* recommended the use of ultrasonic welding, and proposed a continuous spool-to-spool process for attaching the stabilizer to the superconductor in that way.

From time to time various unconventional methods of superconductor processing have appeared in the patent and general literature. GREGORY in a patent granted in 1967 [100] suggested the use of a powder-metallurgy approach to the fabrication of Ti-alloy superconductors. The method was intended to circumvent the difficulties being encountered at the time in preparing large homogeneous ingots of Ti-Nb and Zr-Nb alloy by conventional melting and casting methods. Briefly, the method proposed consisted of taking Ti or Zr powdered metals or hydrides then: (a) blending them with metallic Nb powder; (b) rolling to a "green" strip (say 6" x 3/8" x 0.040"); (c) dedydriding if necessary; (d) sintering at 1400-1800° C; (e) roll-compacting to full density; (f) diffusion annealing again at 1400-1800° C; (g) cladding in stabilizer if desired; (h) cold working and heat treating to final condition. Heavy cold work was recommended, but in one experiment after only 80% reduction by cold work, followed by an anneal for 1 h/550° C, a 4.2-K J_c at 40 kOe of 1.6×10^5 A cm^{-2} was achieved.

Finally attention is drawn to an *in-situ* process for Ti-Nb-base superconductor fabrication reminiscent of the various *in-situ* or precipitation approaches that have been proposed for A15 composite superconductor fabrication. OLIVEI [101] has made an experimental study, with analysis, of the parameters which control the directional solidification from the melt of a filamentary superconductor in a resistive matrix. The ternary systems Ti_{52}-Nb_{43}-Cu_5 and Ti_{50}-Nb_{10}-Cu_{40} were the subjects of the investigation. Reliance was placed on a principle due to MOLLARD and FLEMINGS who showed that it is possible to grow an aligned eutectic-like composite from any melt provided that a plane solidification front can be maintained, a condition which is satisfied if the ratio of thermal gradient (G) to growth rate (R) is sufficiently large, and convection sufficiently well suppressed. For

example with values of G/R of $\sim 30 \times 10^5$ K cm^{-2} s^{-1} the alloy Ti_{50}-Nb_{10}-Cu_{40} yielded a rod-like precipitate structure, while decreasing G/R to 15×10^5 K cm^{-2} s^{-1} caused a transition to plate-like precipitate morphology. It is unlikely that a Ti-Nb alloy capable of competing with modern composites can be produced by this method, nevertheless, the results obtained were sufficiently interesting to warrant continuation of the work described with the possibility of other applications in mind.

SECTION 8

CONVENTIONAL A15 SUPERCONDUCTORS

8.1 The Superconducting A15 Compounds

8.1.1 Formation of the Compounds

The four important classes of superconducting compounds are drawn from: (a) the cubic transition-metal carbides and nitrides with the B1 (NaCl-type) structure [102]; (b) the hexagonal Laves phases with the C14 ($MbZn_2$-type), C15 ($MgCu_2$-type), C36 ($MgNi_2$-type) structures [103]; (c) the Chevrel phases -- ternary compounds of the general formula MMo_6S_8 [104]; (d) transition-metal-base compounds with the A15 or Cr_3Si (formerly β-W-type structure. At the present time the latter are the most technically important and are therefore the subject of this and the following Section.

There are seventy-six known A15 compounds. At least forty-six are superconductors, and of these the six listed in Table 8-1, which have transition temperatures higher than 15 K, have received the most attention. Phase diagrams for all six binary systems are readily available [106] and do not need to be reproduced here. It is interesting to note that in their modes of formation the six compounds exemplify four classes of metallurgical reaction, *viz:* (a) solid-state order-disorder transformation at the stoichiometric composition; (b) congruent solidification from the melt; (c) peritectoid (solid-state) reaction; (d) peritectic solidification. These modes are represented schematically in Figures 8-1(a) through (d), respectively. The manner in which the six high-T_c compounds form, and the temperature at which they do so are listed in Table 8-2.

TABLE 8-1. TRANSITION TEMPERATURES (T_c) AND 4.2-K UPPER CRITICAL FIELDS (H_{c2}) OF SIX BINARY AND TWO PSEUDOBINARY A15 COMPOUNDS [105].

Compound	T_c K	H_{c2}(4.2K) T
V_3Ga	15.4	23.6
V_3Si	17.1	23.0
Nb_3Sn	18.3	26.0
Nb_3Al	18.9	29.5
Nb_3Ga	20.3	33.0
Nb_3Ge	23	37.0
$Nb_3(Al_{0.5}Ga_{0.5})$	19.0	31.0
$Nb_3(Al_{0.7}Ge_{0.3})$	20.7	41.0

TABLE 8-2. MODES OF FORMATION AND REACTION TEMPERATURES FOR SIX BINARY A15 COMPOUNDS -- after DEW-HUGHES [5, pp. 145-153].

Compound	Mode of Formation	Reaction Temperature °C	Homogeneity Range
V_3Ga	order-disorder reaction	1300	21-31.5 at.% Ga (1010°C) 21-29 at.% Ga (600°C)
V_3Si	congruent solidification	1935	19-25 at.% Si (1800°C) 24-25 at.% Si (<1200°C)
Nb_3Sn	peritectic solidification	2130	18 at.% Sn (2130°C) ∿18-25.1 at.% Sn (<1800°C)
Nb_3Al	peritectoid reaction	1730	24.5 at.% Al (1730°C) 19-22 at.% Al (1000°C)
Nb_3Ga	peritectic solidification	1860	21 at.% Ga (1860°C) ∿19.7-20.6 at.% Ga (<1000°C)
Nb_3Ge	peritectic solidification	1900	18 at.% Ge (1900°C) 15-18 at.% (≤1500°C)

8.1.2 Technically Important A15 Compounds

If the six phase diagrams are consulted and intercompared [106], it will be noted that in only the V-Ga and Nb-Sn systems do the A15 compounds possess higher melting points than the competing intermetallic compounds with other stoichiometries. It is this property which permits V_3Ga and Nb_3Sn to be formed by the direct reaction of V or Nb with liquid Ga or Sn, respectively, as in the production of superconducting ribbons, but excludes the other A15 compounds from formation by this technique. It turns out also that only V_3Ga and Nb_3Sn are amenable to formation by the "bronze process", a solid-state-procedure involving a diffusion couple between the transition-metal (TM) and a Cu-SM (Ga or Sn) solid solution (or bronze).† However, as pointed out by LUHMAN [108], an explanation for this must be in terms of the appropriate ternary TM-Cu-SM-phase diagrams and the relationships between the stabilities of the phases present to those of the desired A15 compounds. Thus, although several of the compounds listed in Table 8-1 have very attractive transition temperatures and upper critical fields, as a consequence of their relatively high stabilities, only V_3Ga and Nb_3Sn have been produced on a commercial scale.

8.2 Conventional Processing of A15 Superconductors

8.2.1 The CVD Process

An early successful method of preparing Nb_3Sn ribbon took advantage of the chemical vapor deposition (CVD) technique [109]. In principal this consisted of a reduction by hydrogen of the mixed halides of Nb and Sn in the presence of a suitable heated substrate such as the alloy Hastelloy. In

† SM signifies "simple metal"; i.e., non-transition metal.

practice, HCl is added to the mixed vapors to suppress the formation of solid $NbCl_3$; and gases such as O_2, CO, and CH_4 are added in order to improve the critical-current density. The CVD method has also been successfully applied to the preparation of Nb_3Ga [110] and Nb_3Ge [111][112].

8.2.2 Evaporation and Sputtering

Other methods of depositing A15 compounds onto continuous substrates are electron-beam (EB) evaporation-and-deposition and sputtering. The synthesis of Nb_3Sn, V_3Al, Nb_3Ge, Nb_3Si, and $Nb_3(Ge,Al)$ using EB techniques has been discussed by HAMMOND [113], and a further review of the subject has been provided by LUHMAN [108, pp. 234, 235]. Sputtering, either high-rate or conventional, has been successfully employed in the preparation of A15 forms of the compounds Nb_3Al and $Nb_3(Al_{0.75}Ge_{0.25})$ [114] as well as Nb_3Ge itself [115][116].

8.2.3 The Surface-Diffusion Process

As mentioned above, both Nb_3Sn and V_3Ga are amenable to formation by means of the "surface-diffusion" technique in which the transition-metal component, usually in the form of a ribbon, is exposed to molten Sn or Ga. The Intermagnetics General Corporation has prepared Nb_3Sn ribbon on a commercial scale by this process, and has used it to wind numerous superconducting magnets. At the National Research Institute for Metals (Japan) a similar process was developed during the 1960's for the preparation of V_3Ga-coated ribbon [117]. As explained by TANAKA *et al.* [118], during its passage through a bath of molten Ga, a layer of VGa_2 is formed on the surface of a V ribbon; then during subsequent heat treatment at 700° C this intermediate compound is converted to V_3Ga_2 and finally to V_3Ga by further reaction with the V substrate. An important discovery was the observation that by adding Cu to the melt, or plating it onto the surface of the V tape, the rate of formation of the desired V_3Ga compound could be significantly enhanced. The Cu was shown to play an active role in modifying

the rather complicated chemistry of the Ga + V → V_3Ga reaction which had then become closely related to the solid-state bronze-process reaction to be considered below.

8.2.4 The Bronze Process

The most important method used in the production of A15 superconductors, and the only one capable of producing multifilamentary conductors is the "bronze process". The metallurgical chemistry of this process which, as mentioned above is applicable only to Nb_3Sn and V_3Ga formation, has been discussed by LUHMAN [108, pp. 228, 229]. Technically, the method is quite straightforward to apply, and is eminently compatible with the usual method of processing Cu/Ti-Nb multifilamentary monoliths, cables, and braids. Thus, to a first approximation, in going from Cu-stabilized Ti-Nb-alloy processing to A15 processing by the bronze method, it is necessary only to replace the Cu of the earlier billet with a bronze, and the Ti-Nb cores by V or Nb ones. The metalworking sequence illustrated in Figure 5-1 is common to both routes, the principal difference being that the final-stage thermo-mechanical processing (i.e., the intermediate heat treatment) of the Ti-Nb is omitted when preparing bronze-processed multifilamentary A15 conductors and replaced, after all the wire drawing and twisting operations have been completed, by heat treatments of several hours at temperatures in the vicinity of 700° C to promote the formation, by solid-state diffusion, of the desired intermetallic compound layer at the interface between the cores and the surrounding bronze matrix. In what follows, the essential features of conventional bronze processing will be outlined.

8.3 Conventional Internal-Bronze-Process Technology

8.3.1 Metalworking

Useful summarizing discussions of conventional bronze processing as it applies to the fabrication of multifilamentary Nb_3Sn conductors have been offered by ZEITLIN *et al.* [62, p. 27], MEYER *et al.* [62, p. 59], and HILLMANN *et al.* [6, p. 17].

As in the processing of multifilamentary Cu/Ti-Nb composites the starting billet can be assembled using either the deep-hole drilling or element-packing techniques. Certainly if two stages of extrusion are required, and Cu stabilizer with associated Ta diffusion barriers are to be installed, the packing of hexagonal-shaped elements will need to be employed at least in the preparation of the second-stage billet.

Since the bronze is the reservoir which supplies Sn to the A15 reaction it must be as homogeneous as possible to ensure uniformity of reaction layer thickness along the lengths of the individual filaments. In order to prevent excessive grain growth the reaction should be as fast as possible, which requires the Sn concentration of the bronze to be close to limit of solid solubility. According to the phase diagram, the following points terminate this range: 13.5 wt.%(798° C), 15.8 wt.%(520-586° C), and 11.0 wt.% (350° C). Thus, if a bronze concentration of 15.8 wt.% is chosen (cf. [108, p. 237]), care would have to be taken to ensure that all metalworking took place within the temperature range 500 $\sim$ 600° C. If during extrusion, adiabatic heating to temperatures greater than 600° C takes place in parts of the billet, hot-short embrittlement (by second-phase precipitation) could be expected. For this reason bronze concentrations of 13.0 wt.% [62, p. 29][6, p. 62] or 13.5 wt.% [6, pp. 18, 39] are preferred.

The Nb/bronze billet is assembled using "white-glove" or semi-clean procedures and evacuated overnight to a pressure of 8×10^{-6} torr prior to electron-beam sealing [62, p. 30][6, p. 18]. If desired this may be followed by a consolidation step to increase the packing density from somewhat more than 90% to 98-99%. With regard to extrusion, all three of the

process variants illustrated in Figure 5-6 have been used. Conventional extrusion is the most common procedure; a typical set of specifications, according to ZEITLIN *et al.* [62, p. 31] is given in Table 8-3.

At Vacuumschmelze the preferred technique is indirect extrusion in which the absence of billet/container friction assists in the establishment of laminar flow through the die. A typical set of extrusion parameters according to HILLMANN *et al.* [6, p. 19] is given in Table 8-4.

The applicability of hydrostatic extrusion with its potential for very high reduction ratios to the extrusion of experimental Nb/bronze billets has been explored by MEYER, FIORENTINO, and others, whose results are reported in the book, MANUFACTURE OF SUPERCONDUCTING MATERIALS [62, pp. 59-73] and elsewhere [51, p. 76]. The parameters listed in Table 8-5 serve to describe the extrusion of a small 19-element experimental billet through a hexagonal-apertured die.

An intercomparison of the three sets of parameters presented in Tables 8-3 through 8-5 reveals the great advantage of hydrostatic extrusion in terms of both stem speed and extrusion ratio.

Two stages of extrusion are generally used in order: (a) to enable a sufficiently large numbers of small-diameter ($\sim$ 5 μm) filaments to be present in the final wire; (b) to enable stabilizing Cu to be introduced into the interior of what is to become a monolithic conductor or strand. Three stages of extrusion are less common than two, although examples of it have appeared in the literature [6, pp. 27-36]. Following the extrusion, the rod is reduced to wire first on the draw bench and finally by means of the multidie machine just as in Ti-Nb processing. 13-wt.% bronze, if selected for the matrix alloy, work-hardens rapidly, and unlike Cu/Ti-Nb, the bronze/Nb composite requires frequent annealing at temperatures around 550° C during rod and wire drawing. At first, annealing is administered after every 60% reduction in area, but in later stages a frequency of 80 $\sim$ 90% reduction between anneals is adequate as the wire approaches its final size from about 5 $mm^{\emptyset}$ to about 0.25 $mm^{\emptyset}$.

TABLE 8-3. CONVENTIONAL EXTRUSION -- A SET OF TYPICAL PARAMETERS

Bronze concentration	13 wt.% Sn
Bronze/Nb ratio	2:1
Billet preheat temperature	650±10°C
Exit temperature	700-725°C
Container diameter	9.047 cm
Die aperture	2.844 cm
Die angle (included)	90°
Extrusion ratio	10.1:1
Ram speed	13 mm s^{-1}
Maximum extrusion force	657-710 tons (6.6-7.1 MN)

C-2

TABLE 8-4. INDIRECT EXTRUSION -- A SET OF TYPICAL PARAMETERS

Bronze concentration	13.5 wt.% Sn
Billet temperature	700-750°C
Container diameter	17.5 cm
Die aperture	5 cm
Extrusion ratio	12.25:1
Ram speed	1 mm s^{-1}
Extrusion force	720°C: 12.0 MN
	750°C: 9.1 MN

TABLE 8-5. HYDROSTATIC EXTRUSION -- A SET OF EXPERIMENTAL PARAMETERS

Bronze concentration	10 wt.% Sn
Bronze/Nb ratio†	~3.2:1
Billet temperature	750°C
Liner diameter	6.0 cm
Die aperture (across-flats)	0.56 cm
Die angle (included)	45°
Extrusion ratio	99:1
Stem speed	34 mm s^{-1}
Extrusion pressure	peak : 1540 MN m^{-2}
	runout: 1295 MN m^{-2}

† To permit the high reduction ratio specified it was found necessary to enclose the 19-element Nb/bronze assembly in a thin Cu jacket with attached Cu nose-cone. The Cu was subsequently removed by etching.

8.3.2 The Solid-State Reaction

(a) The final step in multifilamentary A15 composite processing, taken after all deformation processing including twisting has been completed, is the heat treatment needed to convert the Nb filaments, or at least their outer layers, into the desired A15 compound. The goal of the heat treatment is to produce a homogeneous stoichiometric Nb_3Sn layer, as thick as possible (if the Nb filaments are not to be completely consumed) and with the fine grain size needed to ensure effective grain-boundary flux pinning. Since the last two requirements tend to be in conflict a compromise between layer thickness and grain size must be sought.

(b) A qualitative example of the growth of an Nb_3Sn reaction layer at 700° C from a 10 wt.% Sn bronze onto 5-$\mu m^{\emptyset}$ Nb filaments is given in Figure 8-2. The disposition of the various components of the reacted composite after 30 h of the heat treatment is depicted in Figure 5-3; noticeable are: (i) the complete absence of Cu from the Nb core and the reaction layer; (ii) an appreciable and apparently uniform level of residual Sn remaining in the matrix between the various reaction layers. A detailed study of the composition profiles in Nb_3Sn reaction layers has been undertaken be SMATHERS and LARBALESTIER [119]. The time-dependence of the reaction-layer thicknesses at 700° C is plotted in Figure 8-4 together with some results from the literature describing reactions at the same temperature between a 10 wt.% Sn bronze and Nb filaments in the following conditions: (i) unalloyed; (ii) with 0.5 wt.% Zr; (iii) doped with 0.75% Zr in the form of ZrO_2 precipitates.

(c) Indications of the effect of heat treatment on the Nb_3Sn grain size, and in turn the influence of grain size on bulk-pinning-force density are given in Figures 8-5 and 8-6, respectively. Displayed in these figures are: (i) the results of SCANLAN *et al.* [121] who used the "external-diffusion method", in which Sn is applied externally to a Cu/Nb composite, in order to achieve the desired reaction at the Nb surfaces; (ii) the results of SHAW [122] who formed the reaction layer on the internal surfaces of Nb-1% Zr tubes from a nominally 13-wt.% Sn bronze onto Nb filaments.

According to SHAW [122] a pinning-force maximum occurs for grain sizes of between 400 and 700 Å (0.04-0.07 μm) which, according to his data, as listed in Table 8-6, calls for heat treatments in the vicinity of 10 ∿ 30 h at 700° C or about 10 h at 750° C.

(d) The speed of the solid-state reaction increases rapidly with the activity of the Sn, and with it the critical current density of a layer of given thickness. SUENAGA *et al.* [124] have compared the J_c's and the thicknesses of reaction layers formed when a given heat treatment was applied to Nb filaments exposed to bronzes of various Sn concentrations. They showed that after 60 h/700° C, for example, the layer thickness increased from about 1 μm to 4.5 μm as the Sn concentration was raised from about 6.5 to 13 wt.%. MURASE *et al.* [126] have plotted *versus* Sn concentration (10-75 at.%) the Nb_3Sn layer thickness formed on the internal surfaces of Nb tubes filled with Sn-rich bronzes in response to heat treatments of 96 h/700° C. As a consequence of the high Sn activity, the layers so formed were about an order of magnitude thicker than those achieved in the conventional bronze-matrix process referred to above.

ADAM *et al.* [126] have investigated the fabrication and properties of commercial Nb_3Sn conductors prepared using both 10 wt.% and 13.5 wt.% Sn bronze as a result of which it was possible to conclude that the higher concentration bronze led to a 71% improvement in the 12-T critical-current density. The influence of diffusion time and temperature on $J_c(B)$ for fields between 5 and 15% has been investigated by HILLMANN *et al.* [6, p. 25] from which it may be concluded that the design field must be taken into consideration before the heat-treatment conditions are finally decided upon.

(e) Obviously if a large average critical-current density is to be achieved in the composite, it is no more satisfactory to have a thick reaction layer of low bulk-pinning force than a thin layer with a high one. The desired result is achievable only by maximizing the *product* of layer area and pinning-force density. Experiments in which heat-treatment times and temperatures have been varied in such an attempt to determine the optimal processing conditions for Nb filaments imbedded in a 13.5-wt.% Sn bronze matrix have been conducted by HILLMANN *et al.* [6, pp. 17-34] whose results are summarized in Figure 8-7. As pointed out by the authors of that figure,

TABLE 8-6. AVERAGE GRAIN SIZES AND FILM THICKNESSES FOR BRONZE-IN-TUBE[†]-REACTED Nb_3Sn -- after SHAW [122]

Strand Diameter mm	Filament (Tube Diameter) μm	Reaction Time(h)/Temperature (°C)	Grain Size Å	Layer Thickness μm
0.20	8	10/650	300	∿0.2
0.51	15	20/700	600	0.5
0.30	12	30/700	800	0.9
0.20	8	10/750	680	0.37
0.30	12	10/800	1250	0.7

† Number of tubes in strand ∿400.

although the greatest bulk pinning force density is exhibited in the reaction layer formed after 50 h/600° C (Figure 8-7(b)), it is too thin (Figure 8-7(a)) to yield a useful layer thickness (area). The best product of area and pinning-force is achieved after about 100 h at between 680 and 720° C (Figure 8-7(c)).

8.3.3 Variants of the Bronze Process

(a) External Tin Reserviour. As an alternative to having the Nb rods, hence filaments, embedded in a uniform bronze matrix, some advantages accrue from performing all the metalworking operations on Nb in Cu, plating the finished strand with Sn, and diffusing it in from the outside. Numerous descriptions of this process have appeared in the literature (e.g., [124]) the most recent being that of ROSNER *et al.* [6, pp. 69-79] of Intermagnetics General who have developed the idea into a commercial process. ROSNER *et al.*, in a detailed description of what was referred to as the "external bronze process", have compared its advantages with those of the conventional internal-bronze method, coming to the following conclusions [6, p. 77]:

Advantages of the Internal-Bronze Process

(1) The bend-strain tolerance is superior as the filaments can be located close to the conductor's neutral axis.
(2) Since the reacted conductor has a smooth surface, it can accept a coating of film-type insulation.
(3) The maximum size of the conductor is not limited by diffusion lengths.

Advantages of External-Bronze Process

(1) The manufacturing costs are considerably less than those of the competitive process.
(2) Third elements can be introduced into the matrix in order to enhance J_c. Using *internal*-bronze processing

this can only be accomplished by sacrificing some of the Sn in order to keep the total solute content within the solid-solubility range.

(3) The external reservoir of pure Sn is responsible for the maintenance of fast kinetics throughout the reaction period, which leads in turn to a thicker higher-J_c reaction layer than is possible *via* the external-bronze route.

(4) Finally, having been developed for conventional multifilamentary strand production, the external-bronze method can be equally well applied to the "*in-situ*" process, to be discussed below, in which pseudofilaments of Nb are produced by mechanical elongation of Nb precipitates, formed during the solidification of Nb-Cu melts.

(b) Internal Tin Reservoir. In 1974 HASHIMOTO *et al.* described an alternative internal-bronze process in which the Sn reservoir consisted of a Sn-rich Sn-Cu alloy residing at the core of an annular arrangement of Cu-clad Nb filaments which were, in turn, surrounded by a tube of pure Cu [127]. Since the components of the composite are all ductile and are not appreciably subject to work hardening during the drawing process, such an assembly is amenable to being drawn down to final wire size without intermediate annealing. During final heat treatment at 700-780° C, the Sn diffuses out of the central regions to react with the erstwhile Cu-clad Nb filaments.

8.4 Design and Critical-Current Optimization of Conventional Nb_3Sn Composite Conductors

8.4.1 Conductor Design

(a) Introduction and Disposition of Copper. The general principles of stabilization, quench protection, and a.c. loss reduction have been considered in earlier sections of this review. The filaments of a composite monolith, cable, or braid must be made sufficiently small if the requirements of dynamic stability or low hysteretic loss are to be satisfied. They must also be associated with sufficient suitably disposed pure Cu to satisfy the dynamic flux-jump stability requirement as well as to impart cryostability under whatever criterion has been chosen by the designer.

Filament size can be very quickly disposed of. According to ADAM *et al.* [126], in bronze-process Nb_3Sn the highest J_c values are attained in reaction layers of the order of 1 μm in thickness. It follows, in the interests of minimizing the volume fraction of unreacted Nb, that the filaments should have diameters of about 2.5 to 5 μm. Such sizes are well below the range wherein dynamic flux-jump stability might be a problem and, with regard to a.c. loss, are of a size below which surface loss would negate any attempts to further reduce a.c. hysteretic loss by making the filament diameters still smaller.

Associated with dynamic flux-jump stability is a large ratio of thermal to electromagnetic diffusivity as gauged by the ratio $(K_{SC}/\rho_{ST})\ (1-\lambda)$, where K_{SC} is the thermal conductivity of the superconductor and $\rho_{ST}/(1-\lambda)$ is the effective or transverse resistivity of the composite. Since the depleted bronze still has a high residual resistance ratio, the low average resistivity is achieved by incorporating islands of high-conductivity Cu within the composite, as illustrated in Figure 8-8. Since these are introduced into the billet generally prior to the second stage of extrusion, they must be protected from contamination during intermediate annealing and final heat treatment by being enclosed in "diffusion barriers". These are to be

considered in more detail below. Alternatively the double-stage strand may be clad in an outer jacket of high-conductivity Cu as in Figure 8-9. According to LEE and SCOTT [6, p. 38] such an arrangement may be preferable if the anticipated disturbance is mechanical in origin and occurs outside the strand. Indeed the two most likely classes of disturbance are flux-jumps (eliminated by dynamic stabilization) and both microscopic and macroscopic (stick-slip) thermomechanical interlayer frictional effects of the types which have been discussed recently by IWASA and colleagues [128].

There is considerable freedom in the way in which high-purity Cu can be incorporated into the basic strand if the internal-bronze process is employed. On the other hand, if the Sn is to be applied externally, it must obviously be given free access to the innermost Nb filaments. Although the strand depicted in Figure 8-8 was fabricated from a 13.5-wt.%-Sn internal bronze, it is conceivable for such a structure to be compatible with external tinning. Otherwise in a monolithic strand, the Cu must be present as a protected centrally located core, or it could be added during subsequent cabling in the form of: (i) a substrate (i.e., a strap about which the strands are cabled, Figure 8-10); (ii) additional Cu wires, Figure 8-11.

In describing the size of a multifilamentary Nb_3Sn conductor, since filament diameters are uniformly within the range 2.5 $\sim$ 5 μm, unlike Ti-Nb filaments that can have any value between that and $\gtrsim$ 100 μm depending on application, it is sufficient to a first approximation simply to specify the number of filaments.

(b) Diffusion Barriers. In order to prevent Sn from the bronze from contaminating the Cu stabilization during intermediate annealing and final heat treatment, it is necessary to separate the bronze and Cu components of the composite with a diffusion barrier. Ta, which is mechanically compatible with both of the other components, and whose reaction with Sn at the temperatures concerned is insignificant, is the most usual choice. In the finished composite the Ta layer is several filament diameters in thickness, values of 8 ± 2 μm to 15 ± 3 μm being typical. To improve its workability, steps are usually taken to ensure a

small grain size, one way of doing so being to replace a single-wall Ta sheath by multiple layers of Ta foil in the form of a so-called "jellyroll". From a metallurgical standpoint Nb itself could be employed as a diffusion barrier. However, if left untreated, the reaction layer which would form on it could be a possible source of instability; since as pointed out long ago by WIPF [129], a hollow tube is less flux-jump stable than a solid tube of the same diameter. This is because the moment an increasing magnetic field reaches the inner wall, any further increase of it will be accompanied by a sudden demand for the extra flux needed to establish a uniform field (rather than a continuation of the flux gradient) in the bore. To eliminate this as a potential difficulty the reaction layer would need to be suppressed. The Harwell group have succeeded in "poisoning" the bronze with regard to the Nb_3Sn reaction by arranging for the Nb barrier to be separated from the bronze by a thin layer ($20 \sim 30$ μm^t) of commercial ~ 0.26 wt.% P phosphor-bronze [6, p. 41]. The properties of the Nb/Nb_3Sn-shell diffusion barrier have been the subject of a recent magnetic study by SHEN [130]. Although no flux-jump instability was observed with the untreated Nb-base barrier, considerable flux trapping was encountered which of course could be reduced by P-poisoning with the aid of an additional phosphor bronze layer. The use of Nb as a diffusion barrier reduces fabrication difficulties in bronze-process composites and leads to corresponding cost savings. However, both untreated and P-poisoned Nb/Nb_3Sn-barrier multifilamentary composites do appear to possess higher hysteretic losses than does the same conductor processed with Ta barriers. Whether this will be reflected significantly in the *total* loss of the magnet system will depend, of course, on the details of the conductor and magnet design.

(c) A.C. Loss Characteristics. It has already been pointed out that the metallurgically based need for micron-size filaments automatically ensures minimal hysteretic a.c. loss. With regard to interfilamentary eddy-current loss, the residual bronze, after completion of the reaction heat treatment, has a higher resistivity then pure Cu and influences the filamentary

twist-pitch requirements in a manner comparable to that of the "dirty Cu" or the Cu-Ni of Cu/Ti-Nb-base composites. A.C.-loss requirements of *high-amperage* Nb_3Sn conductors can be satisfied by appropriate multistrand-cable design.

8.4.2 Flux Pinning and Optimization

Phenomenological nonmechanistic studies of flux pinning and the applicability of scaling laws to its magnetic field and temperature dependences have been undertaken by MATHUR *et al.* [131], SUENAGA and WELCH [6, pp. 131-142], and LUHMAN [108], who has developed some empirical equations for fitting the reduced-field dependence of the bulk-pinning force.

Recognizing that in Nb_3Sn ribbon, contributions to flux pinning could be made both by grain boundaries and the second-phase particles that are introduced for the purpose of grain-size refinement, SCANLAN *et al.* [121] set out to evaluate the relative importance of their roles. In order to do so, the critical-current densities of ribbons were compared with those of multifilamentary conductors having similar grain sizes and in which second-phase particles did not have to be added to achieve the necessary grain refinements. The results of this work led to the conclusion that grain boundaries serve as the principle flux pinners and that if second-phase particles increase the bulk pinning strength, they do so through the medium of grain refinement. This conclusion was reiterated by SCHAUER and ZIMMERMANN [132] who went on to note that the maximum volume pinning force in multifilamentary Nb_3Sn increased monotonically with grain-boundary density for grain diameters in the range 2000 to 300 Å (cf. Figure 8-6).

As pointed out by BARTLETT *et al.* [133], who studied stress effects in multifilamentary wire, flux pinning in Nb_3Sn can be augmented by the effect of strain fields. Furthermore, as suggested by LUHMAN and SUENAGA [134], the flux pinning in Nb_3Sn shows signs of enhancement by the product of martensitic transformation induced by the differential contraction that occurs between the Nb_3Sn and its bronze coating. In support of this contention, MADSEN and HILLS [135] demonstrated that this additional pinning could be made to disappear when the compressive stresses in the Nb_3Sn were released by an etching away of the bronze (cf. also [136]).

Returning to the influence of grain size on bulk pinning strength, SHAW's work [122] referred to above (cf. Figure 8-60) has suggested the existence of an optimal grain size centered at about 450 ∿ 650 Å. Subsequent workers have tended to agree with this; for example WEST and RAWLINGS [137], in a transmission electron microscopy study of commercially produced multifilamentary Nb_3Sn composites, have found the pinning force to be maximum at a grain size of about 800 Å. PANDE and SUENAGA [138] have produced a flux-pinning model to represent the same problem but have coupled the peak in F_p *versus* grain size with its attainment of five times the flux-lattice spacing. This result is reminiscent of matching theory, a general discussion of which, but within a different context, has been offered by SCHULTZ and FREYHARDT [139].

All workers agree that a fine grain size is essential to strong bulk flux pinning -- at least in the magnetic field range where pinning is important. However, at very high fields when flux-lattice shear reduces the effectiveness of any optimal pinning arrangements, the critical-current density at a given field becomes dominated by H_{c2} which in turn is a function of the degree of stoichiometry, hence order, of the A15 compound. Thus, as SCHAUER and SCHELB [123] have discovered, in order to optimize J_c over the entire field range a two-stage final heat treatment should be administered, for example: 524 h/625° C followed by 30 min 800° C. The first reaction converts the Nb to fine-grain Nb_3Sn, while the second heat treatment serves to increase both T_c and H_{c2} *via* an improvement in the stoichiometry of the previously formed compound.

8.4.3 Multicomponent Alloying

Numerous attempts have been made to improve on the properties of bronze-process Nb_3Sn through the addition of alloying elements either to the bronze matrix, the outside of the conductor if external diffusion is employed, or to the Nb core. The result sought has either been a direct improvement in the superconducting properties of the Nb_3Sn reaction layer or an indirect influence on its critical current density *via* grain size refinement. Simple-metal and metalloid additions which have been investigated

include Mg, Zn, Al, In, Ga, Tl, Ge, Si, and Pb. Whether or not these were expected to substitute for the Sn in the Nb_3Sn layer, this in fact seldom happened; indeed, as pointed out by LIVINGSTON [140], alloying elements are more likely to be incorporated into the Nb_3Sn if they are initially present in the Nb component. This excludes the elements referred to above which are only sparcely soluble in Nb, and in any case would, if present, severely harden it. On the other hand neighboring transition elements will dissolve readily in Nb without severely reducing its ductility. Examples are the group-IV elements Ti, Zr, and Hf, and the group-V element Ta, the influences of all of which on the superconducting properties of the reaction layer have been examined.

(a) Transition-Element Additions to Niobium. In earlier studies in which considerable attention was devoted to the effect of Hf additions to the Nb core [6, pp. 1-15][141][142], and more recent ones dealing with all three group-IV transition elements, [143] TACHIKAWA has reported that 2-at.% (and 2 ~ 5 at.% in the case of Hf) additions increase the rate of growth of a fine-grained reaction layer by factors of 2 to 3. Ti, which is more soluble in Nb_3Sn than either Zr or Hf, can be introduced into the reaction layer either from the core or, even more readily it seems, from the matrix. In the latter case, of course, there is no reduction at all in core ductility. In an intercomparison of the effects of Ti, Zr, and Hf additions on the properties of the reaction layer, TACHIKAWA *et al.* [144] have noted that these three elements, when present in small amounts, all increase the T_c of Nb_3Sn by a few tenths of a degree, maxima occurring at 2 at.% (Ta and Zr) and 5-10 at.% (Hf). Aided by increases in both ρ_n and T_c, increases in H_{c2} of about 4 T result from the additions of Ti and Hf. With regard to J_c, whose high-field value is improved by the presence of the group-IV elements, Ti produces a larger effect than either Zr or Hf. At 15 T the J_c of Nb-Ti(2 at.%)/Cu-Sn (7 at.%) is several times larger than that of the basic Nb/Cu-Sn(7 at.%).

The effects of Zr additions to the starting Nb have also been studied by SUENAGA *et al.* [120][123] whose results have been discussed by LUHMAN [5, p. 248]. It turns out that whereas the J_c of *undoped* Nb_3Sn

decreases relatively rapidly with increasing reaction-layer thickness, when Zr or ZrO_2 are present, although the initial J_c is severely depressed, the decrease is much less rapid, so much so that the undoped and doped J_c *versus* layer-thickness curves intersect (at about 1.5 μm for J_c (4T) and about 3 μm for J_c (10T)). It seems that the initial heterogeneously nucleated Nb_3Sn is coarsely granular, hence of relatively low J_c, but that the presence of the dopant stabilizes the grains against rapid growth as the heat treatment continues. The influence of Ta additions (up to 34 at.%) to the Nb cores of laboratory monofilaments were first investigated by LIVINGSTON in fields of up to 9 T [140]. As a result it was discovered that small additions of Ta increased the high-field critical-current density of Nb_3Sn and decreased its field dependence, observations which held the promise of considerable improvement to the high-field properties of technical multifilamentary superconductors. The beneficial effects of Ta additions to the Nb cores have been confirmed by ROSNER *et al.* [6, p. 75] who have also pointed out that the increases in J_c so obtained are in addition to any improvement which might be won through the use of a high-Sn bronze. In repeating these experiments using cores of Nb, Nb-3Ta, -7Ta, -10Ta, and -20Ta, SUENAGA *et al.* [145] were unable to confirm any Ta-induced improvement in J_c at the 10-T level of applied transverse field but did show: (i) that H_{c2} increased monotonically with increasing Ta content, although T_c decreased; (ii) that J_c (16T) underwent an increase by a factor of about 2 in response to the addition of 7 wt.% Ta to the Nb core. Such a high-field J_c enhancement was regarded as being an important step in the development of Nb_3Sn conductors for fusion magnets.

(b) Simple-Metal Additions to the Bronze. In an extension of the study referred to at the beginning of the previous section, TACHIKAWA noted that Hf additions to the core plus Ga additions to the bronze increased T_c by 0.6 - 0.9 K and H_{c2} by 6-7 T which of course resulted in an increase in the high-field (> 15T) current-carrying capacity [6, pp. 1-15][141][142]. With regard to the influence of Ga itself, HORIGAMI *et al.* [146] have shown as a result of measurements in fields of up to 18 T that its presence has

the effect of increasing H_{c2} and with it the high-field J_c. In an extension of this investigation to fields of up to 23.5 T, DEW-HUGHES and SUENAGA [147] attempted to produce conductors which combined the superior low-field J_c of undoped Nb_3Sn with the improved high-field performance of the Ga-containing material. In some cases small amounts of Al (125 at.%), Sn (2.2 at.%), and Zr (1 at.%) were added to the Nb core and Al to the Cu-Sn-Ga matrix, whereupon it was found that the presence of 1 at.% Zr in the core led to the highest J_c. It was confirmed that Ga could be incorporated into the reaction layer up to a maximum of 3 at.% and that it raises H_{c2} (4.2 K) from 19 $\sim$ 20 T to $\sim$ 25 T while having little effect on T_c.

Of course the penalty for adding Ga to the bronze matrix is a reduction in its Sn level if the total solute concentration is to be confined within the range of solid solubility, but this is no longer a problem if external diffusion is employed.

The results of a detailed study of the effect of 0.5 at.% addition to Mg to the bronze matrix have been reported by TACHIKAWA [6, pp. 1-15][141]. It was found that although no appreciable changes in the T_c or H_{c2} of the reaction layer could be detected its rate of growth was considerably enhanced leading to a doubling of its thickness for a given reaction time. As a result of the presence of Mg an increase in the critical current was noted due primarily to an increase in the thickness of the reaction layer but assisted by a small though significant increase in its J_c.

AKIHAMA *et al.* [62, pp. 37-46][148] have reported on the effects of Al, Ga, In, Tl, and Pb additions to Nb_3Sn. Experiments on arc-melted samples showed that, although T_c was practically unaffected, in each case H_{c2} underwent an increase due to an increase in the normal-state resistivity, a result which augured well for corresponding improvements in the high-field critical-current density. Then after selecting In and Pb as additives, the work was extended to a study of the properties of surface-diffused tapes which were then also found to exhibit rapid increases in H_{c2} (4.2 K) at small doping concentrations. Finally, some preliminary comparative measurements on the influence of In on the critical current of surface-diffused tapes were made, with encouraging results. With regard to bronze-processed

material, DEW-HUGHES and SUENAGA [147] have reported that of the various third elements, Zn, Al, Ga, In, Si, Ge, and Pb which have been added to the bronze, the only one which has been observed to become incorporated into the reaction layer (cf. LIVINGSTON [140], above) is Ga the effects of which have already been described.

8.4.4 Kirkendall Porosity

According to KIRKENDALL†, atomic diffusion across the boundary of an A/B couple takes place not by the direct interchange of A- and B-type atoms (which would require an equality of the diffusion coefficients) but as independent events involving an exchange of the two types of atom, respectively, with vacancies. After interdiffusion has gone on for some time, residual vacancies tend to accumulate as macroscopic voids about small inclusions and, in the case of composite materials, at cold-welded interfaces. Thus, in two-stage multifilamentary composites, the Kirkendall effect, if unhindered, can be responsible for cracks along the interfaces between the primary filament colonies and for a splitting-off of what was once the can of the second-stage extrusion billet, especially if external-diffusion is employed.

EASTON and KROEGER [149], who appear to have been the first to draw attention to this problem, pointed out that void accumulation in the internal-bronze-processed multifilamentary conductor that they studied, could result in mechanical-property deterioration. They noted furthermore that the deterioration was aggravated by increases in the reaction time administered in attempts to increase the reaction-layer thickness and optimize its J_c. Drawing attention to successes obtained with void healing in Cu-Ni couples, EASTON and KROEGER predicted that void formation in Nb/bronze composites could be inhibited by the application of hydrostatic pressure during heat treatment.

As indicated above, the Kirkendall effect, if unchecked, is particularly serious in externally diffused bronze-processed conductors. However, COGAN *et al.* [150], working on the assumption that the voids which

---

† cf. primary references in this section.

produced such a catastrophic cracking-away of the outer layer of the strand during reaction, were nucleating at unidentified particles residing at the cold-welded interface lying just below the circumference of a strand, and that they could be dissolved-away by prior annealing, discovered that Kirkendall porosity in the reacted strand could be completely eliminated if heat treatments of 16 h at 450, 550, 650, and 750° C were administered prior to the application of the external Sn. But as pointed out by COGAN, ROSE *et al.* [151], in the most recent paper of their series, the pre-annealing approach although eminently successful in treating the typical small-diameter strand (diameter $\sim$ 0.25 mm) is not so for large-diameter composites and obviously inapplicable in conjunction with *internal-bronze* processing. For these the second alternative initially proposed by EASTON and KROEGER [149] must be put into operation. ROSE's group at M.I.T. discovered: (i) that depending on strand diameter, a critical external pressure existed above which void formation was eliminated, e.g., 300-500 psi for 0.25 $mm^{\emptyset}$ composites, rising to 1,000-2,000 psi for 0.5 $mm^{\emptyset}$ material; (ii) in reacted composites which were already porous, external-diffusion-generated external voids could be healed by a further heat treatment (10 h/650° C) under a pressure of 2,300 psi, while if the voids were internal (i.e., adjacent to the filaments) as in internal-bronze-process conductors, they could be eradicated by heat treatment (24 h/700° C) at a pressure of 15,000 psi -- a process known to the technical community as "hot isostatic pressing" or HIP.

SECTION 9

UNCONVENTIONAL A15 SUPERCONDUCTORS

9.1 Introduction

9.1.1 Origins of the Bronze Process

Nb_3Sn was the earliest A15 superconductor to be prepared in wire form. A mixture of Nb and Sn powders was packed into a Nb tube which was then drawn down to wire and heat treated at temperatures between 970 and 1400° C for up to 24 h to promote the formation of the desired compound [152]. Subsequently, the powder-metallurgical approach -- known as the "Kunzler method" after its originator-- was extended to the fabrication of solenoids by the "wind-and-react" technique in which a Nb-clad "green" mixed-powder wire was wound to its final form prior to reaction heat treatment. Kunzler's method, which was first described in 1961, was the precursor of the several powder-metallurgical approaches currently being used to prepare pseudomultifilamentary stabilized composite conductors. Coming quickly on the heels of the powder process was the discovery by SAUR and WURM [153] that a superconducting Nb_3Sn layer could be formed on the surface of a Nb wire by exposing it to either molten Sn or its vapor, a method which was to lead eventually to the GE and IGC methods for the fabrication of Nb_3Sn-ribbon conductor on a commercial scale. The RCA method in which superconducting ribbon was prepared by the chemical vapor deposition (CVD) of Nb_3Sn onto a Ni-base alloy (Hastelloy) substrate was first described by HANAK, STRATER, and CULLEN [109] in 1964. Subsequently, as indicated by ECHARRI and SPADONI in a review of Nb_3Sn-conductor fabrication [154], more elaborate ribbon-conductors, incorporating Cu for stabilization and stainless steel for strengthening, were to be developed.

The conventional method of producing multifilamentary A15 superconductors is the solid-state-diffusion process -- described in Section 8 -- in which rods of an unalloyed transition-metal (TM) imbedded in a Cu-alloy

matrix (say, Cu-SM) are drawn down to strand size before being heat treated to promote solid-state-diffusion accompanied by a reaction to convert the TM-cores to TM_3SM. In Japan, the solid-state-diffusional route to A15 superconductor processing had its beginnings in an early (1967) observation by TACHIKAWA [118] that the Ga-rich compounds formed on the surface of a V wire immersed in molten Ga could be more readily converted into the V_3Ga phase if the encrusted wire is plated with Cu before heat treatment for 10 h/700° C. Subsequently, based on this discovery, TACHIKAWA [155] went on to suggest that V_3Ga tapes and multifilamentary wires could be produced by "composite diffusion" rather than "surface diffusion" [6, pp. 1-15]. In the U.S. a solid-state-diffusion process for producing multifilamentary Nb_3Sn wire was first suggested orally by KAUFMAN and PICKETT at a meeting of the American Physical Society and again at the 1970 Applied Superconductivity Conference in Boulder, CO [156]. The first *explicit* account of the Tachikawa-Kaufman-Pickett method to be published in the general literature was by SUENAGA and SAMPSON who had applied their method to the preparation of V_3Ga [157] and V_3Si [158] multifilamentary composites. The history of these early endeavours has been described recently by SUENAGA [7, p. 202] who played an important role in multifilamentary A15 composite processing. It is clear, however, that no one person or group is to be assigned principal credit for the discovery of the solid-state diffusion approach to the preparation of multifilamentary A15 conductors; GEBALLE and HULM in review article [159] have attributed it to Tachikawa, however, it is generally referred to simply as the "bronze process".

9.1.2 Unconventional A15 Superconductors

As indicated in several places above, the bronze process had been successfully applied to the fabrication of Nb_3Sn, V_3Ga, and V_3Si in multifilamentary form. The other binary A15 compounds listed in Table 8-1 are not amenable to preparation by this process. Nb_3Al can be formed in various ways by the direct reaction of Nb with Al. Nb_3Ga can be formed by arc melting a mixture of the constituent elements, and was the first binary compound to exhibit superconductivity above 20 K [160], while A15 Nb_3Ge has been successfully prepared only by sputtering, under suitable conditions, onto a heated substrate [161].

For the purpose of the present discussion any method of A15 conductor preparation that does not involve rod-in-matrix bronze-type processing is referred to as "unconventional", an appellation which therefore applies to: (a) all methods of preparing Nb_3Al multifilamentary conductors; (b) a method of V_3Ga conductor preparation which utilizes precipitation from the concentrated binary solid solution; (c) all powder metallurgical approaches, including the "infiltration" methods, to the fabrication of pseudofilamentary conductors; (d) the so-called "*in-situ*" processing of Nb_3Sn and V_3Ga. Unconventional A15 filamentary conductor processing is motivated by several considerations: (a) with regard to Nb_3Al, whose H_{c2} is higher than that of Nb_3Sn, the bronze route is inapplicable. (b) Powder metallurgy using unalloyed constituents enables large area reductions to be achieved without intermediate annealing. It enables small additions of third and fourth elements, for the purpose of J_c optimization, to be easily made and it also enables very small diameter quasicontinuous filaments to be achieved, and offers the possibility of production-cost reductions. (3) The *in-situ* approach which may also lead to reduced production costs has been shown to yield a conductor with a very attractive high-field overall J_c and excellent strain tolerance.

A15 Nb_3Sn was of course first procduced (*ca.* 1960) using powder metallurgy. In their original paper, KUNZLER *et al.* [152] investigated the critical-current densities, after heat treatment, of Nb tubes filled with elemental powders. They also explored the properties of a mixture of powdered Nb_3Sn and 10% excess Sn powder (presumably to act as wetting agent and to react with the Nb tube), whereupon it was discovered that: (a) a stoichiometric mixture of Nb and Sn powder was preferable to an excess of Sn; (b) a starting mixture of elemental powders, with or without excess Sn, is better than the Nb_3Sn + 10% Sn mixture. Some of the more recent powder-metallurgical approaches to be described below might be regarded as hybrids of the Kunzler method with conventional bronze technology in that Cu powder is now the major ingredient of the starting mixture. A more direct descendant of the original Kunzler method is that, due to ELEN, van BEIJNEN, and

van der KLEIN [162][163]. Known as the ECN† technique their method consists of filling pure V or Nb tubes, imbedded in pure Cu, with powdered V_2Ga_5 plus 10 or 15% powdered Cu, or $NbSn_2$ plus 0 or 15% powdered Cu, respectively, performing mechanical reduction and re-bundling, if required, followed by final reaction heat treatment to form the desired A15 compounds.

Various forerunners of the *in-situ* method have been claimed. ROSE has for example pointed out [164] that CLINE *et al.* in 1963 used eutectic transformation in the Nb-Th system to produce, during rapid solidification, fine needles of Nb in a Th matrix. Subsequent swaging and wire drawing extended these needles into fine highly continuous filaments; it was also pointed out in the same paper [164] that VERHOEVEN, FINNEMORE, and others had produced highly regular arrays of Nb precipitate needles by directionally solidifying Nb-Th and Nb-Y alloys. It was not, however, until 1973 when TSUEI demonstrated that Nb or V particles after precipitation from a Cu-Sn or Cu-Si matrix could be extended into filaments by cold work and partially converted to Nb_3Sn or V_3Si by subsequent heat treatment [165][166] that interest in *in-situ* composites began to accelerate. It had needed the intervening invention of the *fabricated* superconducting composite to provide the necessary impetus by directing attention towards the advantages of the multifilamentary superconductor-in-Cu approach.

9.2 Powder Metallurgy

9.2.1 Process Parameters

As pointed out above the first successful process for A15 Nb_3Sn wire was powder metallurgical. At the time heat treatment temperatures within the range 970-1400° C were used to react the powder. It was later pointed out by TACHIKAWA [118] that the presence of Cu, in the form of a

† Netherlands Energy Research Foundation.

plated layer, could catalyze the solid-state reaction, in his case between the Ga-rich phases VGa_2 and V_3Ga_2 and the V cores. In subsequent powder-metallurgical processes, Cu powder has always been an important ingredient, usually for the purpose of providing a normally conducting matrix to support a network of A15-compound filaments, but occasionally to act as catalyst. FLÜKIGER *et al.* [167] have, for example, shown that the mixture Nb(81 at.%) + Sn(16 at.%) + Cu(3 at.%) could be reacted at 650° C. van BEIJNEN and ELEN have experimented with V tubes packed with V_2Ga_5 powder and 5, 10, and 15% Cu powder [162][168], V tubes packed with VSi_2 powder and 5 to 10% Cu [168] and Nb tubes packed with $NbSn_2$ plus 15% Cu [162].

In the powder metallurgical processing of A15 superconducting wire it is necessary to compact the powder while maintaining its purity, perform heat treatment to convert the green compact, or part of it, to the desired compound, and to provide mechanical support to the finished wire. The many years of process development have seen numerous changes in all of these parameters. In the early process stages the reactants need to be supported in some way. By compaction and sintering, the Nb powder can be formed into self-supporting porous rods [169][170]. This is the basis of the "infiltration" methods proposed by PICKUS and colleagues at the Lawrence Berkeley Laboratory. Otherwise the powder must be compacted into tubes of one kind or another. The tubing selected: (a) may enter into the A15 reaction, such as the Nb [162] [163][171] or V [162][168] tubes of the ECN process; (b) may be of Cu [167] [172][173][174] or a Cu-base alloy such as Cu-0.2 wt.% Zr [167][172] or Cu-1.8 wt.% Be [167][172][175][176] in order to provide support during the initial deformation and later to permit externally applied Sn access to the mixed-powder interior of the composite wire; (c) may be of some "structural alloys" such as MONEL [177], steel [178] or cupronickel [179], later to be removed by etching; (d) or may be of Zr-Cu [167] or Cu and lined with a Ta diffusion barrior [176] if the Sn is present internally and it is desired to incorporate unalloyed Cu into the composite for the purpose of dynamically and cryostatically stabilizing the conductor.

Powders used in the ECN process, to be discussed below, are VSi_2 with or without Cu powder as catalyst [168], $NbSn_2$ with [162] or without [163] Cu as catalyst, and V_2Ga_5 with 5-15% Cu as catalyst [162][169]. The more "conventional" powder processes have employed mixtures of: (a) Cu and Nb powders [167][173][178]; (b) Cu, Nb, and Sn powders [167][175]; (c) Cu, Nb, and Sn-35Cu powders [175]; (d) Cu and Nb-4Ta or Nb-7Ta powders [175]; (e) Cu, Nb-7Ta and Al (0.5 wt.%) powders [175]; (f) Cu, Nb, and Al ($\sim$ 1wt.%) or Mg powders [180][181]; (g) Cu, V, and Al (2 at.%) or Mg powders [182][181]. Processes for Nb_3Al and related superconductors have used mixtures of: (a) Nb and Al powders [176]; (b) Nb, Al, and Si powders [183]; (c) Nb, Al, and Ge powders [179][183].

The aim of much of the powder-metallurgical conductor development has been to produce a prefabricated equivalent of the "*in-situ*"-type of conductor (to be discussed below). Materials and process conditions have been chosen so as to enable the Nb-powder component of the mixture to be deformed into long submicron-diameter quasicontinuous filaments. As with the conventionally processed A15 conductors the purpose of the small filament size was to enable all the Nb to be consumed during a solid-state reaction designed to produce a thin ($\lesssim$1 μm thick), hence high-J_c, reaction layer. By way of contrast the ECN technique has been shown to be capable of yielding thick ($\sim$ 30 μm^{ϕ}) fully reacted high-J_c A15 filaments [171].

The four standard powder-metallurgical processes intended for the production of A15 superconductors are the infiltration and ECN processes referred to above, as well as both hot ($\sim$ 1000° C) and "cold" ($\sim$ 500° C) powder processing. These methods and their relative advantages, which have already been critically reviewed by FONER [174][184], are considered briefly below.

9.2.2 The Infiltration Process

The development of the infiltration process for producing ribbons of Nb_3Sn and wires of Nb_3Sn, $Nb_3(Al,Si)$ and $Nb_3(Al,Ge)$ has been reviewed by PICKUS [170].

To product a flexible ribbon conductor, Nb powder in sizes ranging from 15 to 53 μm, prepared by the hydride-dehydride process, was roll-compacted to tape with a thickness of 0.56 mm and a porosity of about 30%, after which it was sintered for 3 min/2250° C in a vacuum of 4×10^{-5} torr. Its post-sintered porosity of about 25% ensured a pore-density greater than the percolation limit (of 15 volume %) and consequently a sponge-like structure of interconnected cells which could become completely filled with molten Sn after bath immersion for 1 min at 850° C. After further cold rolling the infiltrated tape was heat treated for 3 min/950-970° C; the resulting Nb_3Sn microribbons (typically 30 μm in width and 5 μm thick) had a T_c of 18.1 K and contributed an overall 4.2-K J_c of close to 10^5 A cm^{-2} at 10 T.

Wire conductors, according to HEMACHALAM and PICKUS [169][170], were prepared by first compacting 99.9% pure Nb powder (37 to 44 μm size) at 25-30 ksi into self-supporting rods, and sintered them for (10-15) min/(2250-2300)° C in a vacuum of $\sim 6 \times 10^{-5}$ torr. These were immersed for 30 sec in a molten Sn bath at 700° C, encased in monel or Ta-lined Cu, and reduced to wire before reacting for from 1 min to several hours at temperatures of 700° C to 1200° C in an Ar atmosphere. Critical current densities, normalized to the area of the 0.3 mm^{ϕ} composite cores of the Ta- or monel-clad wires, were measured as functions of applied transverse magnetic field and heat-treatment variables. At 16 T, for example, 4.2-K J_c's of about 4×10^4 A cm^{-2} were obtained after 120 min/800° C or 2 min/950° C.

In order to produce $Nb_3(Al,Ge)$ and $Nb_3(Al,Si)$ wires by the infiltration method, immersion of sintered Nb rods in molten baths of either the Al-Ge eutectic at about 600° C or the Al-Si eutectic at 580° C, was followed by reaction heat treatment at temperatures of up to 1700° C and post-reaction annealing at 750° C.

9.2.3 The ECN Process

ELEN and van BEIJNEN of the Netherlands Energy Research Foundation (ECN) have pioneered a powder-metallurgical method for the preparation of stabilized multifilamentary A15 composites with fully reacted filaments $30 \sim 70$ μm in diameter [171]. Initial studies explored the feasibility

of producing Cu-clad filamentary V_3Ga [162][168], V_3Si [168] and Nb_3Sn [162] [163][171] conductors. As indicated in the introductory section, the approach consisted of placing SM-element-rich TM-SM powders such as V_2Ga_5, VSi_2, and $NbSn_2$, either with or without the addition of Cu powder as possible catalyst,† in V or Nb tubes imbedded in pure Cu. Under moderate-temperature heat treatment (550-625° C for V_3Ga [162]; 800-1000° C for V_3Si [168]; 625-700° C for Nb_3Sn [171]) a rather complicated reaction takes place at the interface between the powder and the tube. For example in the $\rightarrow V_3Ga$ reaction [162] Ga and some Cu first diffuse into the V tube producing an unspecified ternary compound, say "X"; V_6Ga_5 then forms at the interface between X and V, growing into both; then V_3Ga is formed between the V_6Ga_5 and the V. Similarly in the $\rightarrow Nb_3Sn$ reaction [163] the compound Nb_6Sn_5 first forms at the interface between the $NbSn_2$ powder and the surrounding Nb tube; this is followed by Nb_3Sn growth at the interface between the Nb_6Sn_5 and the remaining Nb. In the latest of a series of four papers presented at the Applied Superconductivity Conferences in 1974 [168], 1976 [162], 1978 [163], and 1980 [171], ELEN *et al.*, after describing the laboratory preparation of 7-filament and 19-filament strands with filament sizes ranging from 31 to 75 μm and 4.2-K J_c's at 10 T of about 5×10^5 A cm^{-2}, discussed the possible scale-up of the ECN technique towards the fabrication of long lengths of stabilized multifilamentary Nb_3Sn through the hydrostatic extrusion of 150-kg composite billets.

9.2.4 Cold Powder Processing

The cold powder processing method, introduced to MIT by FLÜKIGER has been discussed in a series of articles by FONER and colleagues; references [167], [172], [173], [174], [175], [176], [184], [185] are a partial list. In the basic "cold" powder process, a mixture of high-purity Nb powder -- such

---

† According to ELEN *et al.* [162] Cu does not catalyze either the $\rightarrow V_3Si$ or $\rightarrow Nb_3Sn$ reaction.

as that produced by the hydride-dehydriding of zone-refined Nb -- and Cu powder are packed into a monel tube and cold-compressed to a density of about 80% theoretical; after being electron-beam sealed the resulting capsule is extruded at a temperature not exceeding 100° C and rolled to ribbon. After grinding away the edges to expose the Nb + Cu interior, the ribbon is electroplated with Sn, diffusion heat treated, and reacted at 650 to 850° C to form the Nb_3Sn compound [173]. As described in subsequent reports the basic process quickly underwent improvement and development while preserving its essential characteristics, *viz*: (a) the use, in the starting billet, of high-purity Nb powder with its potential for extreme elongation; (b) the maintenance of "low" temperatures (at least below 500° C in the case of large billets [167] during the deformation processing. The proclaimed advantages of cold powder processing are [167]: (a) the ratio of Cu to Nb can be varied over a wide range; (b) the technique is not restricted to "bronze-process" ingredients; (c) very fine filaments are achievable without the need for rebundling (as in conventional processing) or for dealing with the problems of casting a "homogenous" finely precipitated starting billet as in the *in-situ* method, to be described below, which powder methods were intended to replace.

In the initial laboratory studies it was found that the material of the jacket needed to be monel rather than Cu in order for the Nb to be adequately deformed. Subsequently, to ensure adequate Nb-powder elongation, jackets of Cu-0.2 wt.% Zr and Cu-1. wt.% Be were employed. These, like monel, were stronger than Cu but possessed the additional advantage of being permeable to Sn [167][186], although it was also later recognized that Cu jackets could in fact be used provided sufficiently large area reductions were to be administered. A typical set of critical-current results is given in Figure 9-1 which indicates, for example, that the average 4.2-K J_c (excluding jacket) for a Cu-35Nb-19Sn composite processed in a Cu-Zr jacket is 6×10^2 A cm^{-2} at 15 T while that of Cu-35Nb-26Sn processed in the stronger Cu-Be jacket is 1×10^4 A cm^{-2} in the same field.

An additional advantage of cold powder processing is that Sn powder can be mixed in with the starting Nb and Cu powders thereby eliminating the need for external Sn plating and diffusion and removing the

attendant strand-diameter limitations of about 0.25 ∿ 0.5 mm [175]. In keeping with the so-called "one-step" philosophy, and at the same time to ensure that the component powders possessed equivalent hardnesses during processing, the Sn powder was later replaced by powdered Sn-35Cu alloy [175]. In a further development of the powder process [175] unalloyed Nb powder was replaced by Nb-4Ta and Nb-7Ta, in order to increase the high-field J_c following the work of LIVINGSTON [140] with conventionally processed composites, cf. Section 8.4.3(a).

In laboratory-scale experiments, powder diameters of about 40 μm were used. But with scale-up in mind much coarser powders, about 150 μm in size, can be contemplated. These have the advantage of a lesser propensity towards contamination by oxygen [176].

Cold powder processing has also been employed in the laboratory-scale preparation of Nb_3Al [176], $Nb_3(Al,Ge)$ [179][183], and $Nb_3(Al,Si)$ [183] composites. The elementary powders were mixed in the correct proportions and loaded into either Cu [176] or cupronickel [179] tubes prior to cold working by swaging and rolling, or wire drawing, after which high-temperature reaction heat treatments were administered -- for example several hours at 700 to 1000° C under He for Nb_3Al [176] and 15 sec/1700° C under 10^{-5} torr, followed by many hours at 725° C (after removal of the cupronickel sheath) in the case of $Nb_3(Al_{0.75}Ge_{0.25})$ [179]. Some typical results for Nb_3Al are given in Figure 9-2.

9.2.5 Hot Powder Processing

The term "hot" refers to the fact that in the powder-metallurgical process advocated by FREYHARDT and colleagues at the University of Göttingen [178][181][182][186] the initial billet extrusion, prior to the subsequent wire-drawing operations which are all performed at room temperature without intermediate anneals, takes place at temperatures of about 800 to 1000° C. At first reported by SCHULTZ, BORMANN, and FREYHARDT in 1978 [178] the method consisted of compressing a mixture of Cu and Nb (∿ 6 μm) powders into a steel container and preheating them for 2 h/> 1000° C prior to extruding

at about 1050° C. After removal of the jacket, the extruded product was cold drawn to an area reduction ratio of 1370, galvanically plated with Sn and reaction heat treated at temperatures 400 to 750° C. Unfortunately, because of the oxygen pickup inherent in this version of the hot-compaction process the Nb particles underwent serious hardening† and failed to elongate sufficiently to confer the desired degree of interfilamentary conductivity. Studies of the microhardness and transition temperature of the processed Nb revealed that oxygen, initially adsorbed on the particle surfaces, had dissolved to the extent of 2 to 3 at.%, its equilibrium solubility at 1050° C, during hot extrusion [187]. As a result, the 4.2-K J_c in fields as low as 5 T was less than 10^3 A cm^{-2}. Subsequent research quickly removed the obstacle of oxygen contamination and led to a process with considerable potential for commercial scale-up.

The remedy selected was to provide a means of *in-situ* purifying the Nb during hot extrusion. The process then acquired important advantages over the cold-powder route in that it was no longer restricted by the need for ultrahigh purity in the *starting* powder; a second advantage of hot extrusion is that it can take place at considerably lower extrusion pressures.

As *in-situ* reducing agents the elements Al, Zr, Hf, Mg, and Ca, and their relative affinities for oxygen, as listed in Table 9-1, were considered. Generally about 1% of them would be sufficient to bind all the free oxygen in the compact. It was found, however, th . although the binding enthalpies for oxygen of Zr, Hf, and Ca were higher than that of Al, these elements were relatively ineffective in the role expected of them. This had to do, apparently, with the fact that since the former three elements are severe hardeners of Cu, as evidenced by the existence of the intermetallic compounds Cu_3Zr, Cu_5Hf, and Cu_5Ca, their presence inhibited the co-deformation of the Nb powder particles, whereas this was not the case for Al, and indeed Mg, which are soluble in Cu at the levels under consideration. An example of the ductilizing influence of the addition of 1 wt.% Al to a Cu-plus-20 wt.% Nb

---

† To a Vickers hardness of 350 kg mm^{-2} as compared to the 90 kg mm^{-2} of large-size high-purity powders [176].

TABLE 9-1. BINDING ENTHALPIES OF OXYGEN IN VARIOUS OXIDES [187]

Oxide	Al_2O_3	ZrO_2	HfO_2	MgO	CaO
Binding enthalphy kJ/(g atom O)	536	540	570	603	636

powder compact is given in Figure 9-3(a); Figure 9-3(b) which serves as a control, depicts a typical Cu-plus-undeformed Nb-powder microstructure. The oxide particles do not appear to have impaired the deformability of the composite. Any excess Al or Mg dissolves in the matrix.

Of course in the hot-powder approach, the Sn must be applied by external diffusion at the end of the process. In this regard the method does suffer from the strand-diameter limitation referred to above. Heat treatments at temperatures of 500 to 650° C have been used for times of up to eight days depending on the Nb-filament diameter [187]. Some typical results are presented in Figure 9-4 in which it can be seen, for example, that for Cu plus 20 wt.% Nb plus up to 2 wt.% Al the 4.2-K J_c was 7×10^4 A cm^{-2} at 10 T and 1×10^{-4} A cm^{-2} at 15 T.

Since the binding enthalpy of V to oxygen is similar to that of Nb, the hot-powder process with about 2 at.% Al or Mg gettering can be equally well applied to the production of Cu/V composite strands prior to Ga plating, and reaction heat treatment at 500-600° C for several days. As expected the high-field 4.2-K J_c's of the V_3Ga wires were considerably greater than those of Nb_3Sn, Figure 9-4. For example, typical values are $(2 \sim 4) \times 10^4$ A cm^{-2} at 16 T.

The strong gettering action of Al augurs well for the production of Nb_3Al composites using hot powder metallurgy, an approach which does not yet seem to have been adopted. As in cold-powder processing some interest has been taken in improving the high-field J_c by replacing the unalloyed Nb powder by Nb-Ta [180]. The effects of adding extra simple-metal components to the "bronze" (i.e., to the Sn plating) have also been examined. Although the influence of In on the high-field J_c is slight, Ga in moderate amounts is extremely beneficial, Figure 9-5.

An intercomparison of the 4.2-K J_c's of wires prepared by various methods is presented in Figure 9-4 with reference to which it can be stated that hot powder processing compares very favorably with the alternative "conventional" and "unconventional" approaches. Furthermore, because of the lower extrusion pressures possible with the hot process, large billets ($\sim$ 100 kg) can be extruded at reduction ratios of up to about 40:1. The

product can then be further reduced at ratios of 10^3:1 to 10^5:1 without further annealing to yield strands containing filaments of diameters between 0.1 and 0.5 μm. Such small filaments are amenable to complete conversion to the A15 phase at temperatures as low as 500-600° C leading to high overall J_c's especially in the V_3Ga composites [182].

9.3 Solid-State Reaction Between Elements

Several attempts have been made to prepare Nb_3Al conductors from their bulk unalloyed constituents. Starting procedures involved the insertion of Nb rods into an Al matrix [188] or Al rods into a Nb matrix [189]. The former approach was adopted by HAFSTROM [188] who assembled seven Nb rods in an Al matrix encased in a Nb jacket, swaged the composite down to wire, and subjected it to a short reaction heat treatment at 1800-1900° C in an induction coil, followed by an ordering heat treatment of 48 h/750° C. 4.2-K J_c's in excess of 10^5 A cm^{-2} at 7 T were obtained. In experiments on Al-plated monofilaments reacted at 1900° C and ordered at 750° C it was found that 1% of Zr added to the Nb accelerated the growth of the Nb_3Al layer [188]. Adopting the converse component-assembly approach EAGER and ROSE [189] prepared multifilamentary composites consisting, before reaction heat treatment, of Al rods imbedded in a Nb-1% Zr matrix. To start with, ¼-in.$^{\emptyset}$ Al rods were inserted into ¼-in. I.D. x ½-in. O.D. Nb-1% Zr tubes which were then reduced by swaging to 1.4 $mm^{\emptyset}$. Nineteen of these packed into a monel tube were again swaged down and further reduced by wire drawing. At this stage the monel could be removed by etching and the composite reacted for 1 h/1600° C to form the A15 phase. Of course successive stages of rebundling and drawing could be administered in order to produce finer and finer threads of Al. The finer the filament, the lower the reaction temperature hence the smaller the grain size of the A15 layer and the higher its J_c. Indeed 36,000 filaments packed into a tape of dimensions 2.5 x 0.1 mm^2 were found to undergo A15 reaction after only 10 min/1100° C. An interesting property of the Al-in-Nb approach is that, on account of the relatively high

diffusivity of the Al, longitudinal pores appear at the sites of the original Al wires [189] an effect which could undoubtedly be exploited to provide interconnecting channels to facilitate the access of liquid He to the A15 layers.

TOGANO and ROSE [190] have used a modification of the Al-in-Nb procedure in order to prepare multifilamentary $Nb_3(Al_{0.75}Ge_{0.25})$. Rods of high-purity Al-Ge alloys were prepared for insertion into 1/8-in. I.D. x 1/4-in. O.D. Nb tubes. A group of seven of these were packed into another Nb tube which was swaged and drawn to 0.5 mm^{ϕ} prior to a reaction heat treatment of 1 min/1800° C, following which T_c could be optimized by a further anneal of 1 week/750° C. As with bulk Nb_3Al, the J_c tended to be rather low due to the excessive grain growth which accompanied heat treatment at such a high temperature [190]. But as indicated above, this tendency can be combatted by reducing the scale of the composite to enable the reaction to take place at a significantly lower temperature. Some Nb-Al microcomposites which take advantage of this principle are considered in the next section.

9.4 Laminated Microcomposites

As indicated above, the temperature needed to form the A15 compound by solid-state reaction can be significantly reduced if the Nb and Al diffusion distances are decreased by reducing the geometrical scale of the composite. Thus, if the Al (in Nb) or Nb (in Al) rods of the previous section are replaced by multiple laminates of alternate Nb and Al foils the reaction temperature can be halved. In the pioneering experiments of CERESARA *et al.* [191], thin foils of Nb and Al wire laid one on top of the other and tightly rolled about a small copper cylinder to form what in the U.S. is referred to as a "jellyroll" [192]. This roll was inserted into a Cu tube and the assembly was rod rolled and wire drawn to a diameter of 0.2 mm. During reaction of 750-950° C the entire jellyroll was consumed and replaced by a mixture of A15 Nb_3Al and unreacted Nb [191]. The optimal

heat treatment was 6 h/850° C and the process yielded a 4.2-K J_c of 1.8 x 10^5 A cm^{-2} at 6.4 T in the reacted zone. The next step consisted of taking seven or nineteen of these jellyrolls and inserting them into the appropriate number of holes drilled in a solid Cu cylinder prior to reduction to some final strand diameter of, say, 0.4 mm [193][194]. In the experiment described by CERESARA *et al.* [193][194] the unreacted composite contained jellyrolls about 50 μm in diameter composed of helical layers of Al and Nb of thicknesses 0.2 μm and 0.8 μm, respectively. Heat treatments of several hours at temperatures of 800, 850, 900, and 950° C served to almost completely react the Al to A15 Nb_3Al. Again a 4.2-K J_c in the compound of (1-1.5) x 10^5 A cm^{-2} at 6.4 T was obtained. Subsequently, with a view to controlling the stoichiometry of the A15 compound and the fraction of unreacted Nb, ANNARATONE *et al.* [221] investigated the superconducting properties of the jellyroll-base Nb-Al composite as a function of Al-foil thickness.

In the meantime, LARSON, LUHMAN, and MERRICK [195] had been exploring an alternative technique for producing microlaminates of Nb/Al as well as Nb/Sn. The technique selected was dry ball milling in which a charge of Al (or Sn) and Nb powders was milled using Nb grinding balls. During such a milling process, particles become fractured and re-cold-welded together again causing mechanically alloyed laminated particles to be created. As grinding proceeds a steady-state condition becomes established wherein, although the composite particle size tends to remain constant, the internal structure is continually being refined. When grinding was deemed complete, the mechanically alloyed powders were packed in Ta-lined Cu tubes which were then drawn down to 1 $mm^{\emptyset}$ prior to moderate-temperature heat treatment. The Nb-plus-Sn composites were heat treated for (1-10) h/(750-850)° C to produce a J_c in the wire of 3.75 x 10^5 A cm^{-2} at 4 T. The Nb-plus-Al composites after heat treatment at temperatures between 800 and 950° C yielded T_c's and 4.2-K J_c's similar to those reported by CERESARA *et al.* [191] for jellyroll-processed material.

In further extensions of this investigation into the properties of jellyroll microcomposites CERESARA *et al.* [194] performed small-coil testing,

ASDENTE *et al.* [196] investigated a.c. losses, while DEW-HUGHES [192] measured high-field J_c's in order to determine whether the low-field promise of these materials was realized at fields of up to 21 T, but with disappointing results.

In a recent extension of the method of CERESARA *et al.*, workers at Teledyne Wah Chang, Albany (TWCA) have developed what they refer to as the "modified jellyroll method". In this, the contents of an entire extrusion billet are assembled by simply rolling up a laminate of Cu foil and "expanded" Nb foil, along with bronze and/or Ta foils if desired, Figure 5-5. After metalworking, the longitudinally directed segments of the Nb mesh become extended into long fine filaments. Although mechanically cross-connected at regular intervals the separation between the points of contact is sufficiently great (>> 10 m) that currents which might otherwise be induced to circulate around the continuously interconnected pathways of the mesh, can easily be limited by twisting [197].

9.5 The Solid-State Precipitation Process

The "solid-state precipitation" process [198] is defined as one in which a homogeneous, concentrated, quenched, bcc TM-SM solid solution, after deformation to ribbon or wire, is induced to form in a controlled way by moderate-temperature heat treatment, a near-stoichiometric A15 TM_3SM precipitate. It has been recently advocated, with reference to prior work, as a processing method for A15 superconductors by MORRIS' group at the Lawrence Berkeley Laboratories (LBL). Variations of the method have of course been considered from time to time by others. It has been applied both to V_3Ga for which the bronze process is successful and to Nb_3Al for which it is not.

With regard to the latter, WEBB has shown that the bcc disordered stoichiometric alloy, preserved during quenching from 1925° C, can withstand without fracture a variety of cold-working operations prior to being annealed

for about half an hour at 950 or 1700° C, during which conversion to the A15 structure takes place [199]. The LBL method might be regarded as a sophisticated development of this approach [200][201]. It starts with an off-stoichiometric solid solution, of composition about Nb-Al (18 at.%), formed by arc melting, homogenization for 1 h/1930° C, and quenching into iced brine [200]. Samples were then warm-rolled to tape at 300-400° C and precipitation heat treated according to the following prescriptions:

Nb-Al (17.7 at.%): 90% deformation plus (3-120) h/750° C;
Nb-Al (17.7 at.%): 99% deformation plus 2 h/750° C;
Nb-Al (18.8 at.%): 90% deformation plus 6 h/750° C.

The results were semicontinuous networks of fine equiaxed A15 particles, 300-1000 Å in size, in a Nb matrix. 4.2-K J_c's achieved were 5×10^3 A cm^{-2} at 10 T to 10^4 A cm^{-2} at 14 T depending on the degree of deformation-by-rolling and the Al concentration.

PICKUS *et al.* [170] have developed this idea into a continuous conductor-fabrication process. They start with an Al rod clad in a Nb matrix as in some of the methods discussed in the previous section. The binary composite is swaged and drawn down to wire, in-line heated for 30 sec/1950° C to form a core of concentrated bcc Nb-Al solid solution and rapidly He-gas quenched. The alloy can then be directly age-transformed to the A15 phase by annealing at 850 to 1000° C as in the method just described. Alternatively the solid solution can be deformed by rolling; this results in a fine network of twins which, since they act as nuclei for A15 precipitation during subsequent aging are responsible for an *in-situ* filamentary-like precipitate morphology.

The method described above for Nb_3Al was based on a series of prior related studies of V-Ga and its reaction kinetics [198][201][202]. As described by HONG *et al.* [198], V-Ga alloys with concentrations of 17 $\sim$ 19 at.% Ga were arc melted and homogenized for 24 h/1350° C before being quenched into water. During the quenching, A15 precipitation was suppressed and it tended to remain so during subsequent warm rolling (at about 800° C) to a

thickness reduction of about 75%. After aging for a range of times at temperatures between 600 and 1000° C an A15 precipitate with an aging-time-dependent T_c was developed. On aging at temperatures between 650 and 800° C a maximum T_c of 14.8 K was attained. According to the equilibrium phase diagram, Figure 9-6, the composition of the equilibrium A15 phase expected to develop in this temperature range would be so far off stoichiometry ($\lesssim$ 20 at.% Ga) that its T_c would be less than 10 K. The high T_c observed, almost equal to the 15.7 K of stoichiometric V_3Ga, is in keeping with the thermodynamic tendency for the small precipitates which form from highly supersaturated solid solutions to be rich in solute content [198]. It was concluded [202] that the technique just described was capable of leading to a monolithic process for V_3Ga wire or tape. Indeed as noted above PICKUS *et al.* [170] have already demonstrated a model process, based on the solid-state-precipitation principle, for the production of Nb_3Al wire.

9.6 The *In-Situ* Process

9.6.1 Principle of the Method

Stemming from some earlier work on rapidly quenched metals was the discovery by TSUEI [165] that 3-g ingots of alloys such as Cu_{93}-Nb_5-Sn_2 and Cu_{90}-$V_{7.5}$-$Si_{2.5}$, after induction melting and cooling at a rate of about 1000° C s^{-1}, were able to be rolled into wires, and furthermore that after heat treatments of typically 2.5 days/600° C or 5 h/800° C were able to carry substantial supercurrents at 4.2 K. This work was reported to the superconductor community in 1974 [166] and attracted sufficient attention that by 1979 scale-up to 10-kg ingots had already taken place [203] and the method was under consideration for development into a continuous commercial process for A15 superconductors. The principle of the method can be described with reference to the binary Cu-Nb phase diagram, a recent version of which is reproduced in Figure 9-7. The constituent elements are fully miscible in the liquid phase and almost completely immiscible when solidified. Then

on account of their difference in melting points, during cooling the Nb is the first to precipitate out of what is to become an almost pure Cu matrix. The precipitate morphology has been considered in detail in several articles [172][203][205]. Unlike Nb powder, the *in-situ* Nb precipitate is relatively oxygen-free and, surrounded by Cu, can be readily elongated to long ribbon-like-fibers by cold work. In Tsuei's initial experiments, Sn was introduced into the starting alloy and during heat treatment reacted with the Nb to form stringers of A15 compound; subsequently the Sn was to be applied by external diffusion at the end of the metalworking process. Again, superconductivity in the initial experiments was believed to take place *via* the discontinuous filaments and by proximity effect across the contacts between them [165], and indeed this was probably true in composites whose Nb levels were as low as 5 at.% (i.e., *ca.* 7 wt.% or vol.%). In subsequent studies with more concentrated alloys (10-12 wt.% Nb) ROBERGE and FIHEY [206][207] noted that if the Cu was etched away, the precipitate structure remained self-supporting, and that superconductivity must in these alloys have been taking place along continuous metallic paths through a sponge-like, three-dimensional network. At the same time it was recognized that although the percolation threshold for spherical objects is about 15 vol.% this is not necessarily the case for flower-like dendritic precipitates whose effective radii are considerably larger than those of volume-equivalent spheres. Indeed for the kinds of precipitate encountered, the percolation threshold was estimated to be about 10 vol.%, Figure 9-8. Subsequent workers agree that both the proximity effect *and* the percolation mechanisms are operative, depending on the Nb concentration and the strength of the applied field [208].

9.6.2 Site Percolation Connectivity and the Proximity Effect

As indicated above, and with reference to Figure 9-8, the percolation limit for rosette-like precipitates is about 10 wt.% (vol.%) Nb. After elongation and reaction it is, however, possible for large current densities to be supported by a P.D. of less than 1 μV across the sample in alloys with Nb levels even lower than 7 wt.%, Figure 9-9. DAVIDSON, BEASLEY, and

TINKHAM [209] have constructed a model for the resistivity of a composite consisting of discontinuous, overlapping but noncontacting, superconducting rods in a normal-metal matrix by means of which it was possible to show that the resistivity of such materials could be so small as to be indistinguishable from "zero" except with the aid of a SQUID-type voltmeter. Using such an instrument DAVIDSON *et al.* [209] demonstrated that the resistivity of one of their samples with 5 at.% Nb was no greater than 3×10^{-17} Ω cm, suggesting that a supercurrent was being conducted by proximity effect across the lap-junctions between successive filaments [210]. However, even in high fields when the proximity effect is no longer operative, it can be shown that the resistivity of an array of highly elongated discontinuous superconducting fibers is still low enough as to be technically useful.

According to BEVK *et al.* [208][211], for an array of highly elongated filaments produced by an area reduction R_e, whereas the longitudinal current density in the filaments is $J_{\parallel} = J/\lambda$, where J is the overall current density and λ is the volume fraction of the superconductor, the transverse current density coupling filaments across the matrix is $J_{\perp} \sim J/(\lambda^{1/2} R_e^{3/2})$; thus, $J_{\perp}/J_{\parallel} = \lambda^{1/2}/R_e^{3/2}$. For 300-Å filaments 3 mm in length [210] R_e would have been about 10^3; then with $\lambda = 0.1$, $J_{\perp}/J_{\parallel} = 10^{-5}$. It follows that a longitudinal supercurrent of 10^6 A cm^{-2} in the filaments can be supported by a transverse current density of only 10 A cm^{-2}, easily achievable by proximity effect if the applied transverse field is sufficiently low (cf. [233]).

Under the conditions just described the energy dissipated in the Cu is less by a factor $(J_{\perp}/J)^2$ than it would be in pure Cu alone. In other words the effective longitudinal resistivity of the composite is given by $\rho_{eff}/\rho_{Cu} = (J_{\perp}/J)^2 = (1/\lambda)(1/R_e)^3 = (1/\lambda)(d_f/L_f)^3$ where (d_f/L_f) is the diameter/length ratio of the filaments, results which had already been given by DAVIDSON *et al.* [209] (cf. also [207]). Again, using $\lambda = 0.1$ and $R_e = 10^3$, $\rho_{eff}/\rho_{Cu} = 10^{-8}$, leading to $\rho_{eff} = 10^{-16}$ Ω cm which is below the detectability threshold of conventional circuitry.

Summary. At Nb levels *beyond the percolation threshold* of about 10 wt.% for irregular precipitates, the composite is continuously conducting; when elongated, the filaments are mechanically interconnected at distances of the order of a filament length. *Below the percolation threshold* and at large area reduction ratios, proximity effect will lead to continuous superconductivity at low fields; at high fields finite transverse normal currents, $J_{\perp}$, influence the resistivity while if R_e is sufficiently large (the filaments sufficiently elongated) the resistivity may still be below the limit of practical detectability [209].

9.6.3 Melting and Casting Methods

Detailed studies of melting and casting procedures, and crucible materials, for the preparation of *in-situ* Cu/Nb starting ingots with masses of up to 40 kg [212] have been undertaken by VERHOEVEN *et al* at Iowa State University [213][214]. Using induction melting followed by chill casting into a water-cooled Cu mold the effects of contamination introduced by various crucible materials were examined [213]. Of the four materials Al_2O_3, ZrO_2 (CaO stabilized), ZrO_2 (Y_2O_3 stabilized) and Y_2O_3 the latter produced the least contamination. ThO_2 was better still except for poor thermal shock resistance. BN although outstanding in this regard contributed B contamination. The use of graphite lowered the oxygen level but contaminated the melt with some 2000 ppma of C. The C pickup was observed to change the Nb dendrite morphology from long and thin to shorter and thicker [213]. This was subsequently found to have a detrimental effect on J_c to such an extent that steps were later taken, when graphite liners were used, to coat them with ZrO_2 [214] although difficulties have at times been encountered in putting this procedure into practice [215].

Consumable arc melting offers the greater potential for scale-up. In the initial experiments [213], 5-cm$^{\emptyset}$ castings were prepared by double consumable arc melting starting with a coaxial Nb-in-Cu electrode. Subsequently, 10 cm$^{\emptyset}$ castings were made using this procedure, and also by an

improved method in which the starting electrode consisted of three Nb plates imbedded in matching slots in a Cu rod [212] in order to improve the spreading of the arc and the melting pattern. Using this electrode geometry, ingots as large as 15 kg (7.5 cm^{ϕ}) and 30 kg (10 cm^{ϕ}) were double-melted in graphite-lined Cu molds. Finally, in a J_c-optimization study, in order to eliminate C contamination and its detrimental influence on Nb-dendrite morphology, the usual graphite lining of the water-cooled Cu mold was replaced with a split graphite liner flame sprayed with ZrO_2 (CaO stabilized), or plasma sprayed with ZrO_2 (Y_2O_3 stabilized)--a more durable coating. The results of this study [214] enabled it to be concluded that the 12-T J_c's of the C-free *in-situ* wire, fabricated from starting ingots prepared in the manner indicated, were as good if not better than the best reported values for powder-processed or bronze-processed wire. The microstructural and superconductive properties of wire prepared from chill-cast and arc-melted starting materials are intercompared in reference [203].

9.6.4 Precipitate Morphology and Process Control

In ingots prepared by melting Cu-20 wt.% Nb in either Y_2O_3 or ThO_2 crucibles and casting into a water-cooled Cu mold, the Iowa State group obtained Nb dendrites about 1 μm in diameter; after area reduction of about 7000:1 these were forced to assume a ribbon-like shape about 2500 Å wide and 50 Å thick [211]. After tinning and heat treatment for some 3 to 6 days at 550° C sets of parallel Nb_3Sn filaments were formed during the reaction of each ribbon [205]. Since during heat treatment small precipitates grow faster than thick ones, some control of Nb-filament size before tinning, with a beneficial influence on the final reacted J_c, could be exerted by annealing the wire after some intermediate-level of reduction (from 25 mm^{ϕ} to 0.79 mm^{ϕ}) for 1 day/750° C† prior to final reduction to 0.15 mm^{ϕ} [216]. The starting points for these later process optimization studies were 15-kg arc castings of Cu-22.5 wt.% Nb.

---

† It was believed that additional precipitation effects may also have contributed to the improved J_c [216].

In scaling up from a laboratory experiment of this kind to an industrial process the possibility of continuous casting is usually investigated. ROBERGE *et al.* [217][218] have devised a method for the continuous induction melting of Nb and Cu in coaxial tubular form followed by steep-temperature-gradient directional solidification, while TACHIKAWA *et al.* [219] have coupled the continuous nonconsumable arc melting of small previously arc-melted buttons of Cu-V to drawing followed by plating-and-heat-treatment lines.

In the experiments on the continuous casting of Cu-30 wt.% Nb [218] it was recognized that variation of the casting rate provided another opportunity for controlling the dendrite morphology, hence the J_c of the final reacted product. For example, solidification rates of 0.015 cm s^{-1}, 0.07 cm s^{-1}, and 0.15 cm s^{-1} yielded dendrite sizes of 20-40 μm, 5-10 μm, and 1-3 μm, respectively. The latter, after an area reduction of about 1400:1 to 0.25 mm^{ϕ} followed by 3 days/650° C, yielded the highest overall 14-T J_c, *viz.* (2-3) x 10^4 A cm^{-2}.

9.6.5 Tinning Methods and Cryostabilization

In the *in-situ* process as initially suggested, the Sn was part of the starting ingot [165]. However, in further developments of the method, in which higher proportions of Nb were present and consequently larger concentrations of Sn were needed to react it, the application of Sn usually by electroplating was deferred until after all metalworking operations had been completed. As in conventional processing, external-Sn diffusion places a restriction of 0.25 mm ∿ 0.5 mm on the diameter of the wire to be reacted and consequently limits scale-up to large-size strands. According to VERHOEVEN *et al.* [205], the advance of Sn into a 0.15 mm^{ϕ} wire is essentially complete after 1-3 days at 550° C.

In order to fabricate large conductors from *in-situ* material there are several ways in which the Sn-diffusion limitation can be overcome. Some of these possess the additional advantage of permitting unalloyed Cu to be added to the conductor for the purpose of stabilization. Although with the extra components needed to accomplish these goals, the conductor tends to take on the complication of a conventional composite, double extrusion for the purpose of reducing filament size is never required.

The strand may also be plated with bronze rather than Sn. This is claimed to result in a more robust wire eminently suitable for cabling into a high-current conductor [220]. If the *in-situ* material is flattened, large conductor cross sections can be combined with short Sn-diffusion distances. This principle leads directly to the ribbon-like conductor discussed by VERHOEVEN *et al.* [220]. Pursuing this idea, the ribbon may be imagined to be folded into a tube which: (a) encloses a solid Cu cylinder which may [215] or may not [216] be provided with a Ta diffusion barrier and externally plated with Sn; (b) encloses a solid Sn-5 wt.% Cu cylinder which acts as Sn reservoir and is provided with an outer shell of pure Cu [203][220][222][223]. In a production process, the *in-situ* Cu-Nb tube needed for methods (a) and (b) above would be formed by extrusion. As an extension of method (b) above FINNEMORE *et al.* [223] have inserted a cluster of seven Sn cores into a Cu-jacketed *in-situ* billet prior to extrusion, leading to a reactable strand of diameter (excluding the Cu jacket) 0.71 mm [223].

9.6.6 *In-Situ* V_3Ga Process Development

The first attempt to apply the *in-situ* method to superconductors based on Cu-V-Ga was due to TSUEI [224] who has already pioneered the work on Cu-Nb-Sn as well as Cu-V-Si [165]. Subsequently, the technique was explored further by BEVK *et al.* (Harvard) [225] who began with induction-melted samples of Cu-20 vol.% V and FIHEY *et al.* (MIT and IREQ, Canada) [226] who prepared, by arc melting, Cu-V alloys with up to 24 at.% (20 wt.%) V. The Cu-V system differs from Cu-Nb in that, in the former, the components are not completely immiscible in the solid state. At 1120° C for example, although the Cu matrix with 0.8 at.% V is fairly pure, the V dendrites are contaminated by 7 at.% Cu in solid solution [127]. Nevertheless, cast alloys such as those referred to above could be swaged and cold-drawn to various area-reductions of up to 1200:1 [226] or 1600:1 [225] without intermediate annealing, to yield the usual long ribbon-like filaments of, in this case, low-concentration V-Cu alloy.

The V-Ga system was of course of particular interest to TACHIKAWA of the National Research Institute for Metals (Japan) who had pioneered the development of process technology for conventional V_3Ga superconductors [117][118]. Accordingly, in a series of papers he and his group discussed process development [228], commercial scale-up [219], and the superconductive and mechanical properties [229], of Cu-V_3-Ga *in-situ* composites. A continuous casting system was developed, based on either nonconsumable- or consumable-electrode arc melting. In the former case the melting chamber was fed with ingots of either binary Cu-V in case external Ga-diffusion was to be used, or Cu-V-Ga if internal diffusion,† or combined internal-plus-external diffusion were to be employed [219]. In the consumable-electrode process the electrodes were fabricated either from bundles of coaxial V-in-Cu rods or a laminated assemblage of V and Cu plates [229]. The finished wire was Ga coated in an evacuated enclosure by passing it through a bath of the molten metal. After being plated, the wires were annealed for 100 h/450° C and reaction heat treated for 100 h at 500° C in order to optimize J_c. It was noted that this reaction temperature was considerably lower than that needed to optimize bronze-process V_3Ga [229]. As depicted in Figure 9-10, the superconducting properties of *in-situ* Cu-V_3Ga conductors, although strongly dependent on alloy compositions and thermomechanical process parameters, were found to be generally better than those of commercial bronze-process wire, and at high fields were of course very much superior to both bronze-process and *in-situ* Nb_3Sn.

9.7 Flux Pinning and Critical-Current Optimization in Powder-Metallurgical and *In-Situ* Composites

Critical-current optimization in powder and *in-situ* composites is characterized by important similarities as well as differences. The fibrous microstructures of heavily cold worked wires produced by either of these techniques are practically indistinguishable and, therefore, control

† Internal diffusion alone could be employed only if relatively small levels of Ga were needed since it is difficult to cold work alloys with more than 15 at.% Ga.

J_c in comparable ways. An advantage of powder metallurgy is that using it an opportunity exists for incorporating additional metallic elements homogeneously into the composite, whereas in the *in-situ* process they can usually only be satisfactorily introduced along with the Sn if the external-diffusion route is taken.

9.7.1 Powder Metallurgy

In the powder-metallurgical fabrication of Cu-Nb_3Sn composites the influences on the critical-current density of In and Ga [180] as well as Sn and Al [175] additions to the Cu, and Ta additions to the Nb [175], have been investigated. Although In has little effect, Ga becomes incorporated into the reaction layer to the benefit of the high-field J_c[180]. As was found to be the case with conventional composites (cf. Section 8.4.3(a)) the presence of Ta in the Nb also serves to improve J_c [175]. The purpose of adding Sn powder was to eliminate the need for external diffusion and the attendant wire-diameter limit of about 0.25 mm; however, a more uniform product with a higher J_c was obtained when pre-alloyed Sn-35Cu powder was used [175]. Al powder acted as a getter of oxygen and thereby assisted the deformation of the Nb component.

In the optimization of the Nb-Al powder process [176], it was found that J_c could be maximized by appropriately varying the reaction time for a preselected temperature (in this case 800° C) and by varying the Al content of the mixture. J_c could also be encouraged to increase monotonically to some saturation value by increasing the reduction ratio, R_e (up to 1400:1 in this case). The J_c improvement was explained in terms of the effect of Al-filament size on the formation of Nb_3Al; small filaments yielded the highest J_c's the effect of increasing Al-filament diameter being to favor the formation of nonsuperconducting Nb-Al phases.

9.7.2 *In-Situ* Composites

In the *in-situ* composites, the starting binary Cu-TM alloy composition plays an important role in determining the final J_c. This has already been amply demonstrated by the relative performances of a series of Cu-V-18Ga compositions [229], Figure 9-10. With reference to the work of LIVINGSTON [140] and SUENAGA [145] with conventional bronze-processed superconductors, FLÜKIGER [243] has discussed the influence of Ta additions to the melt on the critical-current density and mechanical properties of Cu-$(Nb_{1-x}Ta_x)_3Sn$ *in-situ* wires. It was concluded that although the *in-situ* route offered less control over the composition of the cores than does conventional processing, provided that $x \leq 0.05$, the Ta that did dissolve in the Nb precipitates was responsible for an enhanced J_c, particularly in fields of more than 12 T.

Other important parameters are reaction-layer grain size and the size of the fibers themselves. As with conventionally processed conductors, flux pinning in *in-situ* composites is primarily due to the grain-boundary mechanism [211]. Thus, as the reaction temperature decreases, J_c increases and passes through a maximum located at a temperature of 550° C, Figure 9-11, below which the reaction layer ceases to be stoichiometric [205][223]. Of course if the A15 reaction kinetics can be accelerated, the peak of such a curve will be shifted to lower temperatures, and will consequently be higher. Thus, any addition to the melt, such as Zn, which enhances the activity of the Sn and catalyzes the growth of the Nb_3Sn reaction layer, will result in an improvement in J_c [235].

Filament size and its precursor, Nb-dendrite size, play crucial roles in establishing the critical-current performances of *in-situ* superconductors. In such conductors although the filaments whose sizes are in the range 200-2000 Å are actually discontinuous, their critical-current performances are comparable to those of conventional 2-5 $\mu m^{\emptyset}$ continuous-filamentary A15 composites [210]. At ordinary fields flux pinning is by grain boundaries, and at high fields it seems to be limited by the usual flux-lattice shear. When the filament thickness becomes comparable to the grain size, flux pinning by filament/matrix interfaces is expected to contribute substantially

to the total pinning force. Two new features enter the picture: (a) surface roughness, which replaces the network of grain boundaries as the seat of the energy modulation needed for flux pinning; (b) J_c anisotropy, in response to the high aspect ratio which characterizes the cross-sectional view of the *in-situ* fibers [211].

Critical-current in *in-situ* composites is also controlled by the geometry and geometrical arrangement of the filaments themselves quite apart from any intrinsic pinning-strength considerations. In this regard, J_c is strongly dependent on filament size which is accountable both to the original Nb dendrite size and to the area reduction ratio after casting. There is an optimal pre-reaction Nb-filament diameter, and consequently for a given starting dendrite size, an optimal area-reduction-ratio, $R_{e,opt}$ [214]. With $R_e > R_{e,opt}$, the filaments become sufficiently small that coarsening occurs during Sn-diffusion and subsequent reaction heat treatment at the expense of their continuity [205][214]. With $R_e < R_{e,opt}$, filament elongation decreases and with it J_c, according to the argument advanced in Section 9.6. $R_{e,opt}$ of course depends on the initial dendrite size (and/or the effect of any intermediate conditioning heat treatment [214]) which in turn depends on two important factors: (a) the rate of ingot cooling when some steep-temperature-gradient continuous chill-casting process is employed [172][218]; (b) the C content of the melt which as we have seen depends very strongly on whether or not it has been exposed to the surface of a graphite mold [213]. Much finer dendrites result if the surface of a graphite mold or susceptor is covered with an oxide coating [213] or a BN layer [213][235].

9.8 Stress Effects

9.8.1 Conventionally and Unconventionally Processed Material

The mechanical properties of A15 composite superconductors and the effects of stress (strain) on their critical-current densities have been thoroughly reviewed by LUHMAN [108][6, p. 171], EKIN [6, p. 187] and by other authors in references [6] and [7], and partly for this reason were not discussed in Section 8. One of the important advantages of *in-situ*-processed A15 superconductors is their exceptional mechanical strength [211] and the greater uniaxial-*strain*-tolerance of their critical current densities as compared to conventionally processed material [172], advantages which, according to ROBERGE and FONER [172] are shared by powder-processed composites. In this sub-section the effects of stress on the superconductive properties of powder-processed and *in-situ* composites are briefly reviewed and compared with those of conventionally processed conductors -- a second reason for not treating this topic in the previous section.

9.8.2 *In-Situ*-Processed V_3Ga Composites

Even as late as 1980 much less was known about stress effects in conventional V_3Ga composites than was the case for Nb_3Sn. It was suspected, however, that the performance under stress of conventionally processed conductors with large numbers of very fine filaments would be poor. The reason for this is that the intermediate-temperature annealing needed to facilitate heavy-reduction processing had in this system been noted to produce premature reaction to V_3Ga which is then subject to break-up during subsequent wire drawing [225]. On the other hand, there is ample evidence to suggest that *in-situ* processed V_3Ga possesses not only exceptional tensile strength [219][229] but also a high degree of strain tolerance both in tension [226][228] and under bending [219][228]. A comparison of stress-degradation in *in-situ* Cu-V_3Ga with that of other *in-situ*- and conventionally-processed systems is complicated by: (a) the fact that

differences are encountered between the stress-tolerances of externally diffused and internally diffused material [228]; (b) the sensitivity of the threshold strain, ε_d, for J_c degradation to the V and Ga concentrations [219] [229]. An interesting example of the latter effect is given in Figure 9-12 which shows: (i) the rapid decreases in ε_d with Ga concentration; (ii) that the penalty for an increased tolerance to strain is a reduced critical-current density. Bearing in mind the strong influence that composition has on the results, the tensile properties and J_c-stress dependences of some *in-situ* - processed Cu-V_3Ga conductors are briefly reviewed.

The tensile strengths of these materials are quite remarkable: according to TACHIKAWA *et al.* ultimate strengths ranging from 60 kg cm^{-2} (with (Cu-20 at.% V) + 15 at.% Ga) to 80 kg mm^{-2} (with (Cu-35 at.% V) + 15 at.% Ga) have been recorded, the latter actually being higher than the ultimate tensile strength of a cable consisting of six 55-filament V_3Ga conventional composite strands cabled about a W core [219][229].

A typical example of the influence of tensile stress on the J_c of an *externally* diffused *in-situ* Cu-V_3Ga composite (Cu-21.5 at.% V base) is given in Figure 9-13 from the work of FIHEY *et al.* [226]. The tensile results are characterized by a very weak sensitivity of J_c to tensile stress out to about 500 $\sim$ 550 MN m^{-2}. The decrease which follows creates a slight maximum at ε_m = 0.9 $\sim$ 1.2%. Strains of up to 1% did not result in any appreciable permanent deterioration in current-carrying capacity. Results such as this tend to be confirmed by those of TACHIKAWA *et al.* [219][228] who found that J_c in *internally* diffused *in-situ* Cu-V_3Ga (Cu-20 at.% V base) increased with strain almost imperceptibly up to 1.0 $\sim$ 1.2% before beginning to decrease. Its superiority over conventional Cu-V_3Ga was most impressive: single-core bronze-processed V/Cu-20 at.% Ga tpae (reacted 100 h/650° C) began to deteriorate rapidly after 0.5 $\sim$ 0.6% strain [228].

The bend-test data, expressed in terms of a bend strain ε_b = d/D where d is the wire diameter and D is that of the mandrel, are in accord with the tensile-test results [219][228]. For example the bend-strain at which degradation sets in, $\varepsilon_{b,d}$, was about 1.0% for *internally* diffused (Cu-20 at.% V) + 12 at.% Ga and 0.8 $\sim$ 9.0% for *externally* diffused (Cu-20 at.% V) + 15 at.% Ga, values which may be compared with an $\varepsilon_{b,d} \cong$ 0.5% for conventionally processed single-core V/Cu-19 at.% Ga.

9.8.3 Powder-Processed Nb_3Sn Composites

(a) Cold-Powder-Processed Material. The mechanical properties of cold-powder processed Cu-Nb_3Sn are comparable to those of *in-situ* processed material. Of course as pointed out by FLÜKIGER *et al* [167][185] and ROBERGE and FONER [172] the powder requires an external jacket for support during the early stages of deformation. This may be removed once the powder particles (initially about 40 μm in size) have elongated into filaments (say several mm in length) but may be retained, if need be, to contribute extra strength to the strand. The influence of the cladding material on the tensile behavior of *in-situ* composites is indicated in Figure 9-14. When Cu-35 wt.% Nb-27 wt.% Sn is clad in Cu-0.2 wt.% Zr the strain at maximum J_c is $\varepsilon_m \cong 0.7\%$, while J_c is always higher than its starting value ("no degradation") provided $\varepsilon \leq 1\%$. In the Cu-18.8 wt.% Be jacket, the J_c of Cu-35 wt.% Nb-25 wt.% Sn increases monotonically up to a stress of 800 MN m^{-2}, at which point the strain is again about 1%; obviously this conductor is capable of accepting considerably more than 1% strain without degrading.

(b) Hot-Powder-Processed Material. Stress effects in hot-powder-processed Cu-Nb_3Sn have been considered by FREYHARDT *et al*. [181]. The results of a stress-effect measurement of a Cu-30 wt.% Nb-Sn composite were comparable to those for the Cu-Be-clad conductor depicted in Figure 6-14 in that J_c(16T) increased monotonically up to what appeared to be a maximum at $\varepsilon \cong 0.8\%$. Again it seems that degradation will not occur unless strains considerably greater than 1% are encountered.

9.8.4 *In-Situ*-Processed Nb_3Sn Composites

As with Cu-V_3Ga *in-situ* composites (Section 6.8.2), the *in-situ*-processed Cu-Nb_3Sn composites exhibit remarkably high ultimate tensile strengths. In order to study this effect in more detail on a simplified but closely related system, BEVK *et al*. measured as a function of cold area

reduction, hence filament size, the tensile properties of the original untinned Cu-Nb binary system [208][211][236]. As a result of this work it was concluded that the strength of the composite was not a mixture-rule governed quality dominated by the presence of a high-strength fiber reinforcement, but resided primarily in the heavily work-hardened Cu matrix, whose high dislocation density had been stabilized against dynamic recovery by the presence of an abundance of matrix-filament interfaces [236]. An explanation for the high strength of the reacted composites was couched in these terms although it was recognized that the presence of the A15 compound rather than a Nb filament would require a modification to the model [211].

But as pointed out by BEVK *et al.* [211] a feature of *in-situ* Cu-V_3Ga and Cu-Nb_3Sn composites more important than their strength is the stress-strain tolerance of their critical fields and currents. In order to deal with this adequately, although briefly, it is first necessary to describe the J_c-strain characteristics of conventional A15 composites. It is well known that in bronze-processed conductors after the heat treatment is complete and the material has cooled down to room temperature -- and eventually to 4.2 K -- the excess relative contraction of the bronze matrix places the A15 compound in compression and lowers its H_{c2} and J_c. It follows that under the application of a tensile stress, H_{c2} and J_c should rise and attain a maximum at zero strain in the A15 component. A force-balance equation between bulk strain and the elastic moduli of the components of a simple conventional composite predicted, after insertion of the appropriate data, that the maximum should occur at a bulk strain, ε_m, of about $0.4 \sim 0.5\%$ [237]. For *in-situ* composites on the other hand the maxima occur at considerably higher values of strain, the actual value of ε_m, for a given ratio of superconductor to matrix, depending on the inter-filamentary spacing [237] or what amounts to the same thing, the starting dendrite size [217].

With regard to the latter, FIHEY *et al.* [217] have prepared by varying the rate of directional solidification, aligned dendrites 10 μm and 30 μm in size. After cold area reduction of 500:1 and external Sn diffusion J_c was measured as a function of strain at various fields, whereupon it was found that for the three dendrite sizes specified, $\varepsilon_m = 0.6$,

0.5, and 0.3%, respectively. Similarly, in terms of the final interfilamentary spacing, ROBERGE *et al.* [237] have demonstrated that, whereas $\varepsilon_m = 0.2 \sim 0.3\%$ for a spacing of 1.0 μm (as for a conventional composite) with a filament spacing of 0.3 μm, ε_m had risen to between 0.6 and 0.7%. Assuming $J_c(\varepsilon)$ is symmetrical, the "zero degradation" strains would be double the above values.

This description is restricted to Cu-Nb_3Sn conductors. As pointed out above, the J_c of Cu-V_3Ga is relatively strain insensitive out to ε_m. This distinction is depicted in Figure 9-15 which compares the stress responses of those two classes of *in-situ* A15 conductor with that of a conventionally processed commercial multifilamentary composite.

9.9 A.C. Loss

9.9.1 A.C. Loss in Multifilamentary Composite Superconductors

As pointed out in Section 4, the hysteretic a.c. loss of a composite superconductor can be dealt with in three frequency regimes; in the present treatment only the "low-frequency" behavior is to be discussed. It may also be considered in two applied-field strength regimes depending on whether H_a is less than or greater than H^* the threshold of full penetration (i.e., the applied field whose induction just reaches the center of the conductor†). For H_a parallel to the surface of a plane-parallel slab of thickness w, according to the Bean model:

$$\frac{H^*}{w} = \left(\frac{2\pi}{10}\right) J_c \qquad (9\text{-}1)$$

in the c.g.s.-practical units: oersted, cm and A; and for H_a transverse to a cylinder of diameter, d:

† It is assumed that *both* sides of the conductor are exposed to the field.

$$\frac{H^*}{d} = \left(\frac{4}{10}\right) J_c \qquad (9\text{-}2)$$

In a superconducting/normal composite it is easy to see, using slab geometry as in Figure 9-16, that H^* is reduced by a factor λ, the volume fraction of superconductor in the composite (i.e., $H^*_{comp} = \lambda H^*_{super}$). H^*, being proportional to J_c, is a measure of the bulk pinning strength. With weakly pinned material the induction due to H_a extends much further into the conductor than it would if the pinning were strong, Figure 9-17. It follows that the hysteretic loss due to a field $H_a = H_o + H_m \sin \omega t$, when $H_m < H^*$, is inversely proportional to J_c. Conversely, when $H_m > H^*$, since the magnetic hysteresis increases with J_c, the hysteretic a.c. loss is proportional to J_c. These results are embodied in the following equations for $\dot{Q}_h/V$, the hysteretic power loss per unit volume.

According to the Carr anisotropic continuum model for conventional multifilamentary conductors [32], some of the results of which were outlined in Section 4, the a.c. loss is composed of: a hysteretic term containing a component in H_m^3 if $H_m << H^*$ or is linear in fH_m if $H_m >> H^*$; an eddy-current term proportional to $f^2H_m^2$. These various components are clearly distinguishable by the powers of their frequency and/or field dependences.

In case $H_m > H^*$, the composite conductor simulates a fully penetrated superconducting cylinder with critical-current density $J_{c,mean} = \lambda J_c$ and hysteretic loss given by:

$$\frac{\dot{Q}_h}{V} \cong \left(\frac{8}{3\pi \times 10^8}\right) (d_e \lambda J_c) H_m f \qquad (9\text{-}3)$$

(cf. Equation (4-3)) where d_e represents the "electrical diameter" of the filaments, a quantity which equals w, the filament diameter, when the filaments are fully decoupled and tends to D, the strand diameter, as coupling increases.

The low-frequency, eddy-current loss in a cylindrical composite conductor twisted to a pitch L_p in an alternating transverse field of amplitude H_m has, according to the Carr anistropic continuum model, been

given by:

$$\frac{\dot{Q}_e}{V} \approx \left(\frac{1}{2 \times 10^{16}}\right)\left(\frac{L_p^2}{\rho_\perp}\right) H_m^2 f^2 \qquad (4\text{-}3)$$

where L_p is the twist pitch of the composite and $\rho_\perp$ its transverse resistivity which, if low-resistance matrix/filament contact can be assumed, is given by [44][238]:

$$\rho_\perp = \frac{1 - \lambda}{1 + \lambda} \rho_m \qquad (9\text{-}4)$$

where ρ_m is the resistivity of the matrix.

Equation (9-3) embodies the reason for filamentary subdivision as a means of reducing a.c. hysteresis loss. Clearly the loss per unit volume of superconductor will decrease in proportion to d_e until surface loss provides a limit below which further subdivision would be fruitless. Electromagnetic coupling between filaments will tend to increase their effective diameters; consequently, if the full advantage of the presence of fine filaments is to be taken, they must be decoupled from the external field by twisting.

Equation (4-3) shows that a.c. loss due to eddy-currents crossing the matrix can be reduced in proportion to L_p^2, again by twisting, and in proportion to $\sigma_\perp$ by lowering the effective transverse conductivity of the matrix.

The manner in which a.c. loss in *in-situ* composites can be described in terms of the above considerations is discussed in the following section with reference, principally, to the work of BRAGINSKI *et al.*

9.9.2 A.C. Loss in Un-Twisted *In-Situ* Cu-Nb_3Sn Composites

Important results which can be extracted from a study of a.c. hysteretic and eddy-current losses in *in-situ* composites are: an effective or "electrical" filament diameter, d_e, an effective twist pitch L_{pe}, and the transverse resistivity of the composite, $\rho_\perp$. d_e can be derived from

measurements of eddy-current loss. What kind of loss is being detected can be discerned from the index of its H_m-dependence (cf. Equations (9-3) and (4-3)). The limiting low-frequency hysteretic loss can be derived from the area of the static magnetization loop as measured using a vibrating-sample magnetometer at an applied-field frequency of *ca* 10^{-3} Hz [239]. Hysteresis loss at higher frequencies may be measured calorimetrically if the sample volume is $1 \sim 5$ cm^3, otherwise electronic-wattmeter techniques, which are capable of some four orders of magnitude greater sensitivity, must be used [239].

The best way to estimate the effective filament diameter of the composite is to substitute the results of a high-amplitude a.c.-loss experiment into Equation (9-3); similarly an effective twist pitch can be derived from Equation (4-3) from the results of low-amplitude, low-frequency loss experiments. Some examples are presented below.

The results of a typical hysteresis-loss measurement as performed on a coiled ribbon sample are given in Figure 9-18. Other properties of the sample are listed in Table 9-2. The penetration field H^* is obtained from the position of the change-in-slope of the log $(\dot{Q}_h)$ *versus* log H_m plot where the H_m-dependence changes from cubic to linear. Inserting the value $H^* = 4.0$ kOe into Equation (9-1) yields $w = 64$ μm, which is about equal to the thickness of the ribbon, as expected. As for the estimation of d_e, a substitution of the values of $Q_h/V(\equiv\dot{Q}_h/Vf)$, H_m, and $J_{c,meas}$ into Equation (9-3) again yields 64 μm indicating that the filaments are almost fully coupled. Apart from considerations regarding mechanical interconnection the absence of twist would be expected to contribute strongly to the relatively large effective filament diameter. The question as to whether this can be appreciably reduced by twisting will be addressed below. Before doing so, the results of some eddy-current-loss measurements performed on a wire sample of diameter 132 μm, similar to the wire version of the above ribbon conductor (cf. Table 9-2) will be considered. Log-log plots of low-amplitude a.c.,-loss frequency dependence and field-amplitude dependence both had slopes close to 2 indicating that the eddy-current component of loss was being measured. Inserting data from Figure 9-19 into Equation (4-3) in the

TABLE 9-2. PROPERTIES OF THE SAMPLE WHOSE HYSTERETIC LOSS IS DEPICTED IN FIGURE 9-18 -- after BRAGINSKI *et al.* [240]

Composition	82.3Cu-11.7Nb-6.0Sn
Heat treatment	132h/560°C
SC volume fraction, λ	0.23
Rectangular conductor dimensions	0.580mm x 0.076mm
Cylindrical conductor diameter	0.132 mm
Area reduction ratio (rectangular)	1440
Area reduction ratio (cylindrical)	4470
Filament section	0.25μm x 0.025μm
Filament length	10 ∿ 15 mm
Matrix conductivity, ρ_m	9×10^{-6} Ω cm
Penetration field, H*	4.0 kOe
$J_{c,meas}$ at H*	10×10^{5} A cm^{-2}
Measuring field , $H_m > H^*$	10 kOe
$J_{c,meas}$ at H_m	5.5×10^{5} A cm^{-2}
Hysteretic loss (Q_h/V)	3.0×10^{-1} J cm^{-3}

form:

$$\frac{\dot{Q}_e}{VH_m^2} = \left(\frac{1}{2 \times 10^{16}}\right)\left(\frac{L_p^2}{\rho_\perp}\right) f^2 \qquad (4\text{-}3a)$$

and using a calculated value of $\rho_\perp$ (cf. Equation (9-4)) led to an effective twist pitch L_{pe} = 13 mm, a length, according to Table 9-2, about equal to that of an average filament. Further experiments showed that the eddy-current losses decreased with the reduction ratio R_e and with it the average filament length, a result which suggests that at Nb concentrations beyond the percolation limit there is on the average about one current crossover per Nb precipitate particle (i.e., per filament in the finished wire). Since J_c increases with R_e, there is clearly a competition between current-carrying capacity and the maintenance of a short effective twist pitch.

BRAGINSKI *et al.* [239] have also shown how $\rho_\perp$ can be measured directly. By applying an a.c. field parallel to the axis of a rectangular conductor, the induced current loops will be confined by its thickness w. The transverse resistivity may then be derived from Equation (4-3) in the form:

$$\frac{\dot{Q}_e}{V} = \left(\frac{1}{2 \times 10^{16}}\right)\frac{w^2}{\rho_\perp} H_m^2 f^2 \qquad (4\text{-}3b)$$

By applying this method to a ribbon conductor similar to that considered above, a transverse resistivity of about 2×10^{-8} Ω cm was obtained (equal, incidentally, to that of high-purity Cu at 4.2 K). Using Equation (9-4) $\rho_\perp$ would certainly have been expected to be less than ρ_m ($\sim 5 \times 10^{-6}$ Ω cm) but not two orders of magnitude smaller. Clearly the superconductive transverse current paths resulting from mechanical interfilamentary cross linking are severely reducing the transverse resistivity. Returning to the discussion of effective twist pitch, the use of this new value of $\rho_\perp$ would result in an order of magnitude reduction in the estimated L_{pe}, to about 1 mm, and render any reduction in a.c. loss by twisting even more diffucult to accomplish.

9.9.3 A.C. Loss in Twisted *In-Situ* Cu-Nb_3Sn Composites

A.C. Hysteretic and eddy-current losses of samples of various twist pitches in transverse and longitudinal applied fields have been studied by BRAGINSKI and BEVK [241]. A typical transverse-field hysteretic-loss result is depicted in Figure 9-20. Two important features relating to twist pitch are noticeable: (a) at fields $H_m < H^*$ (i.e., below the bend-point) twisting which increases the penetration of the applied field has increased the hysteretic loss; (b) in the full-penetration region above H^* twisting, by slightly decoupling the filaments, has reduced the hysteretic loss.

The eddy-current-loss results for the samples of Figure 9-20, and one other, are summarized in Table 9-3. The effective twist pitch of the untwisted sample, on the basis of the quadratic law for eddy-current loss reduction (Equation (4-3)), is 4.0 mm -- not out of line with the estimates of the previous section. Presumably a distribution of L_{pe}'s within the range $1 \sim 4$ mm is responsible for the relatively weak decrease in eddy-current loss (by a factor 0.6 instead of 0.2) as the twist-pitch is tightened from 2.8 to 1.25 mm.

9.9.4 A.C. Loss in the Jellyroll Process Conductors

The "jellyroll" process for fabricating multifilamentary Nb_3Al conductor has been described in Section 9-4. In a recent paper, ASDENTE *et al.* [196] have reported on the a.c. loss in these types of material and its response to alteration of the process variables.

A rather detailed investigation of a.c. loss in the "modified jelly-roll" Nb_3Sn conductor of the Teledyne Wah Chang Albany group has been undertaken recently by SHEN [197][242]. The study was prompted by concern that such a structure with otherwise attractive properties might be afflicted by unacceptably large a.c. losses traceable to its inherent multiple connectivity. This initial concern was apparently unfounded, in that although the Nb is present in the starting billet in the form of a close continuous

TABLE 9-3. EDDY-CURRENT LOSS IN SOME *IN-SITU* Cu-Nb_3Sn CONDUCTORS -- after BRAGINSKI AND BEVK [241]

Sample Code	Twist Pitch mm	Experimental Eddy Current Loss 10^{-8} W cm^{-3} kOe^{-2} Hz^{-2}
1	∞	80 ± 20
2	2.8	40 ± 10
3	1.25	$25 \pm \frac{5}{10}$

mesh, after extrusion and wire drawing it becomes so elongated that the nodes connecting the filaments are separated by more than 10 m. It is, therefore, to be expected that twisting to a pitch of say 5 mm should adequately decouple them. Indeed it was found that after so doing, the effective filament diameter in a 450 $\mu m^{\emptyset}$ strand was only 18 μm, practically equivalent to that of an individual 2 μm x 10 μm filament [197].

9.9.5 Summary: A.C. Loss in *In-Situ* Composite Superconductors

(a) Effective Filament Diameter. Hysteretic loss measurements have revealed an effective filament diameter some two orders of magnitude greater than the physical diameter of the filaments [240], particularly when λ exceeds the percolation limit. Indeed when λ increases into the range $0.3 \sim 0.4$ the hysteretic loss approaches that of a solid superconductor of critical-current density λJ_c. Cross-coupling between the filaments is believed to be dominated by proximity effect when λ is below the percolation threshold and a result of actual metallic linkages when λ is above it.

With regard to percolation cross-coupling, FINNEMORE *et al.* [223] [233] in a study of *n/s/n* junctions fabricated from Pb and Cd layers, have shown that the junction supercurrent is field-dependent according to $J_c = H_{co}e^{-H_a/H_{ao}}$. This implies that in small-λ *in-situ* composites cross-coupling, hence hysteretic and eddy-current losses, can be significantly attenuated by the application of a sufficiently strong field. At high fields another cause of hysteresis-loss reduction is the decrease in J_c itself (cf. Equation (9-3) [219][223]).

(b) Transverse Matrix Resistivity. As a result of parallel-field eddy-current loss measurements it was determined that the transverse conductivity of the composite, $\sigma_\perp$, was some two orders of magnitude higher than that deduced by combining λ with the conductivity of the depleted bronze matrix, σ_m [240]. Again, this has to do with one or other of the mechanisms of filamentary cross-linking referred to above. FINNEMORE *et al.* [223] attempted to combat this effect by adding a small amount of Ni to the matrix in order to increase its resistivity, and also noted that twisting

to a pitch of 3 mm reduced the a.c. loss six-fold. The effectiveness of twist is, however, strongly λ-dependent; as BRAGINSKI *et al.* [241] and others [221] have pointed out if λ is to be large, interfilamentary cross-connections will dominate over the usual matrix-mediated transverse currents and twisting will become useless.

(c) Shielding Effects. A property peculiar to *in-situ* composites and the multiple interconnectedness of their filaments is their ability to support circulating supercurrents in the presence of a *d.c.* applied field. In this way *in-situ* composites, in contrast to conventional multifilamentary composites, can become internally shielded [241].

(d) A.C. Loss Reduction. The role of twist in a.c.-loss reduction has just been considered. In untwisted composites the mean distance between interfilamentary current-crossovers serves as an effective twist pitch. For this reason the losses are found to decrease with the average filament length, hence the decrease of the reduction ratio, R_e. Since on the other hand J_c increases with R_e (Section 9.7.2) it follows that a compromise must always be sought between current-carrying capacity and a.c. loss. Thus, FINNEMORE *et al.* [240] have recommended that in the interest of reducing a.c. loss, both λ and the mean filament length (with respect to conductor diameter) should be made as *small* as possible consistent with the attainment of an acceptable J_c.

(e) Conclusion. It is generally agreed that further work needs to be done to increase our understanding of a.c. loss in *in-situ* superconductors to enable further appropriate measures to be taken towards reducing that loss through, for example, alloying and the control of geometry and microstructures [211][240].

FIGURES

(a)

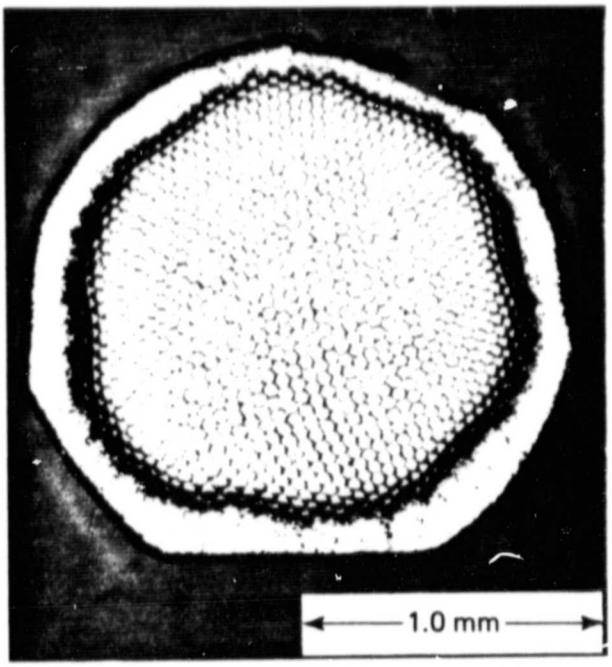

(b)

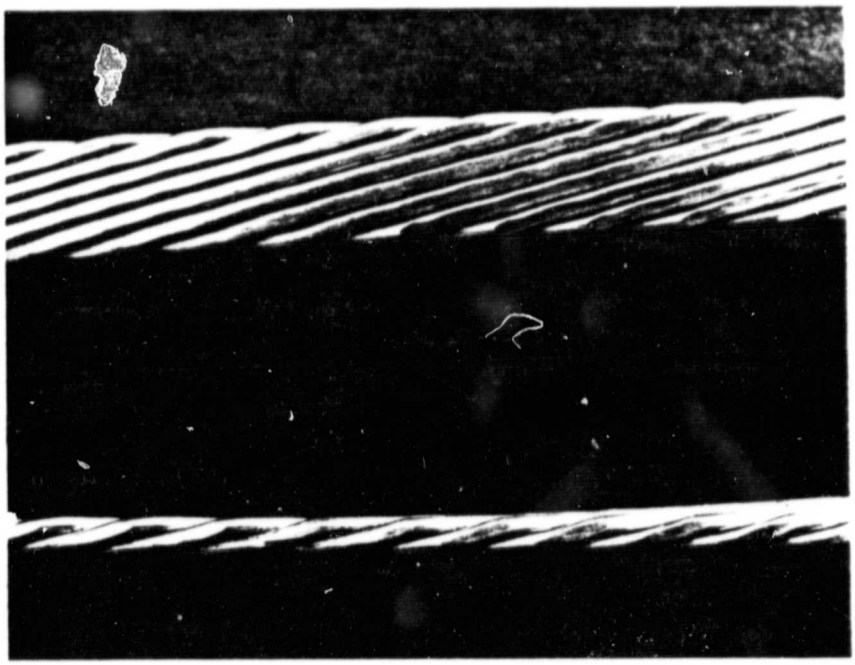

FIGURE 2-1. (a) Optical micrograph of a Cu/Ti-Nb strand; diam., 1.8 mm. (b) Two views of a Rutherford cable wound from such a strand and similar to that intended for the Japanese Large Coil Task 5-T coil windings. Outside dimensions of cable 10.65 x 3.45 mm^2; No. of strands, 11. Cable sample courtesy of Sumitomo Electric Industries Ltd.

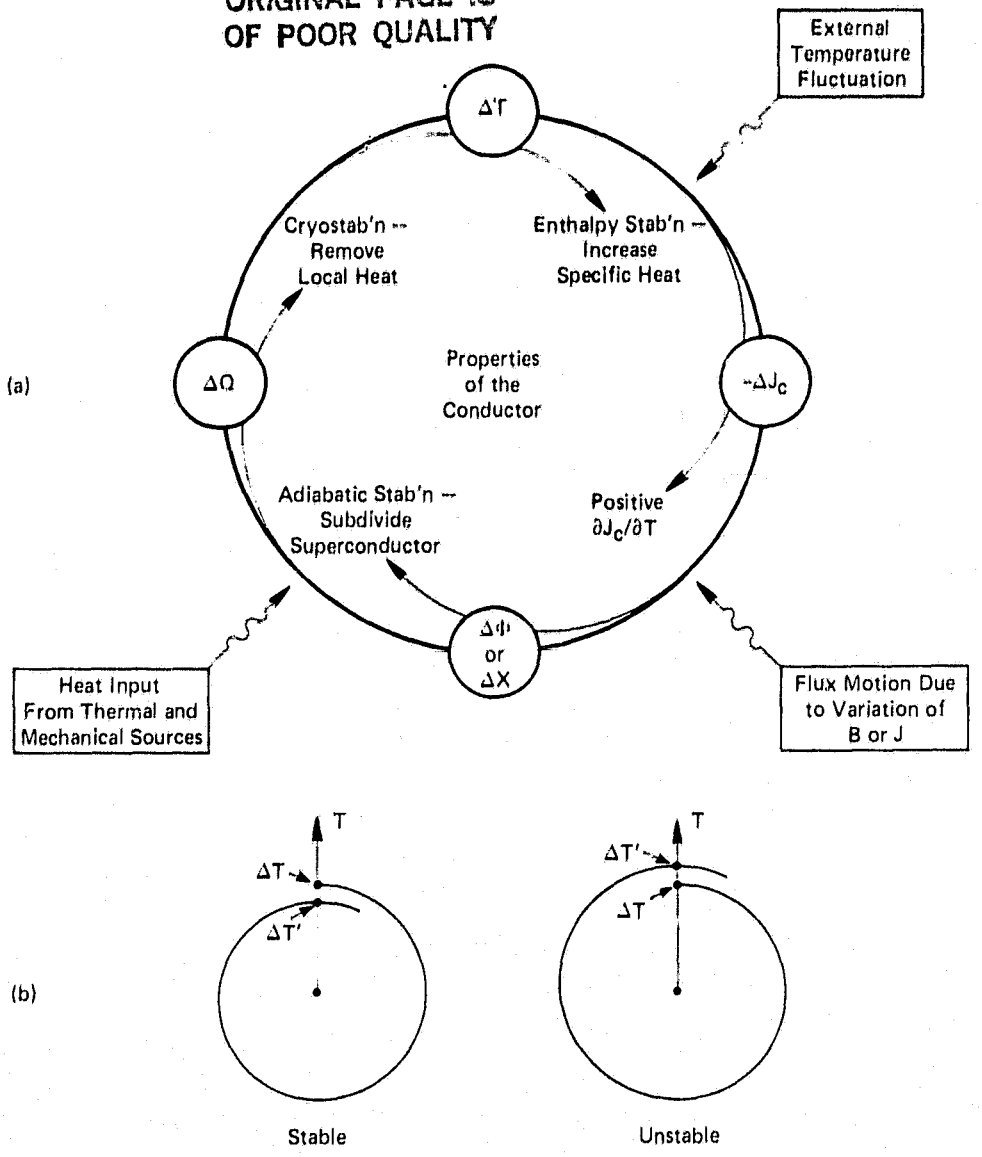

FIGURE 3-1. Diagram representing the cycle of events which govern the stability of a conductor, and the disturbances which set the cycle into motion. Four ways (corresponding to four stabilization techniques) in which the cycle can be induced to spiral inwards (signifying stability) are indicated. The symbols refer to the following incremental quantities: ΔT, temperature; ΔJ_c, critical-current density; $\Delta\Phi$, flux; ΔX, flux penetration; ΔQ, heat.

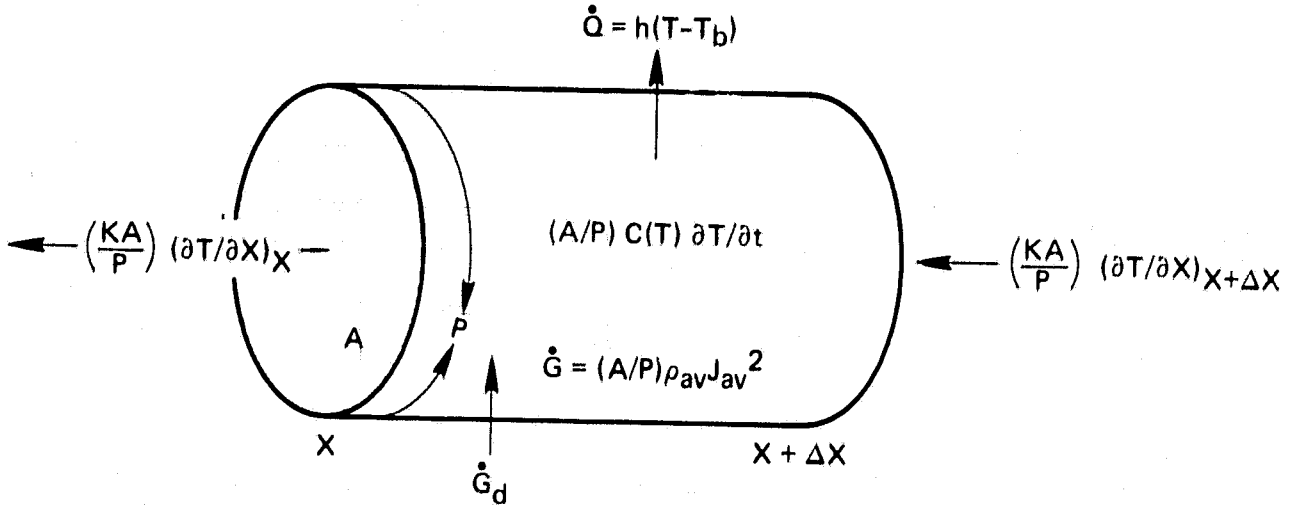

FIGURE 3-2. Representation of a normal zone in a composite conductor indicating the five terms of the energy balance equation controlling cryostability, *viz:* (a) the disturbance $\dot{G}_d$; (b) heat generation, $\dot{G} = (A/P)\rho_{av} J_{av}^2$; (c) storage, $(A/P)C(T)\partial T/\partial t$; (d) conduction, $(KA/P)\partial^2 T/\partial X^2$; and (e) cooling, $h(T-T_b)$.

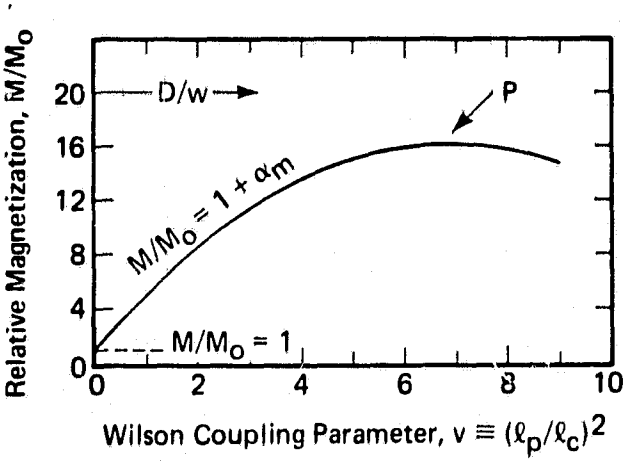

FIGURE 3-3. Variation of relative magnetization M/M_o with Wilson "coupling parameter" $V = (\ell_p/\ell_c)^2$ based on Equation (3-12a) with $\eta_c = 0.8$, $\lambda = 0.5$, and $N = 200$ filaments. According to CARR [30, 31, 32] it is possible to identify α_m as the ratio of the eddy-current to hysteretic losses.

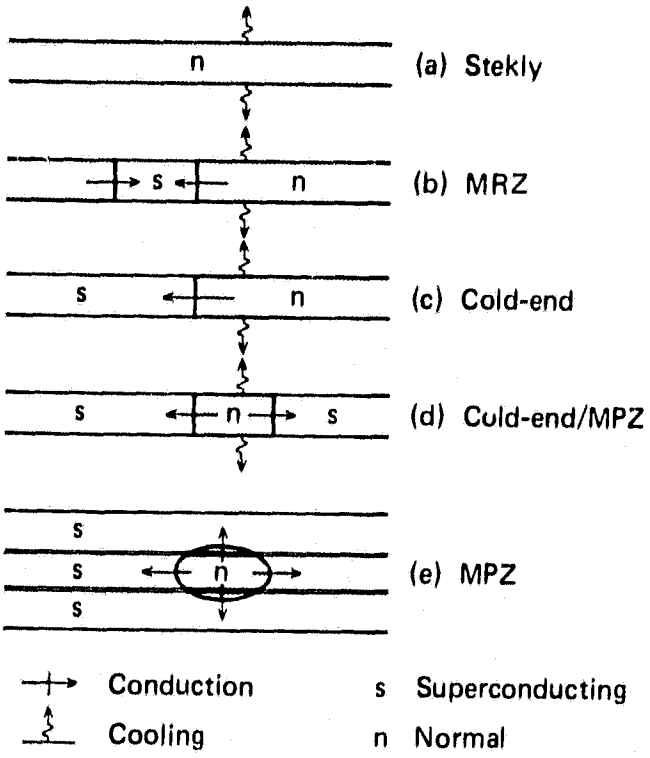

FIGURE 3-4. With reduction in conductor stability as indexed by some parameter which is generally expressed in the form (conductor materials/design) x (conductor average current density) the size of the recoverable normal zone decreases. Condition (a) always vanishes when $\dot{G}_d = 0$; the same conductor will also satisfy condition (c) when conductivity, $K \neq 0$. A less stable conductor will satisfy (c) but not (a). Eventually only a small normal zone will recover spontaneously -- conditions (d) and (e). Between (a) and (c) lies the "minimum recovery zone".

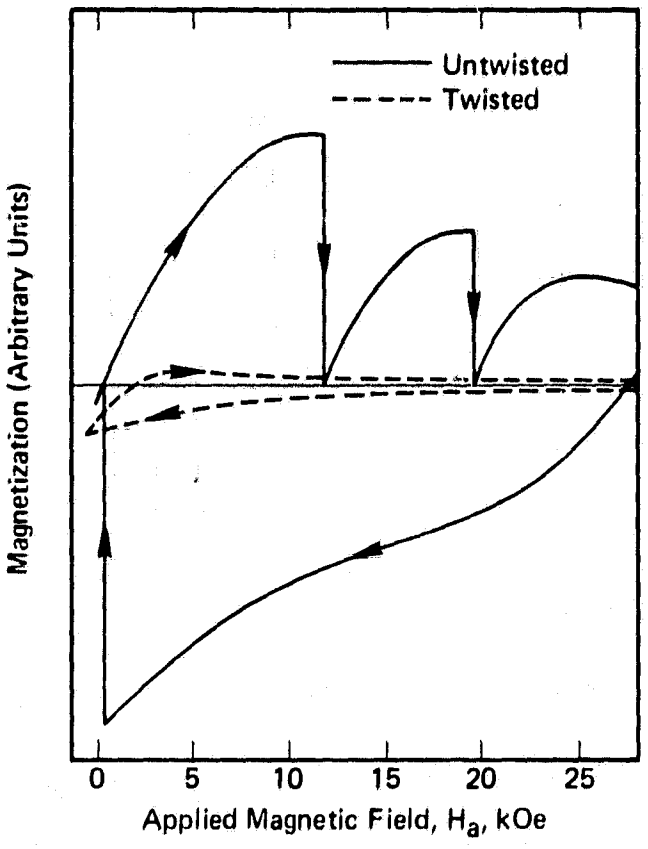

FIGURE 4-1. Influence of twist (pitch = 17 mm) on external pluse-field stability and hysteretic loss in a 361-filament (69 $\mu m^{\emptyset}$) Cu/Ti-Nb (2:1) monolithic conductor (3.2 x 1.3 mm^2) -- after IWASA and MONTOGOMERY [38].

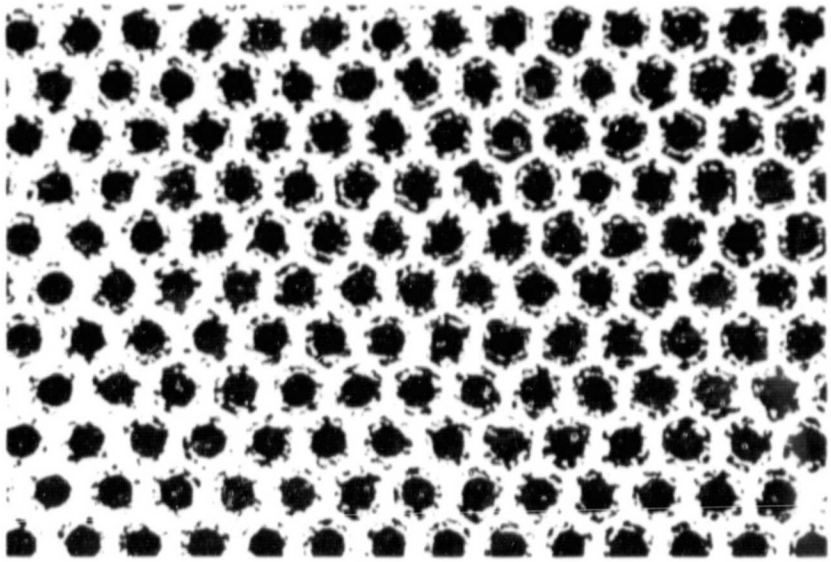

FIGURE 4-2. Interior of a Cu-Ni/Cu/Ti-Nb mixed-matrix basic strand intended for pulsed-magnet cabled or braided conductors. Specifications of the strand depicted are:

Strand diameter (mm)	0.3	Filament number	241
Twist pitch (mm)	5	Matrix/SC ratio	4
Filament diameter (μm)	8	Capacity at 6 T (A)	17

-- micrography courtesy of M. Nagata (Sumitomo Electric Industries ltd.).

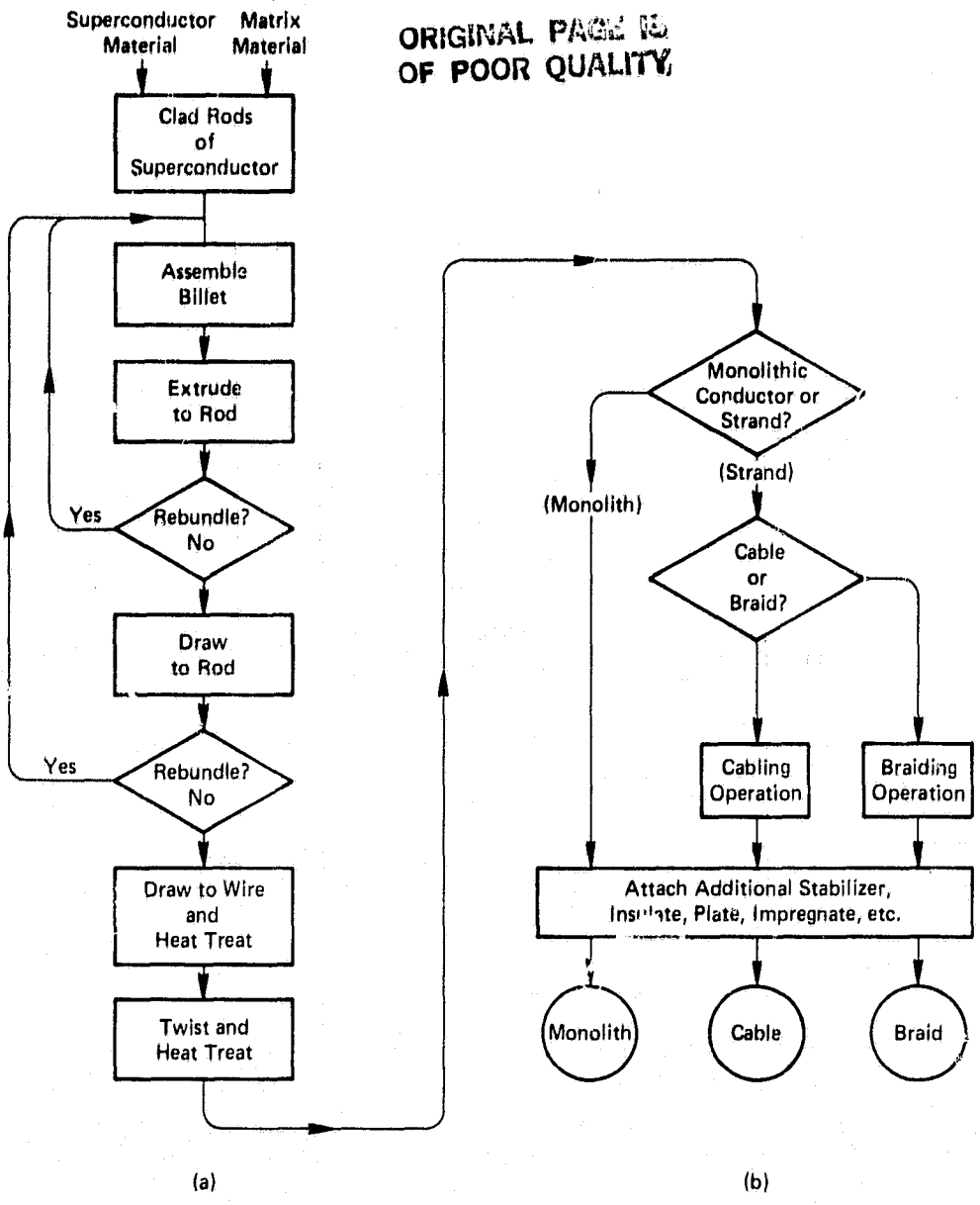

FIGURE 5-1. Flow diagram for superconductor processing. In some cases the drawn and twisted wire (or "monolithic conductor" -- a very thick wire) is the final product. Otherwise many such wires are assembled by means of a stranding process into a cable or a braid. Operation (a) is common to all processes.

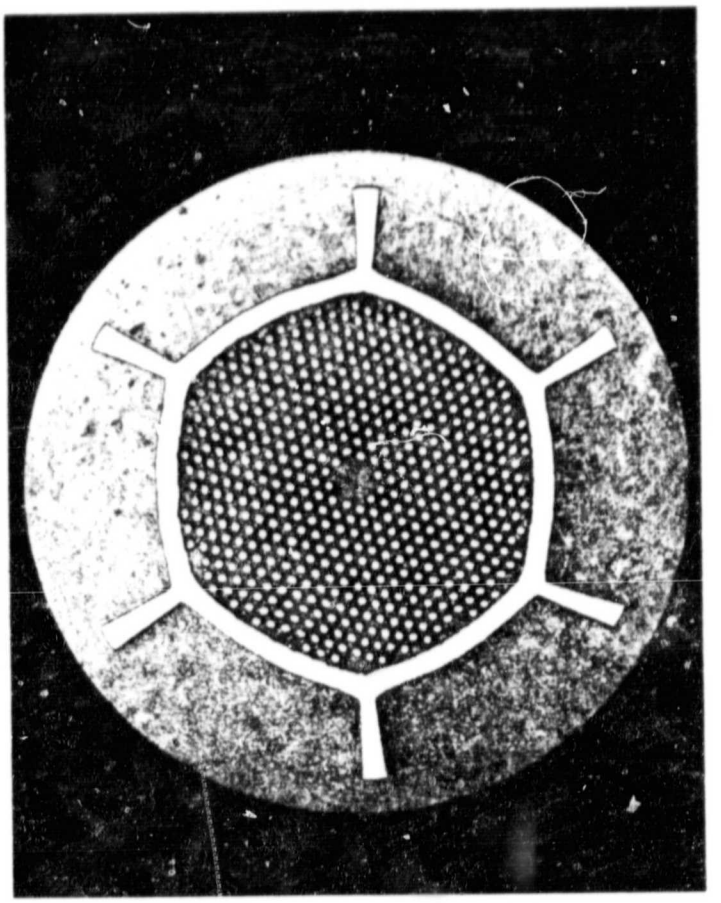

FIGURE 5-2. Advanced mixed matrix basic strand for a 50-kA, 20-MJ, tokamak ohmic heating coil (related to the basic strand of Figure 5-5(c)). Description:

Bare metallic diameter (mm)	:	2.04	Total Cu area (mm^2)	:	2.399 (73%)
Core diameter (mm)	:	1.33	Cu-10Ni area (mm^2)	:	0.356 (11%)
Diameter of fil. region (mm)	:	1.20	Ti-Nb area (mm^2)	:	0.514 (16%)
Fin thickness (mm)	:	0.066	Fil. diameter (μm)	:	34.8
Cu shell thickness (mm)	:	0.098	Fil. number	:	540
Twist pitch (mm)	:	8.1			

-- data from WOLLAN *et al.* [60]; micrograph courtesy of J.J. Wollan (Los Alamos Scientific Laboratory).

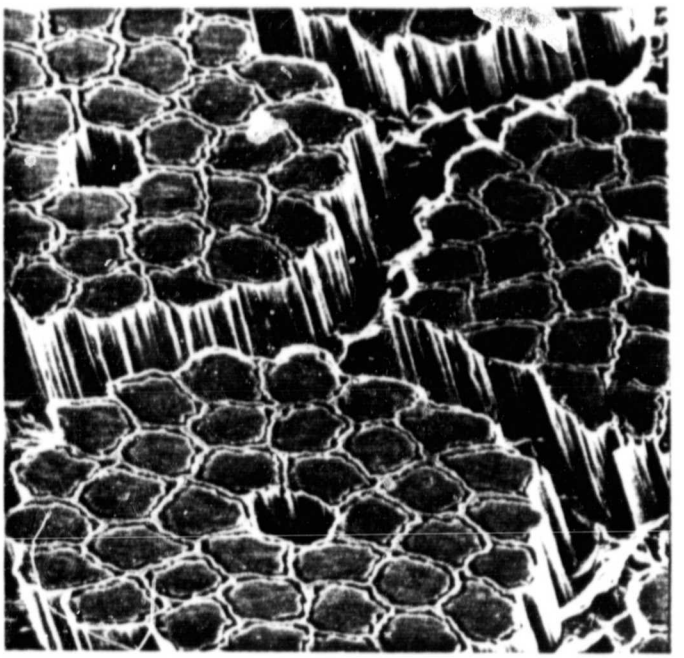

FIGURE 5-3. Primary 35-filament bundle of a 2975-filament double-extruded mixed-matrix composite; strand diameter, 1.45 mm. The Ti-Nb filaments are surrounded by 2 μm of Cu, then by Cu-Ni. The canister (shell) of the primary billet is of impure Cu. The constitution of the conductor is: Cu-Ni/impure-Cu/pure-Cu/SC = 0.25/0.7/1.55/1. In this scanning-electron micrograph, original magnification 650X, the Cu has been removed by deep etching -- micrograph courtesy of H. Hillmann.

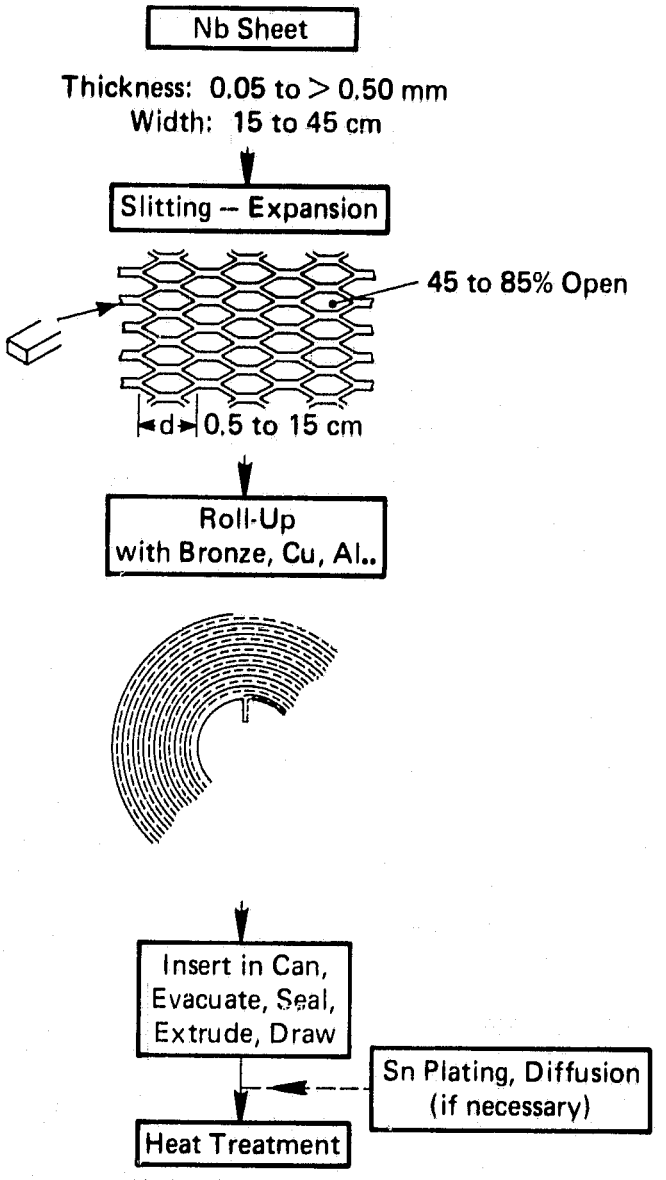

FIGURE 5-4. The modified jellyroll process of Teledyne Wah Chang Albany as described by ROGERGE [7, p. 446].

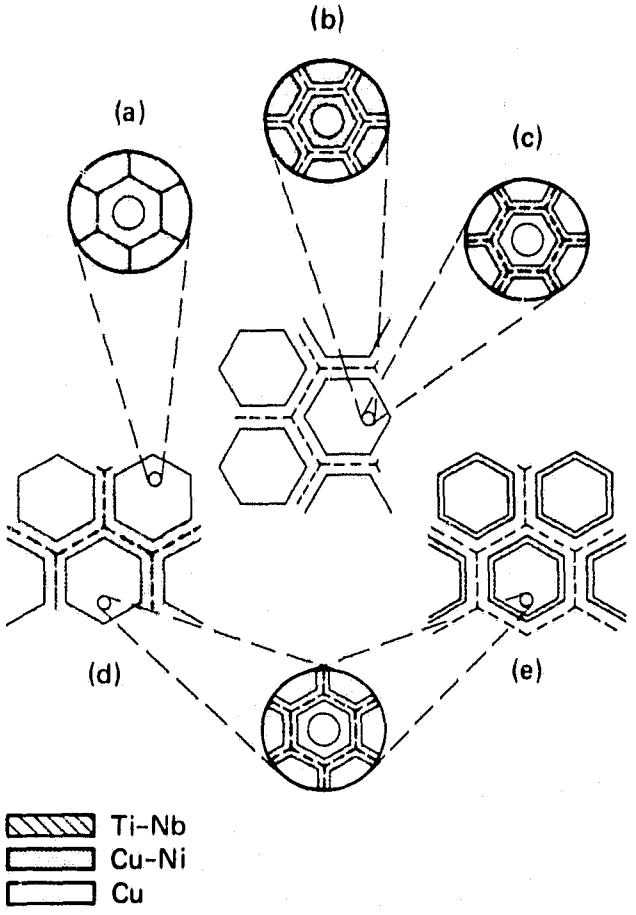

FIGURE 5-5. Schematic representations of three-cell segments of double-extruded monolithic three-component mixed-matrix composites for a.c. or pulsed-field applications. Depicted are groups of primary composites and representative elements of which they are composed (these are equivalent to the basic strands of a cable or braid). Dashed lines are intended to represent prior boundaries between components.

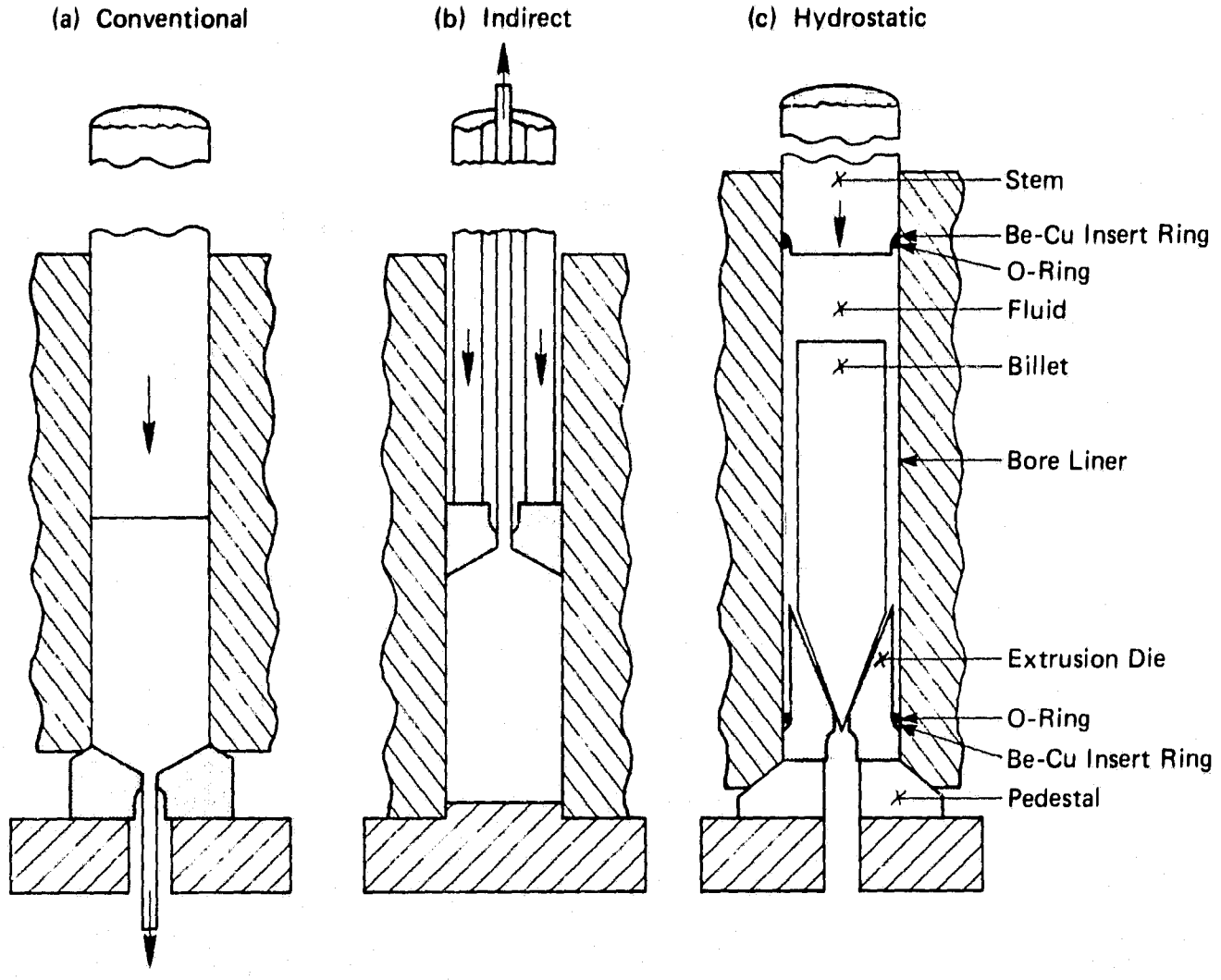

FIGURE 5-6. Schematic representations of the principles of conventional, indirect, and hydrostatic extrusion.

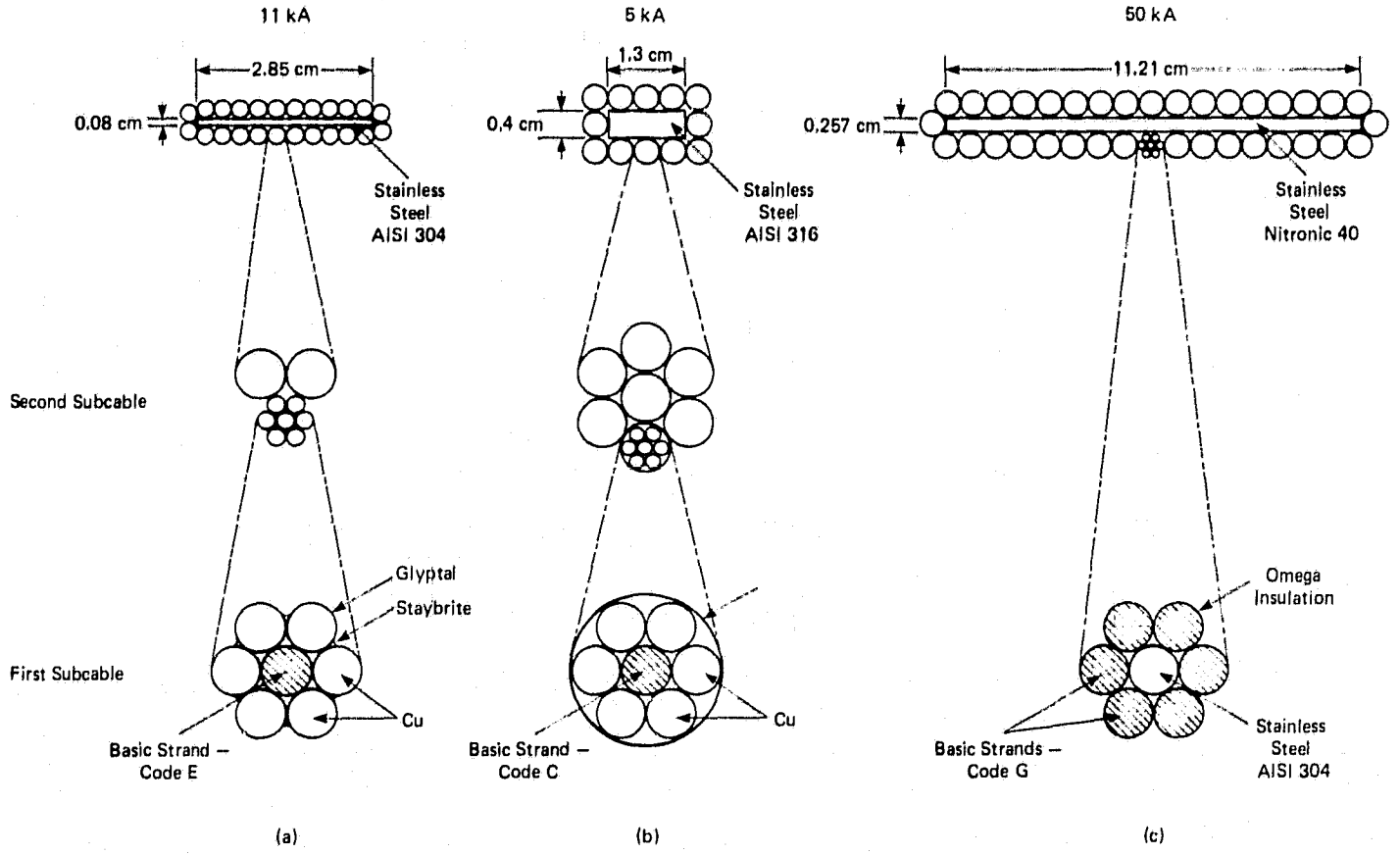

FIGURE 5-7. Three high-current cryostable cables fabricated from six-around-one-cabled basic strands. (a) An 11-kA conductor for a 1.5 MJ model tokamak ohmic heating coil -- after WANG *et al.* [20, 48]; (b) a 5-kA conductor for a 30-MJ magnetic energy storage coil -- after ROGERS *et al.* [49]; (c) a 50-kA conductor for a proposed 20-MJ tokamak ohmic heating coil -- after WALKER *et al.* [60, 71].

FIGURE 5-8. (a Twelve-bobbin planetary strander for the winding of rope (structural steel) or cable (electrical wire). As shown, the machine is not adapted for back-twist, all the bobbin cradles being parallel to one another -- photograph courtesy of A. Blackmore, CEEJ Manufacturing Company, Ont., Canada. (b) Detail of the neighborhood of the cabling point. The strands pass through carbide eyelets in the lay-plate the number of evenly spaced holes in which equals the number of strands being used (in general some bobbins may be vacant) and, guided by the nipple, become cabled about a chisel-shaped mandrel. After leaving the mandrel, the cable is rolled or Turk's headed (double rolled) to size. The mandrel may be replaced by a continuous strip of stainless steel or similar material if a reinforcing core is desired -- after HILLMANN *et al.* [54, pp. 161, 153].

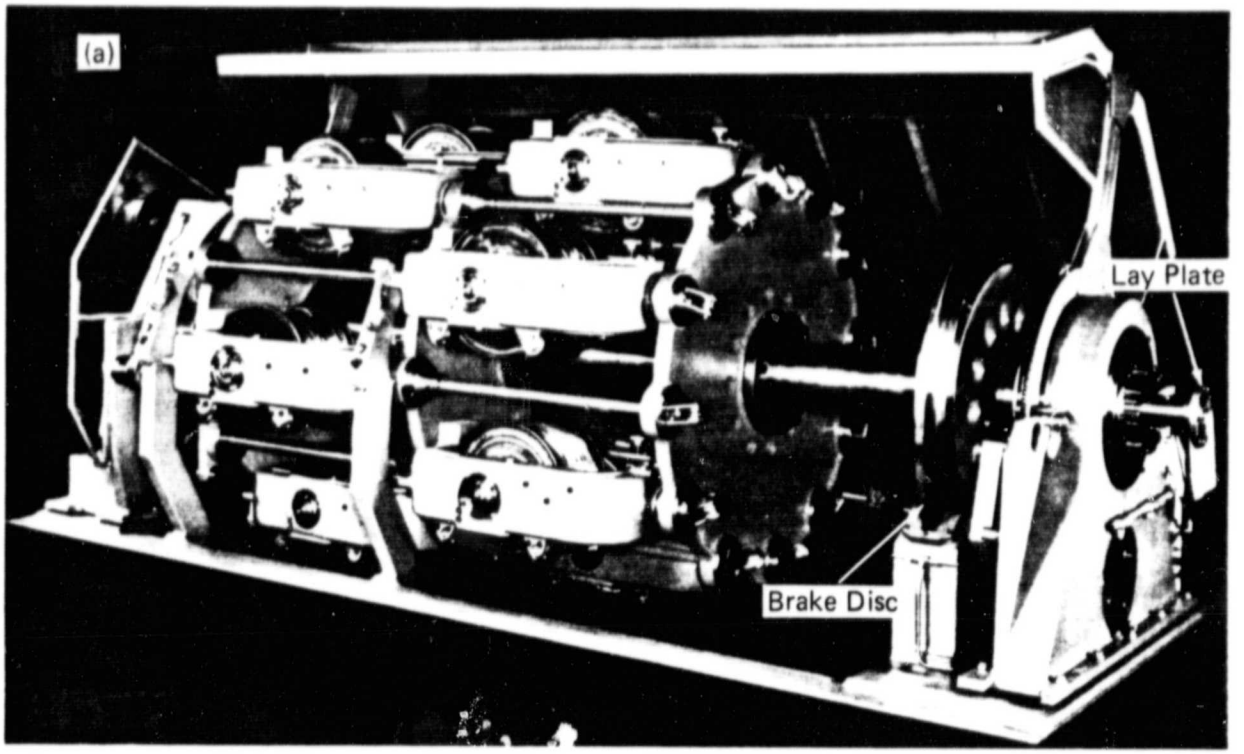

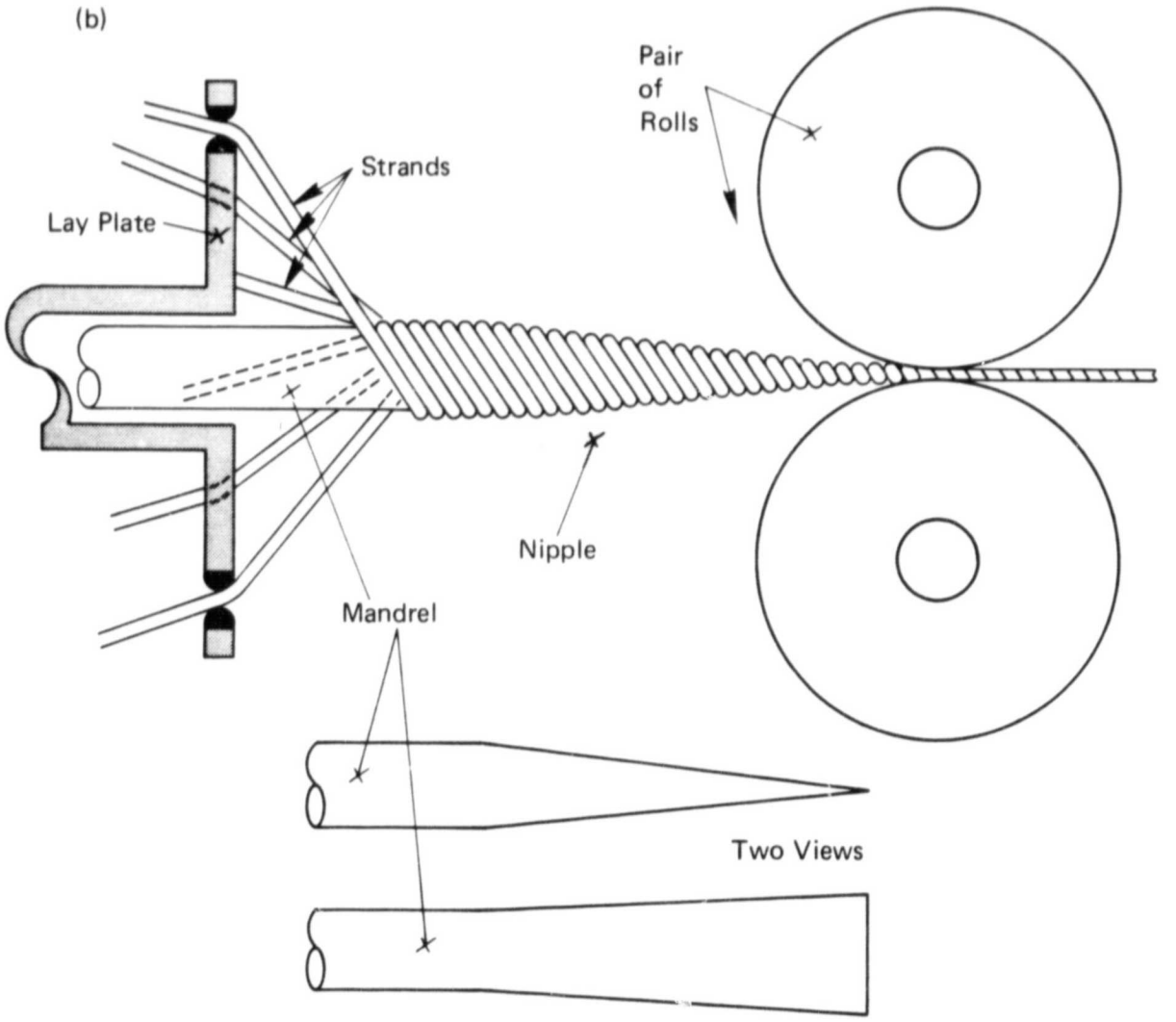

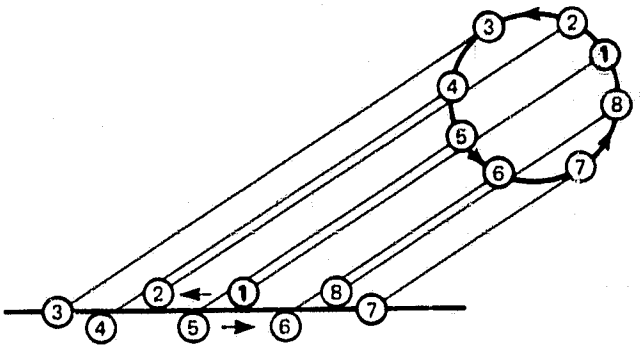

FIGURE 5-9. Diagram indicating transposition in one dimension as the projection of a twisted cylindrical cage; e.g., within the plane, strand #1 is seen to occupy positions between every other pair of strands during one-half-period of the twist; in general a full-period of twist is required to transpose all the strands.

(a)

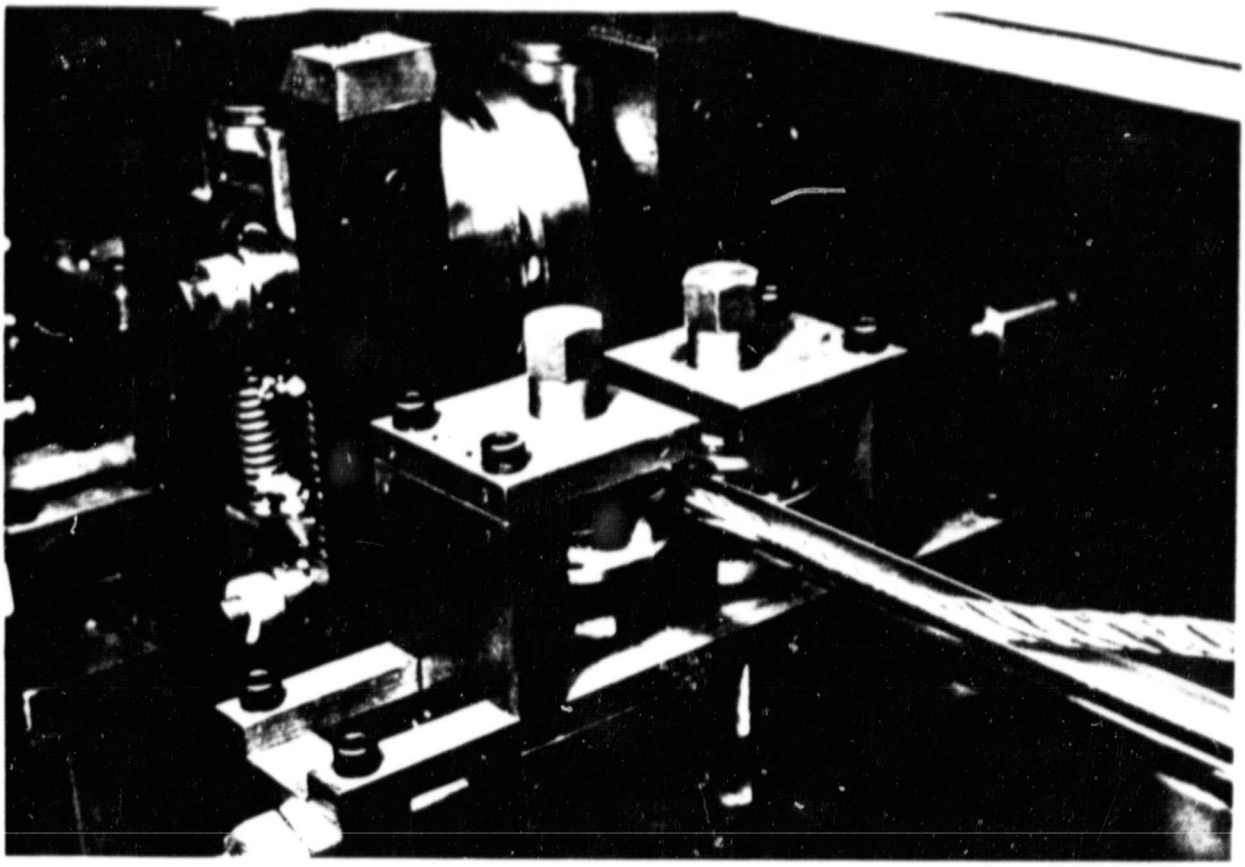

(b)

FIGURE 5-10. Fabrication of compacted cables. (a) Superconducting cable (in the form of six twisted-together triplets -- hence fully transposed) entering the final forming rolls of a tube mill prior to the seam-weld step. Shown is the HFTF conductor. In fabricating the EBT conductor the entering cable was only slightly twisted -- just sufficiently to hold it together. (b) Various stages during the compaction and forming of the conductor -- photographs courtesy of E. Adam and G.L. Taylor, Airco Superconductors.

FIGURE 5-11. Compacted mixed-matrix cable: Scanning electron micrographs after deep etching. Specifications:

Basic Strand Data:

Filament diameter	20 μm
Filament number	517 x 19
Twist pitch	50 mm
Cu/Cu-10Ni/SC ratio	3/0.2/1

Conductor Data:

Dimensions	5 x 2.8 mm^2
Critical current	3 kA at 8T

-- conductor sample and data by courtesy of E. Adam, Airco Superconductors; sample polished and etched by K.L. Hammond, Battelle; micrographs taken by C.R. Barnes, Battelle.

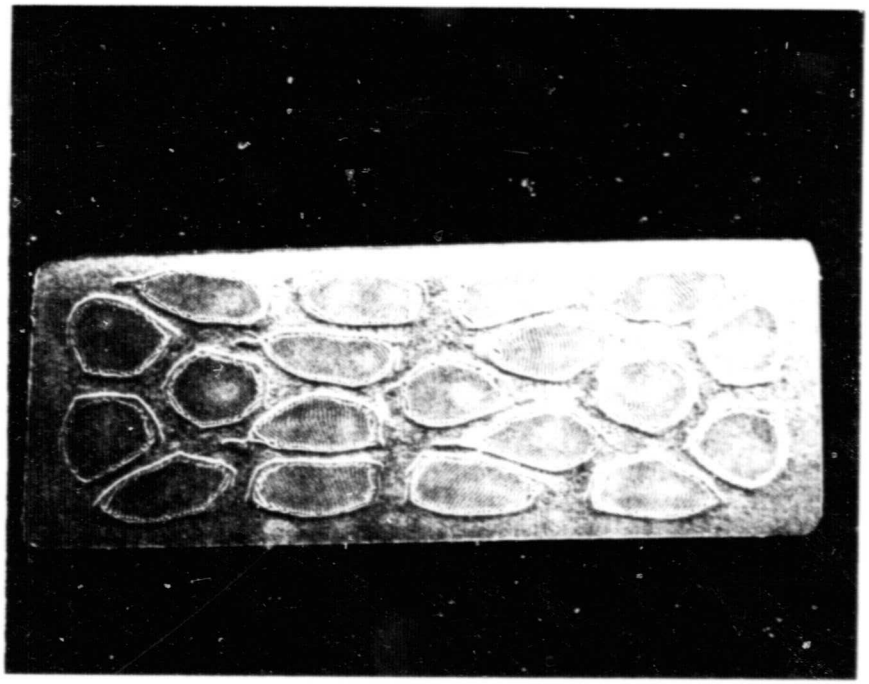

14X

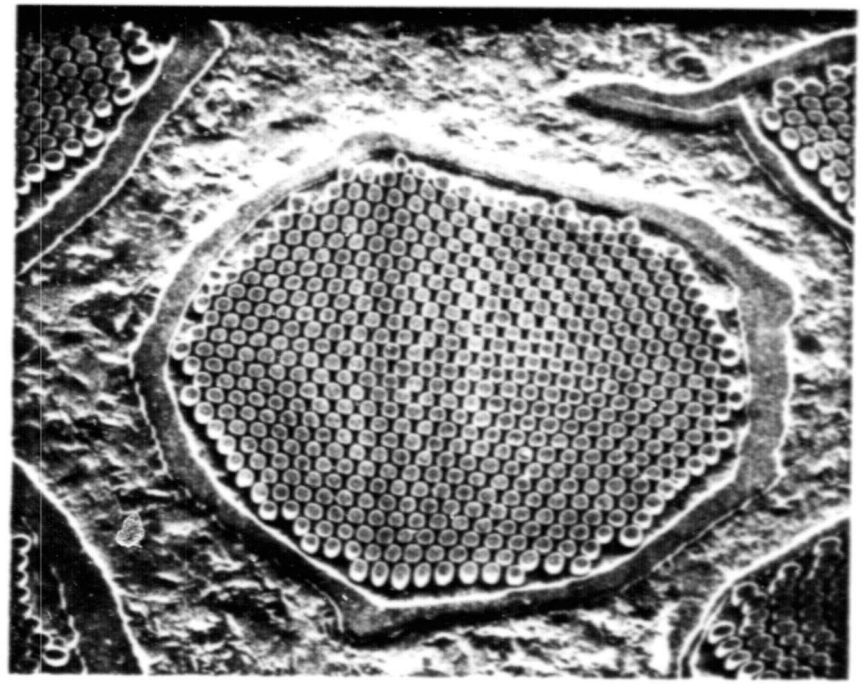

100X

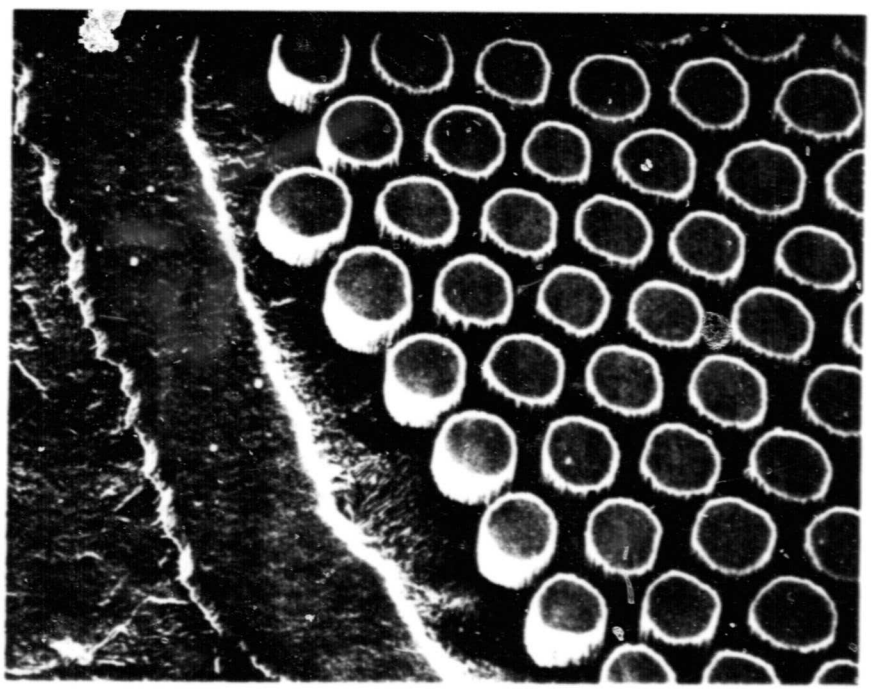

500X

2500X

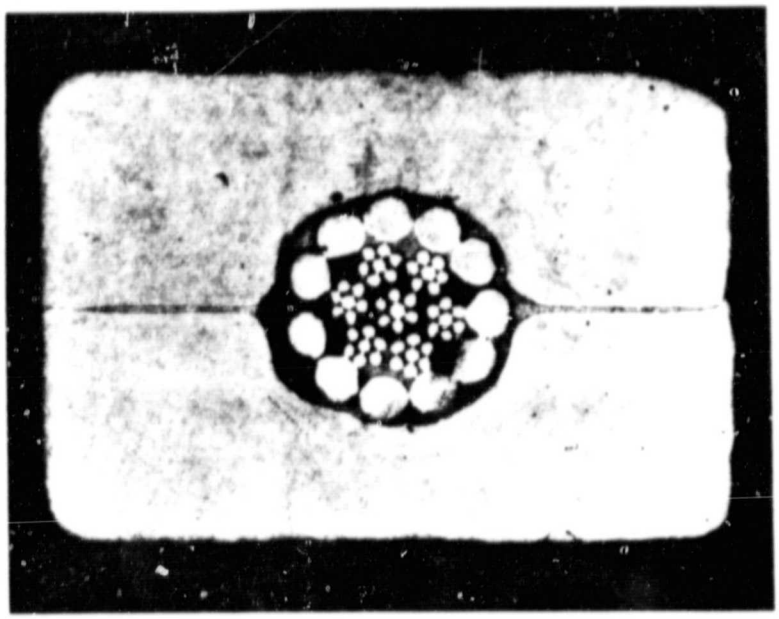

FIGURE 5-12. An Al-stabilized Cu/Ti-Nb hybrid composite conductor intended for a particle-detection magnet at the colliding-beam (ISR) facility at CERN. Eleven 0.6-mmØ Cu/Ti-Nb strands are cabled onto a two-stage six-around-one cabled stainless-steel core and soldered between a pair of grooved 99.9997%-Al strips -- after MORPURGO *et al.* [76].

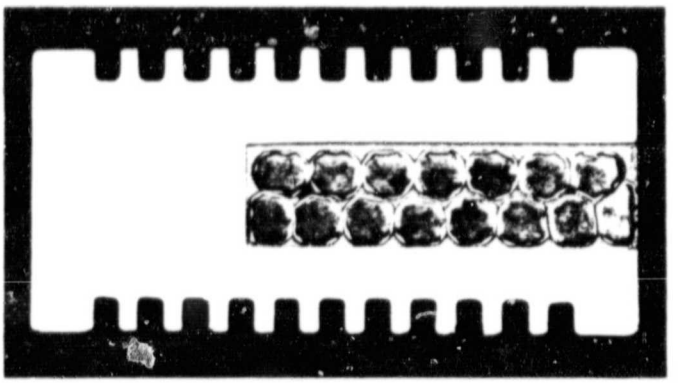

FIGURE 5-13. A 15-strand Cu/Ti-Nb Rutherford cable designed for inclusion in the toroidal field coils of a tokamak fusion reactor, rendered cryostable by being imbedded in a thick Cu strip provided with cooling fins and an oxidized surface. More recent versions of the same conductor show the cable more deeply imbedded and the groove-opening closed with more Cu.

Basic Strand Data:		Conductor Data	
Strand diameter (mm):	2.3	Dimensions (mm^2):	27.0 x 12.7
Filament diameter (μm):	50	Strand pitch (mm):	200
Filament number :	1060	Cu/SC ratio:	8.5:1
Twist pitch (mm):	30	Critical current at 8T (kA):	20.4
Cu/SC ratio:	1.1		

-- micrograph data courtesy of Y. Tanaka, Furukawa, Ltd.

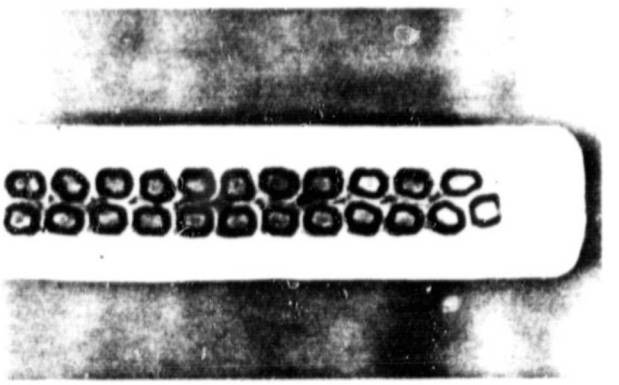

FIGURE 5-14. Hybrid Al/Cu-stabilized cable for the toroidal field coils of a fusion reactor. 23 Cu/Ti-Nb strands are cabled and imbedded in an Al matrix.

Basic Strand Data:		Conductor Data:	
Strand diameter (mm):	1.83	Dimensions (mm^2):	28 x 7
Filament diameter (μm):	23	Strand pitch (mm):	200
Filament number:	1500	Critical current at 8 T (kA):	10.9
Twist pitch (mm):	20		
Cu/SC ratio:	3		

-- micrograph and data courtesy of M. Nagata, Sumitomo, Ltd.

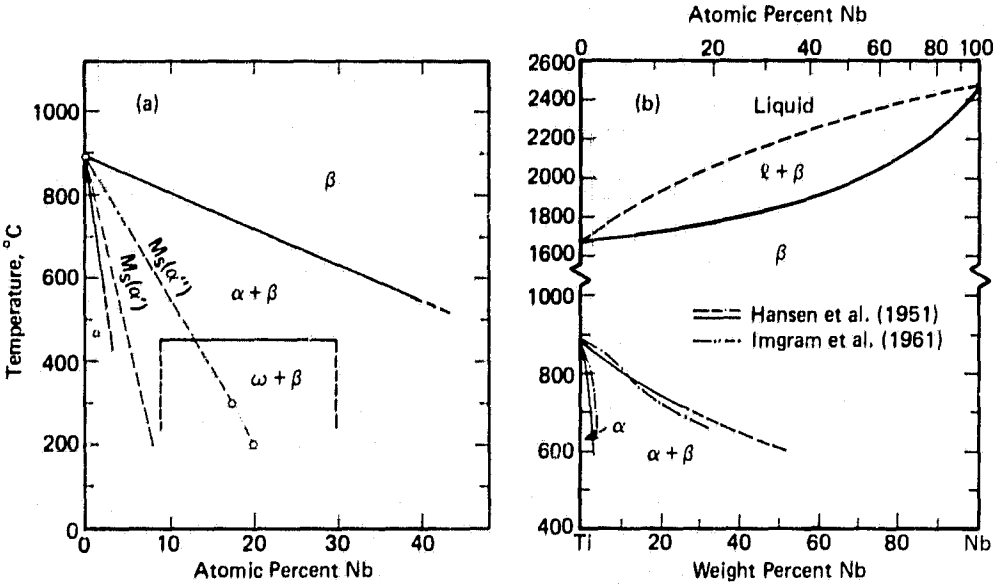

FIGURE 6-1. (a) Metastable-equilibrium phase diagram for Ti-Nb indicating the martensitic α' and α" transi and the isothermal ω+β-phase filed. (b) Equilibrium phase diagram for Ti-Nb from standard sources. The diagrams have been modified by the observation that practically no α-phase precipitation takes place during the aging of alloys with more than 40 at.% Nb [77, 78, 79, 80].

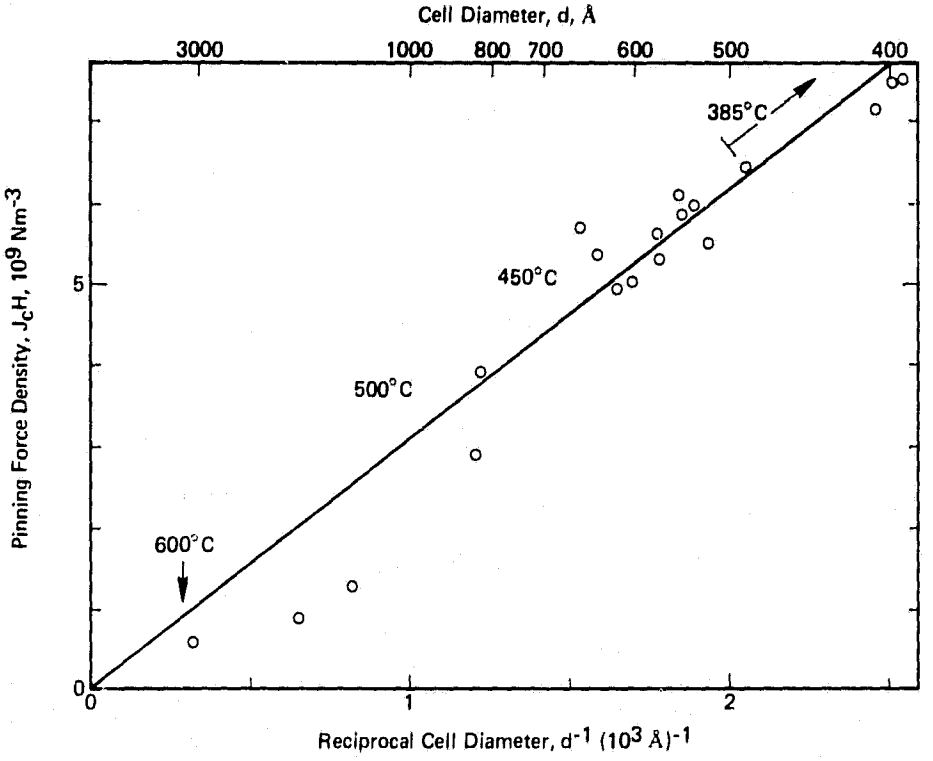

FIGURE 6-2. Bulk-pinning force (J_c.H) at 4.2K and 50 kOe *versus* reciprocal cell diameter for Ti-58Nb, cold worked and heat-treated for one hour at the temperatures indicated -- after NEAL *et al.* [77].

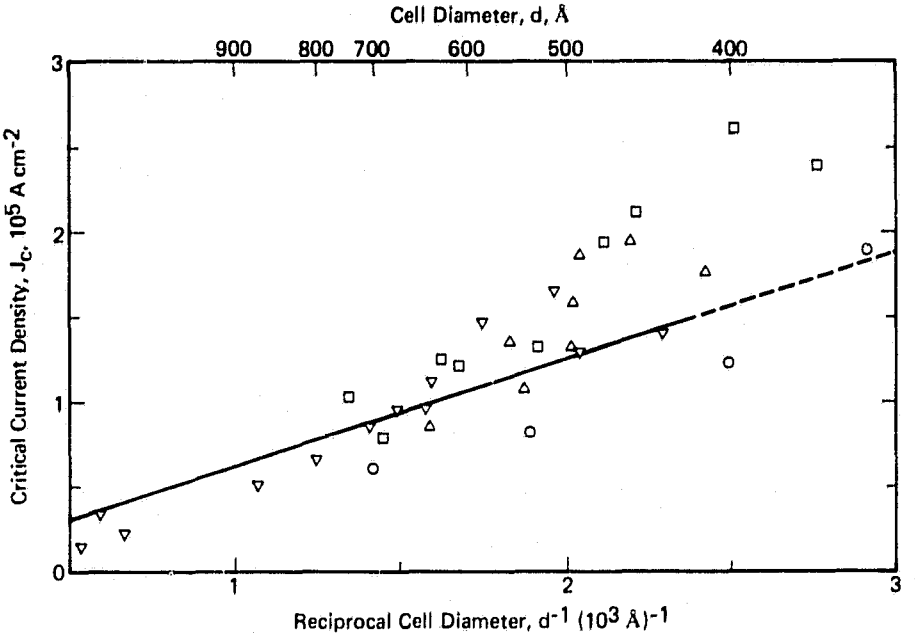

FIGURE 6-3. Influence of precipitation on critical-current density. Critical-current density, J_c(4.2K, 50 kOe), of optimized commercial multifilamentary conductors *versus* inverse cell (subband) diameter. Alloys represented are: Ti-53.5Nb (△); Ti-50.3Nb (○); Ti-49.6 (□); Ti-47.3Nb (▽). The straight line, based on the previous figure, is a repetition of the results of NEAL *et al.* on precipitate-free Ti-58Nb -- after WEST and LARBALESTIER [78].

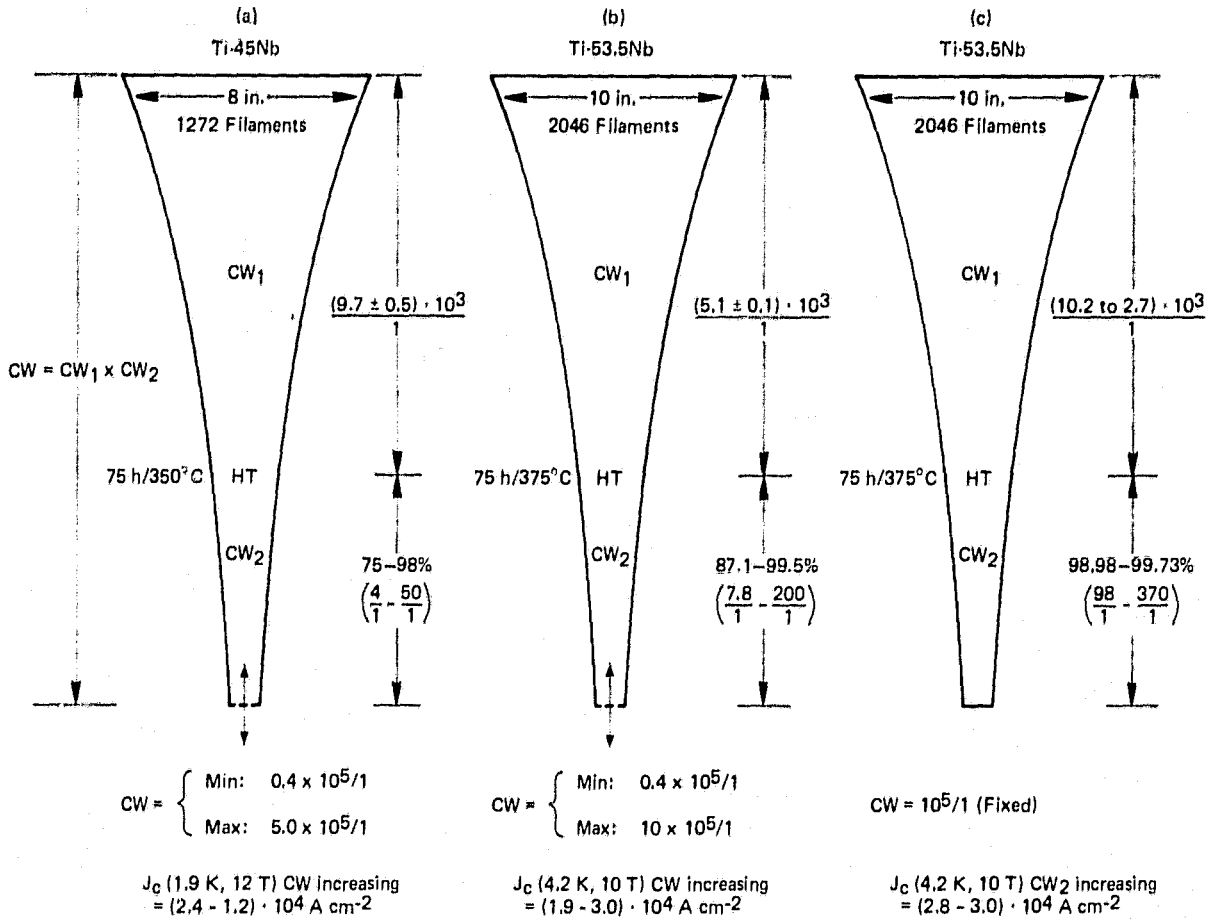

FIGURE 6-4. Schema for comparative studies of the influences of total or final cold deformation on the critical-current densities of singly-heat-treated Ti-45Nb and Ti-53.5Nb multifilamentary Cu/Ti-Nb composites prepared from commercial-size billets. Trends are indicated by listings of the cold-work extrema and the corresponding high-field critical-current densities -- after STEKLY *et al.* [89].

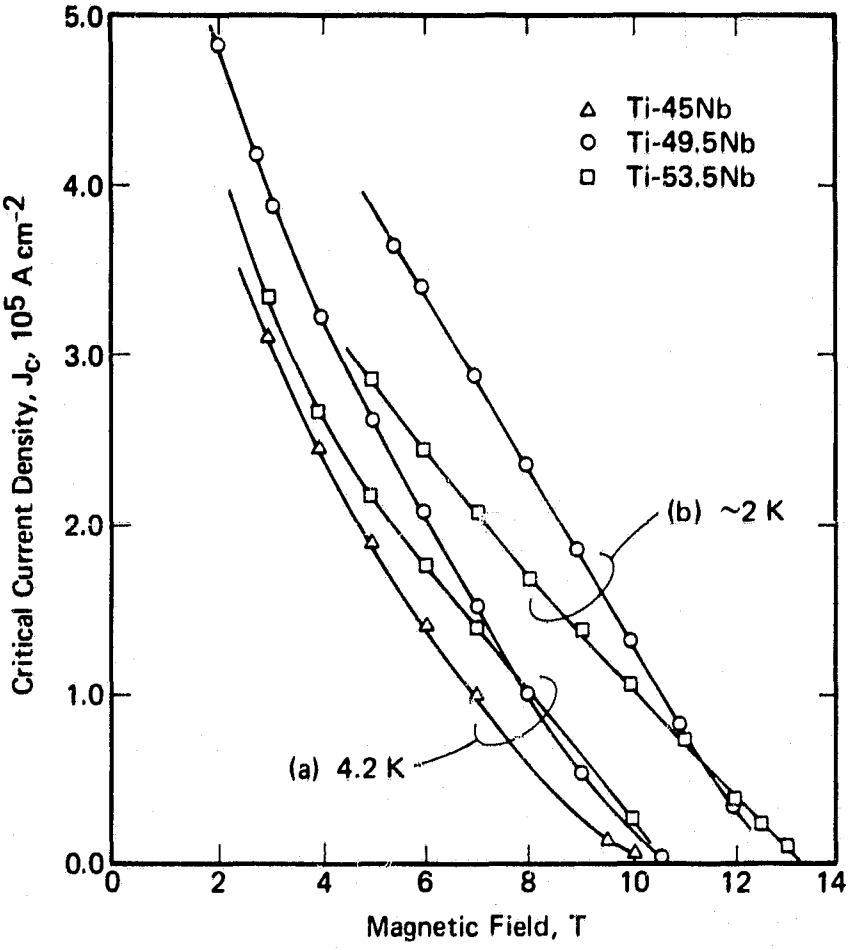

FIGURE 6-5. (a) Comparison of the J_c (4.2K) field dependencies of optimized Ti-45Nb and Ti-53.5Nb as measured by STEKLY *et al.* [89] with that of Ti-50Nb from the work of LARBALESTIER [83, 92]. (b) J_c(~2K) field dependencies of Ti-49.5Nb (at 4.2K) and Ti-53.5Nb (at 2.05K) conductors -- after HAWKSWORTH and LARBALESTIER [92].

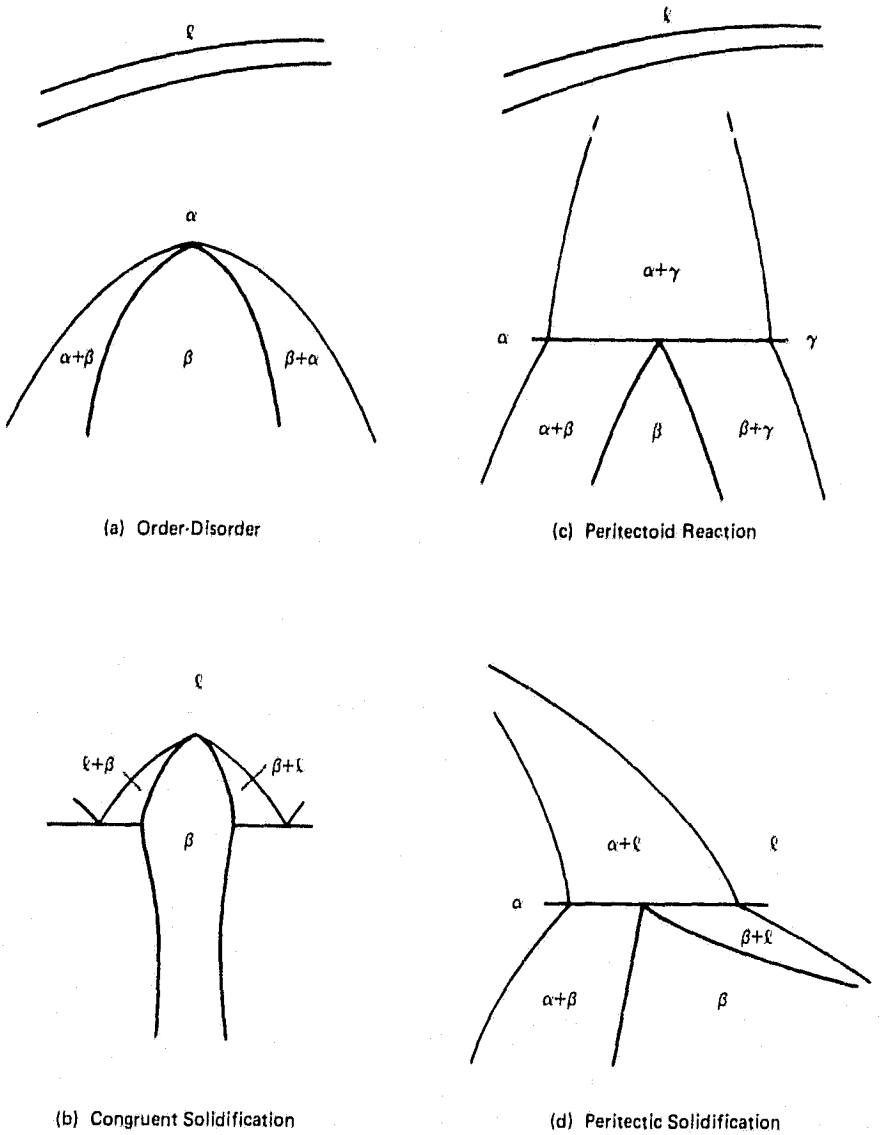

FIGURE 8-1. Four classes of binary compound formation by solidification or solid-state reaction -- after RAYNOR [107] and other sources.

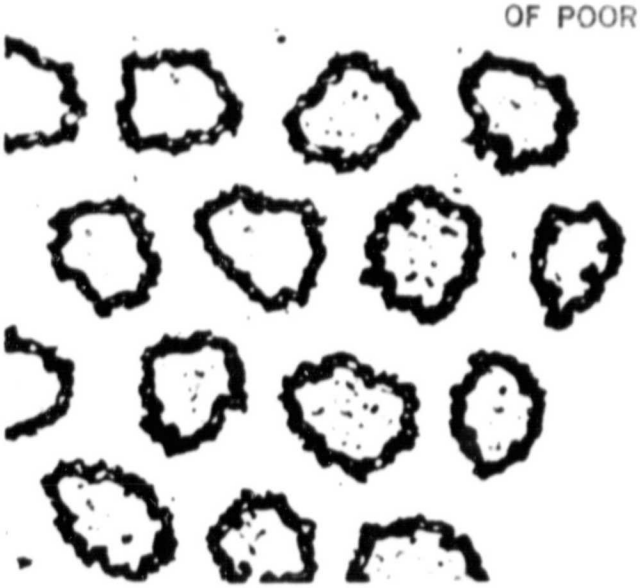

(a) 10 hours

(c) 30 hours

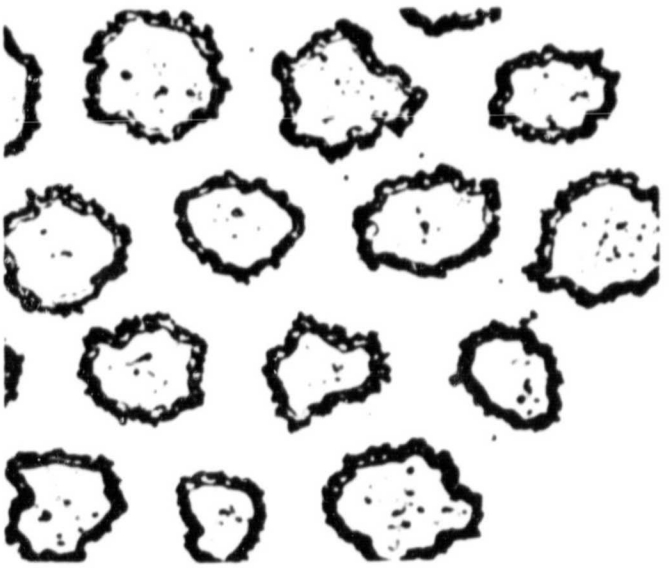

(b) 20 hours

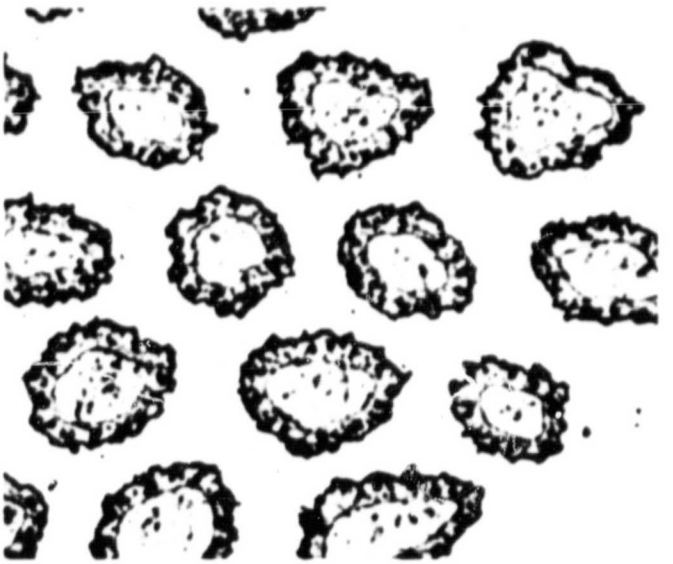

(d) 200 hours

FIGURE 8-2. Formation of the Nb_3Sn reaction layer on 5-$\mu m^{\emptyset}$ (nominal) Nb filaments at 700° C from a 10-wt.%Sn bronze matrix -- after MEYER *et al.* [51, p. 83].

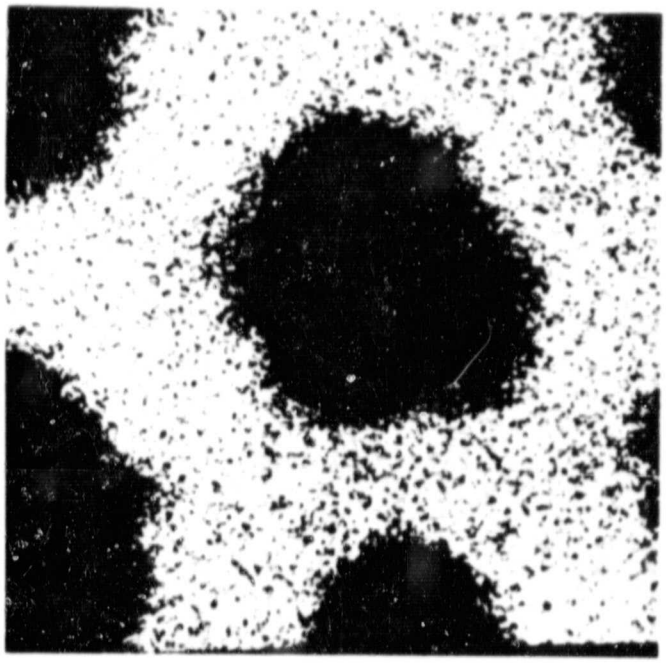

(a) Back-scattered Electrons

(b) Nb x-rays

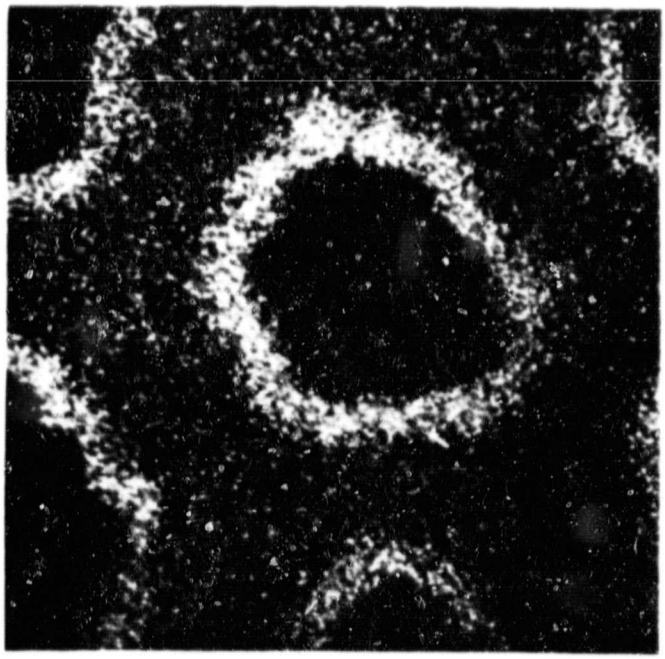

(c) Cu x-rays

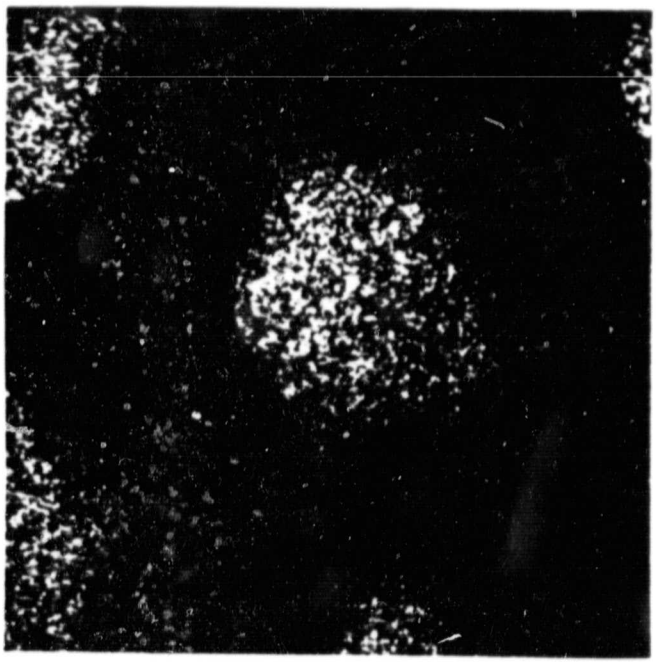

(d) Sn x-rays

FIGURE 8-3. Disposition of the Nb, Cu, and Sn constituents of a Nb/bronze composite after reaction for 30 h/700° C (cf. Figure 8-2) as detected using scanning electron microscopy -- after MEYER *et al.* [51, p. 85].

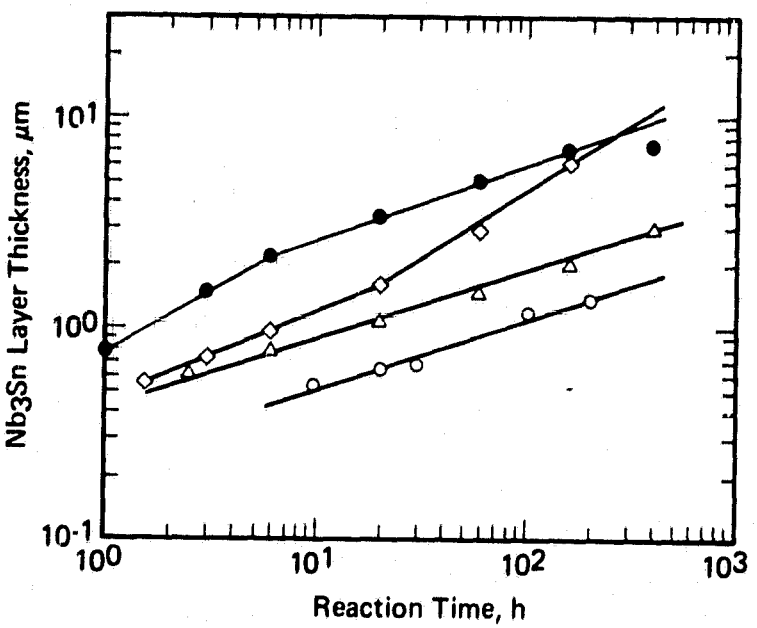

FIGURE 8-4. Thickness of the Nb_3Sn reaction layer formed an unalloyed and doped Nb filaments by solid-state reaction from a 10-wt.%Sn bronze matrix as function of time at 700° C. (a) The composite of Figures 8-2 and 8-3 (O) -- after MEYER *et al.* [51, p. 82]; (b) a similar composite with 25 μmØ filaments (△); (c) a composite with 25 μmØ Nb-Zr (0.5 wt.%) filaments (●); (d) a composite with 25 μmØ ZrO_2-dispersed Nb filaments (◇) -- the latter three results being due to SUENAGA *et al.* [120].

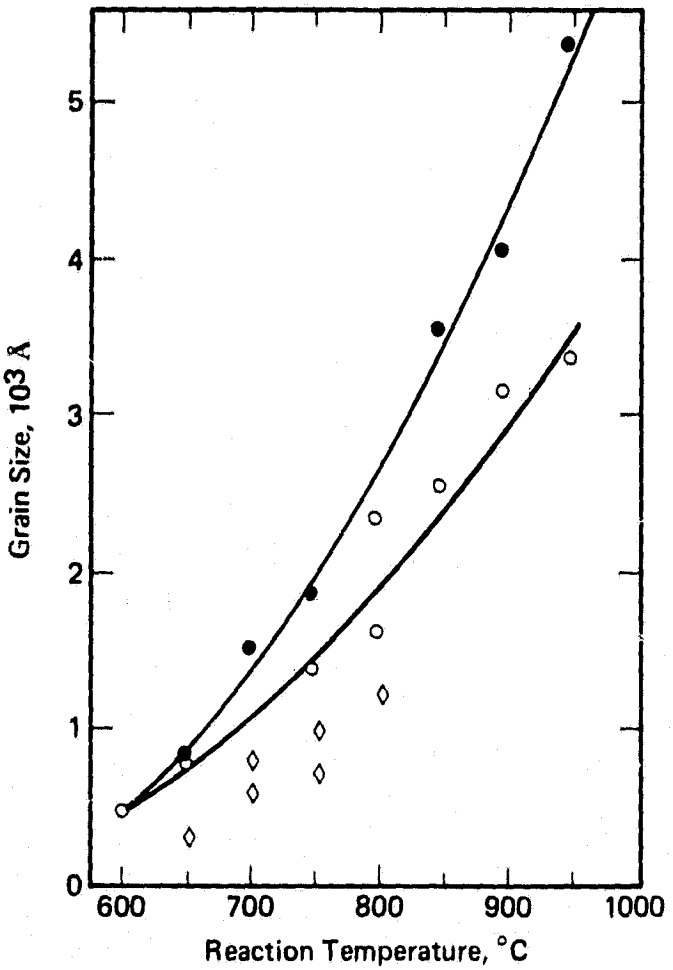

FIGURE 8-5. Average grain size of the Nb_3Sn reaction layer as a function partly of reaction temperature. The data designated ● and ○ are due to SCANLAN *et al.* [121] and refer to grain sizes at a layer thickness of 1 μm (○) and after a reaction time sufficient to fully consume the ∿ 8 μm-thick filaments (●). The data designated ◊ are due to SHAW [122] and are repeated in Table 8-6 -- after SHAW [122].

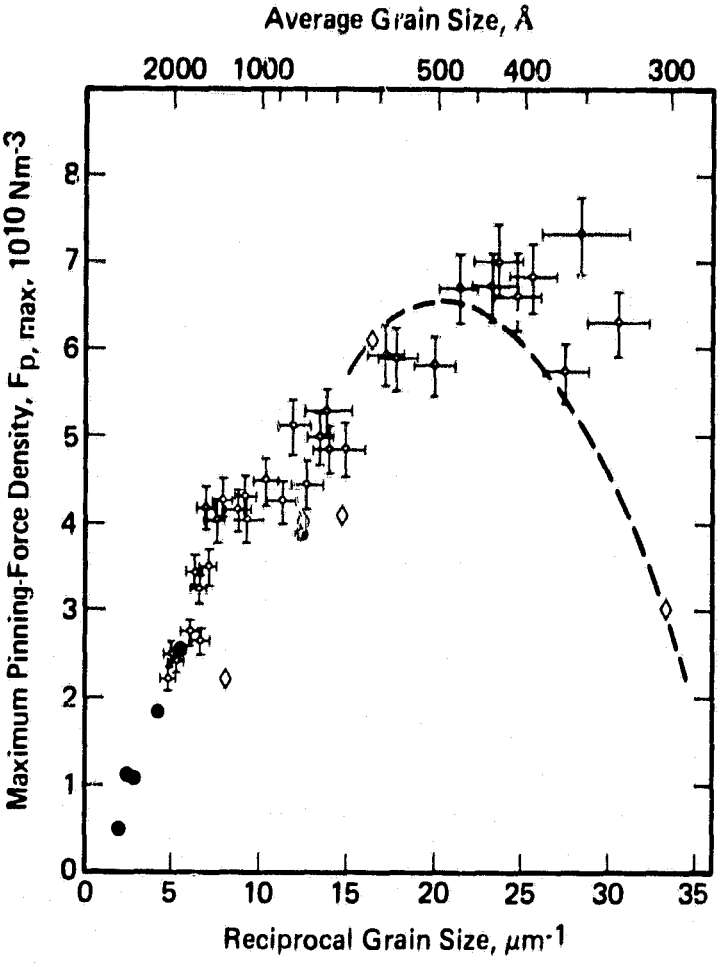

FIGURE 8-6. Bulk-pinning force density as a function of reciprocal grain size in bronze-process Nb_3Sn superconductors: (a) internal diffusion onto Nb filaments from a 13.5 wt.% Sn matrix (⊢◇⊣) [123]; (b) internal diffusion within Nb-1% Zr tubes from a nominal 13 wt.% Sn bronze (◊) [122]; (c) external diffusion *via* Cu onto Nb filaments (●) [121].

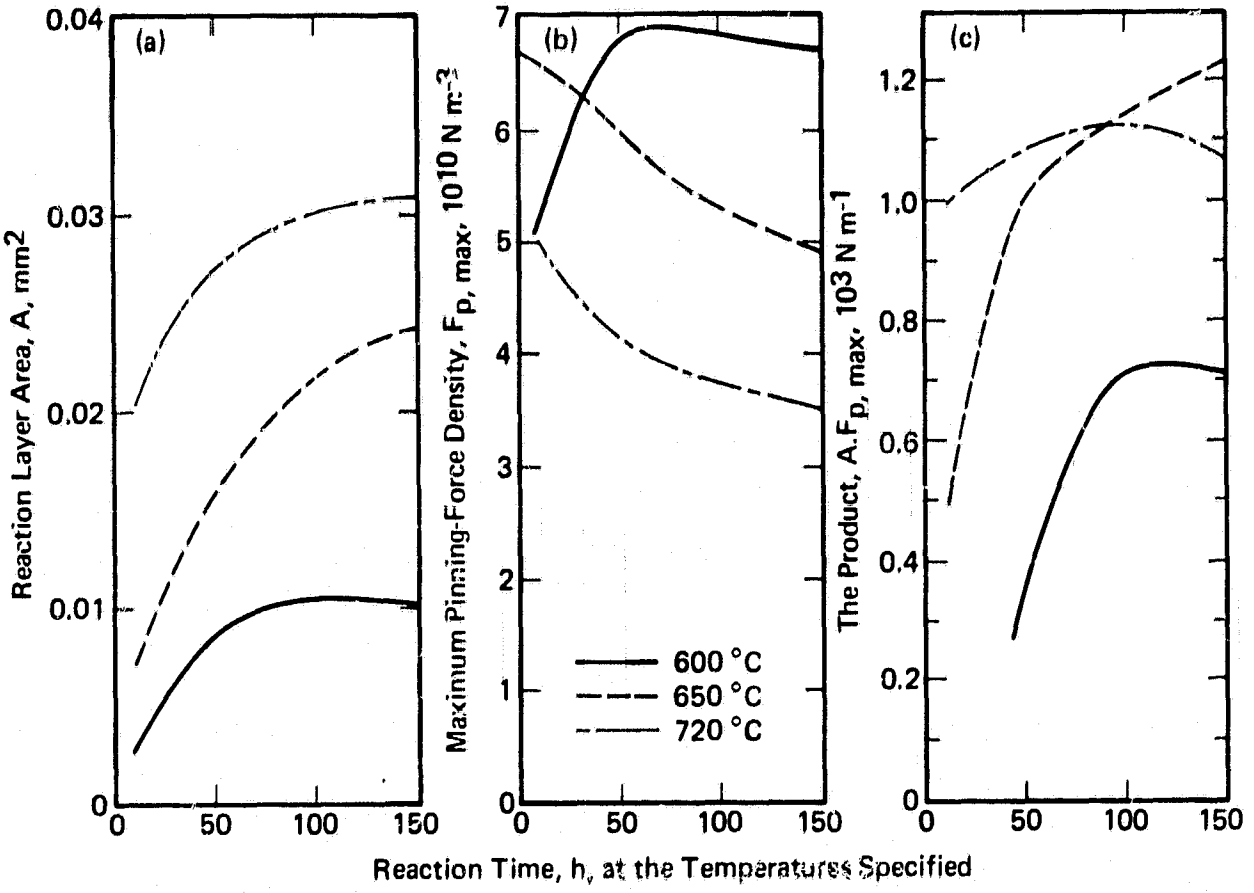

FIGURE 8-7. Influence of diffusion time at the temperatures specified on: (a) the area of the reaction layer; (b) the maximum bulk-pinning force density; (c) the product of the two -- after HILLMANN *et al.* [6, p. 26].

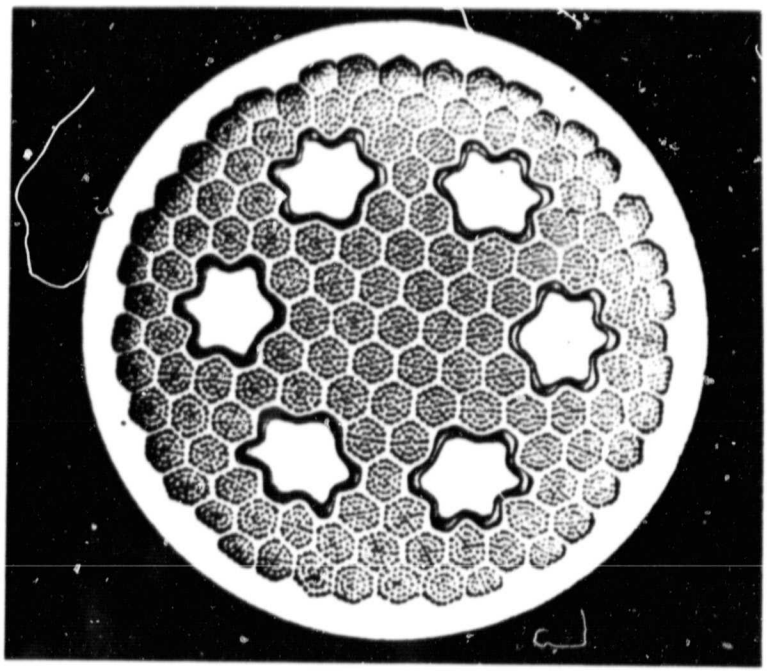

FIGURE 8-8 Harwell/IMI conductor.

Specifications:

Number of filaments	4477
Matrix	tin bronze
Cu/Total ratio	0.15/1
Bronze/Nb ratio	3/1
Diffusion barriers	P-poisoned Nb
Strand diameter	0.7 mm
Critical current (A at 10 $\mu V\ m^{-1}$)	570 350 240 152 at 5 7 9 11 T

-- after LEE and SCOTT [6, p. 37]. Photograph and data courtesy of F. J. V. Farmer, IMI Titanium.

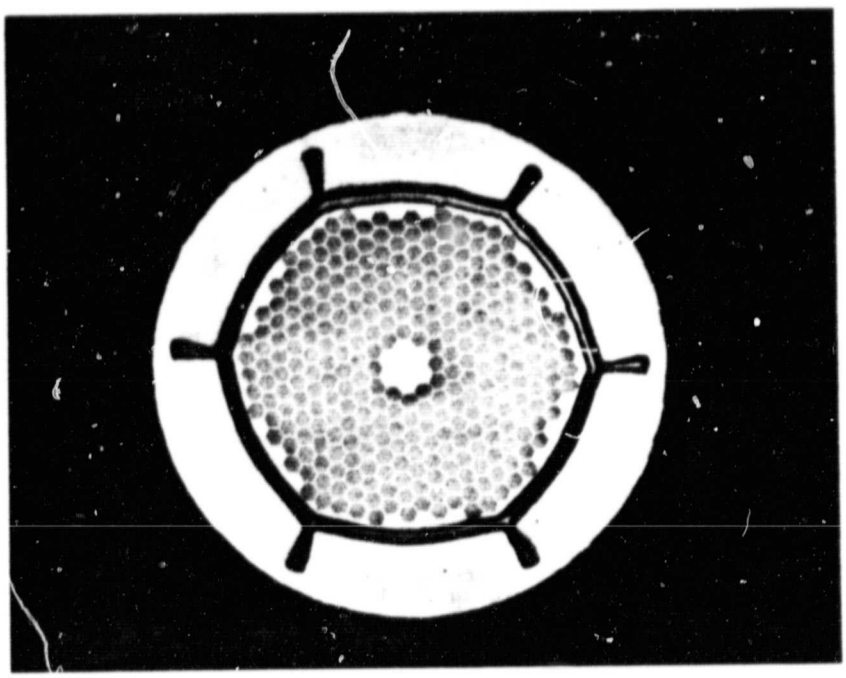

FIGURE 8-9. IGC conductor with 24,480 filaments and a segmented Ta diffusion barrier -- after ROSNER *et al.* [6, p. 74]; photograph courtesy of J.D. Scudiere, Intermagnetics General.

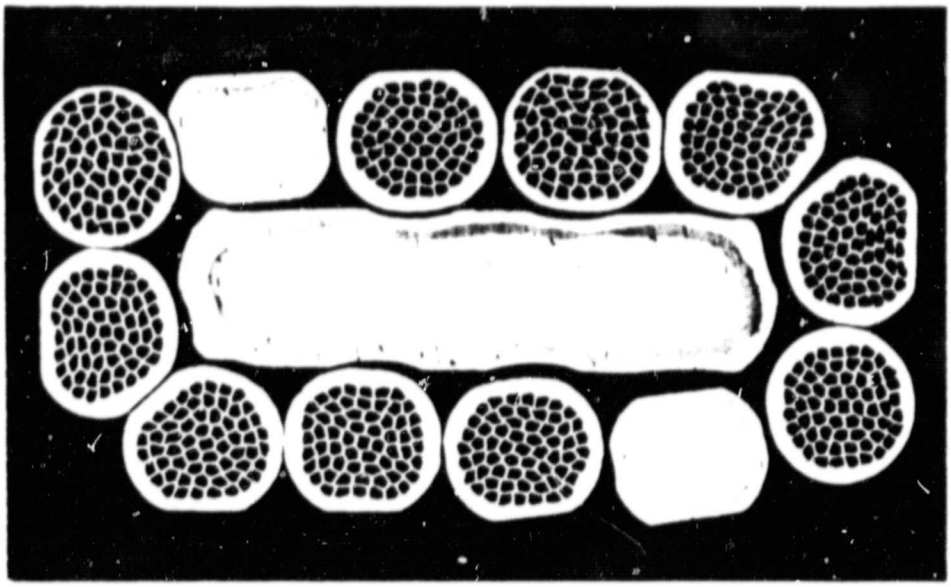

FIGURE 8-10. Vacuumschmelze cable consisting of ten 3,700-filament strands cryostabilized with two Cu strands and a Cu substrate (core), all Ta protected -- after HILLMANN *et al.* [6, p. 23]; photograph courtesy of H. Hillmann, Vacuumschmelze.

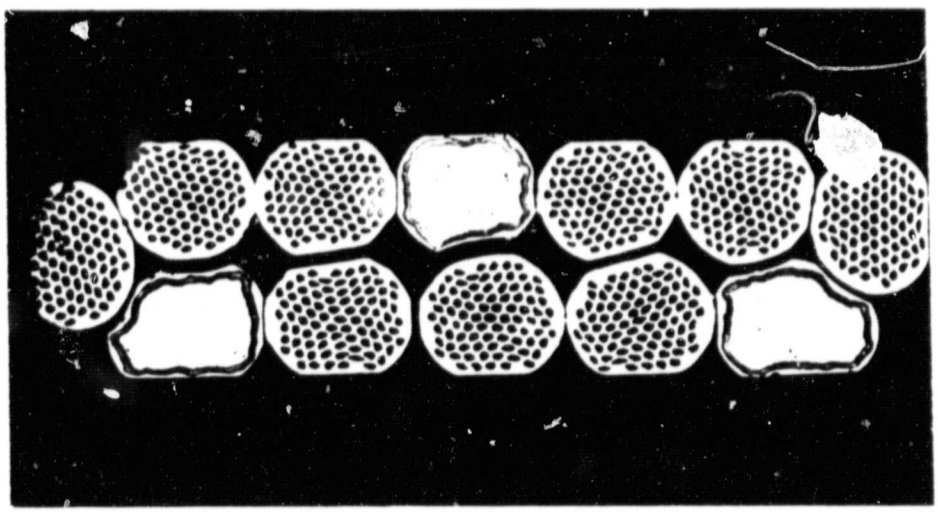

FIGURE 8-11. Vacuumschmelze cable consisting of nine 10,000-filament strands cryostabilized with three Ta-protected Cu strands -- after HILLMANN *et al.* [6, p. 23]; photograph courtesy of H. Hillmann, Vacuumschmelze.

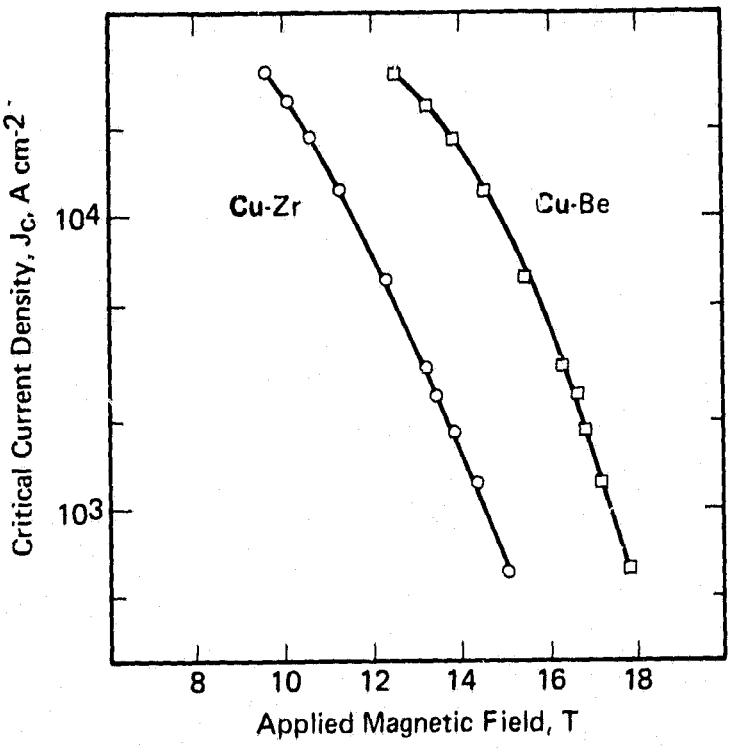

FIGURE 9-1. Influence of jacket material on the critical current density. 4.2-K J_c (overall but excluding jacket) *versus* applied field for cold powder-metallurgy Cu-Nb-Sn conductors processed in *Cu*-Zr (○) or *Cu*-Be (□) jackets at a reduction ratio of ∿ 2000:1. Alloy compositions in wt.% (excluding jackets) were Cu-35Nb-19Sn (○) and Cu-35Nb-26Sn (□) -- after FLÜKIGER *et al.* [185].

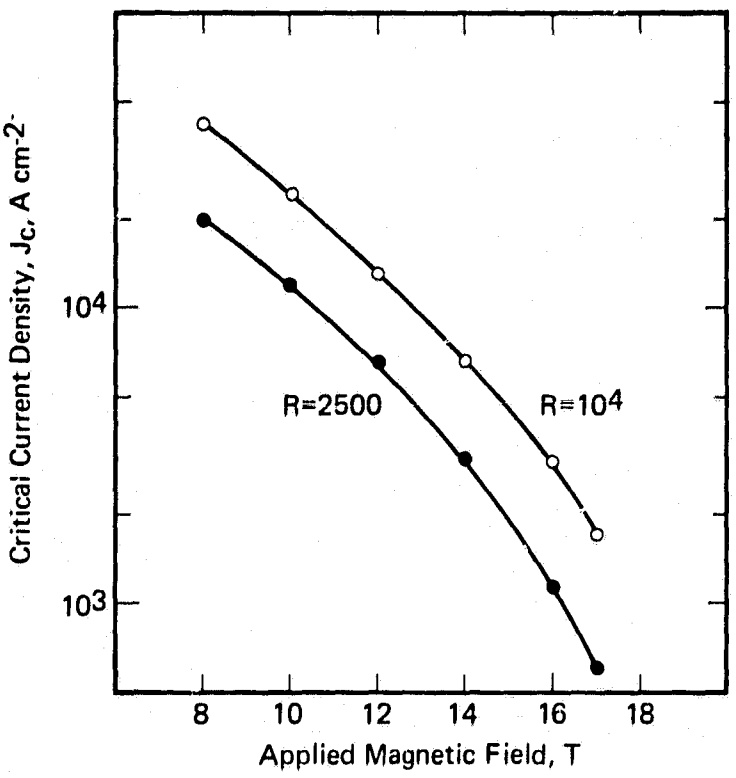

FIGURE 9-2. 4.2-K J_C (overall but excluding Cu jacket) *versus* applied field for powder-metallurgy processed Nb-Al conductors for two specified values of the reduction ratio, R. *Powder sizes:* Nb, 150 μm; Al, 70 μm --- *Composition* (wt.%) *and heat treatment:* Nb-3Al, 16 h/800° C -- after AKIHAMA *et al.* [176].

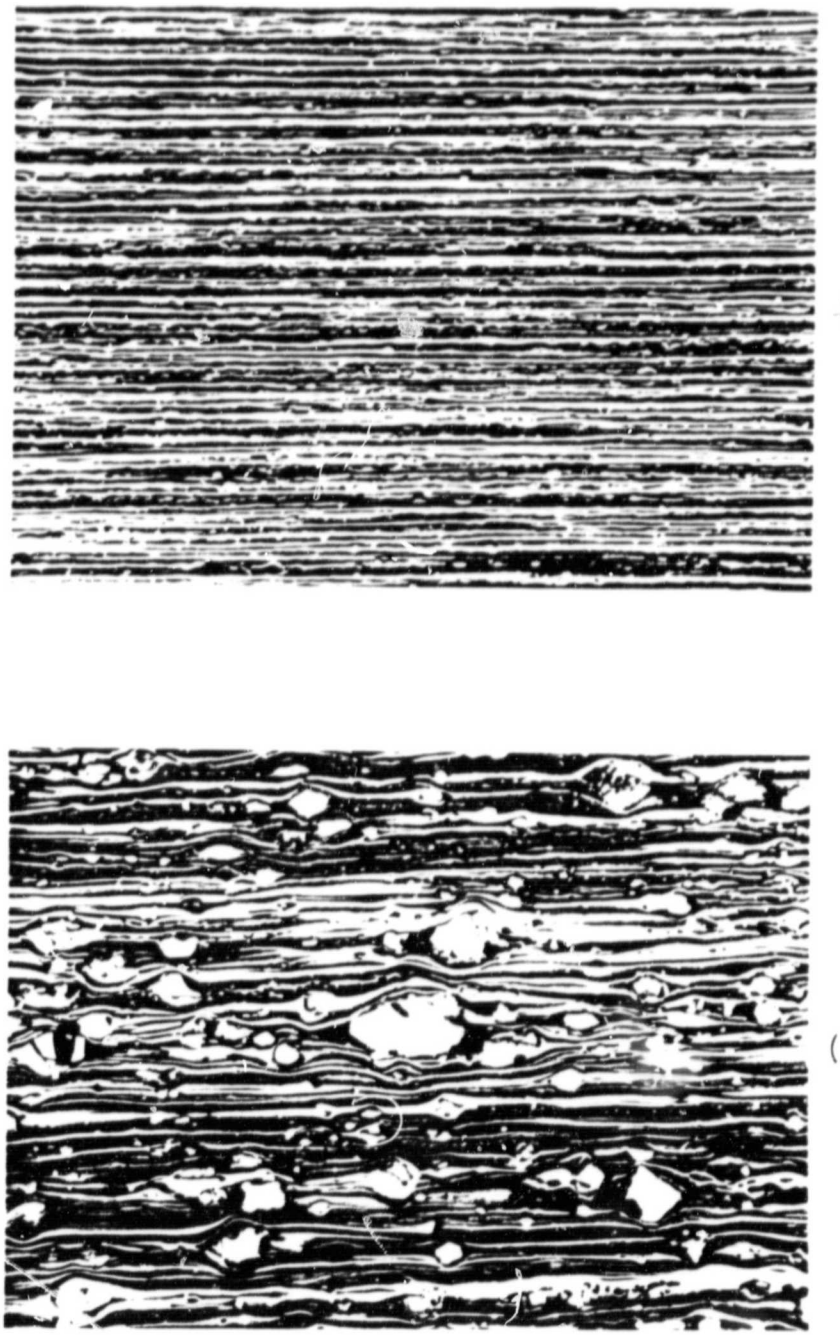

(a)

(b)

FIGURE 9-3. Influence of third-element gettering on the microstructures of hot-extruded and cold drawn (R ≅ 400) Cu-Nb powder composites. Compositions (in wt.%): (a) Cu-20Nb-1Al; (b) Cu-20Nb-4.7Hf -- after WECKER *et al.* [180]; micrographs courtesy of H.C. Freyhardt.

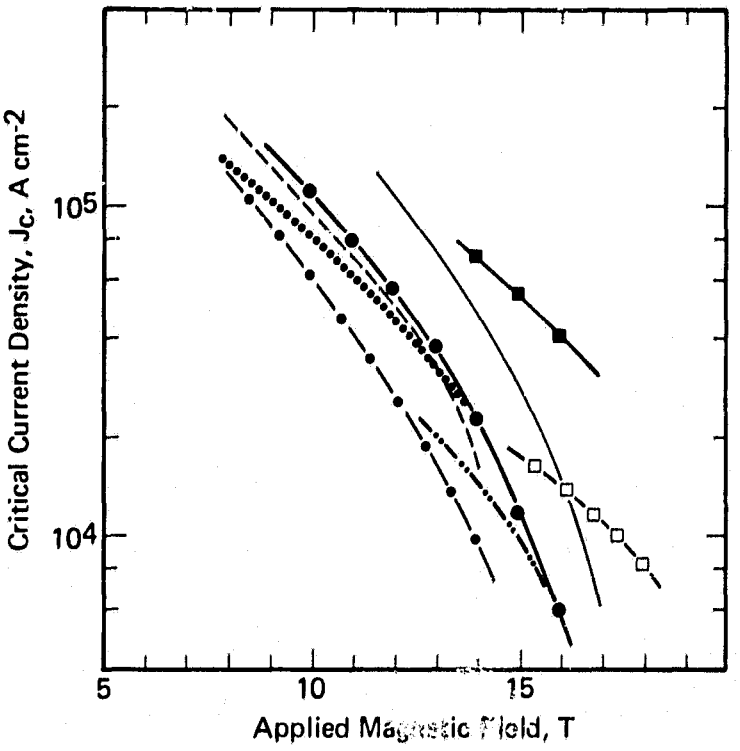

FIGURE 9-4. Intercomparison ofthe 4.2-K J_c field dependences of several Cu-Nb_3Sn and Cu-V_3Ga composites fabricated by various processes. The following compositions are in wt.% -- after BORMANN and FREYHARDT [182].

Nb_3Sn

—●—●—	Cu-30Nb + Sn	BORMANN *et al.* [187]
———	Cu-40Nb + Sn	FLÜKIGER *et al.* [173]
—··—··—	Cu-36Nb + Sn	FIHEY *et al.* [232]
—•—•—	Cu-17Nb + Sn	BEVK *et al.* [243]
--------	Cu-30Nb + Sn	VERHOEVEN *et al.* [220]
·····	Commercial Nb_3Sn multifilament.	HILLMANN *et al.* [244]

V_3Ga

—■—■—	Cu-30V + Ga	BORMANN *et al.* [182]
—□—□—	Cu-14.5V + Ga	BEVK *et al.* [245]

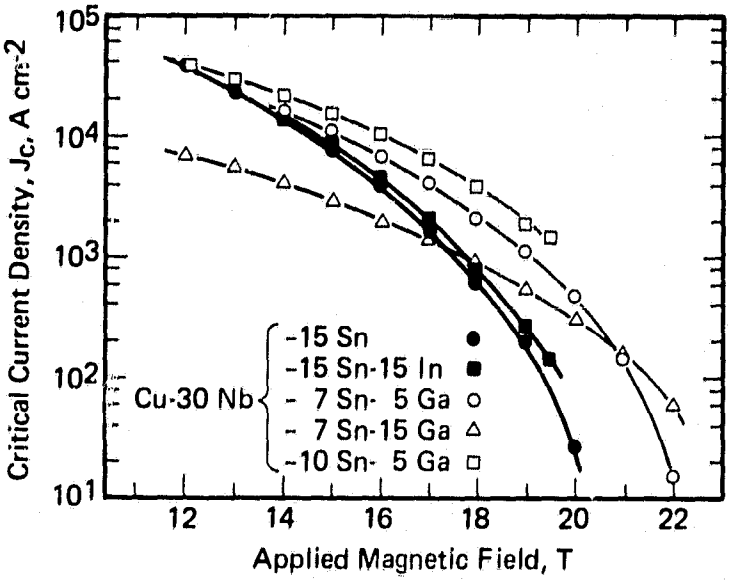

FIGURE 9-5. Influence of Ga and In additions on the critical current density of externally-diffused hot-powder processed Cu-Nb_3Sn composites. Base compositions (wt.%) were Cu-30Nb-7, 10, or 15Sn; additions (in wt.% relative to the total wt. of the composite) were 5Ga, 15Ga, and 15In -- after WECKER *et al.* [180].

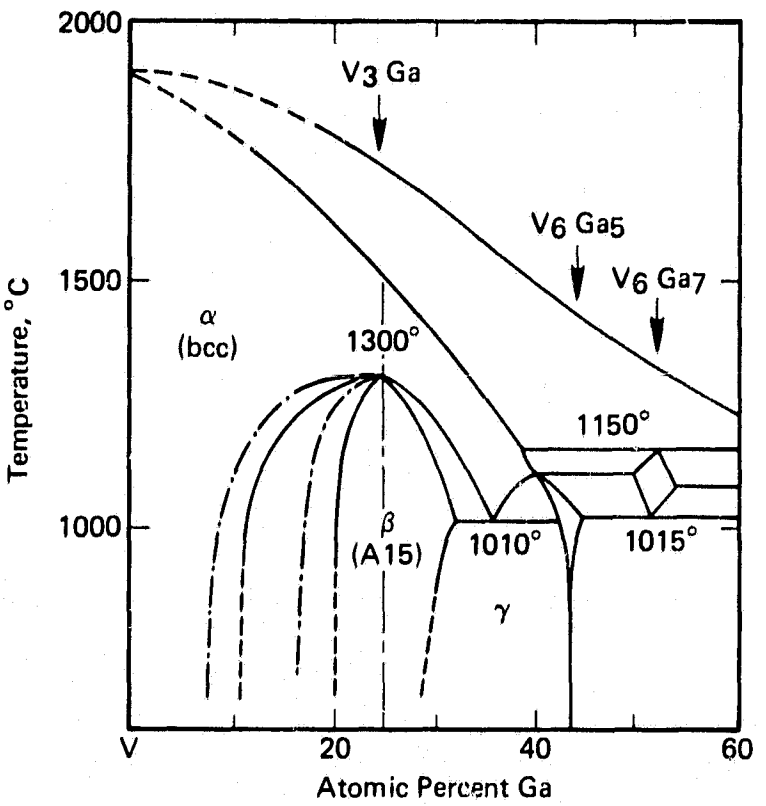

FIGURE 9-6. Portion of the V-Ga equilibrium phase diagram as assembled by HONG, DIETRICH, and MORRIS [198, 202].

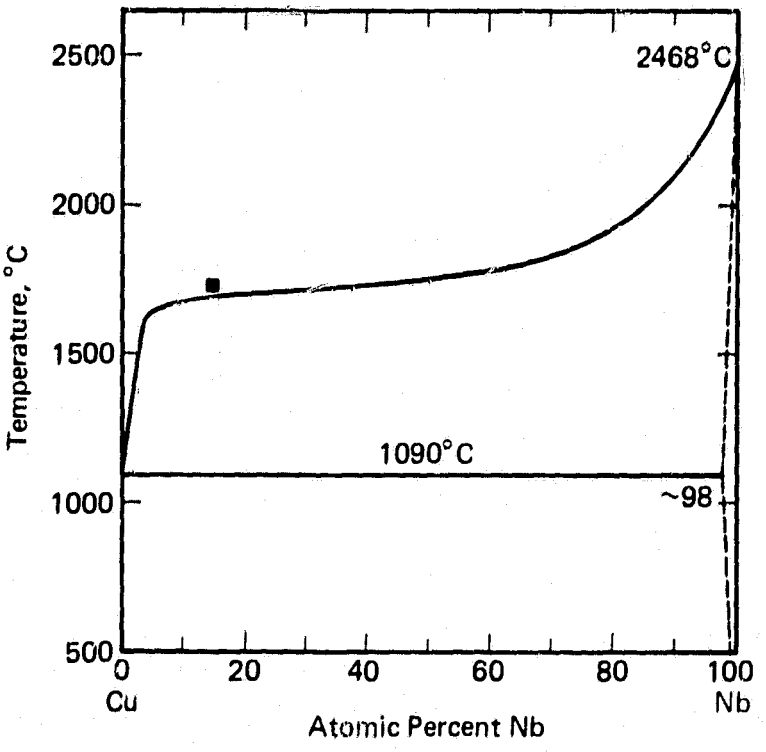

FIGURE 9-7. The Cu-Nb equilibrium phase diagram due to ALLIBERT *et al.* [204]. The limit of solubility of Cu in Nb at 1090° C is 2 at.% Cu [204]. The point designated (■) is due to VERHOEVEN *et al.* [230].

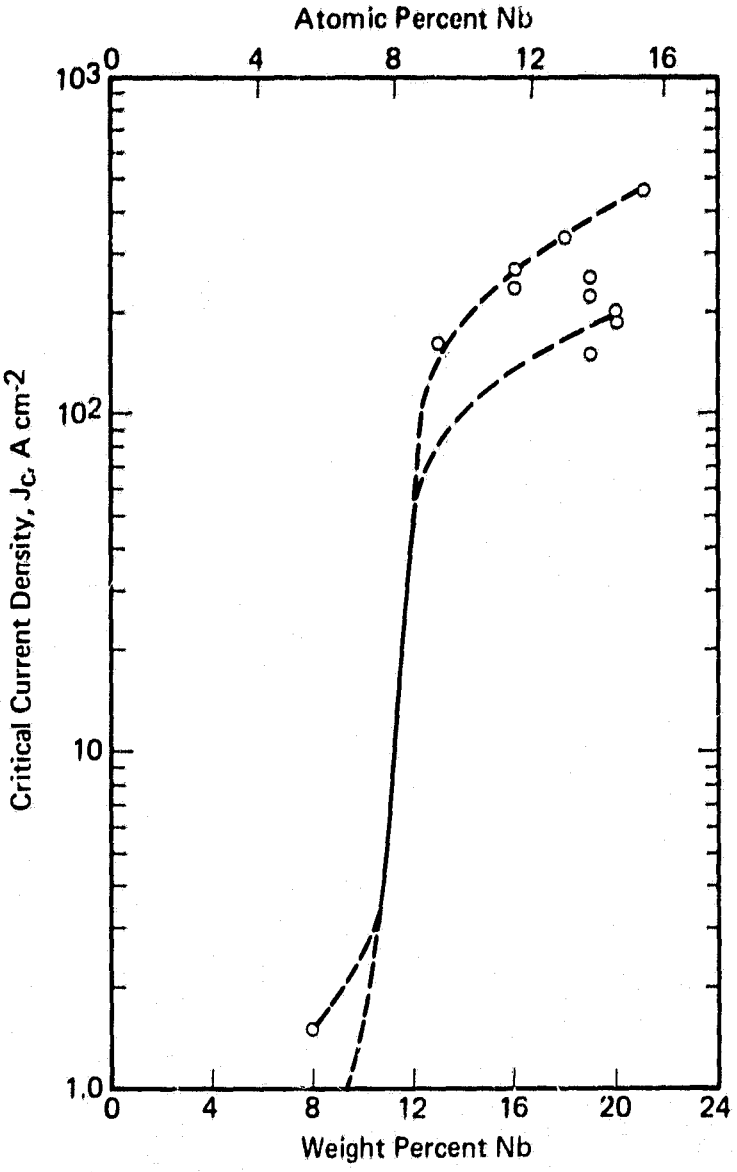

FIGURE 9-8. 4.2-K J_c as function of Nb concentration in as-cast Cu-Nb *in-situ* composites -- after ROBERGE and FIHEY [206].

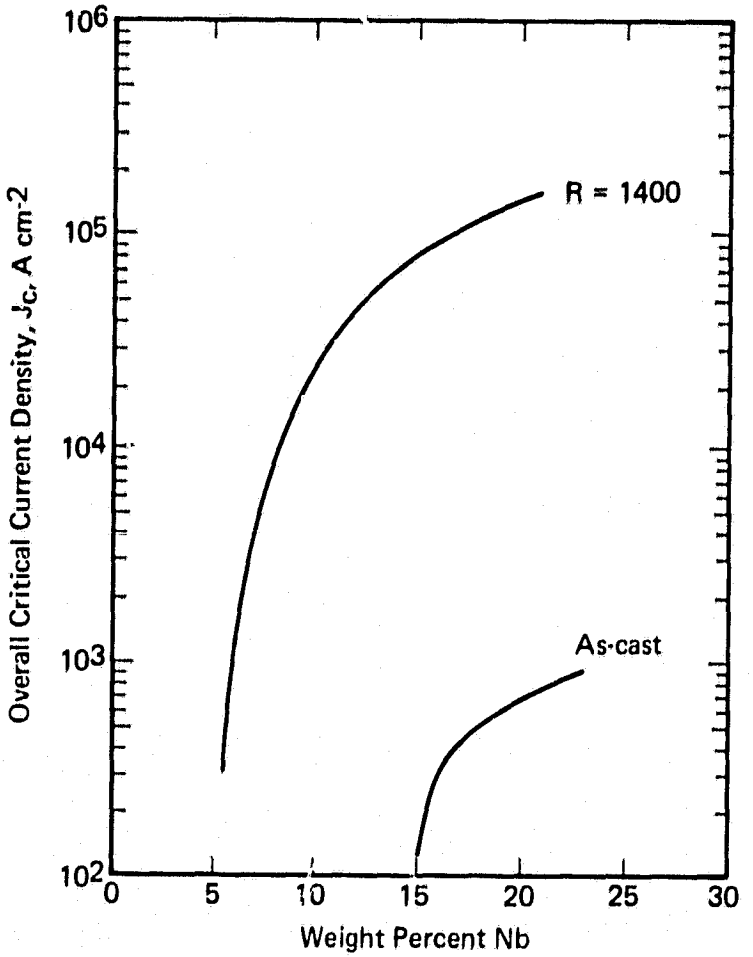

FIGURE 9-9. 4.2-K J_c as function of Nb concentration in cast-plus-deformed-to-wire (R ≈ 1400) Cu-Nb *in-situ* composites -- after ROBERGE and FONER [172].

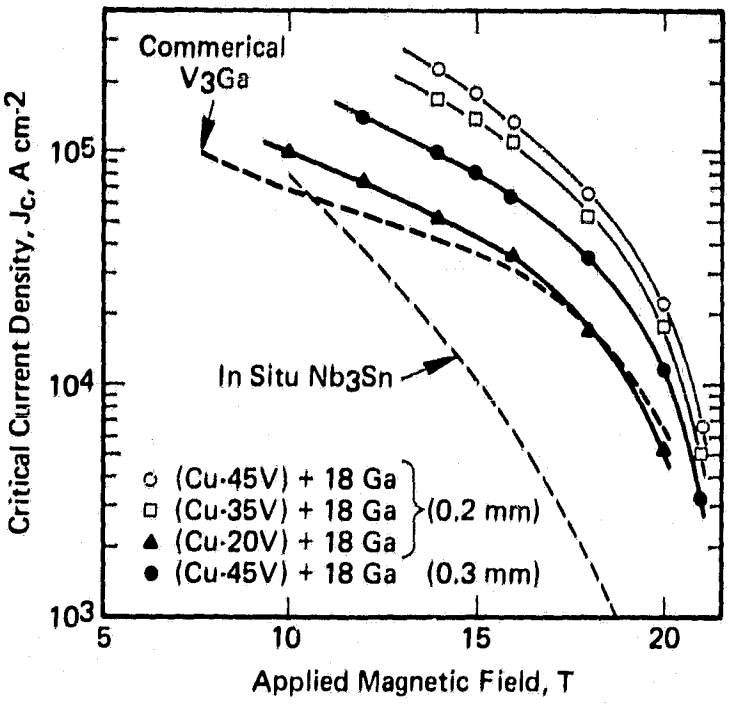

FIGURE 9-10. Comparison of the overall 4.2-K J_c's of *in-situ* processed 0.2-mmϕ and 0.3-mmϕ Cu-V_3Ga wires having the compositions (in at.%) indicated [229] with those of a commercial Cu-V_3Ga wire [231] and an *in-situ* Cu-Nb_3Sn wire [232] -- after KUMAKURA *et al.* [229].

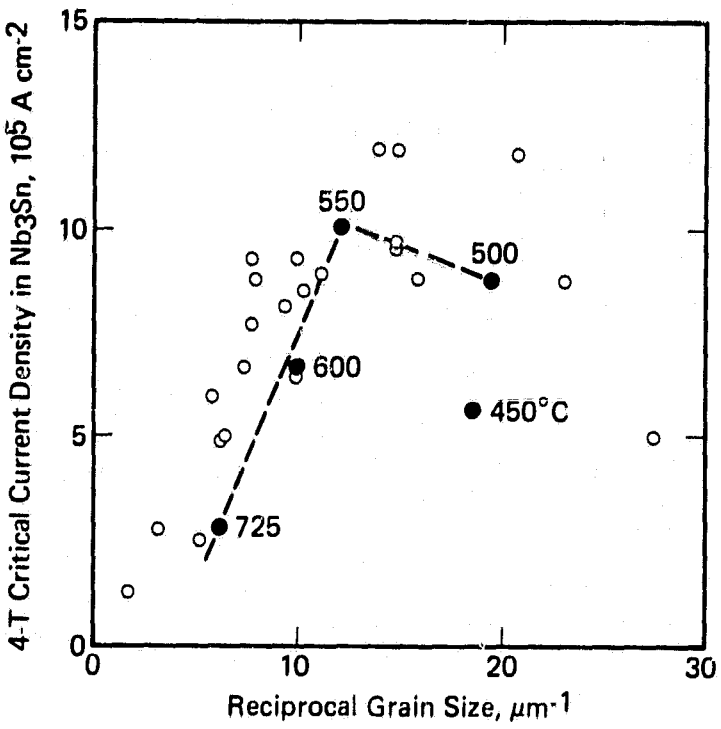

FIGURE 9-11. 4T-J_c as a function of reciprocal grain size for *in-situ*-processed wires (●) heat treated at the temperatures indicated, as reported by FINNEMORE *et al.* [205, 223]. Shown for comparison are some results for bronze-processed Nb_3Sn as reported by MADSEN and HILLS [234] (cf. Figure 8-6) -- after FINNEMORE *et al.* [223].

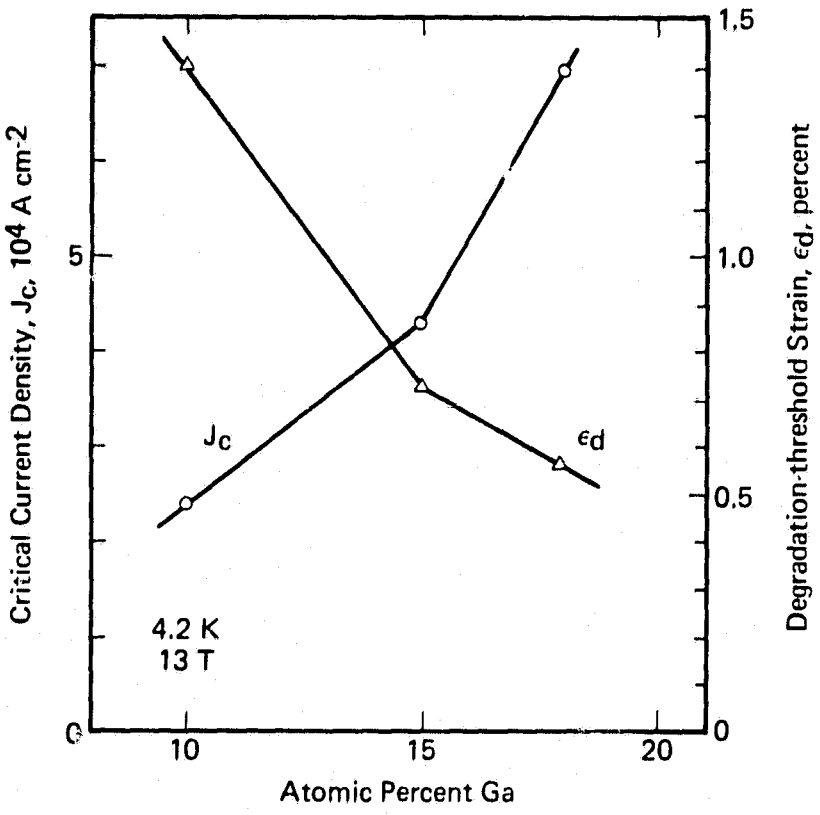

FIGURE 9-12. Influence of Ga concentration on the J_c (4.2-K, 13T) and degradation-threshold strain, ϵ_d, of externally diffused (Cu-35 at.% V) + Ga *in-situ*-processed wire -- after TOGANO *et al.* [219].

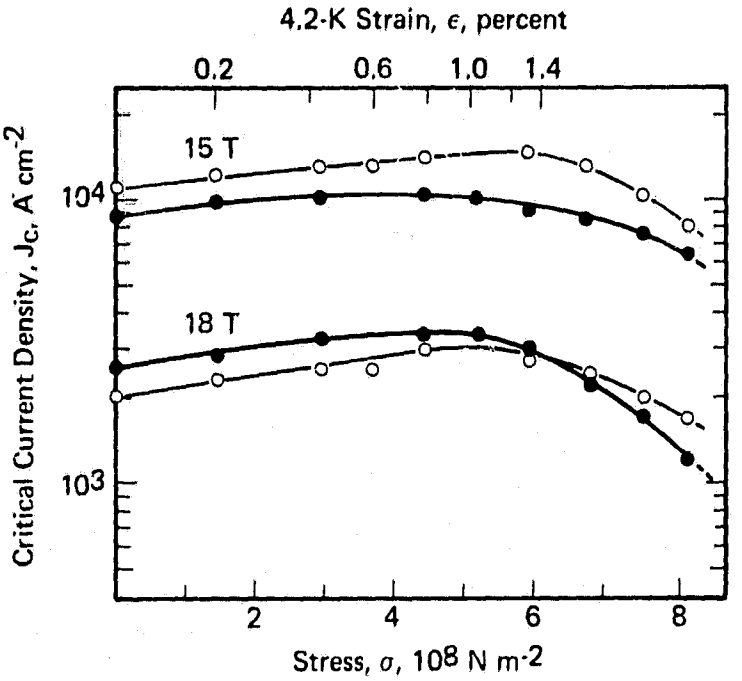

FIGURE 9-13. Influence of stress (and 4.2-K strain with respect to the 0 data) on the overall 4.2-K J_c of an *in-situ* Cu-V_3Ga composite (Cu-21.5 at.% V base) heat treated 1 day/650° C (ō) and 4 days/500° C (●) -- after FIHEY *et al.* [226].

ORIGINAL PAGE IS
OF POOR QUALITY

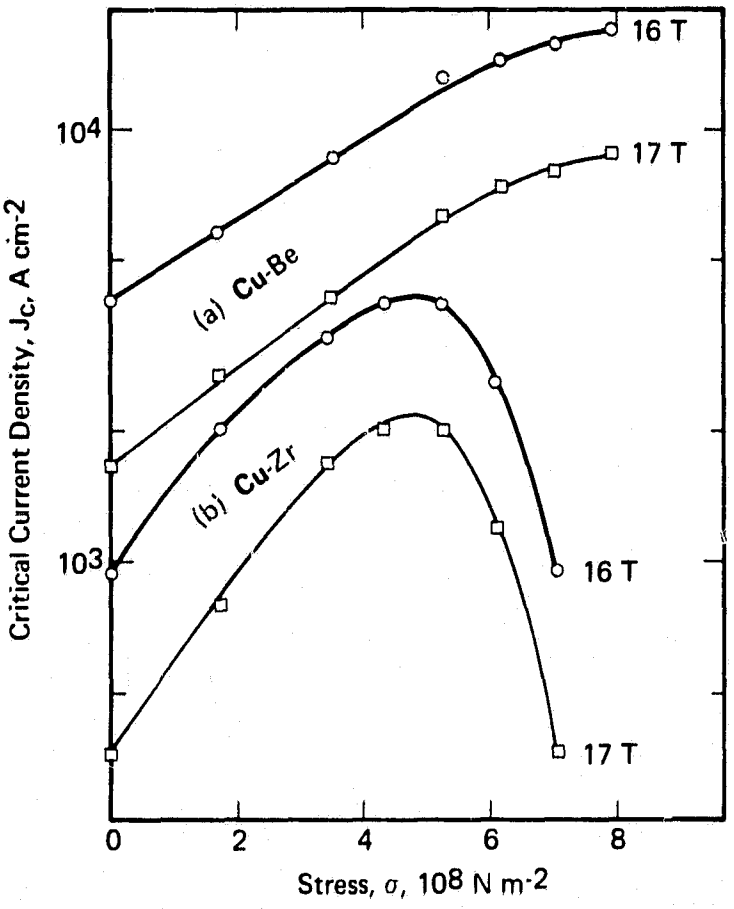

FIGURE 9-14. Influence of jacket material on the stress dependence of the overall 4.2-K critical-current density (excluding jacket) of cold-powder processed Cu-Nb_3Sn composites (R ≅ 2000). Depicted are: (a) Cu-35Nb-25Sn (wt.%) in *Cu*-Be; (b) Cu-35Nb-27Sn (wt.%) in *Cu*-Zr -- after FLÜKIGER *et al.* [185].

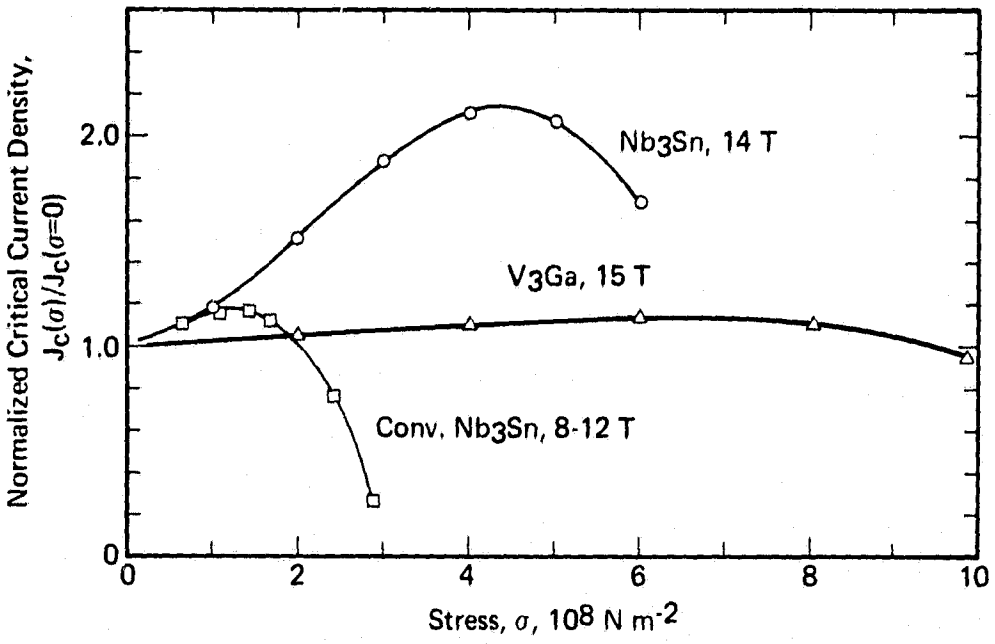

FIGURE 9-15. Intercomparison of the normalized J_c stress dependences, at the fields indicated, of *in-situ* Cu-Nb_3Sn, *in-situ* Cu-V_3Ga, and conventional multifilamentary Nb_3Sn composites -- after ROBERGE and FONER [172].

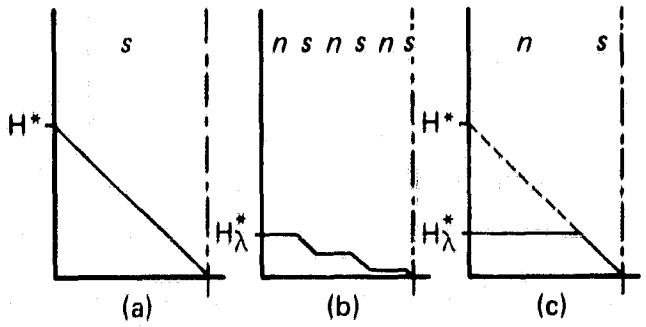

FIGURE 9-16. Penetration of field into: (a) a homogeneous superconductor with critical-current density J_c; (b) a laminated assembly of normal metal (n) and superconductor (s) with the same J_c; (c) a two-element equivalent of (b).

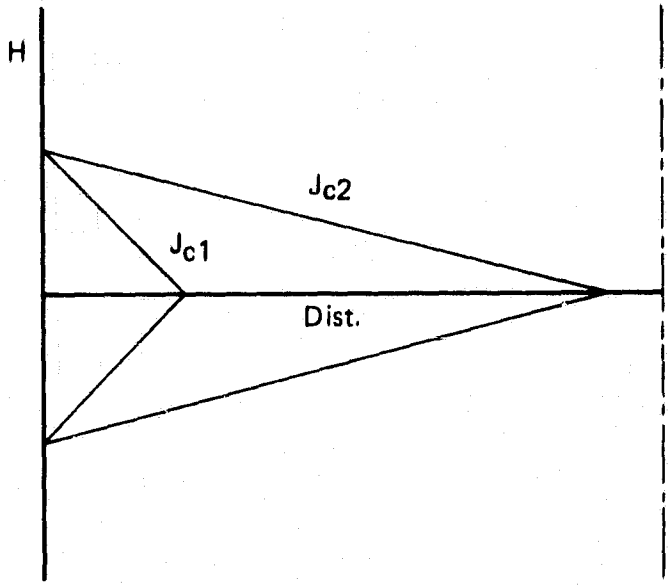

FIGURE 9-17. Penetration of field into a superconductor under two J_c conductors; $J_{c_1} > J_{c_2}$.

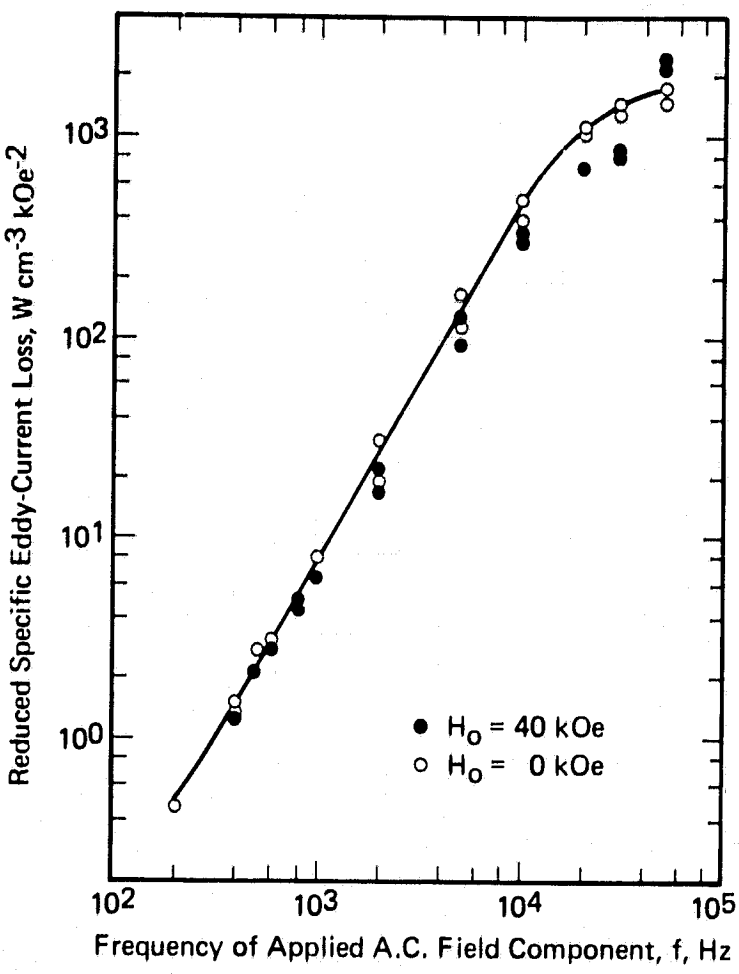

FIGURE 9-18. Hysteretic a.c. loss plotted in the format $\log_{10} (\dot{Q}_h/Vf)$ *versus* $\log_{10} H_m$ (cf. Equation (9-3)). Data: $\lambda = 0.23$, $H^* = 4$ kOe, $J_c(H^*) = 1 \times 10^6$ A cm^{-2} -- after BRAGINSKI *et al.* [240].

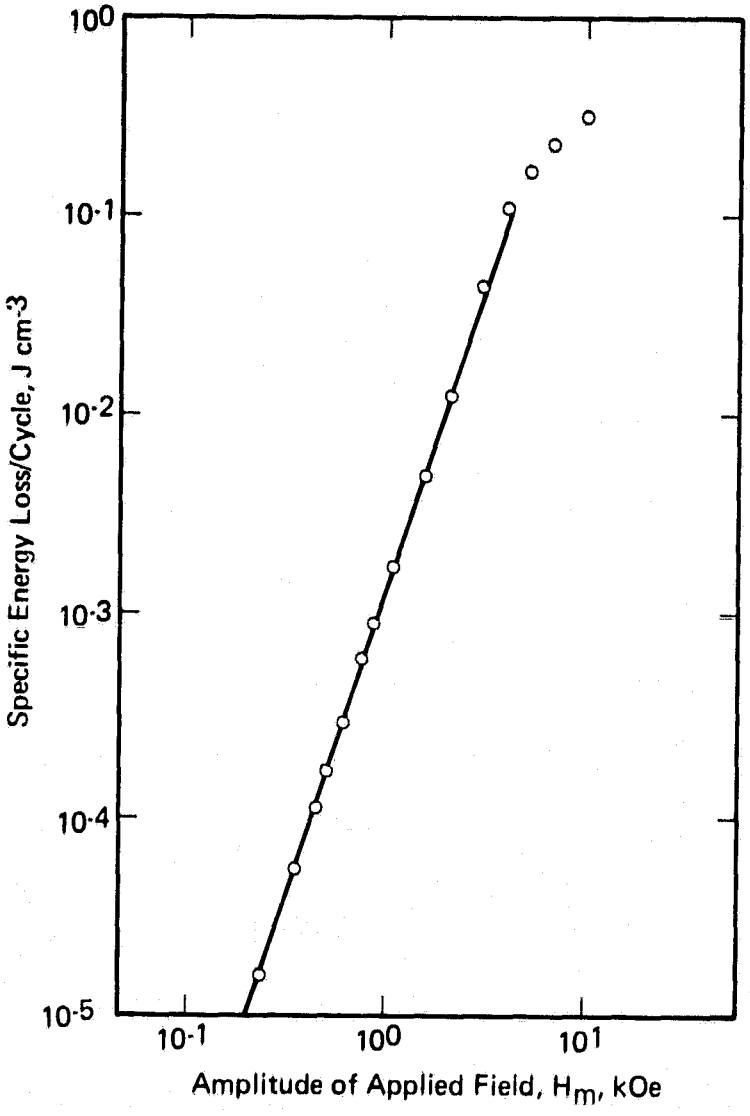

FIGURE 9-19. Frequency dependence of the eddy-current loss plotted in the format $\log_{10}(\dot{Q}_e/VH_m^2)$ *versus* $\log_{10}f$ (cf. Equation (4-4a)) -- after BRAGINSKI *et al.* [240].

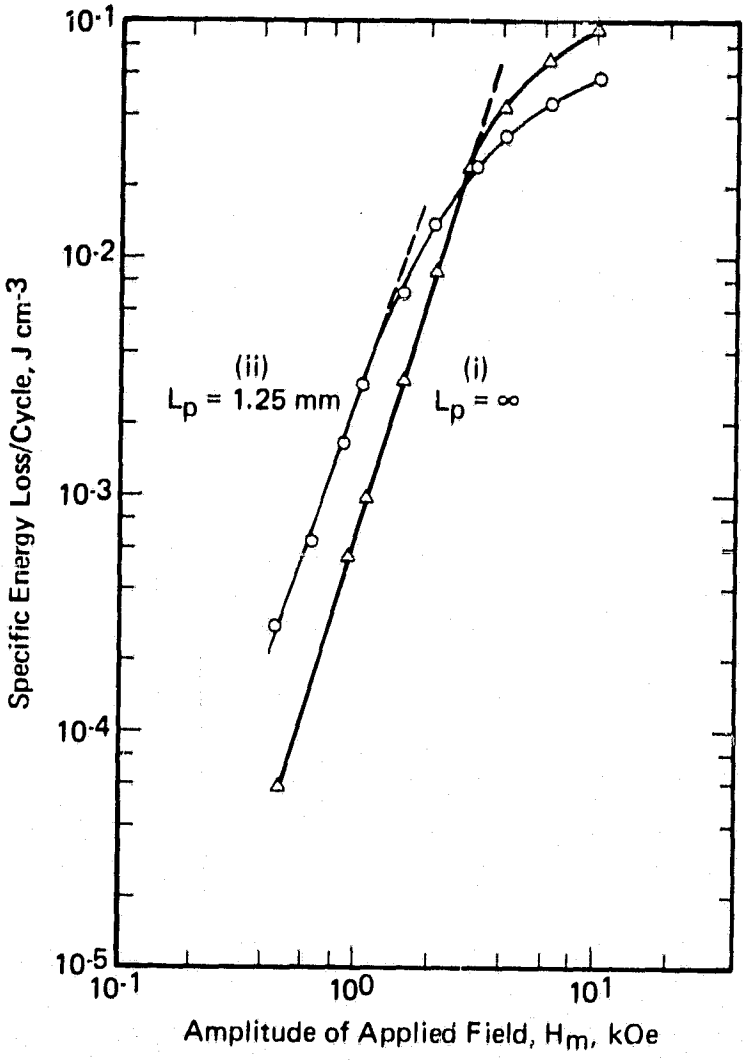

FIGURE 9-20. Influence of twist pitch, L_p, on the transverse-field hysteretic loss. Data: $\lambda = 0.23$, $T = 4.2$ K; (i) *Sample 1, Table 9-3*, $L_p = \infty$, $H^* \geq 3$ kOe; (ii) *Sample 3, Table 9-3*, $L_p = 1.25$ mm, $H^* < 2$ kOe -- after BRAGINSKI and BEVK [241].

REFERENCES

[1] B. T. Matthias, "Superconducting Device Consisting of a Niobium-Titanium Composition", U. S. Patent No. 3,167,692, January 26 (1965).

[2] J. E. Kunzler, E. Buehler, F.S.L. Hsu, and J. E. Wernick, "Superconductivity in Nb_3Sn at High Current Density in a Magnetic Field of 88 kgauss", Phys. Rev. Lett., 6 89-91 (1961).

[3] C. C. Tsuei, "Ductile Superconducting Copper-Base Alloys", Science, 80 57-8 (1973).

[4] J. D. Livingston and H. W. Schadler,"The Effect of Metallurgical Variables on Superconducting Properties", Progr. Mater. Sci., 12 183-287 (1963).

[5] T. S. Luhman and D. Dew-Hughes (eds.), Metallurgy of Superconducting Materials, Academic Press (1979).

[6] M. Suenaga and A. F. Clark (eds.), Filamentary A15 Superconductors, Plenum Press (1980).

[7] S. Foner and B. B. Schwartz (eds.), Superconductor Materials Science--Metallurgy, Fabrication, and Applications, Plenum Press (1981).

[8] D. N. Cornish, J. P. Zbasnik, R. L. Leber, D. G. Hirzel, J. E. Johnston, and A. R. Rosdahl, "MFTF Test Coil Construction and Performance", IEEE Trans. Magn., MAG-15 530-3 (1979).

[9] S. Shimamoto, T. Ando, T. Hiyama, H. Tsuji, K. Yoshida, E. Tada, M. Nishi, K. Okuno, K. Koizuma, K. Oka, and K. Yasukōchi, "Japanese Design of a Test Coil for the Large Coil Task", Proc. 8th Symposium on the Engineering Problems of Fusion Research, Pt III, San Francisco, CA, 13-16 Nov. 1979, IEEE, NY (1980) pp.1174-8.

[10] M. T. Taylor, A. Woolcock and A. C. Barber, "Strengthening Superconducting Composite Conductors for Large Magnet Construction", Cryogenics, 8 317-9 (1968).

[11] M. Young, E. Gregory, E. Adam, and W. Marancik, "Fabrication and Properties of an Aluminum-Stabilized NbTi Filament Superconductor", Adv. Cryo. Eng. (Materials), 24 383-8 (1978).

[12] H. Desportes, J. Le Bars, and G. Mayaux, "Construction and Test of the CELLO Thin-Wall Solenoid", Adv. Cryo. Eng., 25 178-84 (1980).

[13] M. N. Wilson, C. R. Walters, J. D. Lewin, P. F. Smith, and A. H. Spurway, "Experimental and Theoretical Studies of Filamentary Superconducting Composites", J. Phys. D: Appl. Phys., 3 1517-83 (1970).

[14] Y. Iwasa, "Magnetization of Single-Core, Multi-Strand, and Twisted Superconducting Composite Wires", Appl. Phys. Lett., 14 200-1 (1969).

[15] R. R. Critchlow, B. Zeitlin, and E. Gregory, "The Effect of Twist on A. C. Loss and Stability in Multistrand Superconducting Composites", Appl. Phys. Lett., 15 225-7 (1969).

[16] J. L. Duchateau and B. Turck, "Theoretical and Experimental Studies of Magnetic Instabilities in Multifilamentary Nb-Ti Superconducting Composites", IEEE Trans. Magn., MAG-11 350-3 (1975).

[17] J. L. Duchateau and B. Turck, "Dynamic Stability and Quenching Currents of Superconducting Multifilamentary Composites Under Usual Cooling Conditions", J. Appl. Phys., 46 4989-95 (1975).

[18] J. L. Duchateau, B. Turck, L. Krempasky, and M. Polak, "The Self-Field Effect in Twisted Superconducting Composites", Cryogenics, 16 97-102 (1976).

[19] R. A. Popley, D. J. Sambrook, C. R. Walters, and M. N. Wilson, "A New Superconducting Composite with Low Hysteresis Loss", Applied Superconductivity Conference., Annapolis MD (May 1972) IEEE Pub. No. 72CH0682-5-TABSC (1972) pp 516-7.

[20] S. T. Wang, S. H. Kim, L. R. Turner, K. M. Thompson, W. F. Praeg, C. I. Krieger, and R. L. Kustom, "Design and Development of Cryostable Superconducting Ohmic Heating Coils for a Tokamak", Adv. Cryo. Eng., 23 255-64 (1978).

[21] Y. Iwasa and M. W. Sinclair, "Protection of Large Superconducting Magnets: Maximum Permissible Undetected Quench Voltage", Cryogenics, 20 711-4 (1980).

[22] D. T. Read, J. W. Ekin, R. L. Powell, and A. F. Clark, "Definitions of Terms for Practical Superconductors, 3. Fabrication, Stabilization, and Transient Losses", Cryogenics, 19 327-32 (1979).

[23] S. L. Wipf, "Stability and Degradation of Superconducting Current-Carrying Devices", Los Alamos Scientific Laboratory Report LA-7275, Issued December, 1978.

[24] Y. Iwasa, "A 'Critical-Current-Margin' Design Criterion for High-Performance Magnet Stability", Cryogenics, 19 704-14 (1979).

[25] M. A. Green, "Large Superconductor Detector Magnets With Ultra Thin Coils for Use in High Energy Accelerators and Storage Rings", 6th International Conference on Magnet Technology Ptl. Bratislava, Czechoslovakia, 29 August - 2 September 1977 (ALFA, Bratislava, 1978) pp 429-42.

[26] P. F. Smith, M. N. Wilson, C. R. Walters, and J. D. Lewin, "Intrinsically Stable conductors", Proceedings of the 1968 Summer Study on Superconducting Devices and Accelerators, BNL 50155 (C-55) Brookhaven National Lab., Upton NY (April, 1969) pp 913-9.

[27] Z.J.J. Stekly, R. Thome, and B. Strauss, "Principles of Stability in Cooled Superconducting Magnets", Proceedings of the 1968 Summer Study on Superconducting Devices and Accelerators, BNL 50155 (C-55) Brookhaven National Laboratory--Upton, NY (April, 1969) pp 748-64.

[28] Z.J.J. Stekly, R. Thome, and B. Strauss, "Principles of Stability in Cooled Superconducting Magnets", J. Appl. Phys., 40 2238-45 (1969).

[29] Z.J.J. Stekly, "Superconducting Coils--Appendix: Steady State Stability", in The Science and Technology of Superconductivity ed. by W. D. Gregory, W. N. Mathews, Jr., and E. A. Edelsak, Plenum Press 1973, Vol. 2, pp 497-537.

[30] W. J. Carr, Jr., "A.C. Loss in a Twisted Filamentary Superconducting Wire, I", J. Appl. Phys., 45 929-34 (1974).

[31] W. J. Carr, Jr., "A.C. Loss in a Twisted Filamentary Superconducting Wire. II", J. Appl. Phys., 45 935-9 (1974).

[32] J. H. Murphy, M. S. Walker, and W. J. Carr, Jr., "Theory of Alternating Field Losses in Cylindrical Twisted Multifilamentary Superconductors", IEEE Trans. Magn., MAG-10 868-71 (1974).

[33] R. M. Scanlan, J. E. Johnston, P. A. Waide, B. A. Zeitlin, G. B. Smith and C. T. Nelson, "Manufacturing and Quality Assurance for the MFTF Superconductor Core", Proc. 8th Symposium on the Engineering Problems of Fusion Research, Pt I, San Francisco, CA, 13-16 Nov. 1979, IEEE, NY (1980), pp 260-4.

[34] M. S. Walker, "Geometric Reduction of the Critical Current Density in Multifilament Composite Superconductors", Applied Superconductivity Conference, Annapolis, MD (May 1972), IEEE Pub. No. 72CH0682-5-TABSC, pp 477-80.

[35] J. L. Duchateau and B. Turck, "Self-Field Degradation Effect in Adiabatic Conditions", Cryogenics, 14 481-6 (1974).

[36] B. J. Maddock, G. B. James, and W. T. Norris, "Superconductive Composites: Heat Transfer and Steady State Stabilization", Cryogenics, 9 261-73 (1969).

[37] F. R. Fickett, "Magnetoresistivity of Copper and Aluminum at Cryogenic Temperatures", 4th International Conf. on Magnet Technology (Brookhaven National Lab., Upton, NY, September 19-22, 1972), Atomic Energy Commission, Washington, DC (1972) pp 539-41.

[38] Y. Iwasa and D. B. Montgomery, "Threshold Currents of Large Cross-Section Superconductors", J. Appl. Phys., 42 1040-6 (1971).

[39] M. W. Wilson, "Filamentary Composite Superconductors for Pulsed Magnets", Applied Superconductivity Conference, Annapolis, MD (May, 1972), IEEE Pub. No. 72CH0682-5-TABSC, pp 385-94.

[40] F. Sumiyoshi, F. Irie, and K. Yoshida, "Magnetic Field Dependence of AC Losses in Multifilamentary Superconducting Wires", Cryogenics, 19 209-13 (1979).

[41] K. Kwasnitza and I. Horvath, "Measurement of AC Losses in Multifilament Superconducting Wires at Frequencies Between 1 and 100 Hz", Cryogenics, 14 71-6 (1974).

[42] K. Shiiki, K. Ahara, and M. Kudo, "A.C. Loss and Twisting Effect in Superconducting Composite Conductor", Japan J. Appl. Phys., 13 345-50 (1974).

[43] G. H. Morgan, "Theoretical Behavior of Twisted Multicore Superconducting Wire in a Time-Varying Uniform Magnetic Field", J. Appl. Phys., 41 3673-9 (1970).

[44] M. S. Walker, J. H. Murphy, and W. J. Carr, Jr., "Alternating Field Losses in Mixed Matrix Multifilament Superconductors", IEEE Trans. Magn., MAG-11 309-12 (1975).

[45] J. H. Murphy, M. S. Walker, and W. J. Carr, Jr., "Alternating Field Losses in a Rectangular Multifilamentary NbTi Superconductor", IEEE Trans. Magn., MAG-11 313-6 (1975).

[46] J. H. Murphy, D. W. Deis, B. J. Shaw, and M. S. Walker, "Alternating Field Losses in Nb_3Sn Multifilamentary Superconductor", IEEE Trans. Magn., MAG-11 317-20 (1975).

[47] G. R. Wagner, M. S. Walker, D. A. Koop, and C. N. Whetstone, "AC Losses and Critical Current in an Aluminum Stabilized Mixed Matrix NbTi Superconductor Composite", IEEE Trans. Magn., MAG-13 217-20 (1977).

[48] S. H. Kim, S.-T. Wang, and M. Lieberg, "Operating Cheracteristics of the 1.5 MJ Pulsed Superconducting Coil", Adv. Cryo. Eng., 25 90-7 (1980).

[49] J. D. Rogers, H. J. Boenig, J. C. Bronson, D. B. Colyer, W. V. Hassenzahl, R. D. Turner, and R. I. Schermer, "30-MJ Superconducting Magnetic Energy Storage (SMES) Unit for Stabilizing an Electric Transmission System", IEEE Trans. Magn., MAG-15 820-3 (1979).

[50] S. K. Singh, C. J. Heyne, D. T. Hackworth, M. A. Janocko, P. W. Eckels, and J. H. Murphy, "Design of a 400-kJ Pulsed Energy Storage Coil", Adv. Cryo. Eng., 25 81-9 (1980).

[51] G. E. Meyer, E. W. Collings, R. J. Fiorentino, F. J. Jelinek, and D. C. Carmichael, "Experimental Evaluation of Hydrostatic Extrusion for the Fabrication of Multifilament Superconducting Wire", Progress Report to ERDA (Div. of Magnetic Fusion Energy) Sept. 30, 1976.

[52] K. Shiiki, "Effect of Matrix Resistivity on Twisting in Superconducting Composite Conductors", Japan J. Appl. Phys., 13 1875-80 (1974).

[53] C. J. Mole, D. W. Deis, P. W. Eckels, H. E. Haller III, M. A. Janocko, S. A. Karpathy, D. C. Litz, E. Mullan, P. Reichner, Z. N. Sanjana, and M. S. Walker, "A Superconducting 0.54-MJ Pulsed Energy Storage Coil", Adv. Cryo. Eng., 23 57-69 (1978).

[54] H. Hillmann, K. J. Best, H. Hoeflich, J. Rudolph, I. Pfeiffer, and H. Weber, "Hochfeldsupraleiter aus NbTi mit Stromtragfähigkeiten über 3000 A für die Anwendung in Magnetsystemen mit Wechselfeldkomponenten", Vacuumschmelze GmbH, Hanau, Forschungsbericht NT 1022 (April 1979).

[55] F. Levi, "Methods of Producing Magnetic Materials and to the Magnetic Materials so Produced", U.S. Patent No. 3,029,496 (April 17, 1962).

[56] F. Levi, "Method of Producing High Energy Permanent Magnets", U.S. Patent No. 3,239,919 (March 15, 1966).

[57] H. E. Cline, B. P. Strauss, R. M. Rose, and J. Wulff, "Fabrication of an Ultra-Fine Cb-Cu Composite by Drawing", Trans. ASM, 59 132-6 (1966).

[58] R. L. Garwin and A. S. Nowick, "Method of Making Superconductor Wires", U.S. Patent No. 3,370,347 (February, 1968).

[59] D. Dew-Hughes, "Superconducting Materials for Large-Scale Applications", Adv. Cryo. Eng. (Materials), 22 316-25 (1977).

[60] J. J. Wollan, M. S. Walker, B. A. Zeitlin, D. A. Pollock, and S. S. Shen, "Evaluation of a Cryostable Low-Loss Conductor for Pulsed-Field Applications", IEEE Trans. Magn., MAG-17 482-5 (1981).

[61] D. A. Colling, T. A. de Winter, W. K. McDonald, and W. C. Turner, "Superconducting Performance of Production NbTi Alloys", IEEE Trans. Magn., MAG-13 848-51 (1977).

[62] R. W. Meyerhoff (ed.), Manufacture of Superconducting Materials, American Society for Metals, Metals Park, OH 44073 (1977).

[63] B. P. Strauss, R. H. Remsbottom, P. J. Reardon, C. W. Curtis, and W. K. McDonald, "Results of the Fermilab Wire Production Program", IEEE Trans. Magn., MAG-13 487-90 (1977).

[64] H. LeHuy, J. L. Fihey, and R. Roberge, "Continuous High Temperature Gradient Solidification of *In-Situ* Cu-Nb Alloys for Large Scale Development", Adv. Cryo. Eng. (Materials), 28 563-9 (1982).

[65] E. D. Gibson, J. E. Ostenson, J. J. Sue, J. D. Verhoeven and D. K. Finnemore, "Development of Cryostabilized Nb_3Sn-Cu Superconducting Wire Using the *In-Situ* Process", Adv. Cryo. Eng. (Materials), 28 525-34 (1982).

[66] S. S. Shen and W. K. McDonald, "Testing Results of MF-Nb_3Sn Composites Made by a Modified Jellyroll Method", Adv. Cryo. Eng. (Materials), 28 535-43 (1982).

[67] C. W. Curtis and W. K. McDonald, "Production Development Program to Manufacture Cu/Nb 46.5Ti Multifilamentary Wire", Teledyne Wah Chang Albany, Report to Fermi National Accelerator Laboratory under Contract No. 50088 (February 3, 1976).

[68] T. Horiuchi, T. Fukutsuka, K. Matsumoto, and Y. Monju, "Consideration on the Production System of High Field Superconductors", in Workshop on High Field Superconducting Materials for Fusion--U.S.-Japan Cooperative Program, Tokyo (1980).

[69] G. E. Meyer, E. W. Collings, R. J. Fiorentino, F. J. Jelinek, and D. C. Carmichael, "Experimental Evaluation of Hydrostatic Extrusion for the Fabrication of Multifilament Superconducting Wire", Progress Report to ERDA (Division of Magnetic Fusion Energy), June 30, 1975.

[70] W. A. Fietz, R. E. McDonald, and J. R. Miller, "Preparation and Extrusion of Multifilamentary NbTi Conductor Billets", Proc. 6th Symposium on the Engineering Problems of Fusion Research, San Diego, CA, November 18-21, 1975, IEEE, NY (1976), pp 256-60.

[71] M. S. Walker, J. G. Declercq, B. A. Zeitlin, J. D. Scudiere, M. J. Ross, M. A. Janocko, S. K. Singh, E. A. Ibrahim, P. W. Eckels, J. D. Rogers, and J. J. Wollan, "Superconductor Design and Loss Analysis for a 20 MJ Induction Heating Coil", IEEE Trans. Magn., MAG-17 908-11 (1981).

[72] M. A. Janocko, "Lattice Braided Superconductors", IEEE Trans. Magn., MAG-15 797-9 (1979).

[73] C. Spencer, E. Adam, E. Gregory, W. Marancik, P. Sanger, R. Scanlan, and D. Cornish, "Fabrication and Testing of the Nb_3Sn Superconductor for High Field Test Facility (HFTF)", Proc. of 8th Symposium on Engineering Problems of Fusion Research, San Francisco, CA, 13-16 November, 1979, IEEE, NY (1980), pp 245-8.

[74] S. O. Hong, E. Adam, E. Gregory, D. Koop, and W. Marancik, "Fabrication of the NbTi Compacted Monolith Conductor for ELMO Bumpy Torus (EBT-P) Prototype Coils", IEEE Trans. Magn., MAG-17 916-7 (1981).

[75] M. Morpurgo, "Design and Construction of a Superconducting Aluminum Stabilized Solenoid", Cryogenics, 17 89-90 (1977).

[76] M. Morpurgo and G. Pozzo, "Fabrication of an Aluminum Stabilized Superconductor", Cryogenics, 17 87-8 (1977).

[77] D. F. Neal, A. C. Barber, A. Woolcock, and J.A.F. Gidley, "Structure and Superconducting Properties of Nb44% Ti Wire", Acta. Met., 19 143-9 (1971).

[78] A. W. West and D. C. Larbalestier, "Transmission Electron Microscopy of Commercial Filamentary Nb-Ti Superconducting Composites", Adv. Cryo. Eng. (Materials), 26 471-8 (1980).

[79] A. W. West and D. C. Larbalestier, "Microstructure Superconducting Property Relationships in a Fermilab Nb-46.5w/oTi Filamentary Superconducting Composite", IEEE Trans. Magn., MAG-17 65-8 (1981).

[80] A. W. West and D. C. Larbalestier, "α-Ti Precipitation in Niobium-Titanium Alloys", Adv. Cryo. Eng. (Materials), 28 337-44 (1982).

[81] C. Baker, "The Effect of Heat Treatment and Nitrogen Addition on the Critical Current Density of a Worked Niobium 44 wt.% Titanium Superconducting Alloy", J. Mater. Sci., 5 40-52 (1970).

[82] J. P. Charlesworth and P. E. Madsen, "Effect of Heat Treatment on the Superconducting Critical Current of Cold Worked Titanium-45 at.% Niobium. Part I.", Atomic Energy Research Establishment, Harwell, UK, Report No. AERE-R-6534 (October, 1970).

[83] D. C. Larbalestier, "Niobium-Titanium Alloy Superconductors--Present Status and Potential for Improvement", Adv. Cryo. Eng. (Materials), 26 10-36 (1980).

[84] J. Willbrand and W. Schlump, "Einfluss von Ausscheidungsdichte und Teilchengrösse auf die Stromtragfähigkeit von NbTi-Supraleitern", Z. Metallkde., 66 714-9 (1975).

[85] R. Arndt and R. Ebeling, "Einfluss von Gefügeparametern auf die Stromtragfähigkeit von Niob-Titan-Supraleitern", Z. Metallkde., 65 364-73 (1974).

[86] I. Pfeiffer and H. Hillmann, "Der Einfluss der Struktur auf die Supraleitungseigenschaften von NbTi 50 und NbTi 65", Acta. Met., 16 1429-39 (1968).

[87] H. Albert and I. Pfeiffer, "Temperaturabhängigkeit der Festigkeitseigenschaften des Hochfeldsupraleiters NbTi50", Z. Metallkde., 67 356-60 (1976).

[88] H. Hillmann, "Ausscheidungen und Flussverankerung bei Hochfeldsupraleitern aus Niobtitan", Siemens Forsch. u. Entwickl. Ber., 3 197-204 (1974).

[89] Z.J.J. Stekly, H. R. Segal, K. Hemachalam, T. A. de Winter, and D. A. Colling, "Development of NbTi Conductors for 10 T - 14 T Operation", Magnetic Corporation of America, Final Report to U.S. DOE under Contract No. EG-77-C-02-4180 (September, 1978).

[90] E. Helfand and N. R. Werthamer, "Temperature and Purity Dependence of the Superconducting Critical Field, H_{c2}.II", Phys. Rev., 147 288-94 (1966).

[91] D. G. Hawksworth and D. C. Larbalestier, "Enhanced Values of B_{c2} in Nb-Ti Ternary and Quaternary Alloys", Adv. Cryo. Eng. (Materials), 26 479-86 (1980).

[92] D. G. Hawksworth and D. C. Larbalestier, "The High Field J_c and Scaling Behavior in Nb-Ti and Alloyed Nb-Ti Superconductors", Proc. of 8th Symposium on Engineering Problems of Fusion Research, Pt. I. San Francisco, CA, 13-16 November, 1979, IEEE, NY (1980) pp 249-54.

[93] H. Wada, K. Tachikawa, and R. M. Rose, "A Metallurgical Study on Superconducting Ti-Nb Binary and Ternary Alloys", in Titanium '80 Science and Technology (Proc. of the 4th Int. Conf. on Ti, Kyoto, Japan (May, 1980)), ed. by H. Kimura and O. Izumi, published by The Metallurgical Society, AIME, PA (1980) pp 745-53.

[94] M. Suenaga and K. M. Ralls, "Some Superconducting Properties of Ti-Nb-Ta Ternary Alloys", J. Appl. Phys., 40 4457-63 (1969).

[95] T. Horiuchi, Y. Monju, and N. Nagai, "Superconducting Transition Temperatures and Resistive Critical Fields of Superconducting Ti-Nb-Zr-Ta Alloys", Nippon Kinzoku Gakkaishi, 37 882-7 (1973).

[96] T. H. Geballe, "Insulated Superconducting Wire", U.S. Patent No. 3,109,963 (November 5, 1963).

[97] T. Doi and M. Kudo, "Method of Producing Superconducting Strips", U.S. Patent No. 3,710,844 (January 16, 1973).

[98] D. Fairbanks, W. L. Larson, R. N. Randall, and J. Wong, "Composite-Strip-Conductor Containing Niobium-Titanium Superconductor", U.S. Patent No. 3,548,351 (December 15, 1970).

[99] G. Bogner, R. Dötzer, and R. Maier, "Verfahren zur Herstellung von aus supraleitenden und elektrisch normalleitenden Metallen zusammengesetzten Leitern", German Patent No. 1,665,790 (March 18, 1971).

[100] E. Gregory, "Fabrication of Niobium Superconductor Alloys", U.S. Patent No. 3,472,705 (October 14, 1969).

[101] A. Olivei, "Composite Filamentary Superconductors Made From the Melt", Proc. 5th Int. Cryo. Engineering Conf. (Kyoto, Japan, May 7-10, 1974), ed. by K. Mendelssohn, IPC Science and Tech. Press (1974) pp 347-52.

[102] M. C. Ohmer, J. J. Wollan, and J. C. Ho, "Improved Superconducting Properties of Multifilamentary Niobium Carbonitride Wire", IEEE Trans. Magn., MAG-11 159-62 (1975).

[103] K. Inoue and K. Tachikawa, "Upper Critical Fields of Superconducting Laves Phases in V-Hf-X Ternary Alloys", Applied Superconductivity Conference, Annapolis MD (May, 1972), IEEE Pub. No. 72CH0682-5-TABSC, pp 415-8.

[104] S. Foner, E. J. McNiff, and E. J. Alexander, "High Field Properties of Ternary Metal-Molybdenum Sulphides", IEEE Trans. Magn., MAG-11 155-8 (1975).

[105] D. Dew-Hughes, "Superconducting A15 Compounds: A Review", Cryogenics, 15 435-54 (1975).

[106] D. Dew-Hughes, "Physical Metallurgy of A15 Compounds", Reference [5] pp 137-69.

[107] G. V. Raynor, "Phase Diagrams and Their Determination", in Physical Metallurgy, ed. by R. W. Cahn, North-Holland (1965) pp 291-363.

[108] T. S. Luhman, "Metallurgy of A15 Compounds", Reference [5] pp 221-66.

[109] J. J. Hanak, K. Strater, and G. W. Cullen, "Preparation and Properties of Vapor-Deposited Niobium Stannide", RCA Rev., 25 324-65 (1964).

[110] G. W. Webb and J. J. Engelhardt, "Superconducting, Metallurgical and Synthesis Properties of Nb_3Ga", IEEE Trans. Magn., MAG-11 208-13 (1975).

[111] L. R. Newkirk, F. A. Valencia, A. L. Giorgi, E. G. Szkarz, and T. C. Wallace, "Bulk Superconductivity Above 20 K in Nb_3Ge", IEEE Trans. Magn., MAG-11 221-4 (1975).

[112] J. D. Thompson, M. P. Maley, L. R. Newkirk, and R. V. Carlson, "High Magnetic Field Properties of CVD-Prepared Nb_3Ge and $Nb_3(Ge,X)$", IEEE Trans. Magn., MAG-15 516-9 (1979).

[113] R. H. Hammond, "Electron Beam Evaporation Synthesis of A15 Superconducting Compounds: Accomplishments and Prospects", IEEE Trans. Magn., MAG-11 201-7 (1975).

[114] S. D. Dahlgren, "High-Rate Sputtering of Nb-Al-Ge and Nb-Al Superconductors", IEEE Trans. Magn., MAG-11 217-20 (1975).

[115] J. R. Gavaler, "Superconductivity in Nb-Ge Films above 22 K", Appl. Phys. Lett., 23 480-2 (1973).

[116] R. T. Kampwirth, "Critical Current Densities of Magnetron Sputtered Nb_3Ge Films", IEEE Trans. Magn., MAG-15 502-4 (1979).

[117] K. Tachikawa and Y. Tanaka, "Superconducting Critical Currents of V_3Ga Wire Made by a New Diffusion Process", Japan J. Appl. Phys., 6 782 (1967).

[118] Y. Tanaka, K. Tachikawa, and K. Sumiyama, "Formation of Superconducting V_3Ga Compound by a Diffusion Reaction Enhanced by Cu", Nippon Kinzoku Gakkaishi, 34 835 (1970).

[119] D. B. Smathers and D. C. Larbalestier, "Composition Profiles in Nb_3Sn Diffusion Layers", Adv. Cryo. Eng. (Materials), 26 415-24 (1980).

[120] M. Suenaga, T. S. Luhman, and W. B. Sampson, "Effects of Heat Treatment and Doping with Zr on the Superconducting Critical Current Densities of Multifilamentary Nb_3Sn Wires", J. Appl. Phys., 45 4049-53 (1974).

[121] R. M. Scanlan, W. A. Fietz, and E. F. Koch, "Flux Pinning Centers in Superconducting Nb_3Sn", J. Appl. Phys., 46 2244-9 (1975).

[122] B. J. Shaw, "Grain Size and Film Thickness of Nb_3Sn Formed by Solid-State Diffusion in the Range 650-800°C", J. Appl. Phys., 47 2143-5 (1976).

[123] W. Schauer and W. Schelb, "Improvement of Nb_3Sn High Field Critical Current by a Two-Stage Reaction", IEEE Trans. Magn., MAG-17 374-7 (1981).

[124] M. Suenaga, W. B. Sampson, and C. J. Klamut, "The Fabrication and Properties of Nb_3Sn Superconductors by the Solid Diffusion Process", IEEE Trans. Magn., MAG-11 231-7 (1975).

[125] S. Murase, M. Koizumi, O. Horigami, H. Shiraki, Y. Koike, E. Suzuki, M. Ichihara, F. Nakane, and N. Aoki, "Multifilament Niobium-Tin Conductors", IEEE Trans. Magn., MAG-15 83-6 (1979).

[126] E. Adam, E. Gregory, and F. T. Ormand, "Further Developments in Stabilized Multifilamentary Nb_3Sn Superconductors", IEEE Trans. Magn., MAG-13 319-22 (1977).

[127] Y. Hashimoto, K. Yoshizaki, and M. Tanaka, "Processing and Properties of Superconducting Nb_3Sn Filamentary Wire", 5th International Cryogenic Engineering Conference, Kyoto, May 1974, IPC Sci. and Tech. Press (1974) pp 332-5.

[128] O. Tsukamoto, H. Maeda, and Y. Iwasa, "Microslip Degradation in a Braided Superconductor", Appl. Phys. Lett., 39 918 (1981).

[129] S. L. Wipf, "Magnetic Instabilities in Type-II Superconductors", Phys. Rev., 161 404-16 (1967).

[130] S. S. Shen, "Effect of the Diffusion Barrier on the Magnetic Properties of Practical Nb_3Sn Composites", Adv. Cryo. Eng. (Materials), 28 633-8 (1982).

[131] M. P. Mathur, M. Ashkin, D. W. Deis, and B. J. Shaw, "Flux Pinning in Nb_3Sn Multifilamentary Conductors", IEEE Trans. Magn., MAG-11, 255-8 (1975).

[132] W. Schauer and F. Zimmermann, "Temperature Dependence of the Critical Current and Pinning Behavior for Nb_3Sn Filamentary Superconductors", Adv. Cryo. Eng. (Materials) 26, 432-41 (1980).

[133] R. J. Bartlett, R. D. Taylor, and J. D. Thompson, "Stress Effects on Multifilamentary Nb_3Sn Wire", IEEE Trans. Magn., MAG-15 193-6 (1979).

[134] T. Luhman and M. Suenaga, "Effects of Stresses Induced by Thermal Contraction of a Bronze Matrix, on the Superconducting Properties of Nb_3Sn Wires", Appl. Phys. Lett., 29 61-3 (1976).

[135] P. E. Madsen and R. F. Hills, "The Effect of Heat Treatment on the Superconducting Properties of a Multifilamentary Nb_3Sn Composite", IEEE Trans. Magn., MAG-15 182-4 (1979).

[136] R. W. Hoard, R. M. Scanlan, G. S. Smith, and C. L. Farrell, "The Effect of Strain on the Martensitic Phase Transition in Superconducting Nb_3Sn", IEEE Trans. Magn., MAG-17 364-7 (1981).

[137] A. W. West and R. D. Rawlings, "A Transmission Electron Microscopy Investigation of Filamentary Superconducting Composites", J. Mater. Sci., 12 1862-8 (1977).

[138] C. S. Pande and M. Suenaga, "A Model of Flux Pinning by Grain Boundaries in Type-II Superconductors", Appl. Phys. Lett., 29 443-4 (1976).

[139] L. Schultz and H. C. Freyhardt, "Flux Pinning by Regularly Arranged Precipitates in Pb-Na Alloys" in International Discussion Meeting on Flux Pinning in Superconductors, ed. by P. Haasen and H. C. Freyhardt, Akademie der Wissenschaften in Göttingen,1975, pp 168-175.

[140] J. D. Livingston, "Effect of Ta Additions to Bronze-Processed Nb_3Sn Superconductors", IEEE Trans. Magn., MAG-14 611-3 (1978).

[141] K. Tachikawa, "Improvements in Current-Carrying Capacities of A15 Superconductors in High Magnetic Fields", Adv. Cryo. Eng. (Materials), 26 378-87 (1980).

[142] H. Sekine, T. Takeuchi, and K. Tachikawa, "Studies on the Composite Processed Nb-Hf/Cu-Sn-Ga High-Field Superconductors", IEEE Trans. Magn., MAG-17 383-6 (1981).

[143] K. Tachikawa, "Recent Developments in Filamentary Compound Superconductors", Adv. Cryo. Eng. (Materials), 28 29-40 (1982).

[144] K. Tachikawa, T. Takeuchi, T. Asano, Y. Iijima, and H. Sekine, "Effects of the IVa Element Additions to the Composite-Processed Nb_3Sn", Adv. Cryo. Eng. (Materials), 28 389-98 (1982).

[145] M. Suenaga, K. Aihara, K. Kaiho, and T. S. Luhman, "Superconducting Properties of Bronze-Process-Fabricated $(Nb,Ta)_3Sn$ Wires", Adv. Cryo. Eng. (Materials), 26 442-50 (1980).

[146] O. Horigami, T. Luhman, C. S. Pande, and M. Suenaga, "Superconducting Properties of $Nb_3(Sn_{1-x}Ga_x)$ by a Solid-State Diffusion Process", Appl. Phys. Lett., 28 738-40 (1976).

[147] D. Dew-Hughes and M. Suenaga, "Critical-Current Densities of Bronze-Processed $Nb_3(Sn_{1-x}Ga_x)$ Wires up to 23.5 T", J. Appl. Phys., 49 357-60 (1978).

[148] R. Akihama, K. Yasukōchi and T. Osagawa, "The Effect of Ternary Additions to Nb_3Sn on the Upper Critical Field at 4.2 K", IEEE Trans. Magn., MAG-13 803-6 (1977).

[149] D. S. Easton and D. M. Kroeger, "Kirkendall Voids--A Detriment to Nb_3Sn Superconductors", IEEE Trans. Magn., MAG-15 178-81 (1979).

[150] S. Cogan, D. S. Holmes, and R. M. Rose, "On the Elimination of Kirkendall Voids in Superconducting Composites", Appl. Phys. Lett., 35 557-9 (1979); see also S. F. Cogan, D. S. Holmes, and R. M. Rose, "Multifilamentary Nb_3Sn by an Improved External Diffusion Method", Reference [6], pp 91-101.

[151] J. D. Klein, G. Warshaw, N. Dudziak, S. F. Cogan, and R. M. Rose, "On the Suppression of Kirkendall Porosity in Multifilamentary Superconducting Composites", IEEE Trans. Magn., MAG-17 380-2 (1981).

[152] J. E. Kunzler, E. Buehler, F.S.L. Hsu, and J. E. Wernick, "Superconductivity in Nb_3Sn at High Current Density in a Magnetic Field of 88 kgauss", Phys. Rev. Lett., 6 89-91 (1961).

[153] E. Saur and J. Wurm, "Präparation und Supraleitungseigenschaften von Niobdrahtproben mit Nb_3Sn-Überzug", Die Naturwissenschaften 49 127-8 (1962).

[154] A. Eċharri and M. Spadoni, "Superconducting Nb_3Sn: A Review", Cryogenics, 11 274-84 (1971).

[155] K. Tachikawa, Proc. Third International Cryogenic Engineering Conference, Berlin, Iliffe Science and Technology Publications Ltd, Surrey, England, 1970, p. 339.

[156] A. R. Kaufman and J. J. Pickett, "Multifilamentary Nb_3Sn Superconducting Wire", abstracts in Bull. Amer. Phys. Soc., 15 838 (1970) and J. Appl. Phys. 42 58 (1971).

[157] M. Suenaga and W. B. Sampson, "Superconducting Properties of Multifilamentary V_3Ga Wires", Appl. Phys. Letters, 18 584-6 (1971).

[158] M. Suenaga and W. B. Sampson, "Superconducting Properties of Multifilamentary V_3Si Wires", Proceedings of the 1972 Applied Superconductivity Conference, Annapolis, MD,(May, 1972), IEEE Pub. No. 72CH0682-5-TABSC (1972) pp 481-5.

[159] T. H. Geballe and J. K. Hulm, "Superconducting Materials up to Now and into the Future", IEEE Trans. Magn., MAG-11 119-24 (1975).

[160] G. W. Webb, "Superconductivity of Nb_3Ga" in Superconductivity in d- and f-band Metals, ed. by D. H. Douglass, American Inst. of Physics Conference Proceedings No. 4 (1972) pp 139-43.

[161] J. R. Gavaler, "Impurity Stabilization of Nb_3Ge" in Superconductivity in d- and f-band Metals--Second Rochester Conference, ed. by D. H. Douglass, Plenum Press 1976 pp 421-7.

[162] J. D. Elen, C.A.M. van Beijnen, and C.A.M. van der Klein, "Multifilament V_3Ga and Nb_3Sn Superconductors Produced by the ECN-Technique", IEEE Trans. Magn., MAG-13 470-3 (1977).

[163] C.A.M. van Beijnen and J. D. Elen, "Multifilament Nb_3Sn Superconductors Produced by the E.C.N. Technique", IEEE Trans. Magn., MAG-15 87-90 (1979).

[164] R. M. Rose, "Alternative Technologies for Superconductor Fabrication", IEEE Trans. Magn., MAG-15 680-3 (1979).

[165] C. C. Tsuei, "Ductile Superconducting Copper-Base Alloys", Science, 180 57-8 (1973).

[166] C. C. Tsuei, "Ductile Superconducting Cu-Rich Alloys Containing A-15 Filaments", IEEE Trans. Magn., MAG-11 272-5 (1975).

[167] R. Flükiger, R. Akihama, S. Foner, E. J. McNiff, Jr., and B. B. Schwartz, "Progress with Cold Powder-Metallurgy-Processed Superconducting Multifilamentary Composites", Adv. Cryo. Eng. (Materials), 26 337-42 (1980).

[168] C.A.M. van Beijnen and J. D. Elen, "Potential Fabrication Method of Superconducting Multifilament Wires of the A-15-Type", IEEE Trans. Magn., MAG-11 243-6 (1975).

[169] K. Hemachalam and M. R. Pickus, "Studies on Filamentary Nb_3Sn Wires Fabricated by the Infiltration Method", IEEE Trans. Magn., MAG-13 466-9 (1977).

[170] M. R. Pickus, J. T. Holthuis, and M. Rosen, "A15 Multi-Filamentary Superconductors by the Infiltration Process", Reference [6], pp 331-53.

[171] J. D. Elen, J. W. Schinkel, A.C.A. van Wees, C.A.M. van Beijnen, E. M. Hornsveld, T. Stahlie, H. J. Veringa, and A. Verkaik, Development of Stabilized Nb_3Sn Wire Containing A Reduced Number of Filaments", IEEE Trans. Magn., MAG-17 1002-5 (1981).

[172] R. Roberge and S. Foner, "*In Situ* and Powder Metallurgy Multifilamentary Superconductors: Fabrication and Properties", Reference [6], pp 241-57.

[173] R. Flükiger, S. Foner, E. J. McNiff, Jr., B. B. Schwartz, J. Adams, S. Forman, T. W. Eager, and R. M. Rose, "Superconducting Cu-Nb_3Sn Composites Produced by Cold Extrusion of Fine Powders", IEEE Trans. Magn., MAG-15 689-92 (1979).

[174] C. L. H. Thieme, H. Zhang, J. Otubo, S. Pourrahimi, B. B. Schwartz, and S. Foner, "Scaleup of Powder Metallurgy Processed Nb-Al Multifilamentary Wire", IEEE Trans. Magn. MAG-19 (1983), *to be published.*

[175] R. J. Murphy, R. Akihama, S. Foner, and B. B. Schwartz, "Further Development of Powder Processed Multifilamentary Superconductors", IEEE Trans. Magn., MAG-17 989-92 (1981).

[176] R. Akihama, R. J. Murphy, and S. Foner, "Fabrication of Multifilamentary Nb-Al By A Powder Metallurgy Process", IEEE Trans. Magn., MAG-17 274-7 (1981).

[177] R. Flükiger, S. Foner, E. J. McNiff, and B. B. Schwartz, "High Critical Currents in Cold-Powder-Metallurgy-Processed Superconducting Cu-Nb-Sn Composites", Appl. Phys. Lett., 34 763-6 (1979).

[178] L. Schultz, R. Bormann, and H. C. Freyhardt, "Superconducting Properties and Annealing Behavior of Filamentary Cu-Based Composites Produced by Powder Metallurgy", IEEE Trans. Magn., MAG-15 94-6 (1979).

[179] R. Löhberg, T. W. Eagar, I. M. Puffer, and R. M. Rose, "Fabrication and $J_c(H,T)$ Measurements on $Nb_3Al_{0.75}Ge_{0.25}$ Ribbon", Appl. Phys. Lett., 22 69-71 (1973).

[180] J. Wecker, K. Mrowiec, R. Bormann, H. C. Freyhardt, "Optimization of Critical Currents in Cu-Nb_3Sn Microcomposites", Adv. Cryo. Eng. (Materials), 28 495-9 (1982).

[181] H. C. Freyhardt, R. Bormann, and K. Mroviec, "Powder Metallurgically Prepared A15 Microcomposite Superconductors", Reference [6], pp 289-98.

[182] R. Bormann and H. C. Freyhardt, "V_3Ga Micro-Composite Conductors: Preparation and Superconducting Properties", IEEE Trans. Magn., MAG-17 270-3 (1981).

[183] T. W. Eagar and R. M. Rose, "Resistive Measurements on an Improved Nb-Al-Ge Superconducting Ribbon", IEEE Trans. Nuc. Sci., 20 742-3 (1973).

[184] S. Foner, "Powder Metallurgy Processes--A Review of the Status and Promise", Adv. Cryo. Eng. (Materials), 28 41-7 (1982).

[185] R. Flükiger, R. Akihama, S. Foner, E. J. McNiff, Jr., and B. B. Schwartz, "Fabrication on a Laboratory Scale and Mechanical Properties of Cu-Nb-Sn Multifilamentary Superconducting Composite Wires Produced by Cold Powder Metallurgy Processing", Appl. Phys. Lett., 35 810-2 (1979).

[186] R. Bormann, H. C. Freyhardt, and H. Bergmann, "Superconducting A15 Composite Materials", Adv. Cryo. Eng. (Materials), 26 334-6 (1980).

[187] R. Bormann, H. C. Freyhardt, and H. Bergmann, "High-Current A-15 Microcomposite Materials", Appl. Phys. Lett., 35 944-6 (1979).

[188] J. W. Hafstrom, "Metallurgy, Fabrication, and Superconducting Properties of Multifilamentary Nb_3Al Composites", IEEE Trans. Magn., MAG-13 480-2 (1977).

[189] T. W. Eagar and R. M. Rose, "Improved J_c in Mechanically Fabricated Nb_3Al Wires and Ribbons", IEEE Trans. Magn., MAG-11 214-6 (1975).

[190] K. Togano and R. M. Rose, "An Improved Method for Fabrication of $Nb_3(Al,Ge)$ Wire", IEEE Trans. Magn., MAG-13 478-9 (1977).

[191] S. Ceresara, M. V. Ricci, N. Sacchetti, and G. Sacerdoti, "Nb_3Al Formation at Temperatures Lower Than 1000°C", IEEE Trans. Magn., MAG-11 263-5 (1975).

[192] D. Dew-Hughes, "Critical Currents at High Fields in Multifilamentary Wires", IEEE Trans. Magn. MAG-17 561-4 (1981).

[193] R. Bruzzese, S. Ceresara, G. Pasotti, M. V. Ricci, N. Sacchetti, and M. Spadoni, "Experimental Results on Nb_3Al Multifilamentary Wires", Proc. 7th Int. Conf. Eng. Prob. Fusion Research, Knoxville TN, 25-28 October, 1977, IEEE, NY (1977) pp 1255-8.

[194] S. Ceresara, M. V. Ricci, G. Pasotti, N. Sacchetti, and M. Spadoni, "Practical Nb_3Al Wires: Experimental Behavior of Small Scale Solenoids", IEEE Trans. Magn., MAG-15 639-41 (1979).

[195] J. M. Larson, T. S. Luhman, and H. F. Merrick, "Mechanically Alloyed Superconducting Compounds", Reference [62], pp 155-63.

[196] M. Asdente and A. M. Ricca, "AC Losses in Nb_3Al-Nb Layered Multifilamentary Wires", IEEE Trans. Magn., MAG-17 978-80 (1981).

[197] S. S. Shen and W. K. McDonald, "Testing Results of MF-Nb_3Sn Composites Made by a Modified Jellyroll Method", Adv. Cryo. Eng. (Materials), 28 535-43 (1982).

[198] M. Hong, D. Dietderich, and J. W. Morris, Jr., "Development of A-15 (V_3Ga) Superconducting Material Through Controlled Precipitation", J. Appl. Phys., 51 2774-9 (1980).

[199] G. W. Webb, "Mechanical and Superconducting Properties of Nb_3Al", IEEE Trans. Magn., MAG-15 616-8 (1979).

[200] M. Hong and J. W. Morris, Jr., "Direct Solid-State Precipitation-Processed A15 (Nb_3Al) Superconducting Material", Appl. Phys. Lett., 37 1044-5 (1980).

[201] M. Hong, D. R. Dietderich, I. W. Wu, and J. W. Morris, Jr., Microstructure and Properties of A15 Superconductors Formed by Direct Precipitation", IEEE Trans. Magn., MAG-17 278-81 (1981).

[202] M. Hong, D. Dietderich, and J. W. Morris, Jr., "Research on the Monolithic Process of Making A15 Superconducting Materials", Adv. Cryo. Eng. (Materials), 26 327-33 (1980).

[203] J. D. Verhoeven, F. A. Schmidt, E. D. Gibson, J. E. Ostenson, and D. K. Finnemore, "Casting of Dendritic Cu-Nb Alloys for Superconducting Wire", Appl. Phys. Lett., 35 555-7 (1979).

[204] C. Allibert, J. Driole, and E. Bonnier, "Contribution à l'étude du Diagramme d'équilibre de Phases du Système Cu-Nb", Comp. Rend. Acad. Sci. (Paris), 268 Ser. C, 1579-81 (1969).

[205] J. D. Verhoeven, J. J. Sue, D. K. Finnemore, E. D. Gibson, and J. E. Ostenson, "The Morphology and Grain Size of Nb_3Sn Filaments in "In-Situ" Prepared Multifilamentary Nb_3Sn-Cu Composite Wire", J. Mater. Sci., 15 1907-14 (1980).

[206] R. Roberge and J. L. Fihey, "Origin of Superconductivity in Copper Niobium Alloys", J. Appl. Phys., 48 1327-31 (1977).

[207] R. Roberge and J. L. Fihey, "Comments on the Fabrication of "In-Situ" Superconducting Wires in Cu-Nb and Cu-Sn-Nb Alloys", Reference [62], pp 223-31.

[208] J. Bevk and M. Tinkham, "Superconducting Properties and Coupling Mechanisms in In Situ Filamentary Composites", Reference [6], pp 271-87.

[209] A. Davidson, M. R. Beasley, and M. Tinkham, "Remnant Resistance in Tsuei's Composite Superconductors", IEEE Trans. Magn., MAG-11 276-9 (1975).

[210] D. K. Finnemore, J. D. Verhoeven, J. E. Ostenson, E. D. Gibson, and H. H. Sample, "Critical Currents for Superconducting Composites in the 1000-Å Regime", J. Appl. Phys., 50 2867-70 (1979).

[211] J. Bevk, M. Tinkham, F. Habbal, C. J. Lobb, and J. P. Harbison, "In Situ Formed Multifilamentary Composites, Part I: Coupling Mechanisms, Stress Effects and Flux Pinning Mechanisms", IEEE Trans. Magn., MAG-17 235-42 (1981).

[212] J. D. Verhoeven, F. A. Schmidt, E. G. Gibson, J. J. Sue, J. E. Ostenson, and D. K. Finnemore, "Preparation of In-Situ Nb_3Sn-Cu Wire by Consumable Arc Melting", IEEE Trans. Magn., MAG-17 251-4 (1981).

[213] J. D. Verhoeven, E. D. Gibson, F. A. Schmidt, and D. K. Finnemore, "Preparation of Cu-Nb Alloys for Multifilamentary "In-Situ" Superconducting Wire", J. Mater. Sci., 15 1449-55 (1980).

[214] J. J. Sue, J. D. Verhoeven, E. D. Gibson, J. E. Ostenson, and D. K. Finnemore, "On The Optimization of In Situ Nb_3Sn-Cu Wire", Adv. Cryo. Eng. (materials), 28 501-10 (1982).

[215] K. Yasohama, H. Ohkubo, T. Ogasawara, and K. Yasukōchi, "Fabrication of Stabilized In-Situ Nb_3Sn Wire by Consumable Arc Melting and Its Magnetic Behavior", Adv. Cryo. Eng. (Materials), 28 55-62 (1982).

[216] E. D. Gibson, J. E. Ostenson, J. J. Sue, J. D. Verhoeven, and D. K. Finnemore, "Development of Cryostabilized Nb_3Sn-Cu Superconducting Wire Using the In Situ Process", Adv. Cryo. Eng. (Materials), 28 525-34 (1982).

[217] J.-L. Fihey, M. Neff, R. Roberge, M. C. Flemings, S. Foner, and B. B. Schwartz, "High-Temperature-Gradient Casting of *In Situ* Multifilamentary Superconductors", Adv. Cryo. Eng. (Materials), 26 343-9 (1980).

[218] H. LeHuy, J.-L. Fihey, R. Roberge, and S. Foner, "Continuous High Temperature Gradient Solidification of In Situ Cu-Nb Alloys for Large Scale Development", Adv. Cryo. Eng. (Materials), 28 563-9 (1982).

[219] K. Togano, H. Kumakura, and K. Tachikawa, "Studies on 'In Situ Processing V_3Ga Composite Superconductors", IEEE Trans. Magn., MAG-17 985-8 (1981).

[220] J. D. Verhoeven, E. D. Gibson, C. V. Owen, J. E. Ostenson, and D. K. Finnemore, "Fabrication of Superconducting Nb_3Sn-Cu Composites", Appl. Phys. Lett., 35 270-2 (1979).

[221] B. Annaratone, R. Bruzzese, S. Ceresara, V. Pericoli-Ridolfini, G. Pitto, and N. Sacchetti, "Effect of the Thickness of Aluminum Layer on the Transport Properties of Nb_3Al Superconducting Wires", IEEE Trans. Magn., MAG-17 1000-1 (1981).

[222] D. K. Finnemore and J. D. Verhoeven, "A15 Superconducting Composites in the 0.1-μm Region", Adv. Cryo. Eng. (Materials), 26 319-26 (1980).

[223] D. K. Finnemore, J. D. Verhoeven, E. D. Gibson, and J. E. Ostenson, "Preparation and Properties of In Situ Prepared Filamentary Nb_3Sn-Cu Superconducting Wire", Reference [6], pp 259-70.

[224] W.Y.K. Chen and C. C. Tsuei, "Superconducting Copper-Base Alloys Containing Filaments of V_3Ga", J. Appl. Phys., 47 715-20 (1976).

[225] J. Bevk, F. Habbal, C. J. Lobb, and G. Dublon, "Superconducting and Mechanical Properties of *In Situ* Formed Cu-V_3Ga Composites", Adv. Cryo. Eng. (Materials), 26 538-42 (1980).

[226] J.-L. Fihey, R. Roberge, S. Foner, E. J. McNiff, Jr., and B. B. Schwartz, "Multifilamentary V_3Ga Produced By the *In Situ* Process", Adv. Cryo. Eng. (Materials), 26 350-7 (1980).

[227] F. A. Shunk, Constitution of Binary Alloys, Second Supplement, McGraw-Hill (1969), p 300.

[228] H. Kumakura, K. Togano, and K. Tachikawa, "Studies on Cu-V_3Ga Filamentary Superconductors Processed *In Situ*", J. Less-Common Metals, 79 181-90 (1981).

[229] H. Kumakura, K. Togano, and K. Tachikawa, "High-Field Critical Current and Mechanical Properties of In Situ Processed V_3Ga Superconductors", Adv. Cryo. Eng. (Materials), 28 515-24 (1982).

[230] J. D. Verhoeven and E. D. Gibson, "The Monotectic Reaction in Cu-Nb Alloys, J. Mater. Sci., 13 1576-82 (1978).

[231] Y. Furuto, T. Suzuki, K. Tachikawa, and Y. Iwasa, "Current-Carrying Capacities of Superconducting Multifilamentary V_3Ga Cables", Appl. Phys. Lett. 24 34-6 (1974).

[232] J.-L. Fihey, M. Neff, R. Roberge, M. C. Flemings, S. Foner, and B. B. Schwartz, "In Situ Multifilamentary Superconducting Wires Fabricated Using a Controlled High Temperature Gradient", Appl. Phys. Lett., 35 715-7 (1979).

[233] T. Y. Hsiang and D. K. Finnemore, "Magnetic Field Dependence of J_c In SNS Junctions", Solid State Comm., 33 847-8 (1980).

[234] P. E. Madsen and R. F. Hills, "The Effect of Heat Treatment on the Superconducting Properties of a Multifilamentary Nb_3Sn Composite", IEEE Trans. Magn., MAG-15 182-4 (1979).

[235] H. LeHuy, R. Roberge, J.-L. Fihey, G. Rupp, and S. Foner, "The Effects of Additives to the Cu-Nb Melt on the High Field Properties of In Situ Multifilamentary Nb_3Sn Wires", IEEE Trans. Magn., MAG-17 261-4 (1981).

[236] J. Bevk, J. P. Harbison, and J. L. Bell, "Anomalous Increase in Strength of *In Situ* Formed Cu-Nb Multifilamentary Composites", J. Appl. Phys., 49 6031-8 (1978).

[237] R. Roberge, J.-L. Fihey, S. Foner, E. J. McNiff, Jr., and B. B. Schwartz, "The Effects of Mechanical Stresses on the High Field Critical Current Density of *In Situ* Multi-Filamentary Nb_3Sn Wires", Adv. Cryo. Eng. (Materials), 26 530-7 (1980).

[238] W. J. Carr, Jr., J. H. Murphy, and G. R. Wagner, "Alternating Field Losses in Filamentary Superconductors Carrying DC Transport Currents", Adv. Cryo. Eng. (Materials), 24 415-26 (1978).

[239] A. I. Braginski, G. R. Wagner, J. Bevk, and J. P. Harbison, "AC Losses in "In-Situ" Nb_3Sn-Cu Composite Conductors", IEEE Trans. Magn., MAG-15 695-8 (1979).

[240] A. I. Braginski, G. R. Wagner, and J. Bevk, "AC Losses in Untwisted Superconducting Composites Fabricated by An *In Situ* Technique", Adv. Cryo. Eng. (Materials), 26 367-77 (1980).

[241] A. I. Braginski and J. Bevk, "Alternating Current Losses in Twisted In-Situ Composite Wires", Reference [6], pp 321-30.

[242] S. S. Shen, "Magnetic Properties of Multifilamentary Nb_3Sn Composites", Reference [6], pp 309-20.

[243] J. Bevk, J. P. Harbison, F. Habbal, G. R. Wagner, and A. I. Braginski, "Superconducting Critical Properties and AC Losses in a Large Sample of *In Situ* Formed Cu-Nb_3Sn Composite, Appl. Phys. Lett., 36 85-7 (1980).

[244] H. Hillmann, H. Kuckuck, E. Springer, H.-J. Weisse, M. Wilhelm, and K. Wohlleben, "Coil Performance of Multi-Filamentary Nb_3Sn Conductors", IEEE Trans. Magn., MAG-15 205-8 (1979).

[245] J. Bevk, F. Habbal, C. J. Lobb, and J. P. Harbison, "Superconducting Properties of In Situ Formed Cu-V_3Ga Composites", Appl. Phys. Lett., 35 93-5 (1979).